Design and Development of a Two-Photon Absorption Induced Fluorescence Spectrometer and the Investigation of Nonlinear Optical Properties of Organic Chromophores

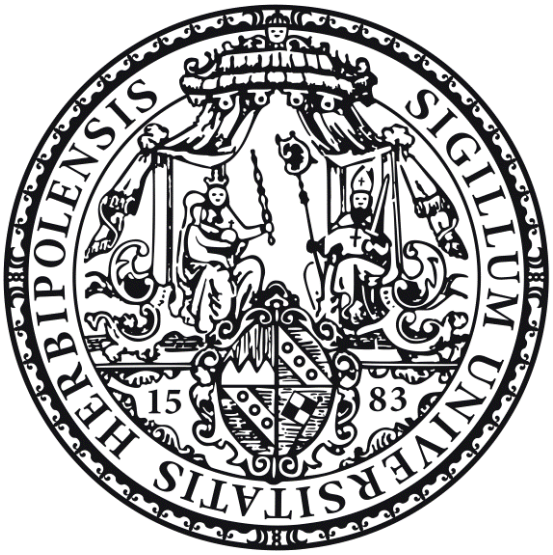

Dissertation zur Erlangung

des naturwissenschaftlichen Doktorgrades der

Julius-Maximilians-Universität Würzburg

vorgelegt von

Evripidis Michail

aus Zypern

Würzburg 2021

Eingereicht bei der Fakultät für Chemie und Pharmazie am

Gutachter der schriftlichen Arbeit

1. Gutachter: Prof. Dr. Christoph Lambert

2. Gutachter: Prof. Dr. Tobias Brixner

Prüfer des öffentlichen Promotionskolloquiums

1. Prüfer: Prof. Dr. Christoph Lambert

2. Prüfer: Prof. Dr. Tobias Brixner

3. Prüfer: Prof. Dr. Tobias Hertel

Datum des öffentlichen Promotionskolloquiums

Doktorurkunde ausgehändigt am

Die vorliegende Arbeit wurde in der Zeit von Oktober 2015 bis März 2021
am Institut für Organische Chemie der Universität Würzburg angefertigt

Mein besonderer Dank gilt

Herrn Prof. Dr. Christoph Lambert

für die Vergabe des vielseitigen und interessanten Themas,
den damit verbundenen Diskussionen die mehr als hilf- und lehrreich für mich
waren, dem Vertrauen und den Freiheiten bei der Bearbeitung

To my parents Theofanis and Maria,
Thank you for believing in me and for your invaluable support

Experiment is the interpreter of nature. Experiments never deceive. It is our judgment which sometimes deceives itself because it expects results which experiment refuses. We must consult experiment, varying the circumstances, until we have deduced general rules, for experiment alone can furnish reliable rules.

Leonardo da Vinci

COPYRIGHTS REMARKS

Parts of this thesis have previously been submitted or published and are reproduced or adapted from:

1. E. Michail, M. H. Schreck, M. Holzapfel, C. Lambert, "*Exciton coupling effects on the two-photon absorption of squaraine homodimers with varying bridge units."*, Phys. Chem. Chem. Phys., **2020**, 22, 18340-18350. (*Chapter 5.1.1*)

2. E. Michail, M. H. Schreck, L. Wittmann, M. Holzapfel, C. Lambert, "*Enhanced two–photon absorption of transoid and cisoid benzodipyrrolenine-fused squaraine dimers: a promising broad energy range optical power limiter."*, Chem. Mater., **2021**, 33, 9, 3121-3131. (*Chapter 5.1.2*)

3. S. Griesbeck, E. Michail, C. Wang, H. Ogasawara, S. Lorenzen, L. Gerstner, T. Zang, J. Nitsch, Y. Sato, R. Bertermann, M. Taki, C. Lambert, S. Yamaguchi, T. B. Marder, "*Tuning the pi-Bridge of Quadrupolar Triarylborane Chromophores for One- and Two-Photon Excited Fluorescence Imaging of Lysosomes in Live Cells."*, Chem. Sci., **2019**, 10, 5405-5422. (*Chapter 5.2.1*)

4. S. Griesbeck, E. Michail, F. Rauch, H. Ogasawara, C. Wang, Y. Sato, R. Edkins, Z. Zhang, M. Taki, C. Lambert, S. Yamaguchi, T. B. Marder, "*The effect of branching one- and two-photon absorption, cell viability and localization of cationic triarylborane chromophores with dipolar vs. octopular charge distributions for cellular imaging."*, Chem. Eur. J., **2019**, 25, 13164-13175. (*Chapter 5.3.1*)

5. Y. Hattori, E. Michail, A. Schmiedel, M. Holzapfel, I. Krummenacher, H. Braunschweig, U. Müller, J. Pflaum, C. Lambert, "*Luminescent mono-, di-, and tri-radicals: bridging polychlorinated triarylmethyl radicals by triarylamines and triarylboranes.",* Chem. Eur. J., **2019**, 25, 15463-15471. (*Chapter 5.3.2*)

and the following Bachelor Theses (supervised by Evripidis Michail):

1. *"Linear and non-linear optical properties of quadrupolar triarylborane chromophores applicable for two-photon excited fluorescence bioimaging"*, A. Hainthaler, Bachelor Thesis, Julius-Maximilians-Universität, Würzburg, **2020**. (*Chapter 5.2.2*)

2. *"Linear and non-linear optical properties of triarylamine meta- and para- conjugated compounds with varying π-bridge electron densities",* C. Rimagmos, Bachelor Thesis, Julius-Maximilians-Universität, Würzburg, **2020**. (*Chapter 6.1*)

Contents

List of Abbreviations and Symbols Used

1PA	one-photon absorption
2PA	two-photon absorption
2PIF	two-photon induced fluorescence experimental technique
$\sigma^{(2PA)}$	two-photon absorption cross-section
β	two-photon absorption coefficient
$N^{(2PA)}$	number of molecules where excited by 2PA process
P_L / F_L	incident laser beam power/flux
$I^{(2PA)}$ / $F^{(2PA)}$	two-photon induced fluorescence intensity/flux
$\varphi_{fl}(\tilde{\nu}_{em})$	fluorescence quantum yield
$n_{fl}(\tilde{\nu}_{em})$	fluorescence detection efficiency
$\Phi(\tilde{\nu}_{em})$	fluorescence quantum efficiency
$\Delta p^{(2PA)}$	fraction of photons absorbed per pulse by 2PA
$\Delta N^{(2PA)}$	fraction of molecules excited per pulse by 2PA
gf	electronic transition between the ground and final excited state (f ← g)
$P_{gf}^{(2PA)}$	two-photon transition probability (for the transition f ← g)
μ_{gf}	transition dipole moment (for the transition f ← g)
$\Delta\mu_{fg}$	permanent dipole moment difference (between the states f and g)
$S^{(2PA)}$	two-photon transition tensor
$\langle\delta^{(2PA)}\rangle$	rotationally averaged 2PA strength
1P-FEA, $r^{(1PA)}$	one-photon fluorescence excitation anisotropy
2P-FEA, $r^{(2PA)}$	two-photon fluorescence excitation anisotropy
$\Omega^{(2PA)}$	polarization-depended 2PA ratio
TD-DFT	time-dependent density function theory
QR-DFT	quadratic-response density function theory

1 Introduction

1.1 The Two-Photon Absorption Phenomenon

At the beginning of the past century one of the most significant events in physics and chemistry, which has been studied extensively experimentally and theoretically, was the interaction between matter and light. This interaction, which is often accompanied by an energy exchange between these two types of elementary particles, gives rise to a wide variety of optical phenomena.[1] As a result, the field of optics has witnessed an enormous growth, leading to the development of revolutionary quantum theories. It was not long before theoretical studies were extended into the regime of the nonlinear optical response of the materials to the applied electromagnetic field. The experimental observation of the nonlinear optical effects became possible after the invention of the laser in 1960, which provided a highly coherent and intense radiation.[2,3]

In 1931, the theoretical physicist Maria Göppert-Mayer predicted the concept of the two-photon absorption (2PA) phenomenon in her dissertation, which was supervised by Max Born at Göttingen University.[4] This prediction was based on the principles of an atom being raised to an excited state by the simultaneous absorption process of two photons. In 1961, the first experimental evidence of 2PA that was performed by W. Kaiser and C. G. B. Garret, reported a 2PA induced fluorescence signal in a CaF_2 crystal containing Eu^{2+} ions by irradiation with 694.3 nm wavelength with a pulsed ruby-crystal laser.[5]

1.1.1 Basic Principles

The 2PA is a nonlinear process in which two photons are absorbed by a molecule (or an atom) "simultaneously". This stepwise process leads to an initial interaction of photon of energy $h\nu_1$ with the molecule, which in turn is being left in a temporarily excited state. This state is not a resonance state of the system due to its very short lifetime, and its existence is derived from uncertainty relations[I]. If a second photon with energy $h\nu_2$ interacts with the molecule within the short lifetime of the state, this then acts as an intermediate state and the molecule can be excited to a higher electronic state. After excitation *via* 2PA, the system in this excited state with energy equal to $h\nu_1 + h\nu_2$ returns to the ground state by the known radiative or/and nonradiative decay pathways. This thesis focuses on the case of degenerate 2PA process as it has been more widely studied, where the two photons belong to the same excitation beam, meaning that they have the same energy $h\nu$. The process of 2PA and the conventional one-photon absorption (1PA) are sketched in Figure 1-1.

[I] Assuming that ΔE represents the uncertainty in energy of the molecular system after the absorption of the first photon, according to the uncertainty principle in which $\Delta t \Delta E \geq \hbar/2$, for the photon energies in the visible and near-IR ranges the order of magnitude of the intermediate state lifetime is 10^{-15} – 10^{-16} s.

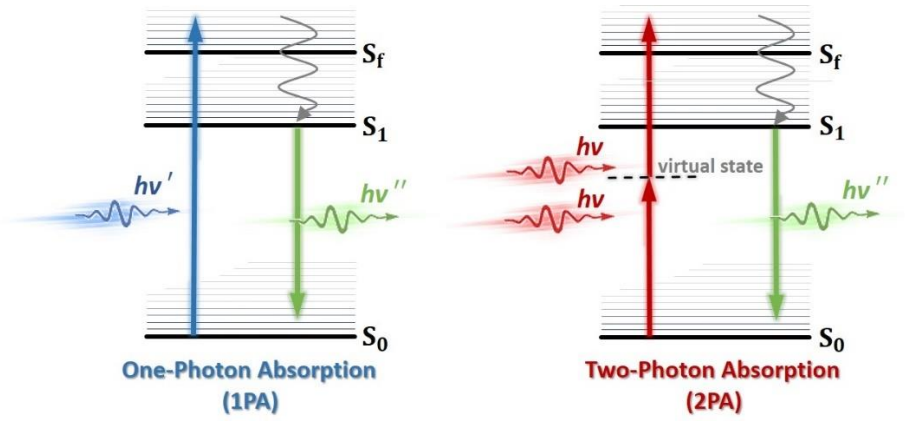

Figure 1-1: Schematic energy state diagram for a molecular system in a 1PA and 2PA process. The blue arrow indicates 1PA transition and the red arrows 2PA transition. The green arrows stand for the fluorescence process and the grey arrows for the internal conversion and vibrational relaxation.

The condition "simultaneous" absorption for the 2PA process is used to indicate that the second photon is required to interact with the molecule within the lifetime of the intermediate state (10^{-15} – 10^{-16} s). Thus, the 2PA process requires high photon flux in the focus laser beam, in order for the two involved photons to be localized in the same restricted space at the same time.

1.1.2 Two-Photon Absorption Cross Section

The 2PA process is quantified through the Lambert-Beer law, which relates the attenuation of a monochromatic beam with intensity I [in W/cm^2] which propagates within a material at a given time:[6]

$$\frac{dI}{dz} = -\beta I^2 \tag{1–1}$$

The absorption mechanism can be represented as a power series expansion of the incident intensity I, where in the regimes of high incident light intensities, the linear absorption order is negligible. Assuming that 2PA is the only nonlinear mechanism, the differential equation (1–1) presents the attenuation of a beam in a material due to 2PA. The 2PA coefficient β is a characteristic macroscopic parameter of the material and is closely related to the 2PA cross section $\sigma^{(2PA)}$ by[7]

$$\sigma^{(2\mathrm{PA})} = \frac{1000\, hv\, \beta}{N_A\, C} \tag{1–2}$$

where *hv* is the energy of the photons, N_A is Avogadro`s number and *C* is the molecular concentration. This is the most common way to quantify the probability that the 2PA process will take place. The molecular 2PA cross section is quoted in the units of Göppert-Mayer GM (where 1 GM = 10^{-50} cm^4 s photon^{-1}, in honour of the theoretical physicist Maria Göppert-Mayer`s fundamental contribution in this phenomenon).

Considering the Lorentz oscillator model for describing the displacement of charges in an organic material upon interaction with an incident electric field,[8] in the case of anharmonic oscillation the polarizability of the material $P(t)$ can be described as a power series in electric field strength $E(t)$ as:[9]

$$P(t) = \chi^{(1)}E(t) + \chi^{(2)}E^2(t) + \chi^{(3)}E^3(t) + \cdots \quad (1–3)$$

Here the quantities $\chi^{(n)}$ are the nth-order optical susceptibilities. The 2PA cross-section $\sigma^{(2PA)}$ is related to the imaginary part of the third-order optical susceptibility $\chi^{(3)}$ as:[10]

$$\sigma^{(2\mathrm{PA})} = \frac{4\pi^2\hbar\omega^2 Im[\chi(3)]}{n^2c^2} \quad (1–4)$$

where $\hbar\omega$ is the energy of the incoming photons and n the refractive index of the material.

1.2 Importance

The 2PA has attracted significant interest both from practical and fundamental research point of view.[11] From the practical aspect 2PA enables a wide range of technological applications in many disparate fields. From the side of the fundamental research, 2PA is a powerful spectroscopic tool to probe molecular properties which can be complementary to the linear absorption spectroscopy.[12-14]

1.2.1 Viewpoint of Technological Applications

Numerous optical applications exploit two main advantages of using two-photon excitation over conventional one-photon excitation. The first results from the fact that the 2PA coefficient depends on the square of the intensity of the light beam used for excitation (as indicated in equation (1–1)). This intensity dependence provides spatial control of optical absorption as the excitation is confined to the perifocal region of the beam.[6] A numerical example, as addressed by Webb and co-workers,[15] indicates that the effective two-photon excitation volume for a 1.2 NA lens at 900 nm is 0.113 μm^3 (femtolitre scale). The second major advantage is that the individual energy of the two absorbed photons is half the energy needed to promote the molecule to an excited state of the corresponding linear transition. Hence, 2PA has attracted significant interest in many different fields, such as biomedical imaging, photodynamic therapy, microfabrication, and others.[16-18]

Excitation microscopy and photodynamic therapy

Two-photon excitation microscopy and photodynamic therapy are two characteristic applications where the 2PA mechanism offers a number of advantages over the conventional 1PA excitation. Excitation microscopy is a fluorescence-imaging technique that can be used for cell imaging of thick biological specimens. In principle, fluorescence is created through excitation of a fluorophore, which serves as a marker that is used due to its highly sensitive and distinct absorption and emission properties.[19] As presented in Figure 1-2, imaging can be achieved by filtering out the excitation light

without blocking the emitted fluorescence.[20] The spatial control of excitation provided by 2PA has led to high (effective) resolution and high-contrast imaging. In conventional one-photon excitation microscopy, the incident light can be absorbed by fluorophores anywhere in the specimen. In contrast, two-photon excitation is induced only in the central area of the focused beam where high power threshold can be reached. The near-infrared wavelengths associated with 2PA is another advantage, because of its lower sensitivity to scattering in the sample and the absorption of tissues is much lower in this optical window. This low-energy wavelength range, which is also called therapeutic optical window (600 – 1350 nm), has its maximum depth of penetration in biological tissues and causes minimum photochemical damage in biological samples.[21-24]

Being motivated by this context, two-photon excitation became a powerful tool for many medical applications with photodynamic therapy being one of the most used. Photodynamic therapy is a clinical treatment for tumours and other diseases that uses photosensitizers and light. When the photosensitizer is excited by light irradiation to a singlet state, through intersystem crossing, the excitation of a triplet excited state is achieved. The latter interacts with the oxygen and generates singlet oxygen ($^1O_2$) which induces apoptotic cancer cells death.[25-27] Therefore, using two-photon induced excitation in photodynamic therapy offers treatment to a deeper-layer cancer with higher selectivity compared to its one-photon counterpart.[28,29]

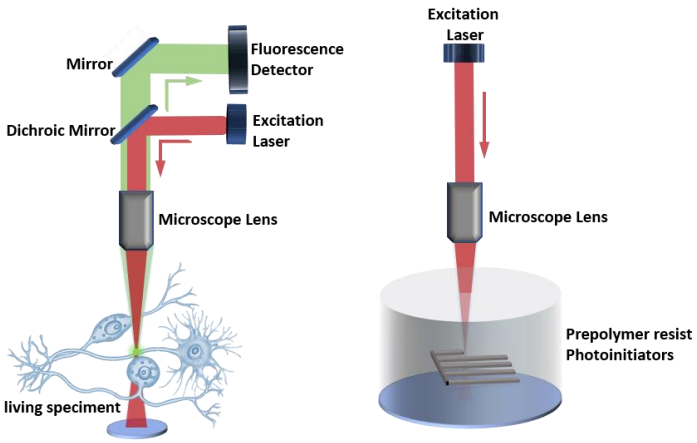

Figure 1-2: Schematic principles of two-photon excitation microscopy (left) and two-photon 3D-microfabrication (right).

Micro- and nano- fabrications

Two-photon excitation is widely used for potential technological applications including 3D-microfabrication and photolithography.[30] A prepolymer resist[II] containing photo-initiators[III], can be

[II] Resist is a light sensitive material which can exist in two types: The negative tone resists in which the polymerization occurs in the region that is exposed. The positive tone resists that behave in the opposite manner upon light irradiation, changes the chemical structure so that it becomes more soluble.

[III] Photo-initiators are molecules that produce reactive species when exposed to radiation and these then react with monomers (or oligomers) to initiate polymer chain growth. Thus, photo-initiators play an important role in the photopolymerization prosses.

excited by monochromatic light and polymerization process takes place in the region of the light exposure.[31] After illumination of the desired structures inside the photoresist volume and the nonilluminated regions can be separated by the elution and thus the polymerized material remains in the prescribed 3D form.[32] A promising 3D-micro and -nano fabrication method is based on two-photon polymerization.[33] As presented in Figure 1-2, the laser beam can be focused deeply in the photoresist volume and the high photon density is created in the focus spot and thus induces two-photon excitation. By controlling the laser beam properties, this localization of 2PA leads to a resolution beyond the diffraction limit, allowing exposure of patterns on the scale of a few nanometres.[34]

This investigation has been progressively employed in the construction of high storage capacity in optical data storages by two-photon lithography, which offers the possibility to record multiple data layers in one disc.[35] This technology enables spatial selective mapping and high-density recording where the data capacity of a disc (120 mm diameter and 10 mm thick) may exceed 200 GB.[36]

1.2.2 Viewpoint of Fundamental Research

Group theory can be used to investigate the way in which symmetry considerations influence the nonlinear absorption such as 2PA. By using point groups, we can determine the possible electronic state accessible by 2PA and gain a deeper understanding of their nature, and therefore generally providing relevant information about optical properties of chemical compounds.[37]

For compounds with symmetry possessing a center of inversion (centrosymmetric), two-photon transition processes between electronic states of the same symmetry are allowed, whereas one-photon transition processes are forbidden.[38] On the other hand, for compounds with no an inversion center (non-centrosymmetric), the one-photon allowed states are also accessible by two-photon transition processes.[39,40]

When a molecule absorbs light, it may be excited from the ground electronic state S_0 with wavefunction ψ_0 to a higher energetically excited state S_f with the corresponding wavefunction ψ_f. The oscillating electric field of the electromagnetic radiation interacts with the electrical charges resulting in a redistribution of the electron density inducing a transition dipole moment μ_{0f} where the transition $S_f \leftarrow S_o$ can be expressed as follows:

$$\mu_{0f} = \int_{-\infty}^{\infty} \psi_f^* \, \hat{\mu} \, \psi_0 \, dr^3 \qquad (1\text{–}5)$$

The integral runs over the coordinates of all electrons and $\hat{\mu}$ is the electronic dipole operator.[41] According to Laporte rule, the transition is allowed if the transition moment integral contains a totally symmetric representation and thus does not vanish. Therefore, assuming a totally symmetric ground state (abbreviated *g* from the German word for even, *gerade*), the final excited state must be unsymmetrical (abbreviated *u* from the German word for odd *ungerade*).

We assumed that the 2PA transition happens in a two-step procedure, where the time-dependent intermediate (virtual) state may be considered as a *u*-state.[42] Then the final state must be a *g*-state, and thus the transition is hereby allowed. If the molecule possesses no center of symmetry, the states cannot be classified as *g* or *u*. Thus, all excited states may be both one- and two-photon allowed. In summary, 2PA can be a powerful spectroscopic tool in combination with the linear absorption spectroscopy. Since the 2PA process is governed by different quantum mechanical rules in molecules that possess an inversion center, the information is complementary to what is obtained from linear spectroscopy. Even in the case when the molecules lacks an inversion center, the same bands should appear in both one- and two-photon absorption spectra, although with different relative intensities, a fact which also provides useful information.[43]

1.3 2PA Spectroscopy

Over the years, several experimental techniques have been proposed to measure the 2PA spectra of organic materials and to determine their 2PA cross section. These experimental techniques can be classified into two types, according to which physical quantity is measured.[44] The direct techniques are based on the measurement of the absorption by the organic material, the indirect techniques on a measurement of a quantity, which is one of the effect of 2PA process, such as induced fluorescence or phosphorescence.[45,46] A third category which is not widely used in the field of 2PA spectroscopy is the wave mixing techniques.[47,48] Wave mixing techniques can be advantageous to measure nonlinear optical parameters besides the 2PA cross section, such as the real and imaginary parts of the third-order susceptibility $\chi^{(3)}$.[49] The indirect experimental techniques can be further categorized as absolute and relative methods. In an absolute experimental measurement, the 2PA cross section is obtained by accurate determination of a series of parameters that are characteristic of the investigated material and the optical experimental setup. On the other hand, in relative methods the 2PA cross section of the sample is determined relative to a secondary reference standard, which has well-characterized absolute 2PA spectra.[50]

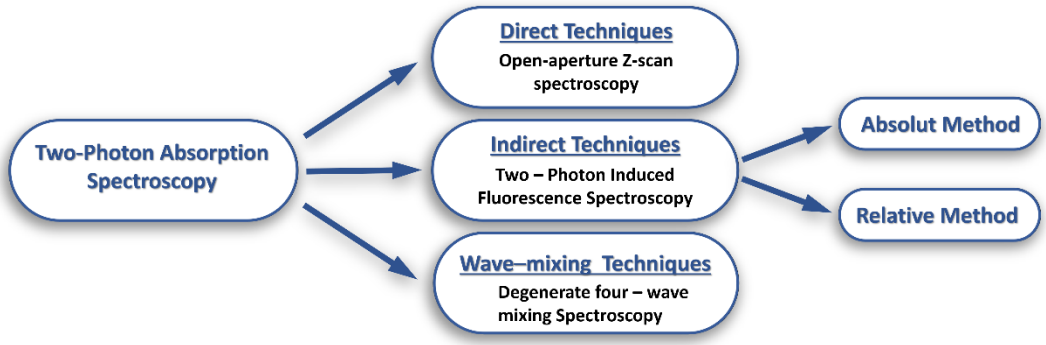

Figure 1-3: Schematic summary of the experimental techniques that are commonly employed to study the 2PA properties of materials.

The classification of the experimental techniques is depicted in Figure 1-3 by giving examples of the established experimental approaches that aim to determine the 2PA spectra of materials. With these techniques, a plethora of spectroscopic information on an appreciable number of molecular compounds has been obtained.

1.3.1 Direct Experimental Techniques

As mentioned before, the direct techniques are based on the measurement of the nonlinear absorption of a sample. As a 2PA process is characterized by a decrease in the transmittance of a sample, the 2PA cross section can be obtained by monitoring these intensity changes when the incident light intensity varies. This can be performed by varying the pulse energy for a given spot size (*e.g.* nonlinear transmission experiment) or the spot size for given pulse energy (*e.g.* Z-scan experiment).[50,51]

Open-aperture Z-scan techniques have been extensively used for determination of nonlinear absorption coefficients and therefore the absorption cross sections of a host of materials. By moving a thin sample mounted on a motorized linear translation stage along the propagation direction (z-axis) of a focused laser beam, the photon flux varies. The transmitted power through the sample is measured as a function of *z*-position of the sample. The resulting transmittance function for a given excitation wavelength has a characteristic shape; where the transmittance is 1 when the *z*-position of the sample is far from the focus of the beam, and as it moves closer to the focus, the transmittance decreases to a minimum value at the focus. As the sample passes through the focus and is moved away in the opposite direction, this trend is reversed. Therefore, by fitting the normalized energy transmittance function to the transmission data obtained from the open-aperture Z-scan measurement, the 2PA coefficient β and consequently the 2PA cross section $\sigma^{(2PA)}$ (see equation (1–2)) may be determined. One major drawback of this method is the difficulty to determine the physical mechanism behind the result, as it bears sensitivity to all types of nonlinear mechanisms such as excited state absorption. Nevertheless, it is a very powerful straightforward-conceptual technique especially for non-fluorescent molecules.

1.3.2 Indirect Experimental Techniques

The indirect experimental techniques are based on the secondary effect of the 2PA process, the most commonly used is the two-photon induced fluorescence (2PIF). By the 2PA a molecule can be promoted to a higher energetically excited state, and after internal conversion to S_1, fluorescence emission is one of the possible outcomes of de-excitation processes to the ground state. Thus, by employing the 2PIF technique, the 2PA cross section may be determined by monitoring the two-photon induced fluorescence signal and so it is possible to obtain the 2PA spectra via an absolute or relative method.

Absolute method

In order to gain insight into the 2PIF measurements, it is essential to examine the relationship between the experimentally measured fluorescence and excitation photon flux. In general, the fluorescence photon flux $F(\tilde{\nu}_{em})$, which is recorded by a fluorescence experimental technique in unit time, may be expressed as:

$$F = N_0\, \varphi_{fl}\, n_{fl} \tag{1–6}$$

where N_0 is the number of molecules which take place in the excitation event and $\varphi_{fl}(\tilde{\nu}_{em})$ is the fluorescence quantum yield, which is the ratio of the radiative decay rate to the total decay rate of the first excited state. $n_{fl}(\tilde{\nu}_{em})$ is the detection efficiency that accounts for the experimental optical setup collection efficiency at the emission energies and depends on several parameters, such as the dispersion of the lens (used for the emission collection), the detector response, the cone angle imaged by the detector, *etc*. In a 2PIF measurement, the average fluorescence signal within an integration time T [in s] is measured, and since usually the excitation source is a pulsed laser with repetition rate f [in Hz], the two-photon induced fluorescence flux $F^{(2PA)}$ is given by the equation (1 – 7).

$$F^{(2PA)} = N^{(2PA)}(Tf)\varphi_{fl}\, n_{fl} \tag{1–7}$$

In order to obtain the molecular 2PA cross section $\sigma^{(2PA)}$, we write the expression for the number of molecules $N^{(2PA)}$, excited by the 2PA process at the illuminated sample volume V ($\vec{r}$ = x, y, z) during each pulse, as indicated in Appendix 8.1.1:[52]

$$N^{(2PA)} = \frac{1}{2} C\, L\, \sigma^{(2PA)} \iint_{V,t} F_L^2\; dV\, dt \tag{1–8}$$

Here, the factor ½ reflects the fact that the fluorescence is induced by the absorption of two photons by a molecule. C is the molecular concentration, which we can assume to be constant at the illuminated volume in time t, L is the thickness of the sample and $F_L(\vec{r},t)$ describes the spatial and temporal distribution of the laser incident photon flux.[46] Let us suppose that the sample is excited by a periodic train of pulses with time width[IV] τ and a Gaussian profile (Δx and Δy spatial beam width[V]) as it propagates along its axial direction (z-axis).[53] Therefore, the corresponding incident photon intensity $I_L(\vec{r},t)$ with peak intensity $I_{0,L}$ for a given energy $\hbar\omega_L$ can be expressed as:

[IV] τ is the laser beam pulse temporal width which is measured at full width at half maximum (FWHM) of the photon flux versus time.

[V] Δx and Δy are the laser beam waist (w_x and w_y) at FWHM on x- and y-axis, respectively. Thus, $\Delta x = w_x\sqrt{2\ln(2)}$ and $\Delta y = w_y\sqrt{2\ln(2)}$.

$$I_{\mathrm{L}} = \frac{F_{\mathrm{L}}}{\hbar\omega_{\mathrm{L}}} = I_{o,\mathrm{L}}\left[e^{-4\ln 2\left(t^2/\tau^2\right)}\right]\left[e^{-4\ln 2\left(x^2/\Delta x^2\right)}\, e^{-4\ln 2\left(y^2/\Delta y^2\right)}\right] \tag{1–9}$$

The quantity enclosed in the first bracket accounts for the temporal profile of the Gaussian excitation laser beam, while the quantity inside the second bracket stands for the spatial profile of the beam. When substituting equation (1–9) into the integral in equation (1–8) the two-photon induced fluorescence photon flux (equation (1–7)) becomes:

$$F^{(2\mathrm{PA})} = \frac{1}{2} C\, L\, \sigma^{2\mathrm{PA}} \frac{I_{o,\mathrm{L}}^2}{(\hbar\omega_{\mathrm{L}})^2}\, (Tf)\left(\frac{1}{8}\left(\frac{\pi}{\ln 2}\right)^{\frac{3}{2}} \tau\Delta x\, \Delta y\right)[\,\varphi_{\mathrm{fl}}\, n_{\mathrm{fl}}] \tag{1–10}$$

Note that the incident photon intensity of the laser beam is an experimentally measurable quantity by using a detector (*e.g.* power meter). The relation between incident pulsed laser intensity $I_{0,\mathrm{L}}$ [in W/m^2] and incident laser power P_{L} [in W] follows the conversion:

$$I_{o,L} = 8\left(\frac{\ln 2}{\pi}\right)^{\frac{3}{2}} \frac{1}{f\tau} \frac{P_{\mathrm{L}}}{\Delta x\, \Delta y} \tag{1–11}$$

Substitute this into equation (1–10), we obtain the two-photon induced fluorescence signal $F^{(2\mathrm{PA})}$ which is detected in a typical 2PIF measurement, and therefore the 2PA cross section can be written as,

$$\sigma^{(2\mathrm{PA})} = \frac{1}{\sqrt{2}}\left(\frac{\pi}{\ln 2}\right)^{\frac{3}{2}} \frac{(\hbar\omega_{\mathrm{L}})^2}{TC\, L}\, (f\tau\Delta x\, \Delta y)\left(\frac{F^{(2\mathrm{PA})}}{{P_{\mathrm{L}}}^2}\right)\left[\frac{1}{\varphi_{\mathrm{fl}}\, n_{\mathrm{fl}}}\right] \tag{1–12}$$

Obviously, the accurate determination of the molecular 2PA cross section requires precise characterization of the excitation laser pulse properties namely temporal (τ) and spatial beam profile (Δx, Δy) for a given excitation energy $\hbar\omega_{\mathrm{L}}$.

Relative method

In the relative method, the latter tedious characterization can be avoided by calibration of the 2PA cross section measurement through the use of a reference compound with well-characterized 2PA spectra. With this method, the determination of the unknown 2PA cross section can be obtained by comparing the two-photon induced fluorescence signal to that of the reference compound, and thus automatically overcomes the necessity of characterizing the temporal and spatial beam profile of the excitation pulse. Moreover, the optimal choice of the reference compound automatically corrects the variations of the detection efficiency term $n_{\mathrm{fl}}(\tilde{\nu}_{\mathrm{em}})$, as will be shown below in Chapter 3.

Thereby, if the excitation beam parameters and the fluorescence collection conditions are the same for both unknown sample S and the reference standard R, then according to the equation (1–12), the

2PA cross section of the sample $\sigma_S^{2\mathrm{PA}}$ may be expressed as a function of the known reference 2PA cross section $\sigma_\mathrm{R}^{2\mathrm{PA}}$:

$$\left[\sigma^{2\mathrm{PA}}(\tilde{\nu}_{\mathrm{ex.}})\right]_\mathrm{S} = \left[\sigma^{2\mathrm{PA}}\left(\tilde{\nu}_{\mathrm{ex.}}\right)\right]_\mathrm{R} \frac{\left[\, q_{\mathrm{fl}}(\tilde{\nu}_{\mathrm{em.}}) n_{\mathrm{fl}}(\tilde{\nu}_{\mathrm{em.}})\right]_\mathrm{R}}{\left[\, q_{\mathrm{fl}}(\tilde{\nu}_{\mathrm{em.}}) n_{\mathrm{fl}}(\tilde{\nu}_{\mathrm{em.}})\right]_\mathrm{S}} \left(\frac{\mathrm{C}_R}{\mathrm{C}_S}\right) \frac{(F_{2\mathrm{PA}})_S}{(F_{2\mathrm{PA}})_R} \tag{1–13}$$

where the quantities with index S refer to the investigated sample compound and those with index R refer to the reference standard compound. The 2PIF relative method is explained and a detailed application of the latter is given in this thesis.

2 Scope of the Work

A powerful concept in physical chemistry is the so-called, “structure-property relationship”, which investigates the relationships among material optical properties and material chemical structure. This approach is based on the optimization of the design and synthesis of novel organic materials in which their optical properties can be tuned to fit a specific technological application (Figure 2-1). The structure-property relations governing 2PA have received increasing attention over the recent years and have been studied both experimentally and theoretically. Therefore, we designed and constructed a two-photon induced fluorescence spectroscopic apparatus in order to examine the 2PA properties of newly synthesised organic molecules. Once this was accomplished, a detailed experimental characterization combined with quantum-chemical computations and theoretical modelling was used as a tool to probe information for the structure-property relationship. The aim of this work is to provide molecular design strategies for materials, which satisfy a certain set of requirements for nonlinear optical applications. Moreover, this study has also been of fundamental scientific interest for the study of basic properties of materials that exhibit 2PA and matter-light interaction.

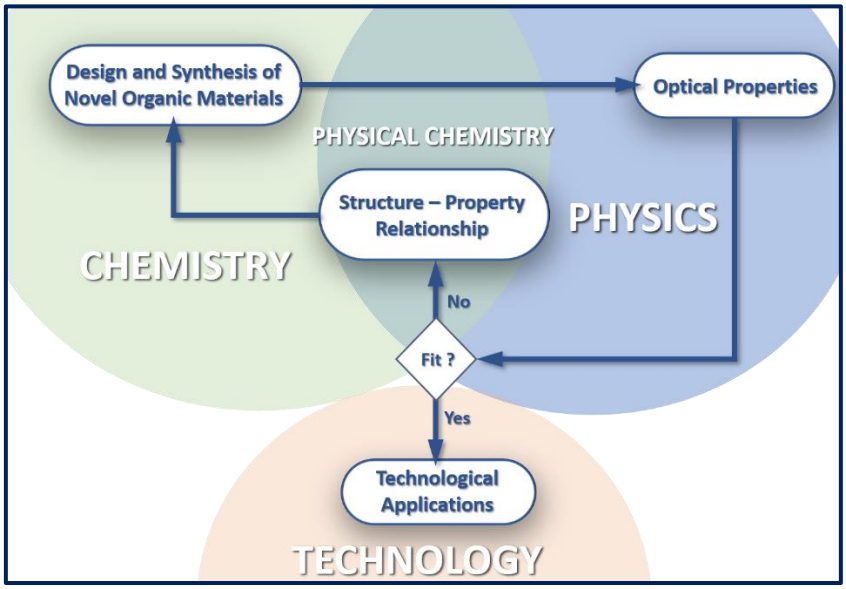

Figure 2-1: Schematic overview of our research approach. In this dissertation this approach refers to the nonlinear spectroscopic properties of organic compounds.

In this contribution, the present thesis is organized as follows: The introduction part, *Chapter 1*, presents the main concept of the 2PA phenomenon and at the same time establishes the theoretical basis of the experimental apparatus. The current *Chapter 2* summarizes the motivation and the objectives of this work.

Then, *Chapter 3* describes the development of the experimental apparatus, providing an experimental protocol. A detailed description of the 2PIF set-up to measure the molecular 2PA cross section which is based on the indirect fluorescence excitation method is presented.

Chapter 4 gives a simplistic picture of the state-of-the-art quantum chemical treatment of the nonlinear optical processes of 2PA, which enables a comprehensive comparison of the theoretical and experimental obtained data, providing a unified view of the nonlinear properties of matter. Moreover, it introduces the polarization-depended 2PA spectroscopy, in order to gain a deeper understanding of the photophysical properties of materials that are not accessible using conversional one- and two-photon absorption spectroscopy, providing information about the nature of the excited states of randomly oriented molecules.

Chapter 5 presents the effects of the molecular structure of several newly synthesised organic compounds on the 2PA spectra and the magnitude of two-photon absorptivity. More specifically, our investigations have been mainly focused on the fundamental understanding of exciton coupling theory, in the special case of nonlinear optical interaction. The studied compounds were gratefully provided by a number of collaboration partners who are named in the respective sections.

An outlook of possible future research directions and technological application proposals, according to some our preliminary studies, is also given in *Chapter 6*. Finally, *Chapter 7* provides a summary of the work done, together with conclusions. It should be noticed that a substantial amount of information and details of the experiments and theory are placed in attached Appendices in *Chapter 8*.

3 Design and Construction of the 2PIF Experimental Apparatus

For the study of the nonlinear optical properties of organic materials, the 2PIF experimental technique based on the relative method was selected. To this end, a 2PIF experimental set-up was designed and developed, which is being utilized to perform 2PA cross section measurements of organic fluorescent compounds in solution. This technique was chosen for being sensitive to 2PA in a broad excitation wavelength range (550 – 1600 nm).

Principles of the 2PIF technique were first introduced by Xu and Webb[54] in 1996, while measurements based on the relative method were first reported by the same group in 1998 by Albota *et al*.[55] Subsequently, several variants have been developed with major improvements in 2008 by Makarov *et* al.[56] The present chapter describes the design and development of the 2PIF experimental apparatus providing a complete experimental protocol. A schematic representation of the 2PIF experimental setup is shown in Figure 3-1, where the red and green pathways stand for the fundamental excitation beam and emission signal path, respectively.

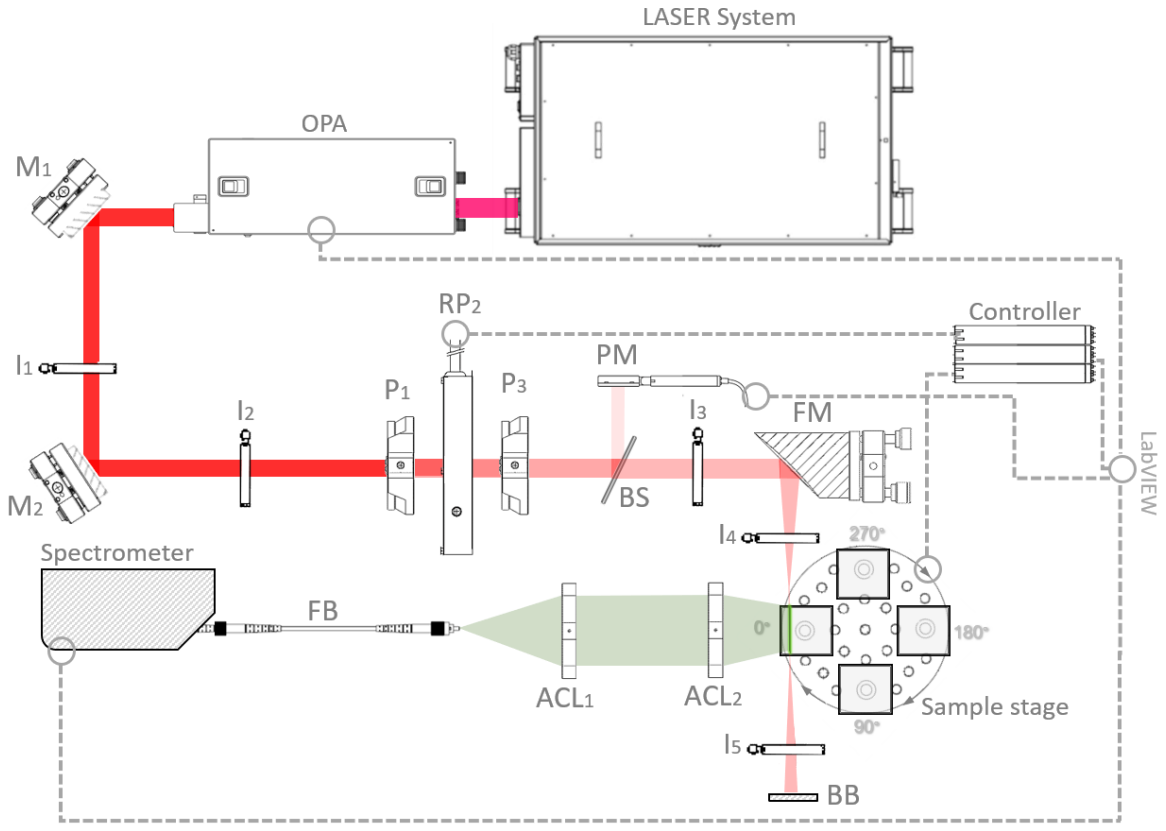

Figure 3-1: Schematic top view of the 2PIF experimental apparatus (not to scale) including the fundamental excitation beam (red) and the fluorescence emission (green). **I_2** - **I_5** – irises, **M_1** and **M_2** – mirrors, **P_1**, **RP_2** and **P_3** – polarizers, **BS** – beam splitter, **PM** – power meter, **FM** – focusing mirror, **BB** – beam blocker, **ACL_1** and **ACL_2** – a pair of achromatic aspherical lenses, **FB** – customized fiber bundle. The dotted lines indicate the connection with the LabVIEW software.

3.1 Experimental Apparatus

For the sake of convenience, the Π–shape apparatus can be divided into three arms: the first arm is responsible for the excitation beam configuration, the second is devoted to the excitation of the sample and the third for the fluorescence collection.

3.1.1 Excitation Beam Configuration Arm

In order to generate excitation light with suitable conditions to produce two-photon induced fluorescence emission, an 1 KHz pulse repetition rate amplified Ti: sapphire laser Solstice from Newport Spectra-Physics was used. The amplifier output delivering 100 fs pulses at 800 nm and 70% of its energy seeds a tuneable computer-driven optical parametric amplifier (TOPAS-C, Light Conversion) which produces the excitation pulses in the range of 290 – 2600 nm. The fundamental laser spectrum was measured with CCD spectrometers (USB4000 for the spectral region 200 – 1000 nm and NIRQUEST for 900 – 2600 nm, Ocean Optics). The TOPAS-C output beam is collimated, and the polarization is vertically or horizontally oriented depending on the spectral region of the emitted wavelength. A series of irises (**I_1** and **I_2**) and mirrors (**M_1** and **M_2**) were used to align the excitation beam to the entrance of the 2PIF experimental apparatus as indicated in Figure 3-1.

A combination of three thin broadband wavelength polarizers (ColorPol®IR 1300 BC5, CODIXX AG) were used to control the intensity and polarization plane direction of the excitation laser beam[I]. The three thin polarizers are placed in row where the second one was positioned in a mechanical rotational mount (PR50PP, Newport) as shown in Figure 3-2.

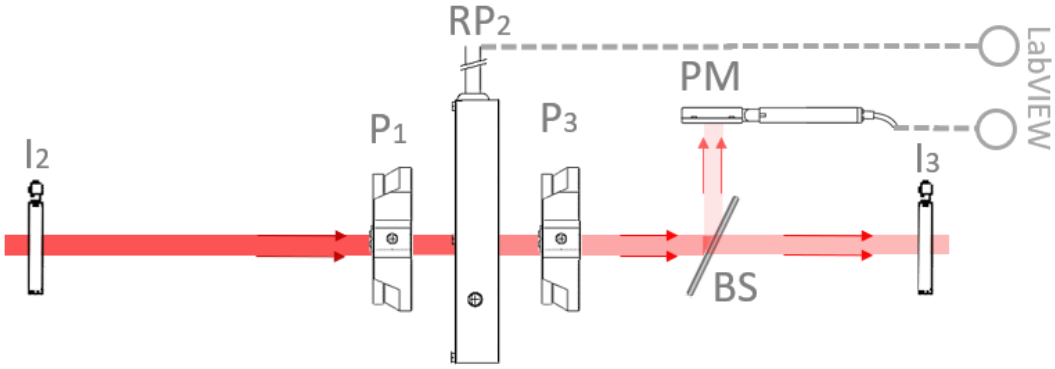

Figure 3-2: Schematic representation of the excitation beam configuration arm; **I_2** and **I_3** – irises, **P_1** and **P_3** – polarizers, **RP_2** – polarizer in a mechanical rotational mount, **PM** – power meter and **BS** – beam splitter. The dotted lines indicate the connection with the LabVIEW software.

[I] The idea came from the Paul Dirac explanation of quantum superposition of states (the so-called "Dirac Paradox") and the Malus' law. The Dirac Paradox states that, as a light passes through a polarizer, its wavefunction can be regarded as in a mixed state, a superposition of horizontal and vertical states. This is being illustrates by the three-polarizer experiment. Introducing an oblique polarizer between two crossed polarizers, which block all light, allows photons to pass through. [57]

The first polarizer, **P_1**, was orientated at 45° in order to provide the same polarization input beam across the different spectral regions from TOPAS-C. The last polarizer **P_3** was oriented at 90°, in order to ensure a vertically polarized excitation beam.[52] Finally, the second polarizer **RP_2** was rotated by 1°/sec and in this way the excitation power varies upon each acquisition. The latter was obtained by applying the Malus' law[II] to the three polarizers according to equation (3–1) where I_{ex} is the transmitted intensity through the third polarizer **P_3**, I_0 is the input intensity which incident to the first polarizer **P_1** and ϑ is the angle (in deg.) of the second polarizer **RP_2**.

$$I_{ex} = \frac{I_0}{2}[\cos^2(45 - \vartheta)\cos^2(45 + \vartheta)] \quad (3–1)$$

The relative average power of the excitation beam at the sample was monitored by the reflective portion of the incident beam to a photodiode sensor **PM** (PD300-UV for the spectral range 200 – 1100 nm and PD300-IR for 700 – 800 nm, Ophir) coupled to an optical power meter (StartLite, Ophir).

3.1.2 Sample Excitation Arm

The laser beam was thereafter slightly focused by an 90° off-axis silver protected parabolic mirror **PM** (Thorlabs, MPD169). The parabolic mirror with an effective focal length of 152.4 mm achromatically focuses the collimated beam *ca.* 10 mm in front of the sample. This provides an almost constant excitation beam cross section passing through the 10 mm long cuvette and at about a *ca.* 2 mm distance through the sample cuvette wall, where the fluorescence is collected. In this way the effect of light scattering by the sample solution is minimized.

The sample solution is filled in a square 10 mm length UV fused quartz glass cuvette and is mounted on a cuvette holder in a precision rotation stage **RS** (Newport, URS75BPP). This stage has the capacity of four cuvettes as shown in Figure 3-3, ensuring that excitation and emission collection is carried out under the same conditions for these four positions on the stage. The stage carries a cuvette with pure solvent (at position 0°), a cuvette with the reference compound (at position 90°) and a cuvette with the under-study sample (at position 180°). There is also the possibility to study a second sample at the fourth position (at position 270°).

The irises **I_4** and **I_5** were used to align the excitation beam such that it passes through the same pathway inside each cuvette for all the excitation wavelengths. The excitation beam is blocked by a beam blocker **BB** after the sample stage.

[II] According to the Malus' law,[58,59] when a plane polarized light incidents on a polarizer the intensity of the light transmitted is directly proportional to the square of the cosine of the angle between the polarization axis of the polarizer and the polarization axis of the incident light.

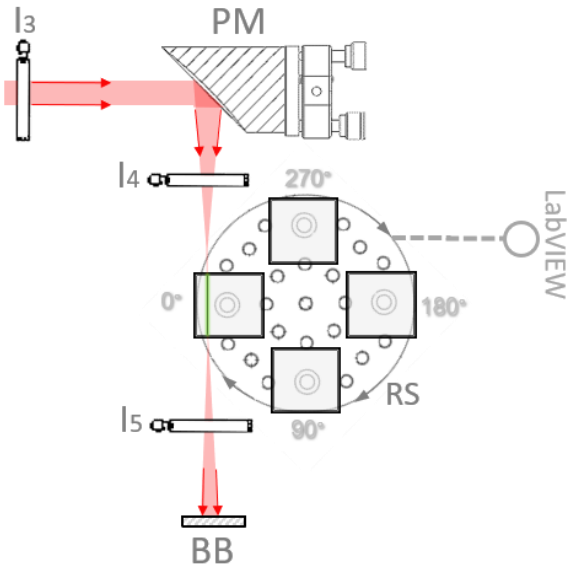

Figure 3-3: Schematic representation of the sample excitation arm; **I_3**, **I_4** and **I_5** – irises, **PM** – 90° off-axis silver protected parabolic mirror, **RS** – precision rotation stage, **BB** – beam blocker. The dotted lines indicate the connection with the LabVIEW software.

3.1.3 Fluorescence Collection Arm

Fluorescence emission takes place isotopically in all directions from every point along the light path. The fluorescence signal is collected at 90° in respect to the laser beam direction by a pair of achromatic aspherical lenses **ACL_1** and **ACL_2** (APAC13 and APAC14, Newport). These lenses, by minimizing the colour and spherical aberration, focus the horizontally elongated image of fluorescence on the entrance of a customized fiber bundle **FB** (BFA105HS02, Thorlabs). The fiber bundle contains 7 fibers arranged in a line configuration at both ends and is responsible for coupling the fluorescence signal into the CCD spectrometer (QE65000, Ocean Optics). The QE65000 spectrometer is a remarkably sensitive spectrometer in the range 200 – 1100 nm, with high quantum efficiency and signal-to-noise ratio due to its cooled (−15 °C) Hamamatsu detector.

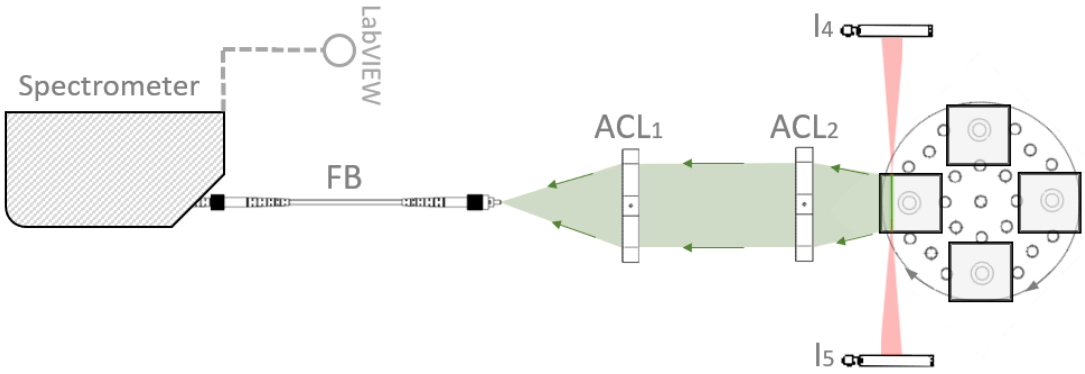

Figure 3-4: Schematic representation of the fluorescence collection arm; **I_4** and **I_5** – irises, **ACL_1** and **ACL_2** – a pair of achromatic aspherical lenses, **FB** – customized fiber bundle and a spectrometer. The dotted lines indicate the connection with the LabVIEW software.

The TOPAS-C output tuning, the excitation power and the acquisition of the fluorescence spectrum, were accomplished through the LabVIEW[III] software.[60,61] The mechanical parts, that are the rotational mount of the second polarizer RP_2 and the precision rotation stage are connected with a motion controller (ESP301, Newport), which is also controlled via LabVIEW software. Appendix 8.3 contains the interface windows between user and the program of the 2PIF apparatus.

3.2 Experimental Procedures

3.2.1 Sample Preparation

All samples were dissolved in pure spectroscopic solvents and all measurements were performed in 10 mm standard quartz cuvettes. The molecular concentration used in the linear absorption and 2PA measurements was in the range 10^{-5} – 10^{-6} M aiming a concentration independent behaviour and the aggregation of the sample could be excluded to prevent self-absorption. Linear absorption spectra were obtained with double beam UV-vis-NIR spectrometers (see Appendix 8.2).

A set of commercially available dyes with well-characterized 2PA spectra have been reported in the literature at selected wavelengths and can be used as a reference for the 2PIF relative experimental technique. The 2PA cross section of these organic compounds, obtained by the absolute 2PIF method, were selected such that their 2PA spans the range 550 – 1600 nm. The selection criteria for a reference compound regarding the 2PA spectra determination are: i) The linear absorption band of reference and sample should partially overlap and ii) the maximum fluorescence peak of both compounds should be as close as possible to each other. iii) Reference and sample compounds must exhibit two-photon absorptivity in the same excitation energy region. In the present dissertation, Rhodamine 6G and Coumarin 485 in methanol, Fluorescein in water pH 11, Coumarin 153 in toluene and DMSO, Perylene in Dichloromethane as well as LDS698 and Styryl 9M in Chloroform were used as reference compounds according to previous works by Makarov *et al.*[62,63] and de Reguardati *et al*.[64,65]

3.2.2 Data Acquisitions

For a given excitation wavelength the measurement was performed by recording the fluorescence spectrum of the investigated compound while the incident excitation power is varied *i.e.* by rotating the second polarizer (**P_2**) by 1° per second. The same procedure is repeated for each cuvette by rotating the sample stage (**RS**) by 90°. For each laser excitation wavelength, a set of fluorescence

[III] LabVIEW is a graphical programming language released by National Instruments, which is liable for the instrumentation, automation control, data acquisition, making real-time embedded systems, as well as for analysing data.

spectra was recorded for each excitation power (as can be seen from the example in Figure 3-5) for the four cuvettes.

The excitation power and the fluorescence spectra were measured simultaneously with the appropriate integration time corresponding to the rotation and 50 acquisitions, while upon each acquisition the excitation energy was varied between 0.2 – 2 μJ ($\vartheta = 50° \rightarrow 0°$). The integration time and the excitation energy range are optional, and they can be defined from the operating LabVIEW program interface. The Figure 3-5 shows the part from of the 2PIF spectrometer interface program, which is designed to plot the recorded fluorescence spectra as function of the excitation power during the measurement, providing complete control of setting the parameters for the 2PIF measurement to the user (see also Appendix 8.3, Figure 8-5). The sets of the obtained experimental data were transferred in the data acquisition analysis LabVIEW program for the determination of the 2PA cross section spectra (Figure 8-6).

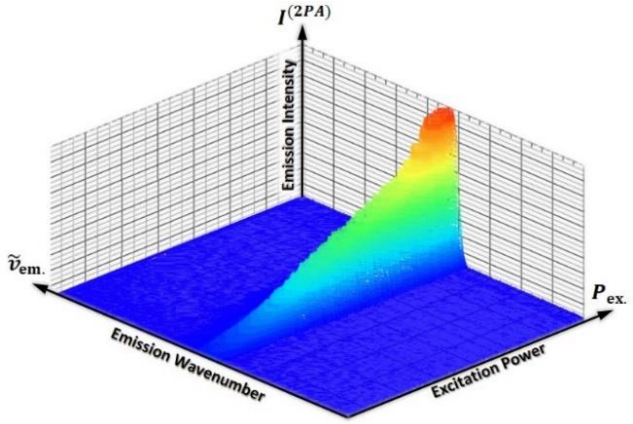

Figure 3-5: The real-time acquisition of the 2PIF spectra while varying the excitation power displayed using the interface program of the 2PIF apparatus. This is an example of 2PIF measurement for Rhodamine-6G in methanol solution at 11000 cm^{-1} excitation laser energy.

3.2.3 Two-Photon Induced Fluorescence Signals

As mentioned before, one major advantage of the 2PIF technique is that it is highly selective for the 2PA process. The 2PA process is verified by the quadratic dependency of the emission signal versus the excitation power. The collected fluorescence spectra are spectrally integrated over the interval of wavelengths between λ_{min} and λ_{max} set by the LabVIEW routine (see Appendix 8.3, Figure 8-6). The fluorescence intensity $I^{(2PA)}$ is measured by integrating the obtained emission spectra for an interval < 10 nm around the emission peak wavelength for each excitation power P_{ex}. By selecting a small spectral width around the emission maximum of reference and sample compounds, a stable and intense signal with reduced background is measured.

Two-photon excitation was verified by fitting the log-log plots of $I^{(2PA)}$ *vs.* P_{ex} with a linear function showing a slope of 2. Data ($I^{(2PA)}$, P_{ex}) which deviate from a slope value in the range 1.95 – 2.05 were

discarded.[IV] An example of this procedure is shown in Figure 3-6, where the black coloured data indicate the excitation power area where the fluorescence signal stems from two-photon excitation. The methodology described here ensures that the 2PA is the only nonlinear process taking place and the small wavelength interval of the fluorescence spectra ensures also that the detection efficiency $n_{fl}(\tilde{\nu}_{em})$ remains almost constant in the wavelength integration region. Any selection of the wavelengths set (λ_{min}, λ_{max}) results in just up to a relative standard deviation[V] of 6%. This indicates that precise experimental results are obtained as they are tightly clustered around the average value.

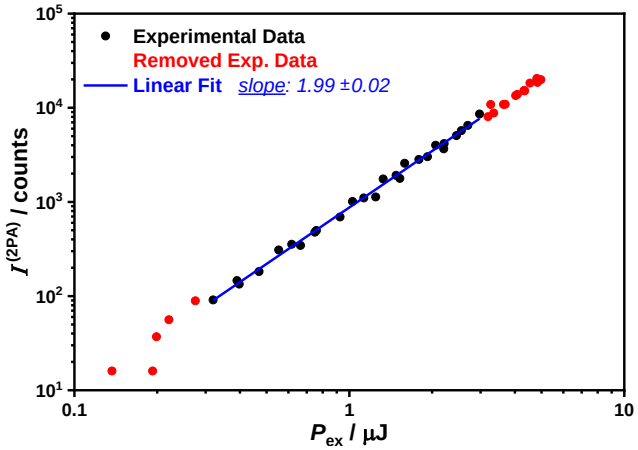

Figure 3-6: Example of the quadratic power dependence by a log-log linear fit of fluorescence Intensity $I^{(2PA)}$ versus the excitation power P_{ex}. This is an example of 2PIF measurement for Rhodamine 6G in methanol solution at 10000 cm^{-1} excitation laser energy. The rejected experimental data are coloured in red.

3.2.4 2PA Cross Section Determination

In the Introduction part, the theoretical framework of the relative method for the determination of the molecular 2PA cross section through the 2PIF spectroscopy was derived. The experimental methodology of the 2PIF spectroscopic apparatus is based on equation (1–11), which was used to determine the molecular 2PA cross section $\sigma^{(2PA)}(\tilde{\nu}_{ex})$. For convenience, the latter equation may be used by introducing the experimentally measurable quantities $\Phi(\tilde{\nu}_{em})$, $I^{(2PA)}(\tilde{\nu}_{em})$ and $P_{ex}(\tilde{\nu}_{ex})$:

$$\left[\sigma^{(2PA)}\right]_S = \left[\sigma^{(2PA)}\right]_R \left(\frac{\Phi_R}{\Phi_S}\right)\left(\frac{C_R}{C_S}\right)\frac{\left\langle\frac{I^{(2PA)}}{P_{ex}^2}\right\rangle_S}{\left\langle\frac{I^{(2PA)}}{P_{ex}^2}\right\rangle_R} \qquad (3\text{–}2)$$

[IV] The rejected experimental data could be due to a bad signal-to-noise ratio or caused by another type of nonlinear phenomenon such as three-photon absorption.

[V] Relative standard deviation (*RSD*) is defined as the ratio of the standard deviation σ to the absolute value of the mean $\bar{\mu}$, $RSD = \frac{\sigma}{|\bar{\mu}|} \times 100\%$.

where, the two-photon induced fluorescence photon flux $F^{(2PA)}$ was replaced by the fluorescence signal intensity $I^{(2PA)}$ which is recorded by the spectrometer. To provide increased accuracy, the term P_L^2 in equation (1–10) was used to normalize the fluorescence signal intensity by dividing the signal $I^{(2PA)}$ by the squared excitation power P_{ex}^2. The < > indicates averaging of the ratio of experimental data ($I^{(2PA)} / P_{ex}^2$). Thus, the 2PA cross section as a function of excitation energy $\sigma^{(2PA)}(\tilde{\nu}_{ex})$ can be determined using equation (3–2), where indices S and R denote the sample compound and reference compound, respectively. C is the concentration of the compounds and Φ is the fluorescence quantum efficiency.

3.2.5 Fluorescence Quantum Efficiency Ratio

The determination of the 2PA cross section through equation (3–2) requires the knowledge of the fluorescence quantum efficiency ratio (Φ_R / Φ_S) which is related to the ratio between the fluorescence quantum yields φ_{fl} of reference and sample as determined by the 2PIF apparatus. This implies that the 2PIF measurements are calibrated with respect to the reference compound`s emission characteristics. In this way, we reduce potential systematic errors and uncertainties because of mismatch in the wavelength calibration of different spectrometer detectors, different source correction functions etc.[65] Thereby, we also take into account the dependence of the detection efficiency at different wavelengths since the fluorescence quantum efficiency ratio comprises also the detection efficiency $n_{fl}(\tilde{\nu}_{em})$. The $n_{fl}(\tilde{\nu}_{em})$ value is generally not known[VI, 66], however it may be evaluated by measuring the amount of fluorescence emitted in the same system under one-photon excitation conditions.[65] This approach requires identical excitation conditions for both sample and reference compounds, as well as that one- and two-photon excitation incident beams pass through similarly exactly the exact same location in the cuvette.

Practically, as the standard procedure for the determination of fluorescence quantum yield $\varphi_{fl}(\tilde{\nu}_{em})$, a relative measurement of the efficiency of the conversion of absorbed light into emitted light of the sample S and the reference R was performed. In this concept, the ratio Φ_R / Φ_S represents the relative quantum efficiency, resulting from the equation for the fluorescence quantum yield calculation.[67]

$$\frac{\Phi_R}{\Phi_S} = \frac{\left(\int_{\tilde{\nu}_{em}} I^{(1PA)}\, d\tilde{\nu}\right)_R}{\left(\int_{\tilde{\nu}_{em}} I^{(1PA)}\, d\tilde{\nu}\right)_S} \frac{\left(1 - 10^{-A(\tilde{\nu}_{ex})}\right)_S}{\left(1 - 10^{-A(\tilde{\nu}_{ex})}\right)_R} \frac{(n^2)_R}{(n^2)_S} \qquad (3–3)$$

As indicated in the latter expression (3–3), the one-photon induced fluorescence signal $I^{(1PA)}(\tilde{\nu}_{em})$ is required for reference and sample compound. By tuning the output of TOPAS-C in the lower excitation

[VI] A method for generating the emission wavelength-dependent correction file is using a series of secondary emission standards, in which their spectra cover the emission wavelength range of the fluorescence based spectroscopic setup as addressed by J. A. Gardecki and M. Maroncelli.[46]

wavelengths, in which the sample and the reference display linear absorptivity, the one-photon induced fluorescence spectra was recorded. The one-photon excitation wavelength was chosen in the overlapping linear absorption band of the reference and the sample (see figure 3-7(a)). The optimal wavelength for one-photon excitation is where the linear absorbances $A(\tilde{\nu}_{ex})$, for the sample and the reference, are similar and the absorption spectrum of both compounds have an almost plateau-like region. The resulting one-photon induced fluorescence spectra (see figure 3-7(b)) was integrated over the same interval of wavelengths (λ_{min} and λ_{max}) as for the 2PA measurements mentioned earlier in the 3.2.3 section. Note that the shape of the one-photon and two-photon induced fluorescence spectra are identical, since both types of excitation result in fluorescence emitted only from the lowest excited state. Moreover, according to the Vavilov-Kasha´s rule[VII],[68] the fluorescence quantum yield under one- and two- photon excitation are equal.[69,70]

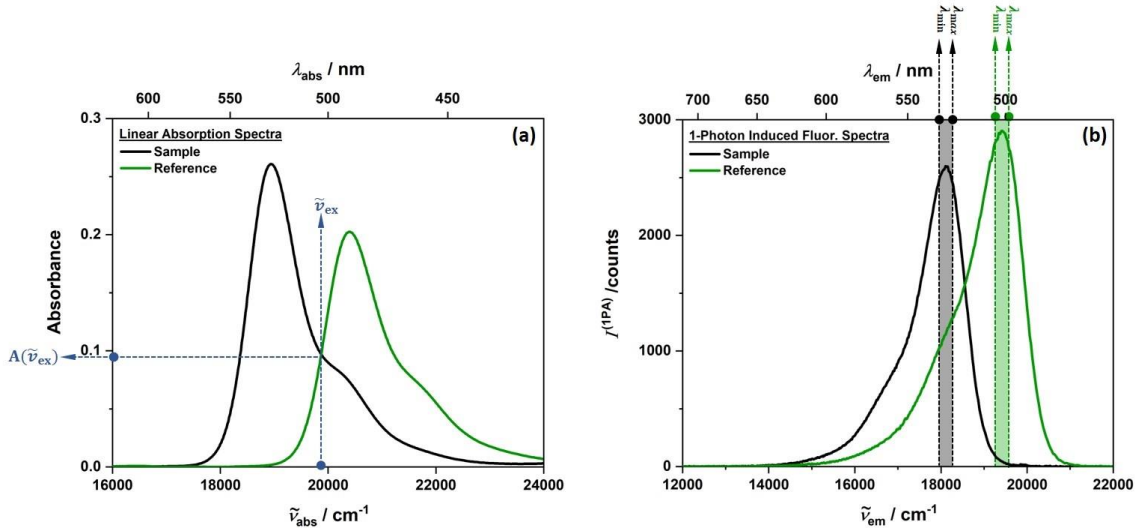

Figure 3-7: (a) Linear absorption spectra and (b) one-photon induced fluorescence spectra of the reference (green) and sample (black) compounds. This is an example of the $\Phi_R/\ \Phi_S$ ratio determination where Rhodamine-6G in methanol and Fluorescein in alkaline water were used as reference and sample compounds respectively.

To provide increased accuracy, the $\Phi_R/\ \Phi_S$ ratio was determined for different excitation wavelengths and different concentrations. The deviation of relative quantum efficiency obtained by this repeated procedure was smaller than 5%, which is sufficiently small. Due to the relative low concentration used in 2PA measurments, the refractive index *n* of the solution was assumed to be the same as that of the pure solvent.

[VII] An excitation to any electronic state S_n (n=1, 2, 3, …) will yield the same fluorescence spectrum as the emission occurs from the lowest excited state S_1. Thus, the properties of fluorescence are independent of the excitation energy.

3.3 Validation and Reliability

3.3.1 Validation of Excitation Conditions

For the purpose of validating the experimental excitation conditions in the 2PIF spectrometer, the examination whether two essential requirements/approximations are met is needed. In particular, by determinating the fractional change of excited state population and of the photon flux during a laser pulse, the validation of excitation regimes in the 2PIF measurments may be achieved. Thus, two essential quantities were obtained; the fraction of absorbed photons $\Delta p^{(2PA)}$ ($\cong p^{(2PA)} / p_0$) and the fraction of excited molecules $\Delta N^{(2PA)}$ ($\cong N^{(2PA)} / N_0$) per pulse by 2PA. Where $p^{(2PA)}$ and $N^{(2PA)}$ are the number of absorbed photons and excited molecules, respectively, per unit volume via 2PA during each pulse. Accordingly, p_0 and N_0 represent the total number of photons and molecules per unit volume in each pulse, respectively. Thus, the two fractional equations can be written as[50]

$$\text{Requirement (i): } \Delta p^{(2\text{PA})} \approx \sigma^{(2\text{PA})} N_0 F_L L \ll 1 \tag{3–4}$$

$$\text{Requirement (ii): } \Delta N^{(2\text{PA})} \approx \frac{1}{2} \sigma^{(2\text{PA})} \tau {F_L}^2 \ll 1 \tag{3–5}$$

where F_L is the excitation photon flux, L *is* the cuvette length that contains the sample solution and τ is the pulse duration. The derivation of the two fractional equation is presented in Appendix 8.1.1. In case that requirement (i) is not valid for a given set of experimental conditions, then the dependence of a measured signal on the square of the incident photons flux is not applicable. On the other hand, the fraction of molecules excited per pulse $\Delta N^{(2PA)}$ is equivalent to the saturation parameters. Thus, if requirement (ii) is valid for a given set of experimental conditions, the ground state of the system is far from being depleted during the pulse. Ground state depletion is one of the most common possible reasons for deviation from the 2PA process, besides stimulated emission and excited state absorption. It will be shown below, that both requirements (i) and (ii) are valid since our experimental set-up has been designed to fall in an excitation regime where both conditions are met. Firstly, let us calculate the photon flux F_L that is being employed in our experiments, where it may be more convenient to express it as a function of laser beam parameters,

$$F_{\mathrm{L}} = \frac{\lambda E}{\pi w_0^2 \tau hc} \tag{3–6}$$

where λ (800 nm) is the excitation wavelength, E is the average energy determined by dividing the average power P_L (1 mW) by the repetition rate f (1 KHz), w_0 (*ca.* 300 μm) is the beam spot size, τ (150 fs) is the pulse duration and hc (1.986 x 10^{-25} Jm) is Planck´s constant multiplied by the speed of light. According to the experimental conditions, a photon flux of 2.6 x 10^{31} photons cm^{-2} s^{-1} is

achieved. The Rhodamine 6G in methanol is chosen as example. Rhodamines are well known Xanthene dyes, which have been extensively used as reference standard dyes for calibration in the 2PIF techniques.[71,72] Based on the 2PA cross section and the experimental parameters presented above, the required excitation conditions can be estimated: $\Delta p^{(2PA)} = 7 \times 10^{-4}$ and $\Delta N^{(2PA)} = 2 \times 10^{-12}$, where the 2PA cross section of Rhodamine 6G in methanol is 90 GM at 800 nm.

3.3.2 Sources of Error

The reference standards, where their 2PA spectra have previously been accurately well-characterized, are vital in the relative 2PIF experimental technique. However, the experimental uncertainties in 2PA spectroscopy are still quite large leading to substantial error of the absolute 2PA cross section values. The experimental errors of the previously available 2PA cross sections of references vary from 30% by Webb, Xu and *co*-authors[46,52] (1996 and 1998), to *ca.* 18% Makarov *et al*.[62] (2008) to 8% Reguardati *et al.*[65] (2017). The reason for this error is most probably that the characterization of the excitation photon flux parameters is still prone to considerable experimental uncertainty.[VIII] However, the 2PA cross section experimental results reported by different research groups and/or using different techniques or setups are in a good quantitative agreement between them (within error margins ~ 10 %).

[VIII] Potential sources of errors in excitation photon flux determination of the 2PA cross section:
Makarov *et al*.:[73] pulse-to-pulse intensity variations ~ 10%, pulse duration determination ~ 5%, beam diameter measurement (for both Δx and Δy) ~ 4%. Reguardati *et al.*:[74] Pulse temporal intensity profile ~ 2%, Beam shape measurements ~ 7%.

4 Quantum-Chemical Treatment of 2PA Process

The perspective aims to better understand the structure-property relationship governing the 2PA processes in organic chromophores requires the use of theoretical approaches. In this Chapter, we illustrate the state-of-the-art methodology for the interpretation of experimental 2PA results and estimation of related quantities, which therefore may be used as design criteria to achieve sizeable values of 2PA cross section. In this context, it is useful to introduce approximations and accompanying computational techniques for explaining the experimental results and estimating intrinsic molecular parameters such as transition dipole moments. We do not intend to describe the quantum-chemical calculations in detail since they have already been given in the literature.[75-77] However, it is important to point out their characteristics and it is instructive to show how they are connected to the nonlinear phenomenon of 2PA.

4.1 2PA Probability

In order to establish the interplay between macroscopic 2PA cross section and quantum-mechanical approaches for addressing the 2PA process, it is instructive first to illustrate the transition probability (f ← g) from the ground state g to a final excited electronic state f.

For the 1PA, the transition probability $P_{gf}^{(1PA)}$ is proportional to the square of the cosine of the angle between the electric vector ($\vec{e}$) of the incident electromagnetic wave and the transition moment vector ($\vec{\mu}$). As it is well established, the transition dipole moment for an *n*-photon absorption process is a rank-*n* tensor in three-dimensional space.[78] Thus, the one-photon transition tensor has rank 1 and the corresponding probability of one-photon induced excitation to the final state f during unit time is:

$$P_{\mathrm{gf}}^{(1\mathrm{PA})} = \frac{\pi\omega}{nc\varepsilon_0\hbar} t F_{\mathrm{L}} \left(\left| \vec{\mu}_{\mathrm{gf}} \cdot \vec{e} \right|^2 \right) g(\omega, \omega_0, \Gamma) \qquad (4\text{–}1)$$

where ω is the angular frequency of the incident monochromatic linearly polarized light, *n* is the refractive index of the medium, *c* is the speed of light, ε_0 is the vacuum permittivity, F_L is the flux of the excitation light and $g(\omega, \omega_0, \Gamma)$ is the normalized line shape function.

Therefore, in the case of 2PA, two electric field vectors ($\vec{e}_1, \vec{e}_2$) are involved and thus the amplitude for the process is given by the double projection of two field vectors onto a molecular tensor. Consequently, the two-photon tensor ($S^{(2PA)}$) has rank 2 and is represented by a 3 x 3 matrix. Taking into consideration two identical photons ($\vec{e}_1 = \vec{e}_2 = \vec{e}$) being absorbed by a molecule causing an electronic transition from the ground state g to a final excited state f, the two-photon transition probability $P_{gf}^{(2PA)}$ of the latter transition is given by the Kramers-Heisenberg-Dirac second order perturbation theory expression:[79]

$$P_{\mathrm{gf}}^{(2\mathrm{PA})} = \frac{1}{2}\frac{\pi\omega^2}{n^2c^2\varepsilon_0^2\hbar^2} t{F_{\mathrm{L}}}^2 \left(\left|\vec{e}\cdot S^{(2\mathrm{PA})}\cdot\vec{e}\right|^2\right) g(2\omega,\omega_0,\Gamma) \qquad (4\text{–}2)$$

where the term in the brackets contains the polarization vector of the two absorbed photons $\vec{e}$ (e_x=*x*, e_y=*y*, e_z=*z*) and the two-photon transition tensor $S^{(2PA)}$, which consists of nine elements with the usual Cartesian indices in the molecular frame (S_{xx}, S_{xy}, S_{xz}, …)[XIV]. The individual tensor elements are quantities which represent the contribution of the strength of the transition from each set of directions α (x, y, z) and β (x, y, z) in the molecule.[81] As will be shown below, $S^{(2PA)}$ is related only to the intrinsic spectroscopic properties of the molecule and the frequencies of the incident photons.

By considering the semiclassical approach we derived an analytical expression for two-photon transition probability through the second order time-dependent perturbation theory which can be found in the Appendix 8.1.2.

4.2 Rotationally Averaged 2PA Strength

With the goal to link the experimental and the theoretical data, a characterization tool similar to the oscillator strength *f*, corresponding to the 2PA is needed. The rotationally averaged 2PA strength $<\delta^{(2PA)}>$ (in a.u.) is an equivalent to the oscillator strength, which in the framework of linear absorption is usually used for comparing experimental and theoretical data.[82] This unitless theoretical quantity, which is independent on any experiment, allows the direct comparison of experimental and theoretical results in the case of 2PA and the quantification of the molecular 2PA cross section.[83] The first expression for the 2PA strength was formulated by Monson and McClain in 1970.[84]

$$\delta^{(2\mathrm{PA})} = \left|\vec{e}\cdot S^{(2\mathrm{PA})}\cdot\vec{e}\right|^2 \qquad (4\text{–}3)$$

Apart from certain constant factors, the 2PA strength $\delta^{(2PA)}$ is given by the product in the bracket in equation (4–2). The experiments of 2PA are usually carried out in solution where the molecules possess a statistical distribution of orientation. Therefore, the 2PA strength must be averaged over all orientations of the molecule to yield:[85]

$$\langle\delta^{(2\mathrm{PA})}\rangle = \delta_F F + \delta_G G + \delta_H H \qquad (4\text{–}4)$$

The brackets <> represent the rotationally average since the computed values are averaged over all possible orientations. Where δ_F, δ_G and δ_H are molecular parameters independent of the incident light and F, G and H are integer constants which depend on the polarization of the incident beam.[84] When the two absorbed photons belong to the same beam with linearly polarized light, the

[XIV] The two-photon transition rate $R_{gf}^{(2PA)}$ ($\cong P_{gf}^{(2PA)} / t$) is proportional to the relative sizes and signs of the nine matrix elements and the Cartesian components of the polarization direction of the light (*x, y, z*), as follows:[80]

$$R_{\mathrm{gf}}^{(2\mathrm{PA})} \propto \left|S_{xx}x^2 + S_{xy}xy + S_{xz}xz + S_{yx}yx + S_{yy}y^2 + S_{yz}yz + S_{zx}zx + S_{zy}zy + S_{zz}z^2\right|^2$$

parameters $F = G = H = 2$ and the molecular parameters $\delta_G = \delta_H$ (because the 2PA tensor $S^{(2PA)}$ is symmetric, $S_{\alpha\beta}$ and $S_{\beta\alpha}$ are equal).[86] Therefore, the term δ_F is proportional to $S_{\alpha\alpha}\bar{S}_{\beta\beta}$ ($\delta_F = |S^{(2PA)}|^2$) and the term δ_G is proportional to $S_{\alpha\beta}\bar{S}_{\alpha\beta}$, ($\delta_F = |\mathrm{Tr}S^{(2PA)}|^2$). Thus, for two-photon excitation by a linearly polarized single beam the equation (4 – 4) reduces to:[78,87]

$$\langle\delta^{(2\mathrm{PA})}\rangle = \frac{1}{15}\sum_{\alpha\beta}\left(2S_{\alpha\beta}\bar{S}_{\alpha\beta} + S_{\alpha\alpha}\bar{S}_{\beta\beta}\right) \tag{4–5}$$

where again α and β represent the molecular Cartesian axis and indicate summation over all *x*, *y* and *z*. The superscript bar indicates complex conjugation. The experimental 2PA cross section $\sigma^{(2PA)}$ can be obtained from the rotationally averaged 2PA strength $<\delta^{(2PA)}>$ in atomic units by[85,88,89]

$$\sigma^{(2\mathrm{PA})} = \frac{(2\pi)^3\alpha {a_0}^5\omega^2}{c}\langle\delta^{(2\mathrm{PA})}\rangle g(2\omega, \omega_0, \Gamma) \tag{4–6}$$

where α is the fine structure constant (7.297 x 10^{-3}), α_0 the Bohr radius (5.292 x 10^{-9} cm), ω the photon energy in a.u (1 eV = 0.03675 a.u.) and *c* the speed of light (3 x 10^{10} cm s^{-1}). Lastly, $g(2\omega, \omega_0, \Gamma)$ refers to the lineshape function with the empirical damping parameter Γ, which describes the spectral broadening effects of an excitation.

In order to apply this expression to a practical spectroscopic situation, we must recognize the fact that the two-photon transition energy cannot be precisely defined. Instead, it is distributed over some range of energies creating an absorption band, which includes the distribution of intensity owing to vibronic transitions. Each electronic state consists of an almost continuous manifold of vibrational levels, which in turn should also be considered in the transition. To this end, we integrate both sides of equation (4–6) with the integral running over transition energies ω. Thus, rotationally averaged 2PA strength can be determined in atomic units from the integrated strength of the 2PA band in the 2PA cross section spectra, divided by the square of transition energies according to:

$$\langle\delta^{(2\mathrm{PA})}\rangle = \frac{c}{8\pi^3\alpha {a_0}^5}\int\frac{\sigma^{(2PA)}}{\omega^2}d\omega \tag{4–7}$$

The numerical application of the rotationally averaged 2PA strength is highlighted through the investigation of the 2PA properties in squaraine chromophores in the next chapter.

4.3 Few-State Model Approximation

The most straightforward method for calculating the 2PA cross section is the few-state model.[90,91] Organic conjugated chromophores typically exhibit only few resonances in the energy region (UV-visible) of their linear absorption spectra. This observation gives rise to the approximation that only few electronic states dominate their optical absorption, thus the few-state-model can describe the observed spectra.

As a starting point let us to consider the analytical expression of the two-photon transition probability $P_{gf}^{(2PA)}$, (see equation (8–28) in Appendix 8.1.2) and the equations (4–2) and (4–3). Thus, the 2PA strength $\delta_{fg}^{(2PA)}$ of the f ← g transition is defined by the summation:

$$\delta_{gf}^{(2PA)} = \left| \sum_{i} \frac{(\vec{\mu}_{gi} \cdot \vec{e})(\vec{\mu}_{if} \cdot \vec{e})}{(\omega_{gi} - \omega)} \right|^2 \qquad (4–8)$$

The key notion is to consider that the sum in the latter expression includes all possible intermediate one-photon resonant states (i) also counting the ground (g) and final (f) states, consisting of infinite number of terms (so-called sum-over-state approximation, Figure 8-1).[92] By employing the few-state model approximation and by applying the rotational-averaging method, as described in detail in Appendix 8.1.3, the rotationally averaged 2PA strength $\langle\delta^{(2PA)}\rangle$ is composed by two terms:[6,93]

$$\langle\delta_{gf}^{(2PA)}\rangle = \frac{4}{15}\left[\underbrace{\left(\frac{{\mu_{gf}}^2 {\Delta\mu_{gf}}^2}{\left(\frac{\omega_{gf}}{2}\right)^2} \left(2\cos^2(\theta_{gf}) + 1\right) \right)}_{D\text{-term}} + \underbrace{\left(\frac{{\mu_{gi}}^2 {\mu_{if}}^2}{\left(\omega_{gi} - \frac{\omega_{gf}}{2}\right)^2} (2\cos^2(\theta_{if}) + 1) \right)}_{T\text{-term}} \right] \qquad (4–9)$$

(a) The first term (*D*-term) contains the change of the squared permanent electric dipole moment upon transition $\Delta\mu_{gf} = \mu_{ff} - \mu_{gg}$ between the ground state and the final excited state, as well as the squared transition moment μ_{gf} between these two electronic states.

(b) The second term (*T*-term) involves two excited states and is strongly dependent on their coupling. It contains the squared transition moment μ_{gi} between the ground state and the intermediate one-photon allowed state and the squared transition moment μ_{if} between the latter intermediate state and the final two-photon allowed state.

The few-state model can be derived under certain assumptions which works well for compounds of well-defined molecular symmetry. As mentioned in the introduction part, the selection-rules for the electric dipole transition depend in a different way on the molecular symmetry. By employing the few-state model formalism, we may describe the different two-photon transition pathways dependent on the molecular symmetry as sketched in Figure 4-1. In this context, the 2PA process for compounds

possessing a center of inversion (centrosymmetric), may qualitatively be described by the three-level model of the $<\delta^{(2PA)}>$, which involves the transition via an intermediate one-photon resonance excited state. At the same time, when compounds lack an inversion center (non-centrosymmetric), $<\delta^{(2PA)}>$ may be described by the two-level model, where only the final excited state mainly contributes to the transition.

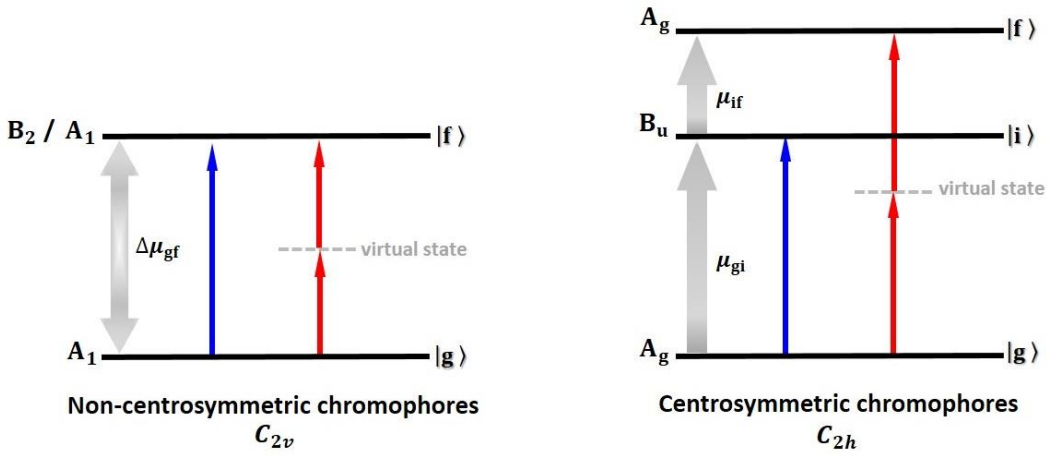

Figure 4-1: Schematic representation of the few-state model formalism: The left panel depicts the two-level model, which describes molecules that lack an inversion center and the right panel depicts the three-level model, which describes molecules which possess a center of inversion.

For some molecules, the 2PA process is no longer dominated by two transitions. In this case, it could be essential to comprise a second transition pathway and thereby form a four-level model. In this thesis we will focus on the cases of three- and two- level model.

Two – level model

In the case of non-centrosymmetric molecules, the ground (g) and the final states (f) are of different parity and thus according to the selection rules the transition f ← g is both one- and two-photon allowed ($\mu_{fg} \neq 0$). Moreover, it is known that a molecule which lacks an inversion center exhibits non-zero permanent dipole moments (μ_{ff}, $\mu_{gg} \neq 0$) which are different in value for different states. Thus, for non-centrosymmetric molecules, the 2PA process is described by the two-level model, where only the final excited state mainly contributes due to the large permanent dipole moment difference $\Delta\mu_{gf}$. Therefore, the *D*-term of the rotationally averaged 2PA strength $<\delta^{(2PA)}>$ (in equation 4–9) became dominant and the *T*-term is neglected due to the transition dipole moments μ_{gi} and μ_{if}, which are very small in comparison to the $\Delta\mu_{gf}$. The rotationally averaged 2PA strength $<\delta^{(2PA)}>$ in the case of the two-level model is given by the equation (4–10), with θ_{fg} being the angle between $\Delta\mu_{gf}$ and μ_{gf}.[94]

$$\langle\delta_{gf}^{(2PA)}\rangle = \frac{4}{15}\frac{(\mu_{gf}{}^2)(\Delta\mu_{gf}{}^2)}{\left(\frac{\omega_{gf}}{2}\right)^2}\left(2\cos^2(\theta_{gf})+1\right) \qquad (4\text{–}10)$$

Three – level model

In case of centrosymmetric molecules, the static dipole moments μ_{gg} and μ_{ff} are equal to zero (μ_{ff}, μ_{gg} = 0) as well as the transition dipole moment between the ground and the final excited state μ_{gf} (due to the selection rules). Hence, the *T*-term now becomes important, and the *D*-term can be neglected, thus the rotationally averaged 2PA strength $<\delta^{(2PA)}>$, in the case of the three-level model, which involves the transition via an intermediate one-photon resonance excited state, is given by the equation (4–11), with θ_{fi} being the angle between μ_{gi} and μ_{if}.[78]

$$\langle \delta_{\mathrm{gf}}^{(2\mathrm{PA})} \rangle = \frac{4}{15} \frac{\left(\mu_{\mathrm{gi}}{}^2\right)\left(\mu_{\mathrm{if}}{}^2\right)}{\left(\omega_{\mathrm{gi}} - \frac{\omega_{\mathrm{gf}}}{2}\right)^2} \left(2\cos^2(\theta_{\mathrm{if}}) + 1\right) \tag{4–11}$$

4.4 Transition Dipole Moment

As reflected in the previous expressions used to determine the rotationally averaged 2PA strength through the few-state model approximation, the transition dipole moment is the major contribution to the enhanced 2PA strength. An electronic transition is accompanied by a substantial intramolecular charge transfer, which causes dipole moment polarizability upon excitation. This pronounced redistribution of π-electron density is correlated with the electron delocalization, which significantly affects the two-photon absorptivity.[95] Thus, the estimation of these transition dipole moments can be a powerful tool for the quantification of the two-photon absorptivity.

Let us turn our attention to the three-level model where the determination of the μ_{gi} and μ_{if} is needed. The transition dipole moments for the transition between the ground state and the first one-photon resonant excited state (μ_{gi}) and between the latter and the final two-photon resonant excited state (μ_{if}) can be derived using experimental data from the linear and two-photon spectra.[96]

It is well established, that the squared transition dipole moment μ_{gi} can be obtained by integrating the main low energy absorption band (i ← g) according to:[97]

$$\mu_{\mathrm{gi}}{}^2 = \frac{3hc\varepsilon_0 \ln(10)}{2000\pi^2 N_{\mathrm{Av}}} \frac{9n}{(n^2+2)^2} \int \frac{\varepsilon}{\tilde{\nu}} d\tilde{\nu} \tag{4–12}$$

Here, N_{Av} is Avogadro`s number and ε is the extinction coefficient [in $M^{-1}cm^{-1}$] at the absorption wavenumber $\tilde{\nu}$. As shown before, the 2PA strength is related to the integrated 2PA cross-section *via* equation (4–7). Thus, replacing the 2PA strength $<\delta^{(2PA)}>$ in equation (4–11) by equation (4–7) yields

$$\mu_{\mathrm{if}}{}^2 = \frac{15}{4}\left(\frac{1}{\mu_{\mathrm{gi}}{}^2}\right) \frac{1}{(2\cos^2(\theta_{\mathrm{if}})+1)} \left(\omega_{\mathrm{gi}} - \frac{\omega_{\mathrm{gf}}}{2}\right)^2 \frac{c}{8\pi^3 \alpha a_0{}^5} \int \frac{\sigma^{(2PA)}}{\omega^2} d\omega \tag{4–13}$$

As input for equation (4–13), the squared transition dipole moment μ_{gi} is obtained *via* the equation (4–12). The energies ω_{fg} and ω_{ig} are estimated from the position of the absorption peaks in the one- and two-photon absorption spectra, respectively. This energetic difference between the virtual state and the one-photon allowed state defines the detuning energy, which (as will be shown in the next chapters) has an important role in 2PA cross section enhancement.

4.5 Two-Photon Fluorescence Excitation Anisotropy

Anisotropy measurements, linked to quantum-chemical calculations, can reveal the spectral positions and determine the mutual orientations of the transition dipole moments from the ground state to higher excited states in relation to the orientation of the emission dipole moment. In this regard, the steady-state one-photon fluorescence excitation anisotropy (1P-FEA) $r^{(1PA)}$ is related to the angle θ^{1P} between the absorption $\vec{\mu}_{abs}^{1P}$ and emission $\vec{\mu}_{em}$ transition dipole moment vectors (see Figure 4-2(a)) by the equation (4–4),[98]

$$r^{(1PA)} = \frac{2}{5}\left(\frac{3\cos^2(\theta^{1P}) - 1}{2}\right) \tag{4–14}$$

where in the range $0° \leq \theta^{1P} \leq 90°$ the 1P-FEA ranges between $-0.2 \leq r^{(1PA)} \leq 0.4$. Clearly, for collinear absorption and emission transition $\theta^{1P} = 0$ and thus $r^{(1PA)} = 0.4$, which is a consequence of the $\cos^2(\omega)$ photo-selection, where ω is the angle between the polarized excitation vector $\vec{E}$ and absorption transition moment vector $\vec{\mu}_{abs}$.[99] Simultaneously for the two-photon fluorescence excitation anisotropy (2P-FEA) $r^{(2PA)}$ the anisotropy value exceeds 0.4 and is as large as 0.57, a fact that can be explained by a new type of photo-selection which depends on $\cos^4(\omega)$ as indicated in Figure 4-2(b).

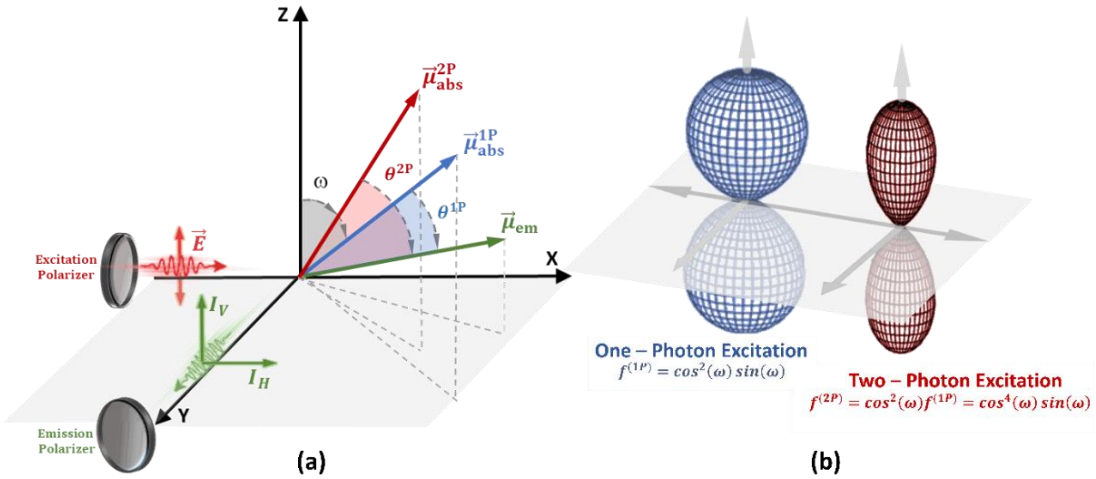

Figure 4-2: (a) Schematic representation of the transition dipole moment vectors for 1P- and 2P-FEA and (b) the orientation distribution of the excited-state population for one- and two-photon excitation with the corresponding one- and two- photon-selection function $f(\omega)$.[80,100]

Thus, in the range $0° \leq \theta^{2P} \leq 90°$ the 2P-FEA ranges between $-0.29 \leq r^{(1PA)} \leq 0.57$. The number of two-photon anisotropy studies is very limited and most of them were performed only within one electronic band. Nevertheless, it seems that in contrast to the conversional 1P-FEA spectroscopy, the 2P-FEA show an almost wavelength independent behavior within several electronic transitions.[101,102]

The 2P-FEA measurements are a powerful tool, since they provide information about the mutual orientation of dipole moments. In this dissertation, 2P-FEA measurements were performed in viscous media in order to determine the angle θ_{fi} in equation (4–11). For the purpose of explaining the anisotropy results, we employed the three-state model with absorption transition dipole μ_{gi} (i ← g) and μ_{if} (f ← i), where i and f are one- and two- photon resonant states, respectively, as explained before and depicted in Figure 4-3(a). In the three-level model, the $r^{(2PA)}$ depends on the mutual orientation of the $\vec{\mu}_{ig}$ transition moment vector, as shown in the diagram of the 2D-space orientation[XV] of these dipoles in Figure 4-3(b).

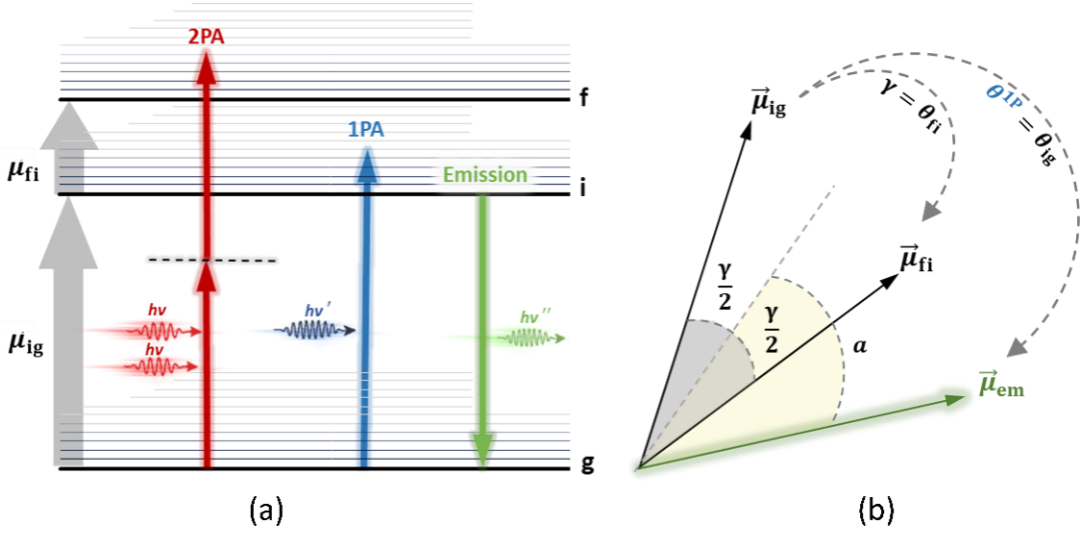

Figure 4-3: (a) The three-level model excitation scheme which is dominated by two major transitions and (b) the corresponding schematic representation of the dipole moment vectors.

The anisotropy values $r^{(2PA)}$ for the three-level model depend on only two angles γ and α. Here, $\gamma = \theta_{fi}$ is the angle between the transition dipole moments $\vec{\mu}_{ig}$ and $\vec{\mu}_{fi}$ and α is the angle between the bisecting line of the angle γ and the emission dipole $\vec{\mu}_{em}$. Thus, the $r^{(2PA)}$ values are given by the expression,[102]

$$r^{(2PA)} = \frac{18\cos\left(\frac{\gamma}{2} - \alpha\right)\cos\left(\frac{\gamma}{2} + \alpha\right)\cos(\gamma) - 7\cos^2(\gamma) + 1}{7(2\cos^2(\gamma) + 1)} \qquad (4\text{–}15)$$

[XV] The transition dipole moment vectors are represented in the 2D-space orientation because in the FEA measurements our interest lies on the relative angle between the dipole moment vectors. In principle, the relationship of their orientation in the 3D-space is taking into consideration the rotational-averaging methods as indicated in Figure 8-2 (see Appendix 8.1.3).

where (see Figure 4-3(b)),

$$\alpha = \left(\theta^{1P} - \frac{\gamma}{2}\right) = \left(\theta_{ig} - \frac{\theta_{fi}}{2}\right) \tag{4–16}$$

Substituting the equation (4–14) into equation (4–15) the hitherto unknown angle θ_{fi} is related to the 2PA anisotropy *via* expression.

$$r^{(2PA)} = \frac{18\cos(\theta_{if} - \theta_{gf})\cos(\theta_{gf})\cos(\theta_{if}) - 7\cos^2(\theta_{if}) + 1}{7(2\cos^2(\theta_{if}) + 1)} \tag{4–17}$$

whereas the angle $\theta_{gf} = \theta^{1P}$ which may be determined by the 1P-FEA. The practical application of the above process will be shown in Chapter 5.

4.6 Polarization-Depended 2PA Ratio

The "new" kind of photo-selection plays an important role in polarization-depended two-photon spectroscopy for the identification of the nature of the excited states of randomly oriented polyatomic molecules.[103] According to the information obtained from equation (4–2), the 2PA probability depends not only on the incident photon flux but also on the polarization of the two involved photons. Moreover, as mentioned above, the 2PA process can be described by the two-photon transition tensor $S^{(2PA)}$ which connects polarization and molecular parameters. W. M. McClain[86] showed that by measuring the dependence of the two-photon absorptivity on the relative polarization of the two involved photons it is possible to determine the symmetry of excited states.

Indeed, the experimentally measurable polarization-depended 2PA ratio $\Omega^{(2PA)}$ allows to distinguish whether the symmetry of states changes or not upon two-photon excitation. This is based on the fact that the $\Omega^{(2PA)}$ is described by the two-photon transition tensor patterns, which is a property of each excited state involved in the transition. The ratio $\Omega^{(2PA)}$ is defined as the ratio of 2PA cross section which is obtained by linear ($\sigma_L^{(2PA)}$) and circular ($\sigma_C^{(2PA)}$) excitation polarized light,

$$\Omega^{(2PA)} = \frac{\sigma_L^{(2PA)}}{\sigma_C^{(2PA)}} \tag{4–18}$$

The relationship between the molecular parameters δ_F, δ_G and δ_H and the exited state symmetry becomes apparent upon examining the two-photon transition tensor $S^{(2PA)}$ elements, which correspond to these terms.[85] Thus, the experimental ratio $\Omega^{(2PA)}$ is related to the two-photon transition tensor $S^{(2PA)}$ by the equation:

$$\frac{\delta_F}{\delta_G} = \frac{3 - 2\Omega^{(2PA)}}{1 + 2\Omega^{(2PA)}} = \frac{\left|Tr.S^{(2PA)}\right|^2}{|S^{(2PA)}|^2} \tag{4–19}$$

As mentioned in subchapter 4.2, for two identical photons, δ_F is a measure of the diagonal $S^{(2PA)}$ elements and the δ_G (= δ_H) value is a measure of the sum of the square of all elements in the transition tensor. Hence, the polarization-depended 2PA ratio $\Omega^{(2PA)}$ varies from 0 to 3/2 for isotropic emission. The systematic determination of the two-photon tensor patterns for each point group is a lengthy exercise and is beyond the scope of the present dissertation. Nevertheless, it is important to emphasize two symmetry rules, which are related to all molecular point groups. Two-photon transitions from a totally symmetric ground state to a nontotally symmetric excited state are required to have $\Omega^{(2PA)}$ = 3/2 (δ_F = 0, trace is zero). At the same time, the transitions to a totally symmetric excited state may have any value in the range 0 to 3/2.[79,104] In order to demonstrate the feasibility of the present technique, as will be shown in the next chapter, we performed polarization-depended 2PA ratio measurements in several investigated compounds.

5 Investigation of 2PA Properties of Organic Chromophores

In terms of complexity of many conjugated chromophores, there is a strong need to probe the relationship between the chemical structure parameters and the 2PA characteristics. In this chapter, several compounds were studied in order to investigate how certain structural parameter effects can affect the magnitude of 2PA cross section and lead to an alteration of their nonlinear optical properties. In particular, this work focuses on the effects that actually define the ability for electron delocalization and the intramolecular charge transfer phenomena, since they are strongly correlated with the two-photon absorptivity. In this thesis, the investigated effects are:

- The exciton coupling interaction between the chromophores
- The bridging unit characteristics
- The branching concept

This knowledge can be used to provide guidelines for the identification of so-called structure-property relations governing 2PA. In order to gain a deeper understanding of the nonlinear properties of the investigated compounds and to give an overview of the 2PA bands, the study of their linear optical properties is requested. In this regard, the steady-state linear absorption properties of all compounds were investigated by UV/vis absorption spectroscopy. The 2PA cross section spectra were determined by the relative 2PIF technique as described in Chapter 3. Many of the results were substantiated by polarization dependent linear and nonlinear optical measurements. Moreover, for more quantitative consideration, density functional theory (DFT) calculations were also performed by Dr. Marco Holzapfel using the Gaussian09[105] and the DALTON[106] program packages. Description of the experimental methodology of the following photophysical study is presented in the Appendix 8.2.

5.1 The Exciton Coupling Effects on the 2PA

As mentioned above, there is a strong correlation between intra-molecular charge transfer and two-photon absorptivity. Thus, the fundamental understanding of exciton coupling theory in the special case of nonlinear interaction is crucial.[107] It is known that increasing the π-conjugation length, thereby enhancing electronic delocalization and charge-transfer phenomena leads to an increase of the 2PA cross section.[108,109] On the other hand, there are several studies dealing with the existence of a limit for the two-photon absorptivity.[110,111] In light of these experiences, several molecular design strategies were proposed for coupling multiple chromophores in oligomers or polymers. In subchapter 5.1.1, we focus on engineering the exciton interaction by altering the coupling unit between the chromophores and in subchapter 5.1.2 on changing the molecular symmetry. Here, in order to explore these impacts on the molecular 2PA cross section we synthesised a series of squaraine homodimers. Among the various functional dyes, which have been in focus of research due to their enhanced 2PA

properties, are squaraines.[112-114] Moreover, due to their rather simple synthetic access of a great variety of monomeric,[115] oligomeric,[116-119] and polymeric squaraine dyes,[120-124] there are extensive possibilities to design a range of superchromophores with tuneable optical properties.[125-127]

5.1.1 SQA-Based Homodimers[l]

It is known that quadrupolar charge distribution and generally large chromophores leads to enhanced 2PA cross section. Recently, our study by Ceymann *et al.*[128] shows that excitonic interaction in squaraine oligomers leads to an enhancement of 2PA. To this end, a series of squaraine homodimers built up from the well-investigated indolenine trans-squaraine parent chromophore **SQA** using a systematic length variation of the bridging unit has been studied. The chemical structure of the investigated squaraine compounds were synthesized by Dr. Maximilian H. Schreck[129,130] and are presented in Figure 5-1. The bridging units increase from a single bond in **dSQA-1**, over an acetylene bridge in **dSQA-2**, and a butadiyne-bridge in **dSQA-3**, to a tolan bridge in **dSQA-5**. Additionally, we also considered different conjugation pathways in e.g. **dSQA-4** vs. **dSQA-3**, and in **dSQA-6** vs. **dSQA-1**. With the intention of investigating the coupling effect of squaraine monomers to yield dimers on their optical properties, the parent monomer **SQA** is also included in this study.

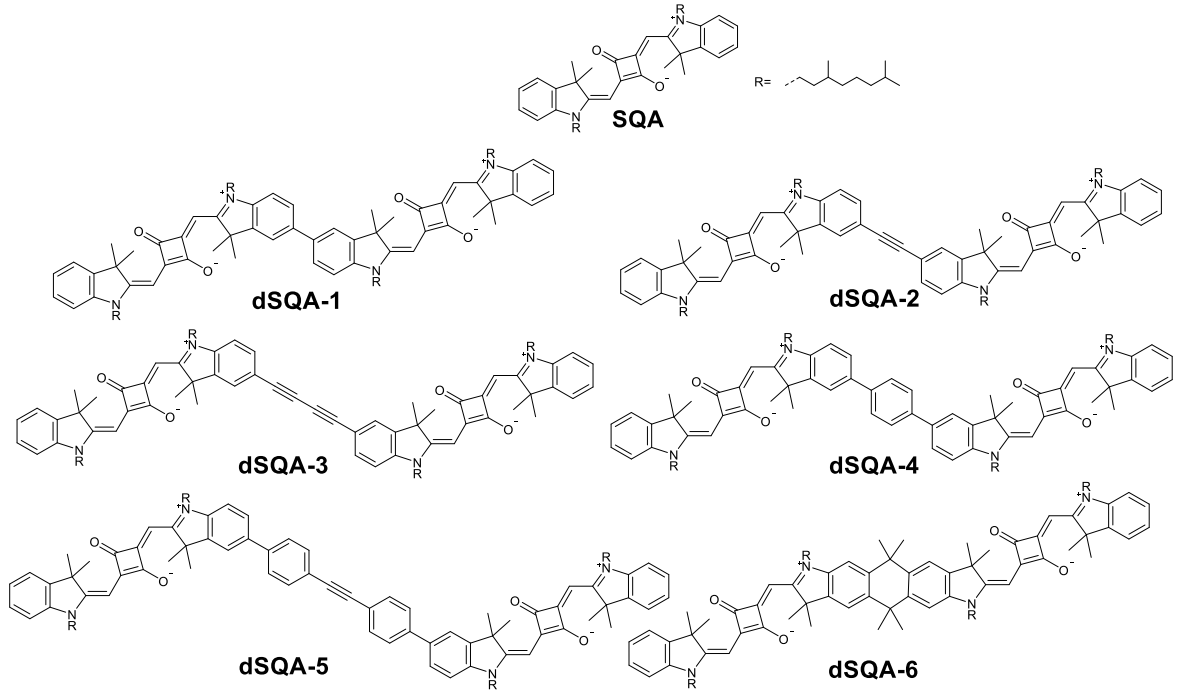

Figure 5-1: Chemical structure of parent squaraine **SQA** and squaraine dimers **dSQA-1**–**dSQA-6.**

[l] Reprinted or adapted in part from: "*Exciton coupling effects on the two-photon absorption of squaraine homodimers with varying bridge units.*" E. Michail, M. H. Schreck, M. Holzapfel and C. Lambert, Phys. Chem. Chem. Phys., 2020, 22, 18340-18350. **© 2020 Royal Society of Chemistry.**

The **dSQA-1** homodimer possesses C_2 symmetry, where **dSQA-2**, **dSQA-3** and **dSQA-6** possess D_{2h} symmetry and **dSQA-4** and **dSQA-5** C_i symmetry. The assignment of the spectral positions of transitions and the determination of their nature is based on the point group symmetry to which the investigated compounds belong. For simplicity, we treat all the homodimers as they belong to the D_{2h} point group since electronically they all exhibit "pseudo centrosymmetric" symmetry. Thus, according to the selection rules of 1PA and 2PA we assume that one-photon transitions are allowed only in electronic states belong to the irreducible representation B_u and the two-photon transitions to states with A_g irreducible representation in all cases.

5.1.1.1 Linear Optical Spectroscopy

The linear optical properties of the monomer compound exhibit typical spectroscopic characteristics of squaraine dyes. In particularly, the linear absorption spectrum features a sharp and intense main band in the red spectral region of the visible spectrum with a weak vibronic shoulder on the high-energy side. The fluorescence spectrum behaves like a mirror image of the monomer absorption accompanied by a small Stokes shift.

The absorption spectra of the homodimers are more complex. Generally, they show red shifted absorption spectra with higher molar extinction coefficients compared to the monomer. All homodimers display strong fluorescence with small Stokes shift. The steady-state linear absorption and normalized fluorescence spectra of the monomer **SQA** and the homodimers **dSQA-1** – **dSQA-6** in toluene are shown in Figure 5-2. The absorption maxima and extinction coefficients of characteristic bands are listed in Table 5-1.

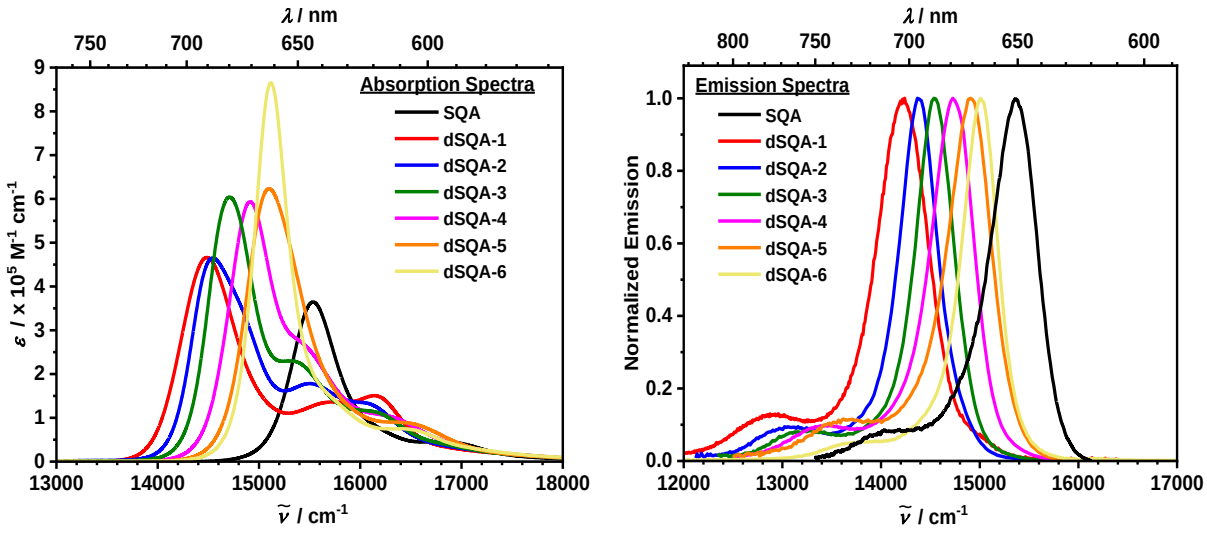

Figure 5-2: Linear absorption (left panel) and normalized fluorescence (right panel) spectra of monomer **SQA** and homodimers **dSQA-1** – **dSQA-6** in toluene.

UV/Vis Absorption

According to the linear absorption spectra of the homodimers, the most intense absorption band in the red spectral region (14500 – 15200 cm^{-1}) is assigned to the $S_1 \leftarrow S_0$ transition accompanied by subsidiary vibronic progression on the high-energy side. In the case of the **dSQA-1** to **dSQA-4** homodimers, an additional absorption band is observed attributed to a second electronic transition $S_2 \leftarrow S_0$. For the **dSQA-5** and **dSQA-6** the upper exciton state is hardly visible as a shoulder to the high energy side of the main peak. Based on the assumption of D_{2h} symmetry, the lowest one-photon exciton state is S_1 (B_u), which results in the first one-photon allowed transition $S_1 \leftarrow S_0$ ($1B_u \leftarrow 1A_g$). The next exciton state S_2 (A_g) can be reached by the two-photon transition $S_2 \leftarrow S_0$ ($2A_g \leftarrow 1A_g$). In principle the latter is forbidden by symmetry as a one-photon absorption process, nevertheless, it is slightly allowed. This is caused by vibronic coupling of the $2A_g$ state to an asymmetric vibration and due to symmetry breaking in the chromophores as will be shown below.[131]

The presence of the two excited states in the homodimer can be conceived as being due to the so-called exciton Davydov splitting of the first excited state of the two coupled parent monomer states.[132] According to the exciton coupling theory, the lowest exciton state S_1 of the **SQA** parent monomer splits in two excited states (S_1 and S_2) in the homodimers and the splitting energy refers to twice the electronic exciton coupling energy, *J*.[133] This means, that half of the energy difference of these two absorption maxima can be used to estimate the exciton coupling energy *J*. Going from **dSQA-1** to **dSQA-6** we observed a gradual decrease of the bathochromic shift of the main absorption band with respect to the parent monomer **SQA** which leads to an enhanced mixing of electronic and vibronic states.[134] The latter observation indicates that the exciton coupling strength of the homodimers decreases by varying the spacer units from **dSQA-1** to **dSQA-6**.

The squared transition dipole moments (μ^2 = dipole strength) for the transitions between the ground state S_0 and the two exciton states (S_1 and S_2) have been estimated by integration of these absorption bands as indicated in Chapter 4 using equation (4–12). The squared transition dipole moments of the squaraine absorption bands of the homodimers show nearly additivity relative to their **SQA** monomer and thus follow the Thomas-Reiche-Kuhn sum rule.[135] The investigated homodimers give similar squared transition dipole moment values (μ^2 = 245 – 269 D^2) proving that no other electronic states are located in this energy range and contribute to the exciton manifold. The squared transition dipole moments μ_{01} of the $S_1 \leftarrow S_0$ transition are also summarized in Table 5-1.

One-photon fluorescence excitation anisotropy

Our aim to correlate the nonlinear optical properties with exciton coupling strength makes the estimation of this quantity an important aspect in this study. To this end, one-photon fluorescence excitation anisotropy (1P-FEA) measurements in viscous poly-THF were performed to estimate the

energy of the S_2 state and therefore of *J* more accurately. The 1P-FEA measurement provides information regarding the orientation of the absorption and emission transition moments of the investigated fluorophore. According to equation (4–14), the 1P-FEA is associated with the angle θ_{01} between the absorption and emission transition moment (see angle θ^{1P} in Figure 4-2(a)).

Except of **dSQA-6**, due to their flexible bridging units, all the other homodimers can exist in different conformers (rotamers) in solution. **dSQA-1** - **dSQA-5** homodimers may form essentially only two different stretched orientations as shown in Figure 5-3: The *Type I* where the long axes of the squaraine monomers is parallel, and the *Type II* in which they possess an angle of *ca*. 120°. Thus, we assume that in case of **dSQA-1** - **dSQA-5** homodimers the solution consists of an equimolar mixture of *Type I* and *Type II* conformers. The latter aspect may explain the observed weakly allowed one-photon transition to the $2A_g$ state which in the *Type II* conformer has lower symmetry and thus breaks the centrosymmetry. In contrast, due to its rigidity the squaraine homodimer **dSQA-6** cannot form rotamers and thus the full transition strength is concentrated in the lower exciton state ($1B_u$) and the upper exciton state ($2A_g$) is not observed. Analogously, the linear absorption spectrum of the **dSQA-6** exhibits the feature of a "*J*-type" dimer showing a 1.5 times higher extinction coefficient than the other homodimers in toluene.

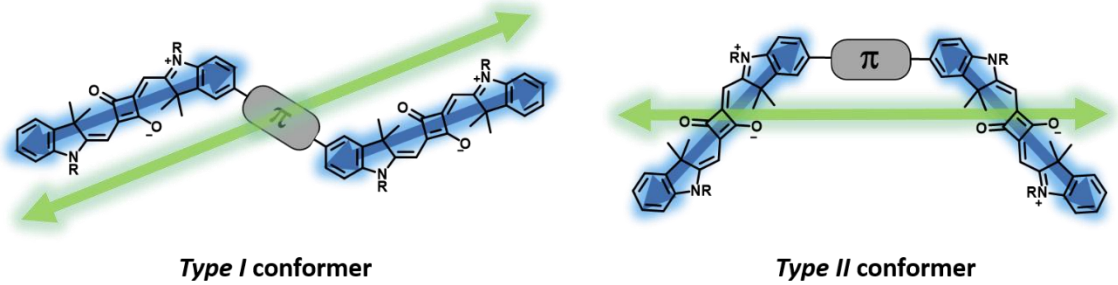

Figure 5-3: The two different types of orientations of the investigated squaraine homodimers **dSQA-1**–**dSQA-5**. The blue and green arrows indicate the transition dipole moments of the lowest energy transitions of the individual **SQA** chromophores and of the whole homodimer, respectively.

Ideally, in case of strong exciton coupling, the lower energy exciton state of all the homodimers should show an anisotropy of $r_{1PA} = 0.4$. This limiting anisotropy value can only be reached due to parallel absorption and emission transition moments of the S_1 exciton state.[98] At the same time, a weak exciton coupling leads to a partial localization of excitation which results in reduced anisotropy values.[136] Indeed, as expected, the experimental anisotropy value r_{1PA} for the **dSQA-1** homodimer at the lower energy exciton state is 0.36, confirming the strong exciton coupling. For **dSQA-5** the 1P-FEA anisotropy value at the red side of the lower exciton band is 0.18. The latter value indicates a complete exciton localization after excitation. In case of *Type I* conformer the transition moment for absorption

and emission are parallel even after excitation, while in *Type II* conformer the angle between the transition moment after excitation is *ca*. 60° which leads to an anisotropy of −0.05. Thus, averaging over the two types of conformers leads to r_{1PA} = 0.175. The anisotropies of the other homodimers are in-between those of **dSQA-1** and **dSQA-5**.

The upper exciton state S_2 should possess a vanishing transition dipole moment for *Type I* conformer. On the other hand, for *Type II* conformer the S_2 state should have the anisotropy of −0.2 since it is polarized along the C_2 axis and thus is perpendicular to the emission transition dipole moment. However, due to the overlap of the two exciton states (S_1 and S_2) the experimental anisotropy of the upper exciton state deviates from r_{1PA} = −0.2. In the homodimer **dSQA-1** the experimental anisotropy value of −0.02 at 16310 cm^{-1} refers to S_2 exciton. The localization of **dSQA-5** leads to r_{1PA} = 0.4 for *Type I* and at the same time to −0.05 for *Type II*, thus, averaging yields r_{1PA} = 0.175 for the S_2 exciton state. Nevertheless, we used this low anisotropy values to assign the $2A_g$ state more precisely and in the following we assign this state with the superscript *r*. In Table 5-1, the estimated S_2 energy region ($\tilde{\nu}^r_{S_2}$) and the exciton coupling derived from these energies (J^r), as well the excitation coupling estimation by the linear absorption spectra are given. The 1P-FEA spectra together with the linear absorption and 2PA spectra in toluene are depicted in Figures 5-7, 5-8 and 5-9, at the end of this subchapter for a more detailed assignment of states.

Table 5-1: The squaraine center-to-center distance, absorption maxima of S_1 and S_2 state, exciton coupling energy, dipole strength of the parent monomer **SQA** and homodimers **dSQA-1** – **dSQA-6** in toluene.

	L /Å	$\tilde{\nu}_{S_1}$/cm^{-1} [ε / M^{-1}cm^{-1}]	$\tilde{\nu}_{S_2}$/ cm^{-1} [b]	J/ cm^{-1} [c]	$\tilde{\nu}^r_{S_2}$/ cm^{-1} [d]	J^r/ cm^{-1} [e]	μ^2_{01}/ D^2 [f]
SQA		15530 [3.64 x 10^5]					127
dSQA-1	17.1	14480 [4.66 x 10^5]	16140	830	16310	920	248
dSQA-2	19.6	14550 [4.65 x 10^5]	16060	760	16290	870	254
dSQA-3	22.0	14720 [6.04 x 10^5]	15400	340	15600	440	269
dSQA-4	21.2	14910 [5.94 x 10^5]	15420	260	15690	390	260
dSQA-5	27.7	15110 [5.94 x 10^5]	-	-	15280	90	252
dSQA-6[a]	18.7	15120 [8.58 x 10^5]	-	-	15900	390	245

[a] See also Ref [136]. [b] Estimated from 1PA absorption spectra. [c] Estimated as $J = (\tilde{\nu}_{S_2} - \tilde{\nu}_{S_1})/2$. [d] Estimated from 1P-FEA spectra. [e] Estimated as $J^r = (\tilde{\nu}^r_{S_2} - \tilde{\nu}_{S_1})/2$. [f] Dipole strength of the total exciton manifold.

In what follows, we do not further discriminate between the *Type I* and *Type II* conformers. Moreover, Spano *et al*.[137], through theoretical investigations, pointed out that the optical properties of the two conformers of **dSQA-1** are rather the same.

Fluorescence Spectroscopy

All the investigated homodimers show strong fluorescence emission with a small Stoke shift ($\Delta\tilde{\nu}$). Their fluorescence spectra resemble that of the parent monomer **SQA** but are shifted to lower energies. This indicates that the fluorescence exclusively originates from the lowest exciton state. The lifetime measurements gave multiexponential decays for all the investigated squaraine compounds and the average lifetimes acquired in this way were used to calculate the transition dipole moment of fluorescence as described in Appendix 8-2. The squared transition moments for fluorescence varies between 147 – 177 D^2 for **dSQA-1** - **dSQA-6** compared to 114 D^2 for **SQA**. Likewise, high fluorescence quantum yields (φ_{fl}) vary between 0.80 and 0.71 and follow the exciton coupling strength, which are obtained for **dSQA-1** – **dSQA-6**. The obtained fluorescence quantum yields are higher than that of the monomer, which is a consequence of the coupled transition moments (superradiance[II]).[138-140] The emission maxima and all the obtained data are summarized in Table 5-2.

Table 5-2: The emission maximum, the Stokes shift $\Delta\tilde{\nu}$, the fluorescence lifetimes τ_{fl} with the relative amplitudes in parentheses, the average fluorescence lifetimes values $\bar{\tau}_{fl}$, the square of the fluorescence transition moments and fluorescence quantum yield φ_{fl} of the parent monomer **SQA** and homodimers **dSQA-1** – **dSQA-6** in toluene.

	$\tilde{\nu}_{em}$/cm^{-1}	$\Delta\tilde{\nu}$/cm^{-1}	τ_{fl}/ns (α_n)	$\bar{\tau}_{fl}$/ ns	μ_{fl}^2/ D^2	φ_{fl}
SQA	15360	170	0.25 (0.09) 1.71 (0.91)	1.69	114	0.62
dSQA-1	14240	240	1.22 (0.53) 2.14 (0.47)	1.78	172	0.80
dSQA-2	14360	190	0.80 (0.22) 1.84 (0.78)	1.73	168	0.78
dSQA-3	14530	190	0.63 (0.06) 1.61 (0.94)	1.59	168	0.74
dSQA-4	14730	180	0.57 (0.13) 1.70 (0.87)	1.64	164	0.77
dSQA-5	14900	210	0.27 (0.07) 1.66 (0.93)	1.64	147	0.71
dSQA-6	15020	100	0.37 (0.02) 1.34 (0.98)	1.33	177	0.71

[II] Superradiant behavior was reported in organic conjugated materials characterized by a head-to-tail interaction between transition dipoles, which can be described as an ensemble of collinear dipoles oscillating in-phase leading to a superradiant state.

5.1.1.2 Nonlinear Absorption Properties

All the homodimers in toluene solution displayed significant 2PA in the investigated spectral region between 15000 – 25000 cm^{-1}. The spectral regions where 2PA resonance occurs can be divided into three sections: The first section is up to 18000 cm^{-1}, in which the 2PA cross section reaches maximum values of *ca.* 400 GM. The second section covers 2PA bands from 18000 to 24000 cm^{-1}, where the 2PA spectra shows a distinct spectral evolution and the 2PA cross section decreases on going from **dSQA–1** to **dSQA–6**. The third section is above 24000 cm^{-1} and shows an extremely high 2PA cross section for all the investigated dimers. The 2PA spectra of the squaraine homodimers, as well as the parent monomer **SQA** in toluene are depicted in Figure 5-4. For a more detailed assignment of exciton states, a comparison of the linear and 2PA spectra with the 1P-FEA spectra for all the investigated squaraine compounds separately, can be found at the end of this subchapter. Our aim is not only to quantify the 2PA cross section of the 2PA bands, but also to determine their origin. Under the light of the two coupled monomers, the simple exciton coupling theory predicts only two possible exciton states. More elaborate orbital coupling and CI mixing schemes indicate the formation of four excited states.[128,141] To gain a deeper insight into the nonlinear properties, we turn our attention to the three spectral sections in detail.

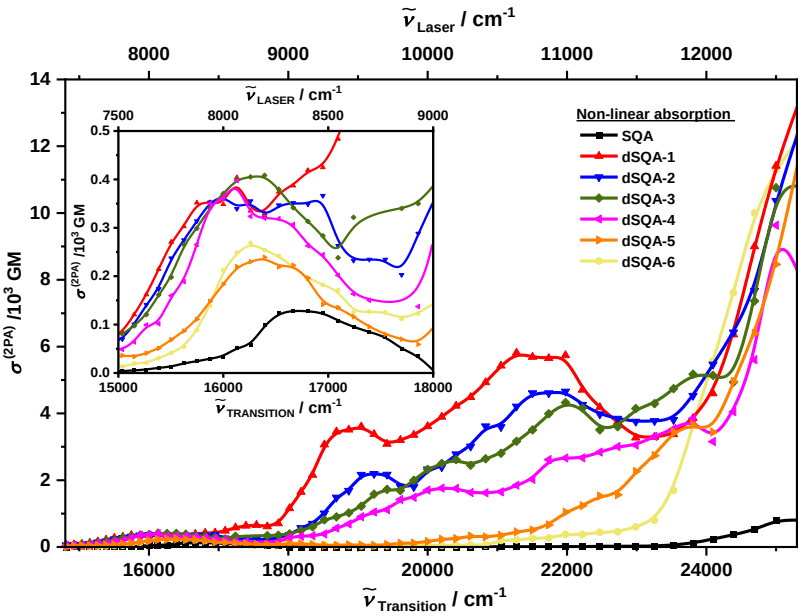

Figure 5-4: 2PA cross-section spectra of monomer **SQA** and homodimers **dSQA-1** – **dSQA-6** in toluene.

The 15000 – 18000 cm^{-1} 2PA region

In the first spectral section all the homodimers exhibit a 2PA band which has a similar 2PA cross section and consists of two overlaid 2PA bands. The first band is caused by vibronic coupling of the otherwise 2PA-forbidden $S_1(1B_u)$ excited state with b_u asymmetric vibrations (Herzberg-Teller effect, $B_u \times b_u \rightarrow A_g$).[116,142] The same 2PA band is clearly visible in the 2PA spectra of **SQA** monomer, where

a cross section of *ca.* 200 GM is reported.[116,128,141] The second band can be ascribed to the two-photon allowed transition $S_2 \leftarrow S_0$ ($2A_g \leftarrow 1A_g$), as mentioned above.

To confirm this hypothesis, the origin of the two 2PA bands in the 15000 – 18000 cm^{-1} spectra region were investigated by polarization-dependent 2PA spectroscopy (see subchapter 4.6). To this end, polarization-depended 2PA measurements for **SQA** monomer, **dSQA-1**, **dSQA-2** and **dSQA-5** homodimers in fluid toluene were performed in order to determine the 2PA polarization-dependent ratio $\Omega^{(2PA)}$. The measurements were recorded by the 2PIF spectrometer, as described in Appendix 8.2 and the results are presented in Figure 5-5 (and the power-dependent verification in Figure 8-4).

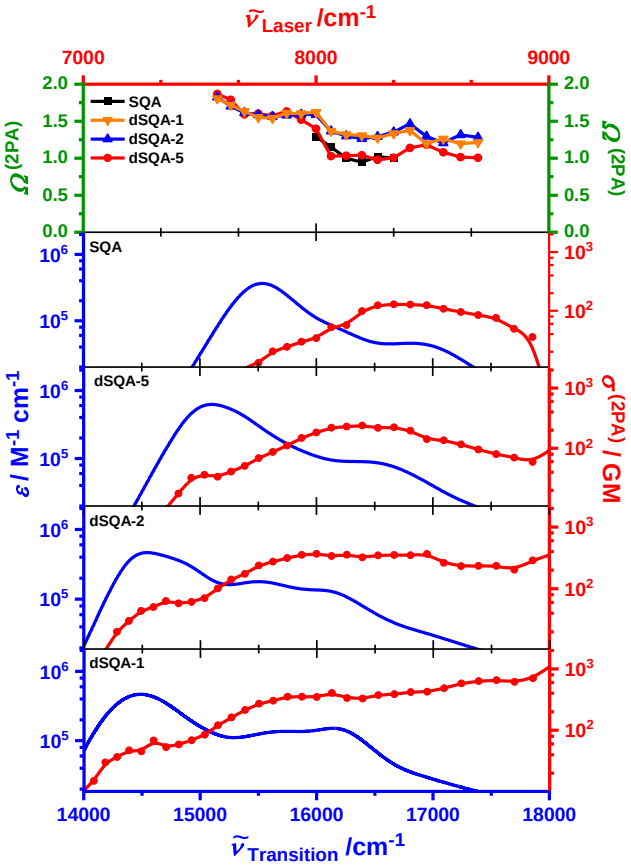

Figure 5-5: Linear absorption (blue line), 2PA (red line) and 2PA polarization-dependent ratio (upper panel) spectra of monomer **SQA** and **dSQA-1**, **dSQA-2** and **dSQA-5** in toluene.

As expected, two regions can be observed, where the value of 2PA polarization ratio tends to a constant value, suggesting two different types of transition in this spectral region. In the lower energy spectral region, where the $S_1 \leftarrow S_0$ transition is located, all the three homodimers as well as the parent monomer **SQA** exhibit $\Omega^{(2PA)} \sim 3/2$. By assuming a totally symmetric ground state S_0 ($1A_g$), this result implies that a transition to a nontotally symmetric excited state takes place ($1B_u \leftarrow 1A_g$). This is, as described above, the same transition as in case of the **SQA** monomer *i.e.* two-photon transition through vibrational coupling $B_u \times b_u \rightarrow A_g$ in an electronic state, which is in principle 2PA forbidden. In

the second spectral region at higher energies, where the energetic position of $S_2 \leftarrow S_0$ transition is located, the $\Omega^{(2PA)}$ varies from *ca.* 1.3 (for **dSQA-1**) to 1 (for **dSQA-5**). This indicates that the transition involves two electronic states with the same symmetry ($2A_g \leftarrow 1A_g$) and thus the upper exciton state S_2 is a totally symmetric excited state and can be reached by two-photon transition.

To further substantiate our experimental results, we performed theoretical calculations[III] using density functional theory (DFT). The linear absorption states were calculated by time-dependent theory (TD-DFT) and the 2PA excited states by quadratic response theory (QR-DFT). Due to inherent DFT problems the computed S_1 state energies for all homodimers are 4000 cm^{-1} higher in energy compared to the experiment. Such blue-shifted bands have been also reported in the literature for DFT calculations of other squaraine dyes.[IV][140,146,147] Nevertheless, for the sake of comparison we shifted all the computed states energies by 4000 cm^{-1}. In this context, the theoretical calculations in this spectral region indicate that the 2PA strengths $<\delta^{(2PA)}>$ decrease from 1500 a.u to 100 a.u on going from **dSQA-1** to **dSQA-5**.

For a more quantitative consideration, we integrated the respective spectral region according to the equation (4–7). The integral is performed over the $S_1 \leftarrow S_0$ and $S_2 \leftarrow S_0$ low energy absorption bands with integration limits 14600 – 17800 cm^{-1}. Thereby, we obtained the 2PA orientationally averaged transition strength $<\delta^{(2PA)}>$ in order to compare the intensity of transitions irrespective of their band shape. The two-photon allowed S_2 state shows significant 2PA strengths, which slightly decreases from *ca.* 3.4 x 10^4 a.u to 1.5 x 10^4 a.u on going from **dSQA-1** to **dSQA-5**. While the theoretical calculations show the same trend with the experimental one, they are about one order of magnitude lower, even taking into consideration that the lower exciton state S_1 contributes to the 2PA strength in this energy region.

All obtained data can be found in tables at the end of this subchapter for all the investigated squaraine compounds in toluene. Specifically, the integrated 2PA strength and the corresponding maximum 2PA cross section are given in Table 5-5. At the same time, all the computed data (transition energies as well as oscillator strengths of 1PA-allowed state and 2PA strengths for 2PA-allowed states) are given in Table 5-6.

The 18000 – 24000 cm^{-1} 2PA region

In the second investigated spectral region between 18000 – 24000 cm^{-1}, we observed a strong and structured 2PA band with the 2PA cross-section decreasing from 5740 GM to 375 GM upon modifying

[III] The theoretical calculations were performed by Dr. Marco Holzapfel.

[IV] The fact that various theoretical methods overestimate the vertical transitions for cyanine-like dyes was intensely investigated and traced back to various reasons, according to the literature. [143-145]

the molecular structure of the π-units on going from **dSQA-1** to **dSQA-6**. Interestingly, the 2PA spectra of the homodimers going from **dSQA-1** to **dSQA-6** approach that of the parent monomer **SQA**.

According to our recent studies by Ceymann *et al*.[128] we assume that four electronic states are experimentally observed up to 23000 cm^{-1}. While the S_1 and S_2 exciton states can easily be derived by exciton coupling theory, the orbital interaction of two monomers gives rise to further two excited states (S_3 and S_4) which are not predicted from exciton coupling theory. In this energy region, the DFT calculations suggest two exciton states S_3 and S_4 which are rather close in energy (at *ca.* 23000 cm^{-1}) with A_g and B_u symmetry, respectively.

Now, we turn our attention to the third exciton state S_3 ($3A_g$) since $3A_g \leftarrow 1A_g$ is the dominant electronic transition in the structured 2PA spectra region between *ca*. 18000 – 24000 cm^{-1}. Therefore, the unexpected large width of this 2PA band might be caused by vibronic progression which, in contrast with the linear absorption spectra, can be enhanced in 2PA.[43,148] The experimental 2PA strength $<\delta^{(2PA)}>$ via equation (4–7), in that spectral region with integration limits 17800 –24000 cm^{-1} yields values between 3 x 10^5 a.u for **dSQA-1** and 2 x 10^4 a.u for **dSQA-6**. These findings are in contradiction with the theoretical calculations, which are about one order of magnitude higher than the integrated 2PA strengths (see Tables 5-5 and 5-6). This is probably due to the experimental 2PA strength associated with a major error as the integration limit, especially at the high energy side, is rather arbitrary.

In order to gain insight into how the exciton coupling interaction affects the magnitude of 2PA strength, we employed the few-state formalism for the investigated symmetric homodimers. As presented in subchapter 4.3, by employing the three-level model, the relation of the rotationally average 2PA strength $<\delta^{(2PA)}>$ is connected with the squared transition dipole moments μ_{13}^2 between the first one-photon resonance excited state S_1 ($1B_u$) and third two-photon-allowed excited state S_3 ($3A_g$) as presented in equation (4–13). The determination of the transition dipole moments μ_{13}^2 allows a fundamental understanding of the corelation between the exciton coupling strength and the 2PA strength as indicated in Figure 5-6. The determined μ_{13}^2 values and the corresponding $<\delta^{(2PA)}>$ results are listed in Table 5-3.

Moreover, two-photon fluorescence excitation anisotropy measurements (2P-FEA) in viscous poly-THF was also performed (see Figure 8-3) in order to determine the hitherto angle θ_{13} as described in subchapter 4.5. Considering an equimolar mixture of *Type I* and *Type II* isomers, the angle θ_{01} and θ_{13}, which were obtained by 1P-FEA and 2P-FEA measurements, respectively, refer to an average value. The maximal 1P-FEA values $r^{(1PA)}$ as well as the corresponding angles between the absorption and emission transition moment θ_{01} are summarized in Table 5-3 with the 2P-FEA values $r^{(2PA)}$ and the corresponding angles θ_{13} between the transition dipole moments μ_{01} and μ_{13}.

Table 5-3: Input values for Equation (4–7) and (4–13) : 1PA and 2PA anisotropy *r*, angles of transition moments θ and state energies ω, 2PA strength $<\delta^{(2PA)}>$ and squared transition moments μ.

	$r^{(2PA)}$[a]	θ_{01}/deg	$r^{(2PA)}$ [at $\tilde{\nu}$/cm^{-1}]	θ_{13}/deg	ω_{01}/cm^{-1}	ω_{03}/cm^{-1}	$<\delta^{(2PA)}>$/a.u.	μ_{13}^2 /D^2
dSQA-1	0.35	16.8	0.41 [21980]	71	14500	21980	477085	63.6
dSQA-2	0.33	20.0	0.28 [21980]	81	14500	21980	353413	53.1
dSQA-3	0.23	32.2	0.17 [21980]	89	14700	21980	322594	53.6
dSQA-4	0.29	25.4	0.38 [21980]	77	14900	21980	222035	38.5
dSQA-5	0.18	37.3	0.13 [22470]	90[b]	15100	22470	96886	18.7
dSQA-6	0.36	15.0	0.50 [22220]	62	15120	22220	16886	2.7

[a] Maximum anisotropy value. [b] This angle refers to the minimum anisotropy of 0.14.

Therefore, in Table 5-4 we also give the determined μ_{13} values for the extreme angles θ_{13} = 0° and 90° which show again the same trend. Although the thereby evaluated μ_{13}^2 is smaller/larger than in case of varying angles, it is clearly indicated that the difference in 2PA strength are caused by the difference of exciton coupling in this series of squaraine homodimers.

Table 5-4: The squared transition dipole moments μ_{13} for the limiting angles θ_{13} = 0° and 90°

	μ_{13}^2 /D^2 (θ_{13}= 0°)	μ_{13}^2 /D^2 (θ_{13}= 90°)
dSQA-1	25.7	77.0
dSQA-2	18.6	55.7
dSQA-3	17.9	53.7
dSQA-4	14.1	42.4
dSQA-5	6.22	18.7
dSQA-6	1.27	3.82

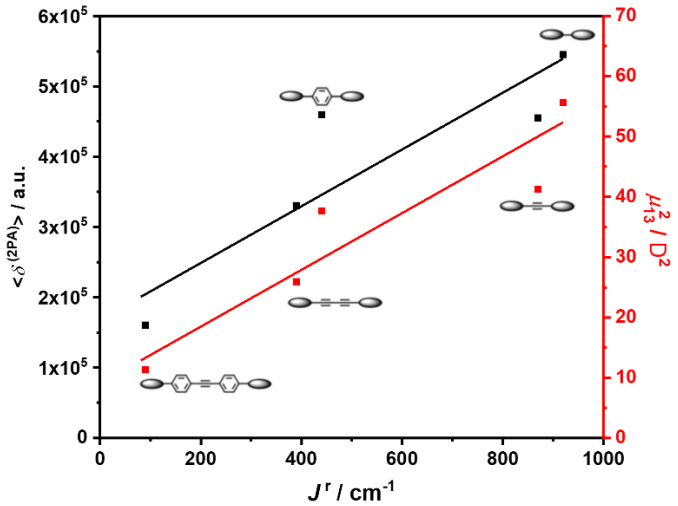

Figure 5-6: Plot of the 2PA strength (black) for the S_3 exciton state and the dipole strength (red) between S_1 and S_2 *vs*. exciton coupling energy for **dSQA-1** – **dSQA-5** in toluene. The linear correlation lines are only a guide to the eye.

The 24000 – 25000 cm^{-1} 2PA region

The third investigated spectral region includes the highest 2PA cross section in the accessible energy range located at *ca*. 25000 cm^{-1}. According to linear and 2PA spectra in this high energy region, all the squaraine homodimers feature two further states; the S_5 state which is 1PA-allowed and the S_6 which is 2PA-allowed.

The linear absorption spectra exhibit a less intense $S_5 \leftarrow S_0$ transition at energies around 26000 cm^{-1} for all the homodimers as well as the monomer **SQA**. In agreement with experiment, the DFT calculations, after renormalization in energy, confirms the existence of the S_5 exciton state at this energy position with $3B_u$ symmetry. Moreover, the latter transition has a moderate oscillator strength for all homodimers as shown in Table 5-6.

For the S_6 state, all the homodimers share the common feature of significant large intrinsic 2PA cross section between 9000 – 13000 GM. According to the three-level model, where the energetic difference between the one-photon resonance excited state and the virtual intermediate state of the two-photon transition tends to zero, double-resonance effect occurs which enhances the 2PA cross-section dramatically.[149,150] As mentioned in subchapter 4.3, this energetic difference called detuning energy is represented by the term $\omega_{01} - \frac{\omega_{03}}{2}$ in equation (4–11). In this respect for states approaching twice the energy of the S_1 state, the 2PA strength $<\delta^{(2PA)}>$ and consequently the macroscopic 2PA cross-section $\sigma^{(2PA)}$ increases strongly.[151] However, due to the existence of the linear absorption at higher energies (> 14000 cm^{-1}) we were unable to cover this 2PA-allowed S_6 state and determine its maximum cross section by using the 2PIF setup. Again, according to the theoretical calculations the latter exciton state S_6 with $4A_g$ symmetry possesses large 2PA strength, on the same order as the $S_3(3A_g)$ state (**dSQA-1** – **dSQA-3**) or even higher (**dSQA-4** – **dSQA-6**).

Table 5-5: 2PA cross sections $\sigma^{(2PA)}$ at selected energies[c] and 2PA strengths $<\delta^{(2PA)}>$ for selected energy intervals of the parent monomer **SQA** and homodimers **dSQA-1** – **dSQA-6** in toluene.

	$\tilde{\nu}_{S_1}$ /cm^{-1}	$\sigma^{(2PA)}$ /GM	$\tilde{\nu}_{S_2}$ /cm^{-1}	$\sigma^{(2PA)}$ /GM	$<\delta^{(2PA)}>^a$ /a.u.	$\tilde{\nu}_{S_3}$ /cm^{-1}	$\sigma^{(2PA)}$ /GM	$<\delta^{(2PA)}>^b$ /a.u.
SQA	15750	24						
dSQA-1	14390	47	16130	397	3.42x10^4	21980	5740	4.77x10^5
dSQA-2	14490	44	16000	360	2.53x10^4	21980	4660	3.53x10^5
dSQA-3	14270	121	16260	405	2.68x10^4	21980	4330	3.23x10^5
dSQA-4	15270	99	16130	397	2.07x10^4	21980	2670	2.22x10^5
dSQA-5	15040	36	16390	239	1.52x10^4	22470	1530	9.69x10^4
dSQA-6	15040	13	16260	269	1.58x10^4	22222	375	1.69x10^4

[a] The 2PA strength covers that of the S_1 and the S_2 state. Integration limits 14600 – 17800 cm^{-1} (19300 cm^{-1} for **dSQA-6**). [b] Integration limits 17800 – 24000 cm^{-1} (23200 cm^{-1} for **dSQA-6**). [c] The wavenumbers for the assigned states are those with a maximum of 2PA cross section and do not necessarily agree with the wavenumbers in Table 5-1.

Table 5-6: TD-DFT (BHandHLYP/6-31G*) and QR-DFT calculated excitation energies (shifted by 4000 cm^{-1}), oscillator strengths *f* and TPA strengths $<\delta^{(2PA)}>$[a].

	S_1 ($1B_u$)	$J = (\Delta E S_1S_2)/2$	S_2 ($2A_g$)	S_3 ($3A_g$)	S_4 ($2B_u$)	S_5 ($3B_u$)	S_6 ($4A_g$)
	f [$\tilde{\nu}$/cm^{-1}]	/cm^{-1}	$<\delta^{(2PA)}>$/a.u. [$\tilde{\nu}$/cm^{-1}]	$<\delta^{(2PA)}>$/a.u. [$\tilde{\nu}$/cm^{-1}]	*f* [$\tilde{\nu}$/cm^{-1}]	*f* [$\tilde{\nu}$/cm^{-1}]	$<\delta^{(2PA)}>$/a.u. [$\tilde{\nu}$/cm^{-1}]
SQA	1.55 [15892]						$1.12x10^5$ [29147]
dSQA-1[b]	3.55 [14666]	786	1540 [16237]	$1.63x10^6$ [22337]	0.01 [22613]	0.09 [27534]	$1.38x10^6$ [28583]
dSQA-2	3.98 [14442]	759	3880 [15959]	$3.06x10^6$ [22342]	0.05 [22577]	0.19 [26163]	$1.64\ 10^6$ [27454]
dSQA-3	4.21 [14460]	657	1810 [15773]	$3.39x10^6$ [22656[c]]	0.14 [22569[c]]	0.34 [25195]	$2.09x10^6$ [27131]
dSQA-4	3.83 [15037]	430	500 [15897]	$7.40x10^5$ [23281]	0.02 [23311]	0.23 [27050]	$1.61x10^6$ [27776]
dSQA-5	4.11 [15156]	238	198 [15632]	$5.30x10^5$ [24011[c]]	0.14 [23924[c]]	1.1 [25679]	$1.75x10^6$ [27050]
dSQA-6	3.72 [15222]	482	105 [16185]	$2.02x10^4$ [23238]	0 [23242]	0.04 [28744]	$1.29x10^6$ [28825]

[a] The symmetry assignments refer to D_{2h} symmetry although the actual symmetry might be different. n-π* excitations with zero oscillator strength and 2PA cross section are omitted. [b] For **dSQA-1** with C_2 symmetry there are very small oscillator strengths *f* also for the "pseudo" g state and, vice versa, TPA cross sections for the u states, but these are negligible. [c] the energetic order of states is reversed concerning symmetry.

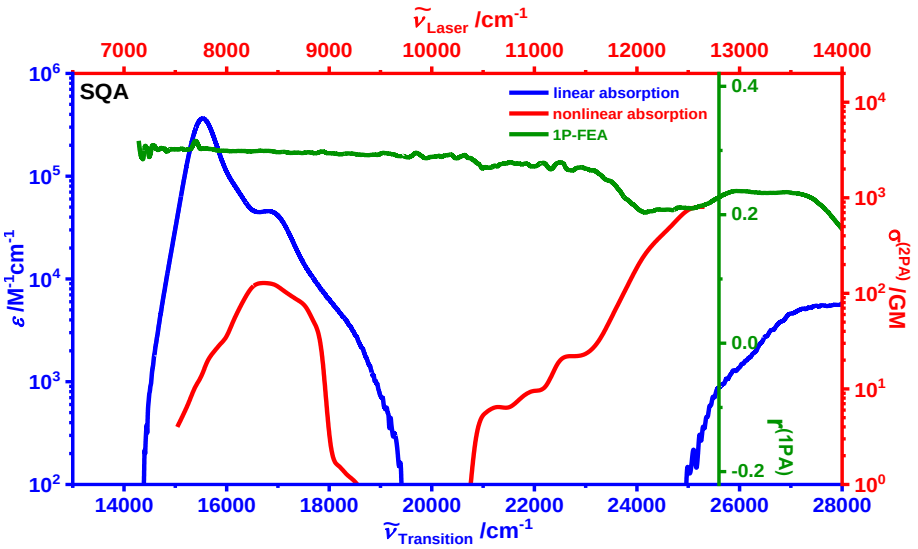

Figure 5-7: A comparison of the linear absorption (blue line), 2PA (red line) and 1P-FEA (green line) spectra of the parent monomer **SQA** in toluene.

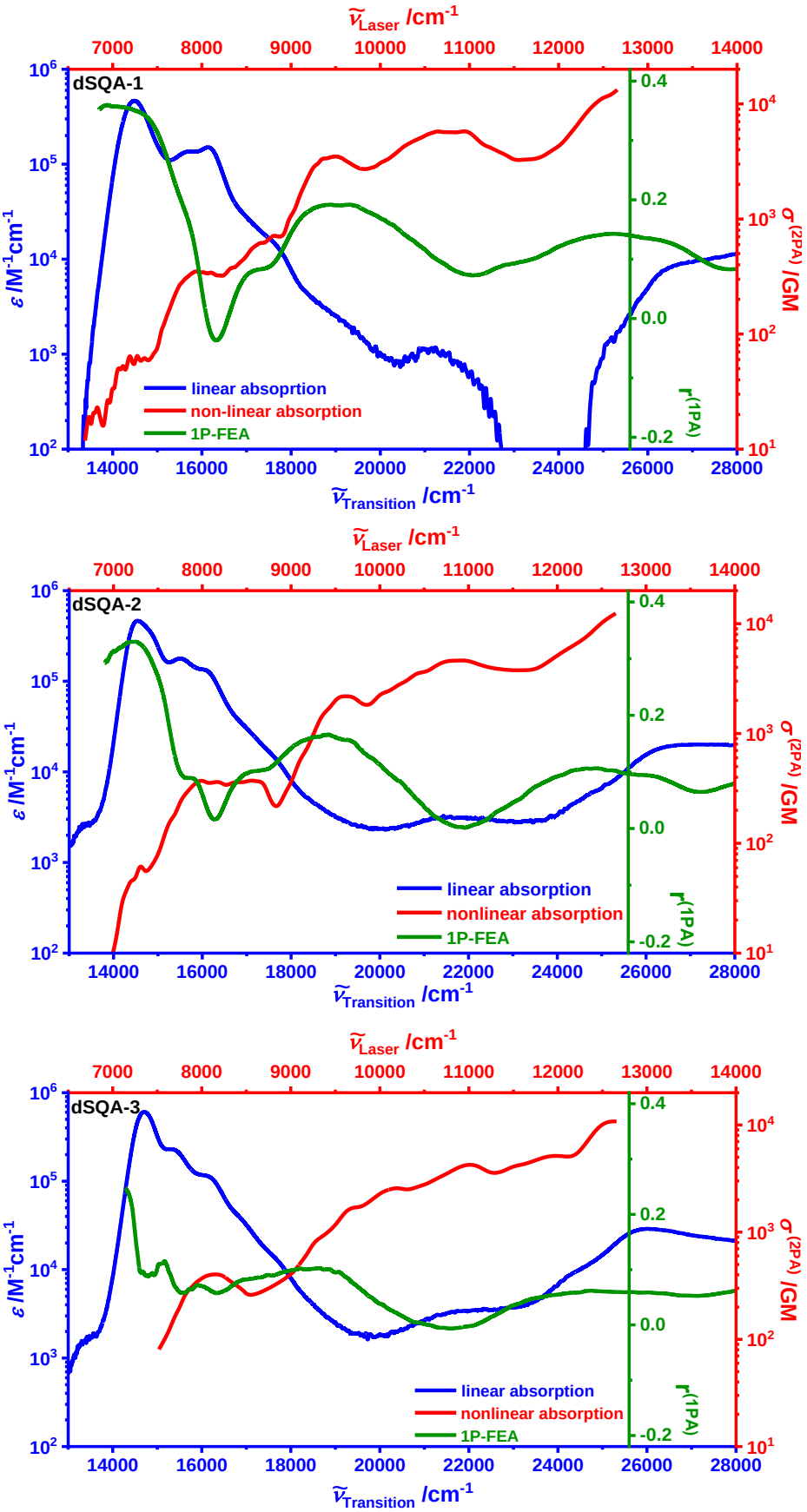

Figure 5-8: A comparison of the linear absorption (blue line), 2PA (red line) and 1P-FEA (green line) spectra of homodimers **dSQA-1**, **dSQA-2** and **dSQA-3** in toluene.

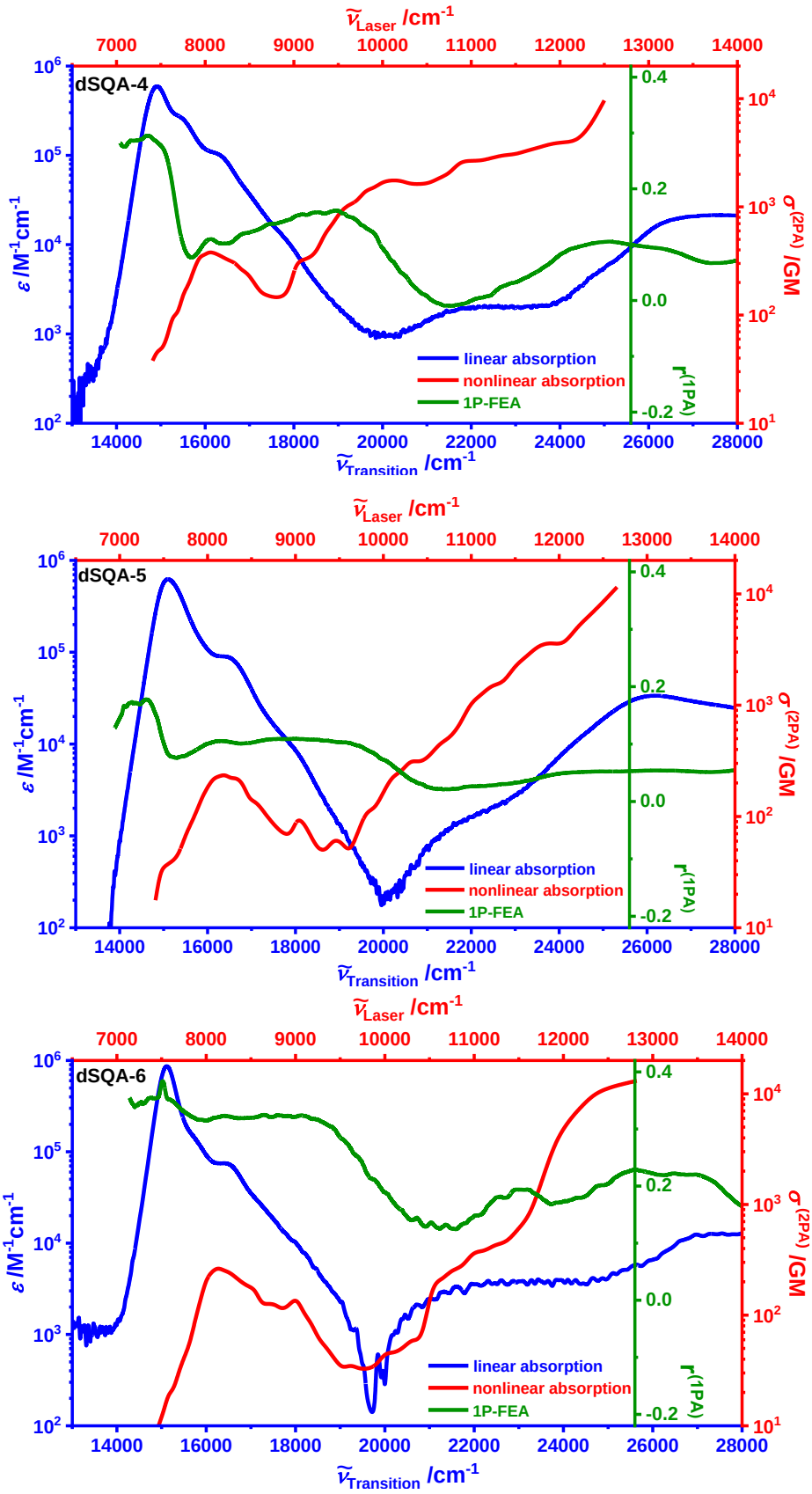

Figure 5-9: A comparison of the linear absorption (blue line), 2PA (red line) and 1P-FEA (green line) spectra of homodimers **dSQA-4**, **dSQA-5** and **dSQA-6** in toluene.

5.1.1.3 Conclusion

To sum up, we have studied a series of squaraine homodimers connected by diverse bridges to probe the correlation between exciton coupling and two-photon absorptivity. The main conclusion, based on the discussed findings, is that the 2PA strength roughly follows the exciton coupling interaction between the squaraine chromophores. The exciton coupling strength and consequently the 2PA strength decreases on going from directly coupled squaraines in **dSQA-1** to **dSQA-5** where the squaraine chromophores are connected through a tolan bridge. One exception is **dSQA-6** which possesses the smallest 2PA cross section although its exciton coupling is quite significant and equals that of **dSQA-4**. Taking into consideration the squaraine center-to-center distance the exciton coupling shows the same trend. On the other hand, in case of **dSQA-6**, where the two squaraine chromophores are connected by a short-saturated bridge, the exciton coupling strength is more similar to **dSQA-4** homodimer with a conjugated phenylene bridge, which in turn places the two squaraines at farther distance. Summarizing, the combination of a short and conjugated bridging unit between the two squaraine chromophores increases the exciton coupling strength and leads to an enhanced 2PA strength in such homodimers. Noteworthy, by tuning the extent of exciton coupling by diverse bridges, sizable values of 2PA cross section up to 5700 GM at *ca.* 11000 cm^{-1} and 12000 GM at 12500 cm^{-1} could be obtained.

Beside these findings, we assigned the spectral positions of transitions and we also characterized them as sketched in Figure 5-10. As can be seen, exciton coupling of the two coupled squaraine chromophores leads to four excited states in the investigated energy region.

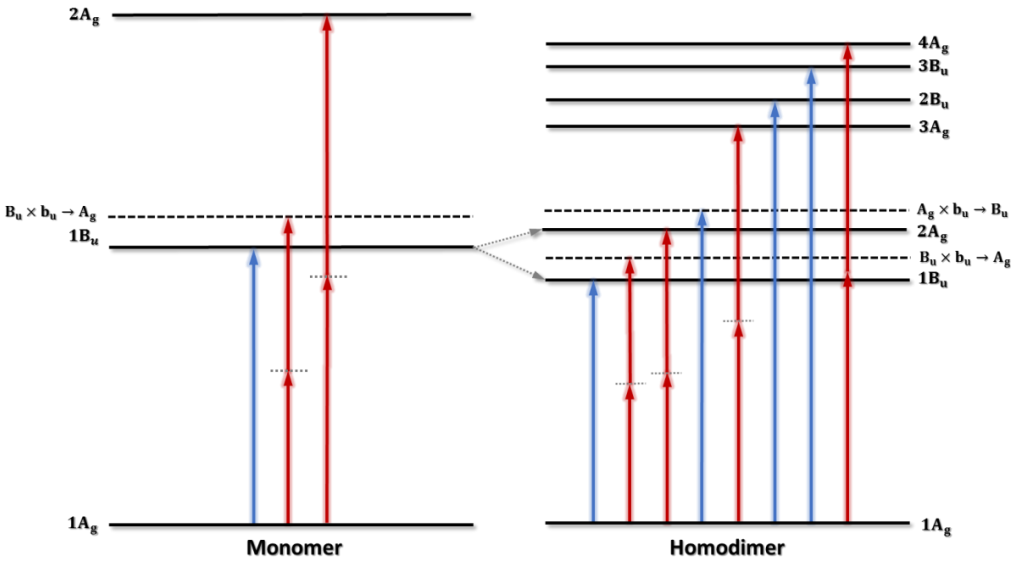

Figure 5-10: Schematic energy state diagram for **SQA** monomer and the homodimers both with D_{2h} symmetry. The blue arrows indicate 1PA allowed transitions, the red arrows 2PA allowed transitions. Uppercase symmetry assignments refer to electronic states, lowercase assignments to vibrations. Energies are not to scale.

The first exciton state of the monomer splits in two excited state in the homodimers, where the first exciton state ($1B_u$) is strongly 1PA-allowed and the second ($2A_g$) is weakly 2PA-allowed. The $2A_g$ states have overall small 2PA cross section which do not vary greatly within the series of homodimers. This can be attributed to the small squared transition dipole moment in the series of squaraine dimers as we deal with chromophores which lack significant local charge-transfer contribution. However, the third exciton state ($3A_g$) is strongly 2PA-allowed and the fourth ($2B_u$) is only weakly 1PA-allowed. In the case of the third exciton state $3A_g$ the corresponding squared transition dipole moment is large and its magnitude follows qualitatively the exciton coupling strength. This could be rationalized by applying the three-level model.

5.1.2 SQB-Based Homodimers[V]

In light of our previous work, we have gained experience in understanding of exciton coupling theory in the special case of nonlinear photophysical properties by altering the coupling unit between the squaraines chromophores. Going a step further, let us add the impact of molecular symmetry on the 2PA properties in the "equation". Thereby, here two rigid benzodipyrrolenine-based squaraine dimers **pySQB*trans*** and **pySQB*cis*,** formed in two isomers were investigated, with *transoid* and *cisoid* configuration, respectively, as shown in Figure 5-11.

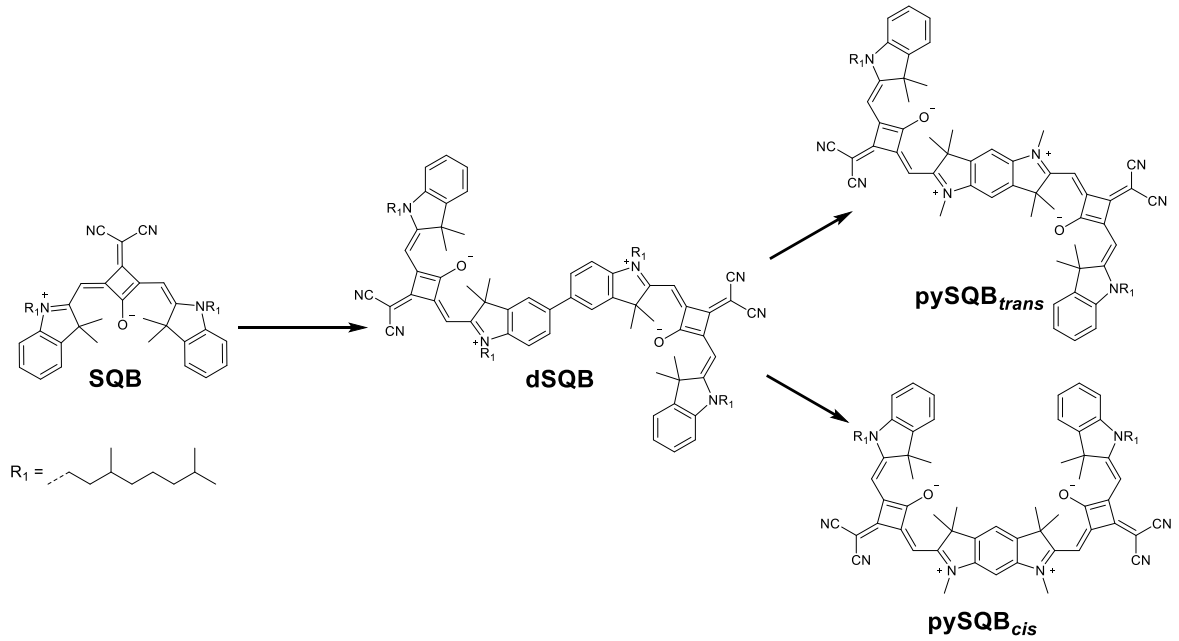

Figure 5-11: Chemical structure of parent squaraine **SQB** and the dimer **dSQB** with biaryl connection and the benzodipyrrolenine squaraine dimers **pySQB*trans*** and **pySQB*cis*.**

[V]Reprinted or adapted in part from: "*Enhanced two–photon absorption and promising broad energy range optical power limiting properties of transoid and cisoid benzodipyrrolenine-fused squaraine dimers.*", E. Michail, M. H. Schreck, L. Wittmann, M. Holzapfel and C. Lambert, Chem. Mater., 2021, 33, 9, 3121-3131.

The two homodimers were also synthesized by Dr. M. H. Schreck,[129] based on two fused indolenine squaraine chromophores **SQB** and share a single benzodipyrrolenine core unit. This benzodipyrrolenine bridging unit ensures that the **pySQB*trans*** and **pySQB*cis*** homodimers exhibit a fixed geometry, where symmetry aspects of the optical properties can be investigated without considering the formation of symmetry breaking due to rotamers/conformers. Employing two different isomeric benzodipyrrolenine bridging units led to two different squaraine dimers, one with *transoid* geometry and C_{2h} symmetry, and one with the *cisoid* geometry and C_{2v} symmetry. Moreover, in order to further substantiate our assumptions, the monomeric parent chromophore **SQB** and the homodimer **dSQB** with a flexible biaryl axis also take part in the discussion. Recently, we investigated the photophysical properties of the **SQB** and **dSQB** compounds, which were addressed in our previous studies by Ceymann *et al*.[128] and Röhr *et al*.[131]

5.1.2.1 Linear Optical Spectroscopy

As expected, the linear absorption spectra of the investigated benzodipyrrolenine homodimers show all the relevant features of the squaraine homodimers as discussed above. Moreover, the fluorescence spectra of both investigated squaraine compounds show approximate mirror image relationship of the respective absorption spectrum of the monomer accompanied with a small Stokes shift. The steady-state linear absorption and normalized emission spectra of the investigated benzodipyrrolenine homodimers are presented in Figure 5-12 in toluene.

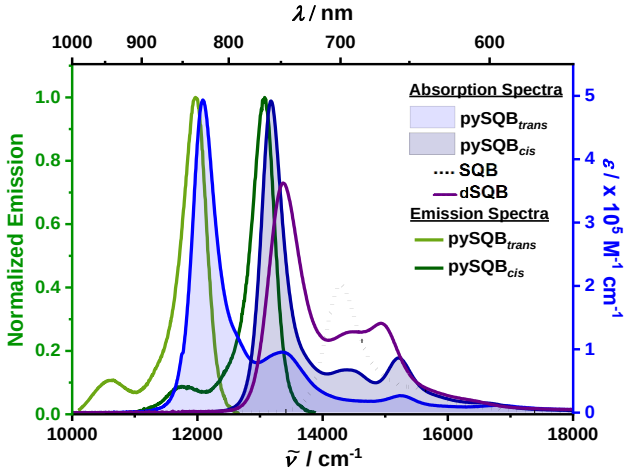

Figure 5-12: Linear absorption and normalized fluorescence spectra of benzodipyrrolenine squaraine dyes **pySQB*trans*** and **pySQB*cis*** in toluene and the absorption spectra of the parent monomer **SQB** and the dimer **dSQB** in toluene.

UV/Vis Absorption

According to linear absorption spectra, squaraine homodimers **pySQB*trans*** and **pySQB*cis*** exhibit a sharp and intense main absorption band in the red spectral region at 12100 cm^{-1} and 13200 cm^{-1}, respectively. This low-energy absorption band is attributed to the $S_1 \leftarrow S_0$ transition accompanied by

a vibronic progression at *ca.* 13200 cm^{-1} for **pySQB**$_{trans}$ and at 14300 cm^{-1} for the **pySQB**$_{cis}$. Furthermore, an additional less intense absorption peak at *ca.* 15200 cm^{-1} for both benzodipyrrolenine squaraines dimers is assigned to the $S_2 \leftarrow S_0$ transition, followed by vibronic progression at around 16700 cm^{-1}. Again, we interpret the presence of this S_2 exciton state within the investigated homodimers as being due to the exciton Davydov splitting of the first excited state of the parent monomer **SQB** as argued above for the **dSQA** homodimers. Furthermore, additional less intense shoulders and peaks are observed between *ca.* 20000 up to 30000 cm^{-1}. A logarithmic plot of the linear absorption spectra of the investigated benzodipyrrolenine homodimers in toluene are depicted in Figure 5-13. For the convenience of representation, the linear absorption spectra of the parent monomer **SQB** and the homodimer with flexible **dSQB** are also shown.

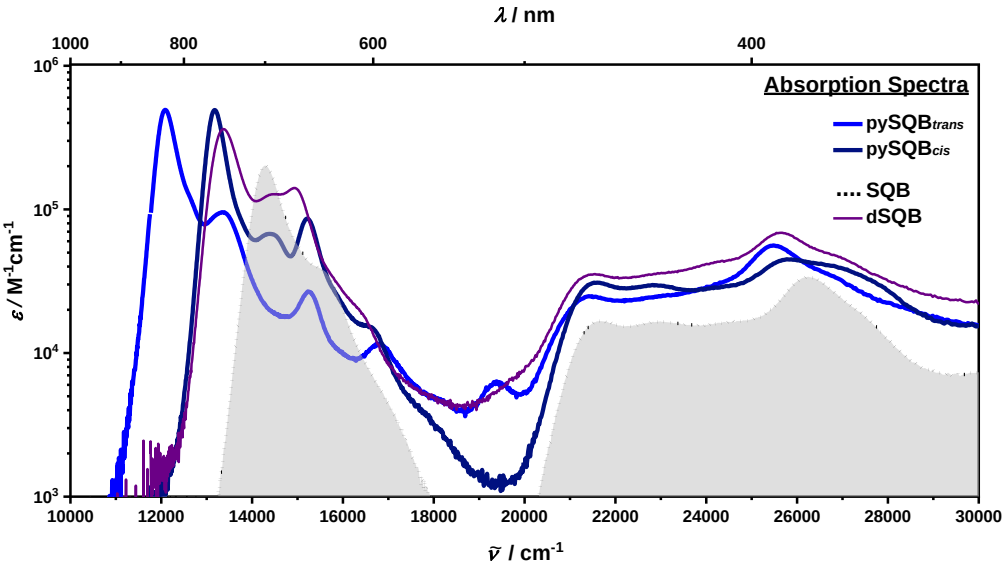

Figure 5-13: A logarithmic plot of the linear absorption of benzodipyrrolenine squaraine dyes **pySQB**$_{trans}$ and **pySQB**$_{cis}$ with the absorption spectra of the parent monomer **SQB** and the dimer **dSQB** in toluene are depicted for comparison.

Again, the exciton coupling strength *J* can be estimated from the linear absorption spectra by taking half of the difference between the absorption maximum of the lower ($\tilde{\nu}_{S_1}$) and the upper ($\tilde{\nu}_{S_2}$) exciton transitions. Thereby, both **pySQB**$_{trans}$ and **pySQB**$_{cis}$ display high coupling strength which yields J = 1580 cm^{-1} for **pySQB**$_{trans}$ and J = 1020 cm^{-1} for **pySQB**$_{cis}$. The larger coupling in the *transoid* **pySQB**$_{trans}$ emphasizes the effect of *para*-conjugation vs. the *meta*-conjugation pathway in *cisoid* **pySQB**$_{cis}$. Moreover, in the case of the **pySQB**$_{cis}$ the localized transition moments possess an angle of *ca.* 120°, as indicated in Figure 5-14, which also reduces dipole-dipole coupling. Here, attention is drawn to the fact that the *para*-conjugation pathway of the central benzodipyrrolenine of **pySQB**$_{trans}$ leads to coupling strength which is about twice as large as that of **dSQB** (J = 800 cm^{-1}). This is caused by the fused nature of benzodipyrrolenine compound´s conjugation way and the somewhat closer distance of the localized transition dipoles compared to **dSQB**.

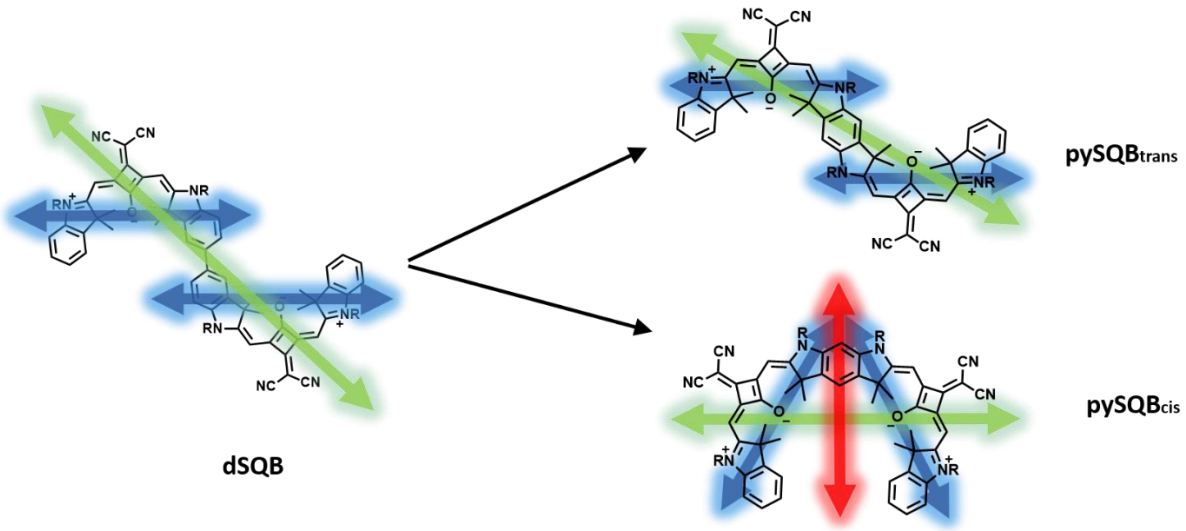

Figure 5-14: The different type of orientations of the dimer **dSQB** with biaryl connection and the investigated benzodipyrrolenine isomers squaraine **pySQB*trans*** and **pySQB*cis***. The blue arrows indicate estimated localized transition moments of the **SQB** $S_1 \leftarrow S_0$ transition, green arrows indicate the transition moments of the **pySQB*trans*** and **pySQB*cis*** $S_1 \leftarrow S_0$ transitions. Finally, the red arrow refers to the allowed $S_2 \leftarrow S_0$ transition of **pySQB*cis***.

Owing to exciton coupling, **pySQB*trans*** shows a dramatic red-shift of 2200 cm^{-1} which is almost twice as large as that of **pySQB*cis*** in respect to the parent monomer **SQB**. The shifting of the $S_1 \leftarrow S_0$ transition in both homodimers can be attributed to *J*-type exciton coupling of localized transition moments, which are assumed to be in a head-to-tail manner in **pySQB*trans***.

At the same time, the absorption spectra of the **dSQB** homodimer, which due to the flexible axis exists in different conformers (rotamers), is a superposition of the spectra of two different conformers. The lowest energy absorption maximum indicates the same bathochromic shift as **pySQB*cis***. This effect can be addressed from the orientation of the transitions in both **pySQB*cis*** and **dSQB** homodimers which are polarized along the long axis of the respective molecules and that molecular arrangement does not affect the relative energies of the conformers to a great extent. Indeed, this assumption is supported by Bredas *et al.*[152] who showed that centrosymmetric *transoid* squaraine conformation and the non-centrosymmetric *cisoid* conformation behave essentially in the same way concerning the properties of exited states.

At the same time, the upper exciton state S_2 located for both **pySQB*trans*** and **pySQB*cis*** homodimers at the same energetic position at *ca.* 15200 cm^{-1} and is blue-shifted compared to the lower exciton state S_1 of the **SQB** by about 960 cm^{-1}. The latter electronic state is energetically close to the upper exciton state of **dSQB** in both benzodipyrrolenine homodimers and as already outline before, is forbidden by symmetry as 1PA process. In the case of that homodimer may form an equimolar mixture of two rotamers. Thus, in both conformers, the out-of-phase arrangement of transition moments breaking

the centrosymmetry and the $S_2 \leftarrow S_0$ transition becomes weakly allowed. In case of **pySQB*trans*** the latter transition is also spectroscopically observable because it gains oscillator strength by vibronic coupling to an out-of-plane bending vibration which breaks the symmetry of the wavefunction. Indeed, while both investigated homodimers show the same extinction coefficient for the S_1 exciton state, **pySQB*cis*** with C_{2v} symmetry, where $S_2 \leftarrow S_0$ transition is allowed and is polarized along the C_2 axis, shows a three times higher extinction coefficient for the upper exciton state S_2 than **pySQB*trans***.
The squared transition dipole moments between the ground state S_0 and the lowest exciton state S_1 have been determined (through equation (4–12)) by integration over the whole exciton manifold (S_1 and S_2) due to difficulties in separation of these two partly overlapping absorption bands. The results are presented in the Table 5-7 with the absorption maxima and extinction coefficients of characteristic bands, as well as the estimated exciton coupling strength which is also listed.

Table 5-7: The absorption maxima of S_1 and S_2 state, exciton coupling energy and dipole strength of the parent monomer **SQB** and dimers **dSQB**, **pySQB*trans***, and **pySQB*cis*** in toluene.

	$\tilde{\nu}_{S_1}$/cm^{-1}	ε_{S_1} / M^{-1}cm^{-1}	$\tilde{\nu}_{S_2}$/cm^{-1}	ε_{S_2}/ M^{-1}cm^{-1}	J/ cm^{-1} [b]	μ^2/ D^2 [c]
SQB [a]	14300	2.02 x 10^5	-	-	-	93
dSQB [a]	13400	3.62 x 10^5	14900	1.40 x 10^5	800	226
pySQB*trans*	12100	4.92 x 10^5	15200	2.65 x 10^4	1580	231
pySQB*cis*	13200	4.92 x 10^5	15200	8.61 x 10^4	1020	195

[a] See also ref. [128] and [131]. [b] Estimated as $J = (\tilde{\nu}_{S_2} - \tilde{\nu}_{S_1})/2$ and verified by 1P-FEA spectra. [c] Dipole strength of the total exciton manifold.

One-photon fluorescence excitation anisotropy

Measurements of the 1P-FEA in viscous poly-THF could give further insight in the energetic position of excited states. The 1P-FEA spectra for both **pySQB*trans*** and **pySQB*cis*** homodimers is depicted in Figures 5-16 and 5-17, in which for sake of comparison a logarithmic plot of 1PA and 2PA spectra with the corresponding symmetry assignment are also shown.
The lowest energy exciton state of benzodipyrrolenine isomers shows an anisotropy of $r_{1PA} \approx 0.4$ which is caused by parallel transition moments of absorption and emission of the excited state S_1. The 1P-FEA values drops to *ca.* $r_{1PA} = 0.2$ at 15600 cm^{-1} for the **pySQB*trans*** compound and to $r_{1PA} = -0.04$ for the **pySQB*cis*** in the spectral region where the $S_2 \leftarrow S_0$ transition is located. Again, the latter reduced 1P-FEA values indicate a pronounced angle between absorption and emission transition moment, where in the special case of an angle of 90° one would expect the smallest possible anisotropy of $r_{1PA} = -0.2$. Our finding suggests more excited states in the region up to 20000 cm^{-1} which cannot be predicted by Kasha`s exciton coupling theory, but which again can be explained by mixing of orbital

configurations.[128] As expected, there is a number of additional states above 18000 cm^{-1} which are visible as anisotropy changes in the 1P-FEA spectra. In case of the **pySQB*trans*** dimer the 1P-FEA spectrum shows a low anisotropy value of r_{1PA} = 0.07 at 19700 cm^{-1} and again a rather high value of r_{1PA} = 0.35 at 21400 cm^{-1}. These findings, which are supported by TD-DFT computations, point towards two additional exciton states S_3 and S_4 that possess $3A_g$ and $2B_u$ symmetry, respectively. At the same time, in **pySQB*cis*** there is a slight increase of anisotropy to 0.13 at *ca.* 18500 cm^{-1} and finally an increase to 0.25 at *ca.* 21400 cm^{-1}, which indicate the presence of two exciton states. However, the joint findings from the 1P-FEA and the DFT computations demonstrate that there is a state in-between, with negligible oscillator strength.

Indeed, because 1PA into S_3 ($2B_2$) which is polarized perpendicular to the C_2 (B_2) axis and S_4 ($3A_1$) which is polarized along the C_2 axis, are overlapping, this leads to the observed reduced anisotropy of 0.13 since averaging of r_{1PA} = 0.4 for parallel absorption and emission transition moments and r_{1PA} = -0.2 for 90° angle between them, yields r_{1PA} = 0.1, which is in agreement with the observation. The DFT computations corroborate these experimental findings and yield a negligible oscillator strength of f = 0.03 for the S_3 ($2B_2$) and an intense 1PA (f = 1.08) for the S_5 ($3B_2$). Furthermore, likewise to the previous study, our results were substantiated by DFT calculations based on the TD-DFT and QR-DFT which were performed by Dr. Marco Holzapfel. Again, due to inherent DFT problems the computed state energies turned out to be generally too high and are therefore empirically down-shifted by 4000 cm^{-1} for the **pySQB*trans*** dimer and 3600 cm^{-1} for the **pySQB*cis***, in order to match with the lowest energy transition (S_1). The results of these calculations are summarized in Table 5-9 and the relative comparison with the experimental 1PA and 2PA spectra is given in Appendix 8.4 (Figure 8-7).

Fluorescence Spectroscopy

The near-mirror image spectra between the fluorescence spectra of the benzodipyrrolenine squaraine dimers and the absorption spectrum of the monomer **SQB** indicate that the fluorescence originates from the lower exciton state. This comes in agreement with the model of exciton coupling and is in accordance with *J*-type aggregate behaviour. This was further supported by the determination of the squared fluorescence transition dipole moments calculated via Strickler-Berg equation using the fluorescence lifetimes and quantum yields (see Appendix 8.2). The absorption dipole strength (μ_{01}^2 = 231 D^2 for the **pySQB*trans*** and μ_{01}^2 = 195 D^2 for the **pySQB*cis***) are very similar (within the experimental error) to those of the corresponding emission dipole strength (μ_{fl}^2 = 204 D^2 for the **pySQB*trans*** and μ_{fl}^2 = 177 D^2 for the **pySQB*cis***). The latter confirms the initial assumption that, in case of the **pySQB*trans*** and **pySQB*cis*** benzodipyrrolenine squaraine dimers, the fluorescence mainly occurs from the S_1 excited state and thus provides Strickler-Berg symmetry.[153] The deviation also reflects

the fact that for the determination of the absorption transition moment we integrated over the whole exciton manifold (S_1 and S_2), while emission refers to S_1 only.

Interestingly, the two investigated benzodipyrrolenine squaraine dimers show significant difference in fluorescence quantum yields φ_{fl}. The **pySQB*trans*** and **pySQB*cis*** compounds possess fluorescence quantum yields φ_{fl} of 0.26 and 0.80, respectively. The average fluorescence lifetimes $\bar{\tau}_{fl}$ for the **pySQB*trans*** and **pySQB*cis*** were found to be 0.86 ns and 2.30 ns, respectively, which nicely correlates with the fluorescence quantum yield values. The time-depended fluorescence measurements were presented in the Table 5-8.

Table 5-8: The emission maximum, fluorescence lifetimes τ_{fl} with the relative amplitudes in parentheses, the average fluorescence lifetimes values $\bar{\tau}_{fl}$, the square of the fluorescence transition moments and fluorescence quantum yield of the parent monomer **SQB** and dimers **dSQB**, **pySQB*trans*,** and **pySQB*cis*** in toluene.

	$\tilde{\nu}_{fl}$ / cm^{-1}	τ_{fl} / ns (a_n)	$\bar{\tau}_{fl}$ / ns	μ_{fl}^2 / D^2	φ_{fl}
SQB [a]	14000	3.46 (1.00)	3.46	81	0.75
dSQB [a]	13100	1.98 (0.42) 3.26 (0.58)	2.73	125	0.68
pySQB*trans*	12000	0.86 (1.00)	0.86	204	0.26
pySQB*cis*	13100	2.30 (1.00)	2.30	177	0.80

[a] See also ref [128] and [131].

5.1.2.2 Nonlinear Spectroscopy

Both benzodipyrrolenine squaraines dimers in toluene feature extremely high 2PA cross-section over the entire manifold of excited states in the spectral region 13000 – 22000 cm^{-1}. It is most remarkable that in the **pySQB*trans*** dimer the 2PA cross section reaches enormous values of *ca.* 14000 GM at 16000 cm^{-1} and 90000 GM at 22000 cm^{-1} which is by far the highest among all the squaraine dimers investigated in our previous studies.[116,128,130] The 2PA spectra of the **pySQB*trans*** and **pySQB*cis*** homodimers are depicted together with the linear absorption spectra in Figure 5-15.

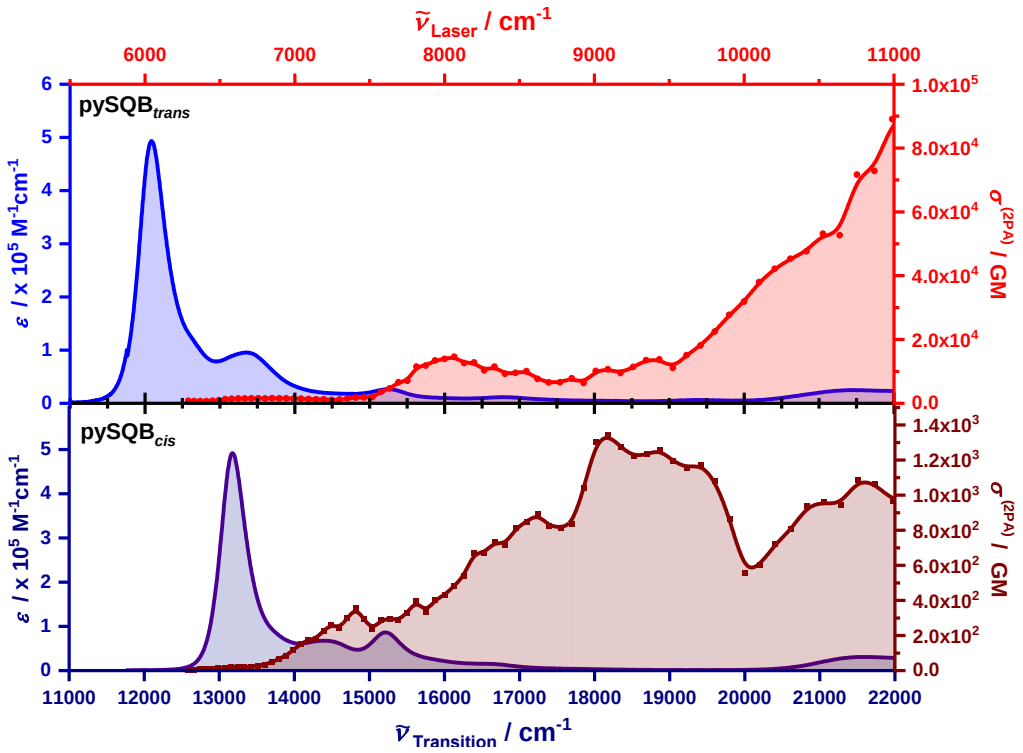

Figure 5-15: A comparison of the linear absorption (blue line) and 2PA cross section (red line) spectra of benzodipyrrolenine squaraine dyes **pySQB$_{trans}$** (top) and **pySQB$_{cis}$** (bottom) in toluene.

*2PA of **pySQB$_{trans}$***

As already outlined above, the **pySQB$_{trans}$** homodimer belongs to the C_{2h} symmetry possessing a center of inversion. Thus, according to the selection rules for the electric dipole transitions, two-photon transition processes from the totally symmetric ground state $1A_g$ to singlet excited states with the same gerade symmetry are allowed, whereas 1PA processes are forbidden. This selection rule is obvious in the lower energy region where the 1PA and 2PA bands can be discerned.

In the spectral region between 13400 – 14500 cm^{-1} the **pySQB$_{trans}$** exhibits the least intense 2PA band with a 2PA cross-section of *ca.* 1600 GM which is due to vibronic coupling of the S_1 (B_u) state. According to the Herzberg-Teller effect,[154] the presence of this two-photon transition is caused by a b_u in-plane bending that couples to the B_u state yielding a totally symmetric wavefunction (B_u x $b_u \rightarrow A_g$).[116,155]

The next 2PA band at 14500 – 17500 cm^{-1} with the maximum 2PA cross section of *ca.* 13900 GM at 16000 cm^{-1} is assigned to the $S_2 \leftarrow S_0$ transition. By taking into account the linear absorption and the 1P-FEA spectra (see Figure 5-16) the corresponding 2PA band is notably blue shifted from the linear absorption band due to enhanced vibronic transitions. Thus, the $2A_g$ state is assigned at 15380 cm^{-1} and the diverse peaks which are located at lower and higher energies appear to be a vibronic progression. At higher transition energies (> 18000 cm^{-1}) the 2PA cross-section rises steadily up to *ca.* 90000 GM at 22000 cm^{-1}. The 1PA and 2PA spectra are highly overlapping between 18000 – 22000 cm^{-1} due to the high state density in this spectral region. However, the 1P-FEA spectra

and the QR-DFT calculations (see below) indicate that this broad 2PA band is caused by a single electronic state $3A_g$ at 19200 cm^{-1} with a broad vibronic progression. Indeed, the QR-DFT calculations predict the strongest 2PA strength of 3.5 x 10^6 a.u. for the latter transition at 19200 cm^{-1}.

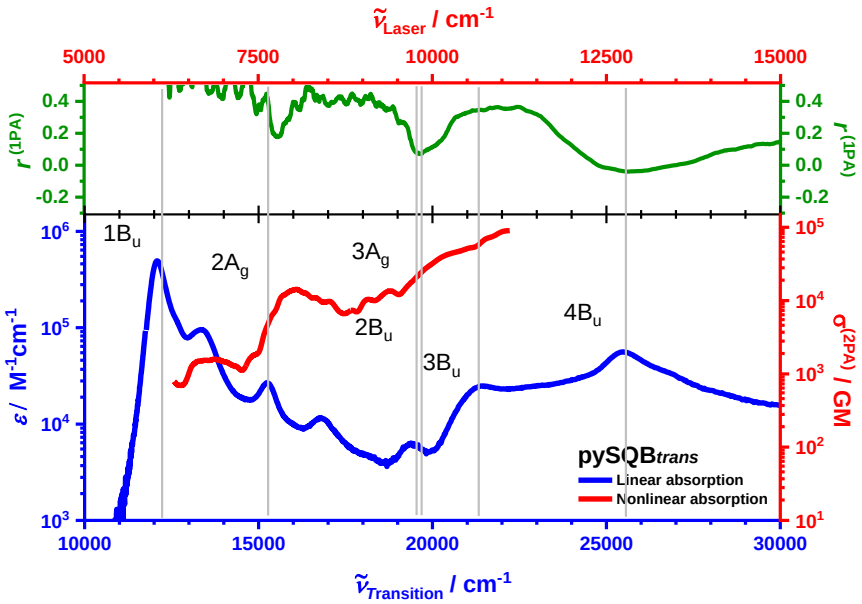

Figure 5-16: A comparison of the 1PA (blue line), 2PA spectra (red line) and FEA (green line) of the **pySQB*trans*** benzodipyrrolenine squaraine in toluene. The gray lines are a guide to the eye and indicate electronic states that can be identified due to changes of their anisotropy *r* and/or peaks in the 1PA/2PA spectra. The symmetry assignments were made with help of DFT calculations.

From the few-state model point of view, using the three-level model we can rationalize that the reason for the fact that the 2PA transition $1A_g \leftarrow 3A_g$ is about one order of magnitude higher than to the transition $1A_g \leftarrow 2A_g$ which is due to the higher transition moment between the $1B_u$ state and the respective 2PA state ($2A_g$ / $3A_g$). By applying the equation (4–11), which relates the rotationally averaged 2PA strength $<\delta^{(2PA)}>$ with the transition dipole moment μ_{12}/μ_{13} between the one-photon resonant excited state $S_1(1B_u)$ and the two-photon resonant excited state $S_2(2A_g)$ / $S_3(3A_g)$ in the three-level model, we obtain that $\mu_{13} >> \mu_{12}$. This can be explained by the small charge transfer contribution for the case of squaraine dyes where $\mu_{12} = \Delta\mu \approx 0$ as is supported by the TD-DFT calculations where for the parent monomer **SQB** a dipole moment difference $\Delta\mu_{12} = 2.8$ D is calculated. It has to be mentioned, that we refrain to give experimental $<\delta^{(2PA)}>$ values through the equation (4–7) like in chapter 5.1.1, because it is difficult to separate the strongly overlapping 2PA bands.

*2PA of **pySQB**$_{cis}$*

In case of the non-centrosymmetric *cisoid* isomer **pySQB**$_{cis}$ with C_{2v} symmetry, the one-photon allowed exciton states are also accessible by two-photon transition process. The **pySQB**$_{cis}$ homodimer exhibits structured 2PA bands with large widths, however with about one order of magnitude smaller values than **pySQB**$_{trans}$. At the lowest exciton transition $S_2 \leftarrow S_0$ ($1B_2 \leftarrow 1A_1$) at 12100 cm^{-1} the 2PA cross section is 20 GM and it rises to *ca.* 360 GM where the vibronic shoulder of the S_1 state is visible. At higher energies where the $S_2 \leftarrow S_0$ ($2A_1 \leftarrow 1A_1$) transition is located the maximum 2PA cross section of 850 GM was not found at the 1PA peak but at the vibronic shoulder at *ca.* 17100 cm^{-1}. The overall highest 2PA cross section (1340 GM) is found at 18200 cm^{-1} for the $S_4 \leftarrow S_0$ ($3A_1 \leftarrow 1A_1$) transition and is confirmed by the QR-DFT calculations which also yield the highest 2PA strength of 3.2 x 10^5 a.u.

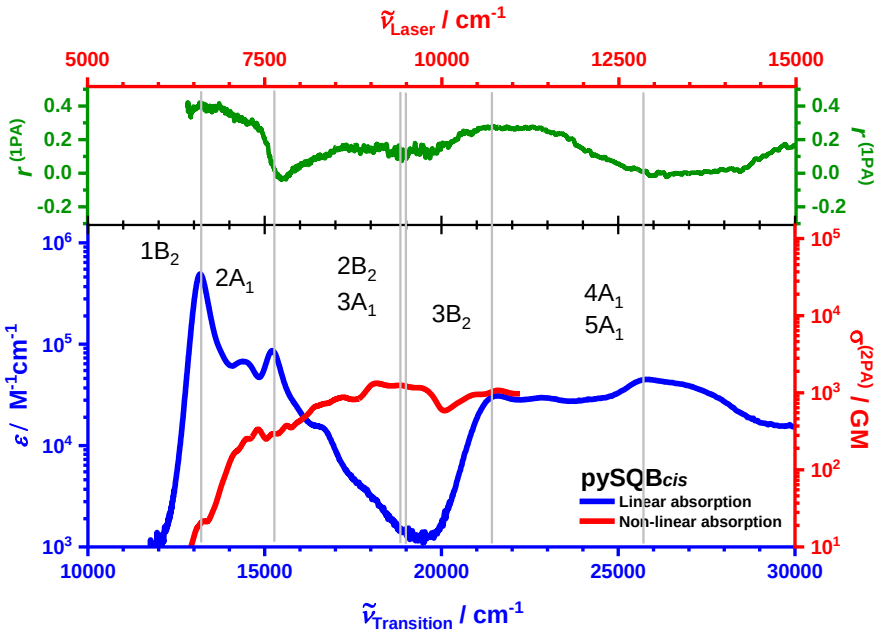

Figure 5-17: A comparison of the 1PA (blue line), 2PA spectra (red line) and FEA (green line) of the **pySQB**$_{cis}$ benzodipyrrolenine squaraine in toluene. The gray lines are a guide to the eye and indicate electronic states that can be identified due to changes of their anisotropy *r* and/or peaks in the 1PA/2PA spectra. The symmetry assignments were made with help of DFT calculations.

Despite the fact that the *cisoid* configuration compound **pySQB**$_{cis}$ is non-centrosymmetric, as it belongs to the C_{2v} point group, the two-level model is insufficient to describe the 2PA strength. By trying to approach the rotational averaged 2PA strength of the diverse transitions by the two-state model through the equation (4–10), we cannot clarify the huge differences of the 2PA cross section that we obtained in the experiment or that is predicted by the DFT computations (e.g. between S_3 and S_4). Large 2PA strengths can be found, if the static dipole moment difference $\Delta\mu_{gf}$ between the ground state and the final 2PA state is large, if the squared transition moment μ_{gf} into that state is intense and

if the angle θ_{gf} between the $\Delta\mu_{gf}$ and μ_{gf} is small. The latter holds for all excitations in A_1 symmetry (e.g. S_2 and S_4), as both the transitions and dipole moment differences are polarized along the C_2 axis. Indeed, the TD-DFT computations yield dipole moment differences of about 2 – 3 D for the transitions $S_1 - S_4$ ($\Delta\mu_{01}$ = 2.34 D; $\Delta\mu_{02}$ = 2.96 D; $\Delta\mu_{03}$ = 2.42 D; $\Delta\mu_{04}$ = 2.34 D). However, even considering the angle term which in the present cases amounts to either 1 or 3, neither the dipole moment difference nor the transition dipole moment can be made responsible for the huge differences of the 2PA cross sections that we obtained experimentally or by theoretical calculations. This leads to the conclusion, that although the **pySQB*trans*** and the **pySQB*cis*** dimers are isomers, the 2PA spectra show that the symmetry has a huge impact on the 2PA cross section, which is about one order of magnitude larger for the *transoid* isomer. In the framework of a three-state model, this behavior can only be explained by smaller transition moments between excited states μ_{if} in **pySQB*cis*** compared to **pySQB*trans*** because the transition moment μ_{gi} into S_1 is very large and dominates the three-state pathways practically equally for both isomers.

Table 5-9: TD-DFT and QR-DFT calculated transition energies $\tilde{\nu}_{\mathrm{tran.}}$, oscillator strengths *f* and 2PA strengths $<\delta^{(2PA)}>$ at BHandHLYP/6-31G*.

	Irred. rep	$\tilde{\nu}_{\mathrm{tran.}}{}^{a}$ / cm^{-1}	*f*	$<\delta^{(2PA)}>$a.u.	Irred. rep	$\tilde{\nu}_{\mathrm{tran.}}{}^{b}$ / cm^{-1}	*f*	$<\delta^{(2PA)}>$/ a.u.
	pySQB*trans*				pySQB*cis*			
S_1	$1B_u$	12 102	2.48	0	$1B_2$	13 146	1.93	2.43 x 10^3
S_2	$2A_g$	14 520	0	8.21 x 10^3	$2A_1$	14 747	0.37	2.14 x 10^3
S_3	$3A_g$	19 197	0	3.47 x 10^6	$2B_2$	19 815	0.03	0.5
S_4	$2B_u$	20 027	0.12	0	$3A_1$	19 868	0.001	3.19 x 10^5
S_5	$3B_u$	23 358	0.94	0	$3B_2$	23 790	1.08	3.56 x 10^4
S_6	$4A_g$	24 440	0	2.14 x 10^5	$4A_1$	24 426	0.35	1.43 x 10^5
S_7	$4B_u$	26 934	0.48	0	$5A_1$	27 756	0.35	3.12 x 10^6
S_8	$5A_g$	28 071	0	5.30 x 10^{10}	$4B_2$	27 790	0.07	1.05 x 10^5
S_9	$6A_g$	29 337	0	2.69 x 10^8	$6A_2$	30 035	0	1.48 x 10^8
S_{10}	$1A_u$	29 767	0	0	$1B_1$	30 035	0	0.4

[a] The calculated energies are shifted by 4000cm^{-1}

[b] The calculated energies are shifted by 3600cm^{-1}.

5.1.2.3 Conclusion

This section provides a continuation of the previous subchapter and considers the exciton coupling effects on the nonlinear optical properties of two benzodipyrrolenine squaraine homodimers with fixed geometry. In this section, the centrosymmetric **pySQB*trans*** with *transoid* geometry and C_{2h} symmetry, and the non-centrosymmetric **pySQB*cis*** with *cisoid* geometry and C_{2v} symmetry were

studied. Both homodimers in toluene solution exhibit extremely high 2PA cross section with those of **pySQB**$_{trans}$ being at least on order of magnitude higher than those of **pySQB**$_{cis}$ over the whole accessible spectral range. Two major conclusions can be drawn from the above study: i) Despite the fact that the two squaraine dimers are isomers, the 2PA spectra indicated that the symmetry has a huge impact on the two-photon absorptivity which is one order of magnitude larger for the *transoid* isomer. ii) The *para*-conjugation pathway in **pySQB**$_{trans}$ increases the electronic coupling of the two chromophores compared with the *meta*-conjugation pathway in **pySQB**$_{cis}$, that is, the substitution pattern of the nitrogen atoms of the central benzodipyrrolenine units. Furthermore, the **pySQB**$_{trans}$, owing *para*-conjugation pathway shows enhanced electronic coupling between the two **SQB** squaraine moieties to about twice of that of the recently investigated **dSQB** homodimer with a biaryl connection.

In the light of the two different molecular symmetries, the selection-rules for the electric dipole transition and consequently the origin of the nonlinear absorption in the two benzodipyrrolenine is also different. Thus, for the centrosymmetric **pySQB**$_{trans}$ compound the excited states with *u*-symmetry are one-photon allowed and the excited states with *g*-symmetry are two-photon allowed. On the other hand, for the non-centrosymmetric **pySQB**$_{cis}$ compound one-photon allowed states are also accessible by two-photon transition process.

Remarkably, the **pySQB**$_{trans}$ dimer features by far the highest 2PA cross section (up to 90000 GM) among all the squaraine homodimer investigated in our previews studies and is -to the best of our knowledge- comparable or even higher than the highest reported 2PA cross section of organic low molecular weight chromophore to date. This strong 2PA cross section in a broad energy range of **pySQB**$_{trans}$ prompted us to measure its optical power limiting behavior as presented in Chapter 6.1.

5.2 Effect of Bridging on the 2PA

The important benefit of intramolecular charge-transfer on 2PA enhancement was quickly recognized, and thus, the functionalization of molecules with an π-electron rich (π-donor, D) or/and π-electron demanding (π-acceptor, A) moieties was demonstrated to further enhance 2PA cross section. J. W. Perry, C. Xu and co-workers firstly proposed the design concept of substantial symmetric charge redistribution, which occurs upon excitation and leads to enhanced 2PA cross section values, high fluorescence quantum yields and simple access to tune the absorption and emission properties.[156] This design strategy has since led to a rapidly growing collection of "push-push" (D-π-D) and "pull-pull" (A-π-A) chromophores, which were characterized by symmetric charge transfer, from the ends of a conjugated system to the middle, or *vice versa* upon excitation.[95,157] Subsequently, much effort was dedicated to these design strategies proposing asymmetrical "push-pull" (D-π-A) as well as quadrupolar compounds.[158,159]

In the search of adequate materials for specific applications, triarylborane chromophore systems offer a potential choice for live-cell imaging by two-photon fluorescence microscopy. The three-coordinate organoboron compounds with trigonal-planar geometry are characterized as a strong π-acceptor moieties, when connected to a conjugated π-system. Thus, the large change in dipole moment upon excitation of these compounds, its planar and highly π-conjugated structure provides an effective π-electron delocalization leading to large 2PA cross section. Moreover, triarylboron compounds were found to be non-toxic, water-soluble and photostable, facts that make them a promising proposal for imaging in live cells.

5.2.1 π-Bridged-Alkynyl Quadrupolar Triarylborane Chromophores [VI]

In collaboration with the group of Todd B. Marder from the Institute of Inorganic Chemistry at the University of Würzburg, we explored a series of quadrupolar A-π-A triarylborane chromophores with five different π-bridges as shown in Figure 5-18. The investigated compounds contain different π-bridges, namely **B1**: 4,4-biphenyl, **B2**: 2,7-pyrenyl, **B3**: 2,7-fluorenyl, **B4**: 3,6-carbazolyl and **B5**: 5,5-di(thien-2-yl)-3,6-diketopyrrolopyrrolyl, and were synthesized by Dr. Stefanie Griesbeck.[160,161] In this regard, we investigated the influence of the π-bridge on the two-photon absorptivity of these compounds. The linear and nonlinear spectroscopic measurements were performed in acetonitrile, as the polarity within cells is more similar to acetonitrile than to water.[161,162]

[VI] Reprinted or adapted in part from: "*Tuning the pi-bridge of quadrupolar triarylborane chromophores for one- and two-photon excited fluorescence imaging of lysosomes in live cells.*", S. Griesbeck, E. Michail, C. Wang, H. Ogasawara, S. Lorenzen, L. Gerstner, T. Zang, J. Nitsch, Y. Sato, R. Bertermann, M. Taki, C. Lambert, S. Yamaguchi and T. B. Marder, Chem. Sci., 2019, 10, 5405-5422.

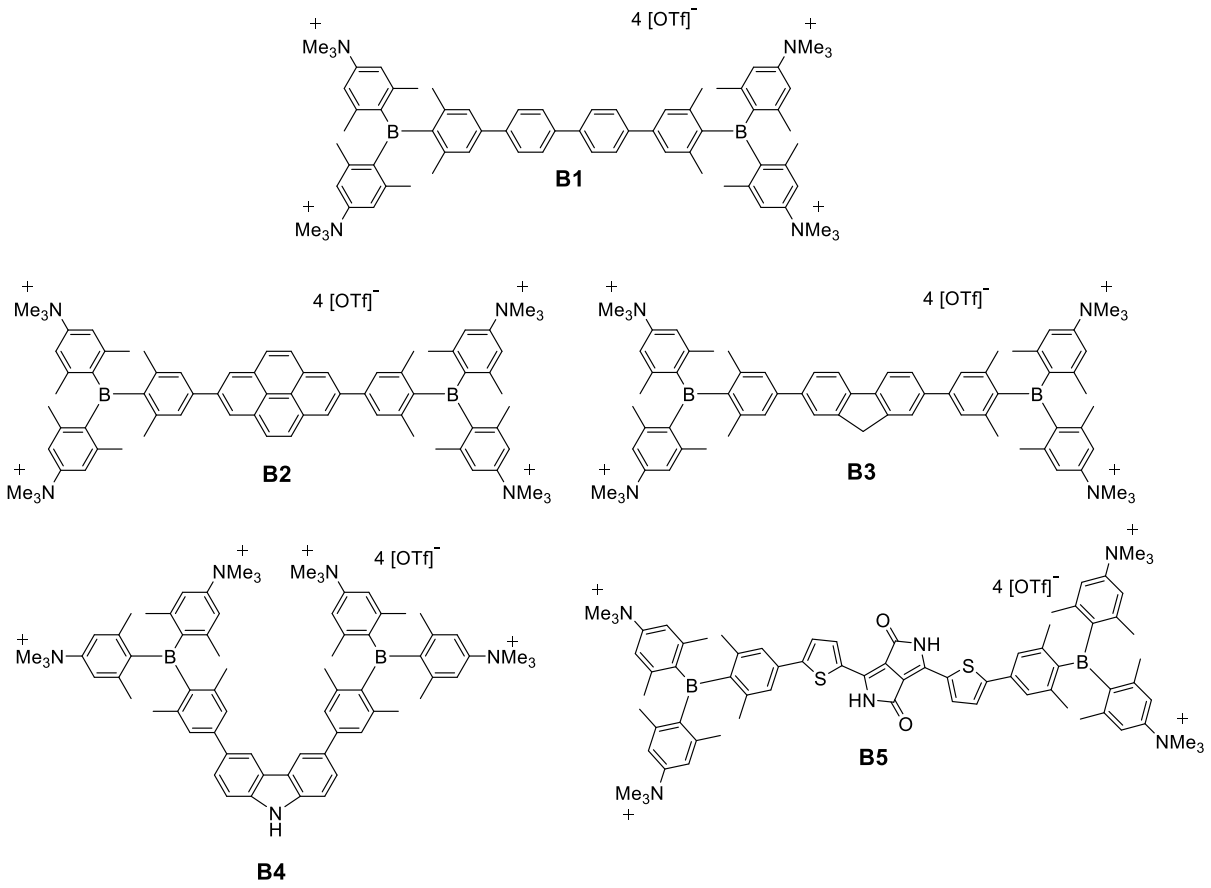

Figure 5-18: Chemical structures of the investigated quadrupolar bis-triarylboranes **B1** – **B5**.

In order to interpret the 2PA bands, it is necessary firstly to pay attention to the linear optical properties of the investigated compounds. The steady-state linear absorption and normalized fluorescence spectra of the bis-triarylborane compounds in dry acetonitrile are shown in Figure 5-19. The linear absorption spectra of the bis-triarylboranes feature a main absorption band from 15000 – 28000 cm^{-1}, which originates from the lowest exciton state S_1. In addition, absorption bands are observed at higher energies from 27000 – 33000 cm^{-1}, which are attributed to transitions into higher energetically electronic states. According to the π-bridge of the compound, the emission spectra can be tuned from 22200 cm^{-1} (blue colour) to 15500 cm^{-1} (light red colour). Moreover, the fluorescence quantum yields vary also with the conjugation pathway, between 0.12 – 0.73 in acetonitrile. In general, all the investigated bis-triarylborane compounds display completely different linear optical properties by changing the π-bridge. This finding proves that the π-π* contribution of the π-bridge becomes very important, since the lowest energy transitions are located on the π-bridge. Interestingly, the dithienyl-diketopyrrolopyrrole compound **B5** exhibits the most red-shifted absorption maximum, a fact which can be explained by enhanced intramolecular charge transfer. Indeed, as will be shown below, compound **B5** exhibits also the highest 2PA cross section value.

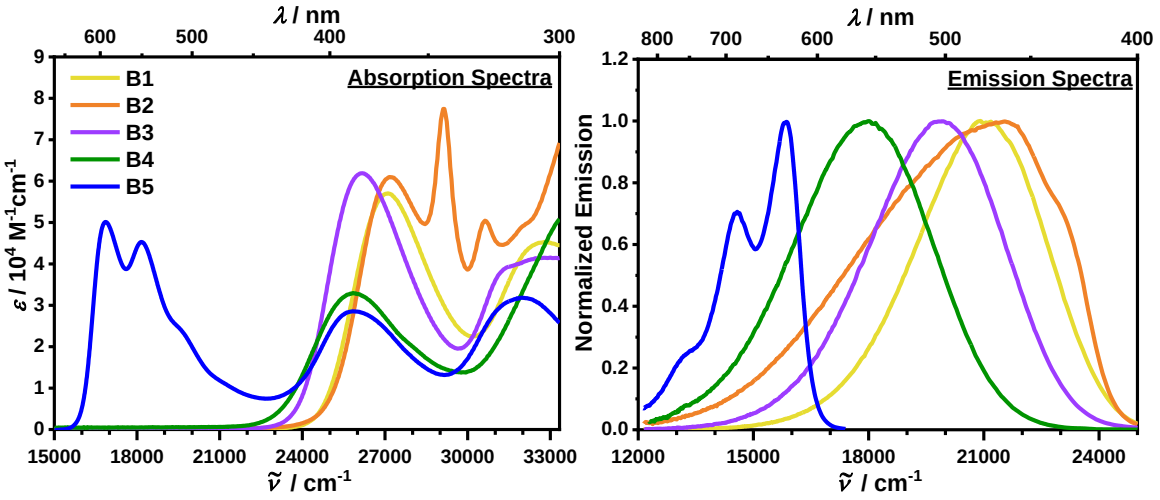

Figure 5-19: Linear absorption (left) and normalized fluorescence (right) spectra of bis-triarylboranes **B1** – **B5** in acetonitrile.

All the bis-triarylborane compounds exhibit large 2PA cross sections and the corresponding 2PA spectra versus the excitation energy are shown in Figure 5-20. We turn our attention to the structured 2PA bands in the spectral region between 12000 – 15000 cm^{-1} (see Table 5-10), which is important for the two-photon fluorescence microscopy applications.[163]

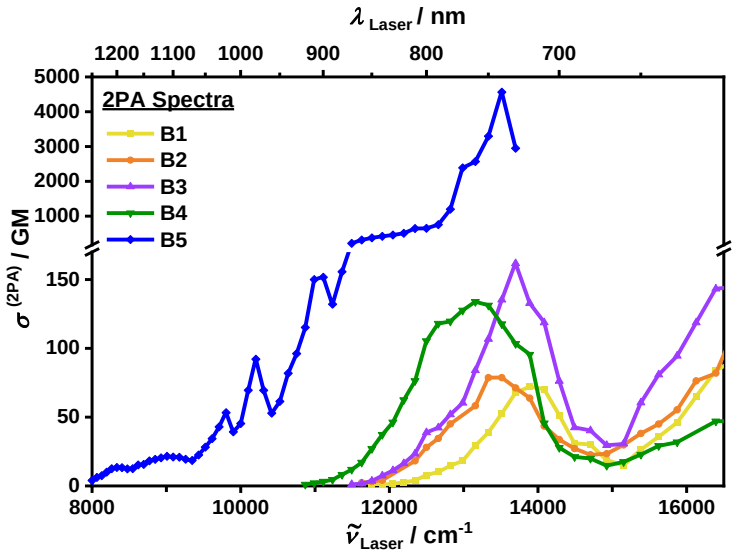

Figure 5-20: Plot of 2PA cross section spectra versus the laser excitation energy of the investigated triarylborane homodimers **B1** – **B5** in acetonitrile.

By reviewing the experimental results from the viewpoint of intramolecular charge-transfer processes, coplanarity has been identified as particularly important to the 2PA cross section.[75,164-166] The biphenyl compound **B1** as the most twisted molecular structure, due to the rotational degree of freedom around the C–C bond of the phenyl axis, has the smallest 2PA cross section of 72 GM. For **B2**, **B3** and **B4** compounds, the planarity was increased by inserting pyrene, fluorene or carbazole moieties. Since the two "phenylene" rings have no twist, taking the advantage of their π-bridge

rigidity, we obtained increased 2PA cross section values of 79 GM for **B2**, 162 GM for **B3** and 134 GM for **B4**. The dithienyl-diketopyrrolopyrrole compound **B5** is the most planar of our conjugated compounds (the angles between the acceptor moieties and the π-bridge are 2.5 times less than in the other compounds)[VII], with the highest 2PA cross section value of 4560 GM.

Beside co-planarity, several structural parameters define the intramolecular charge transfer ability, such as the length and the electron density of the conjugated system. Thus, the **B3** compound has a higher 2PA cross section than **B4**. This is attributed to the shorter conjugation length of the **B4** compound relative to compound **B3**. This is a competitive process, because it is known that increasing the distance over the charge transferred leads to an enhanced 2PA cross section. Moreover, by changing the bridging units from biphenyl (**B1**) to diketopyrrolopyrrole linker (**B5**), the energy of the lowest exciton state S_1 decreases at 16890 cm^{-1} and it comes to resonance with the two-photon allowed state at 27000 cm^{-1} and thereby an increasing of the 2PA cross section is achieved.

A comparison of the linear absorption and the 2PA spectra is shown in Figure 5-21 for the compounds **B1**, **B2** and **B5** which possess a center of inversion, since they belong to the C_i point group. Thus, by following the electronic selection rules, the 1PA maximum is attributed to the $S_1 \leftarrow S_0$ ($1A_g \leftarrow 1A_u$) transition, which is by symmetry forbidden for 2PA. The latter is located at higher energies; $S_2 \leftarrow S_0$ for **B1** and **B5** and $S_3 \leftarrow S_0$ for **B2**. The presence of a shoulder in the 2PA spectra of the three compounds at the energetic position, where the lowest 1PA transition is located, is due to a vibronic coupling to the A_u state with an a_u vibrational mode.[116,167] Accordingly, the linear and nonlinear absorption spectra of the **B3** and **B4** compounds, which possess C_{2v} symmetry as the highest point group and lack an inversion center, are depicted in Figure 5-22. Here, all transitions are both one- and two-photon allowed (1A ← 1A). The symmetry assignments were made with the help of TD-DFT calculations and were carried out by the group of Prof. Marder.

Table 5-10: The absorption maxima of S_1 state with the corresponding extinction coefficients, emission maxima, fluorescence quantum yields and the 2PA cross-sections at selected energies[a] of the investigated bis-triarylborane compounds in acetonitrile.

	$\tilde{\nu}_{S_1}$ / cm^{-1}	ε / $M^{-1}cm^{-1}$	$\tilde{\nu}_{em}$ / cm^{-1}	φ_{fl}	$\tilde{\nu}_{max}^{2PA}$ / cm^{-1}	σ_{max}^{2PA} / GM
B1	27140	5.71 x 10^4	20920	0.73	13890	72
B2	27250	6.08 x 10^4	21645	0.12	13330	79
B3	26210	6.19 x 10^4	19960	0.61	13700	162
B4	25870	3.29 x 10^4	17605	0.38	13160	134
B5	16890	5.01 x 10^4	16207	0.56	13510	4560

[a] The structured 2PA bands between 12000 – 15000 cm^{-1}.

[VII] DFT-optimized geometries of the ground states of all the investigated compounds at the B3LYP/6-31G level of theory were performed by the Prof. Marder group.

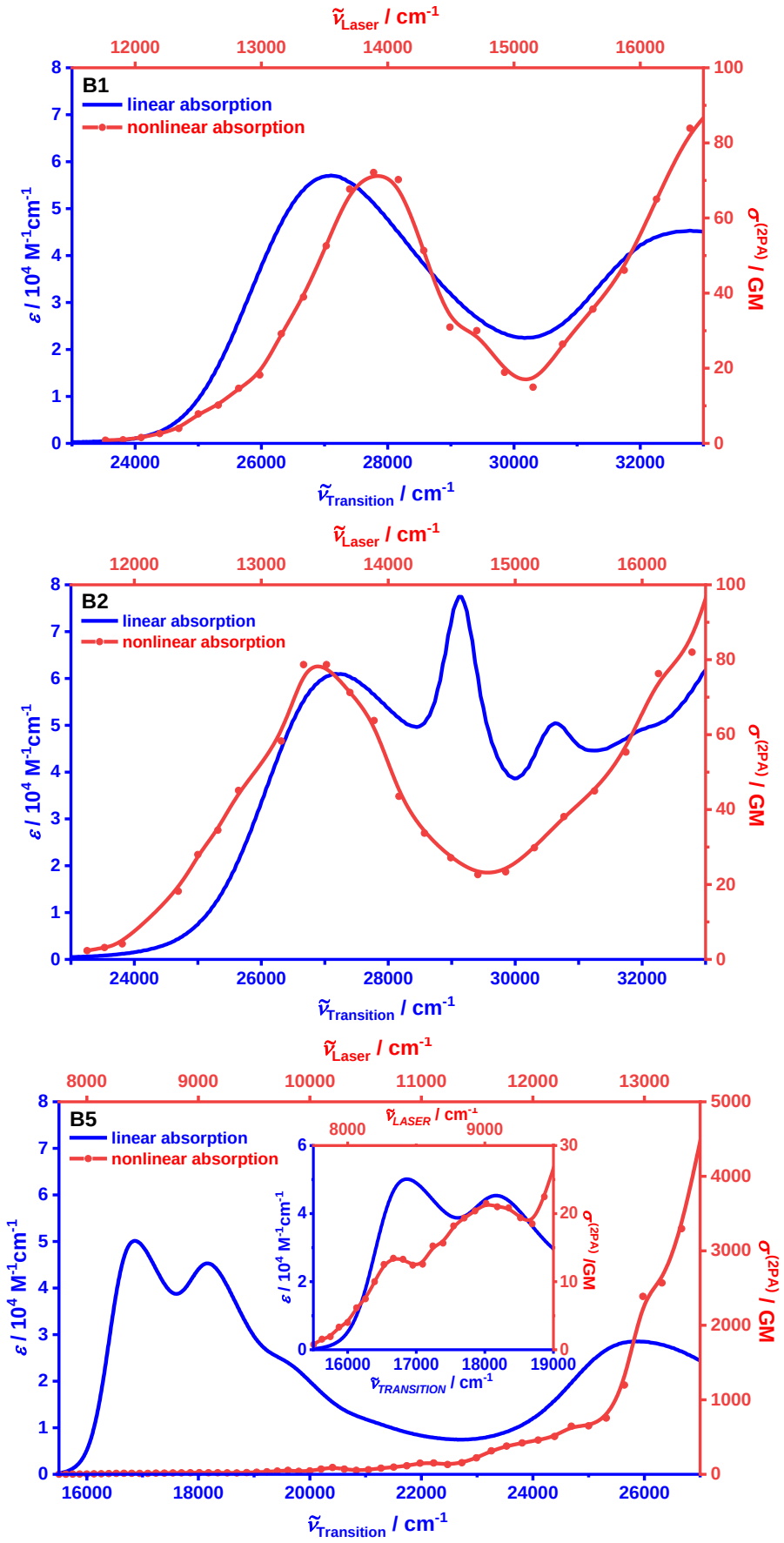

Figure 5-21: A comparison of the 1PA (blue line) and 2PA (red line) spectra of the investigated centrosymmetric (C_i symmetry) triarylborane compounds **B1**, **B2** and **B5** in acetonitrile.

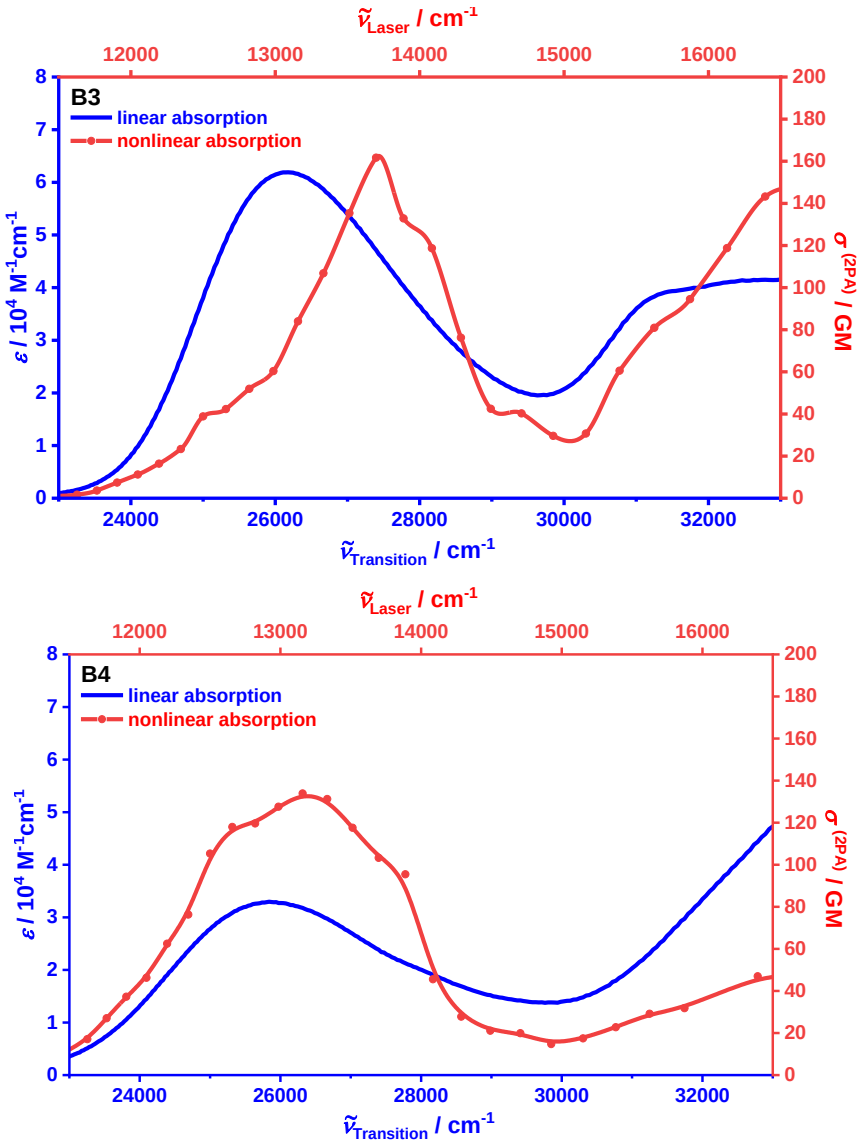

Figure 5-22: A comparison of the 1PA (blue line) and 2PA (red line) spectra of the investigated non-centrosymmetric (C_{2v} symmetry) triarylborane compounds **B3** and **B4** in acetonitrile.

5.2.2 π-Bridged Bis(phenylethynyl)aryl Quadrupolar Triarylborane Chromophores[VIII]

As a consequence of the intramolecular charge-transfer on 2PA enhancement, the extension of the conjugated π-system in symmetric chromophores was proposed to increase the 2PA cross section as it leads to states with extended charge separation.[95,108,168] In this framework, the following section provides a continuation of the previous subchapter, since the optical properties of the investigated compounds could be tuned drastically by using different long bis(phenylethynyl)arene linkers between the two terminal boryl moieties. To this end, in collaboration with the group of Prof. Marder, we

[VIII] Parts of this subchapter have been investigated in a Bachelor Thesis under the supervision of E. Michail: "*Linear and non-linear optical properties of quadrupolar triarylborane chromophores applicable for two-photon excited fluorescence bioimaging*", A. Hainthaler, Bachelor Thesis, Julius-Maximilians-Universität, Würzburg, **2020**.

investigated three quadrupolar triarylborane compounds with long bis(phenylethynyl)aryl linkers; **aB6**: arene=9,10-anthracene, **aB7**: aryl=5,5'-2,2'-bithiophene and **aB8**: arene=1,4-benzene, which were synthesized by Matthias Ferger.[169] The chemical structures are given in Figure 5-23.

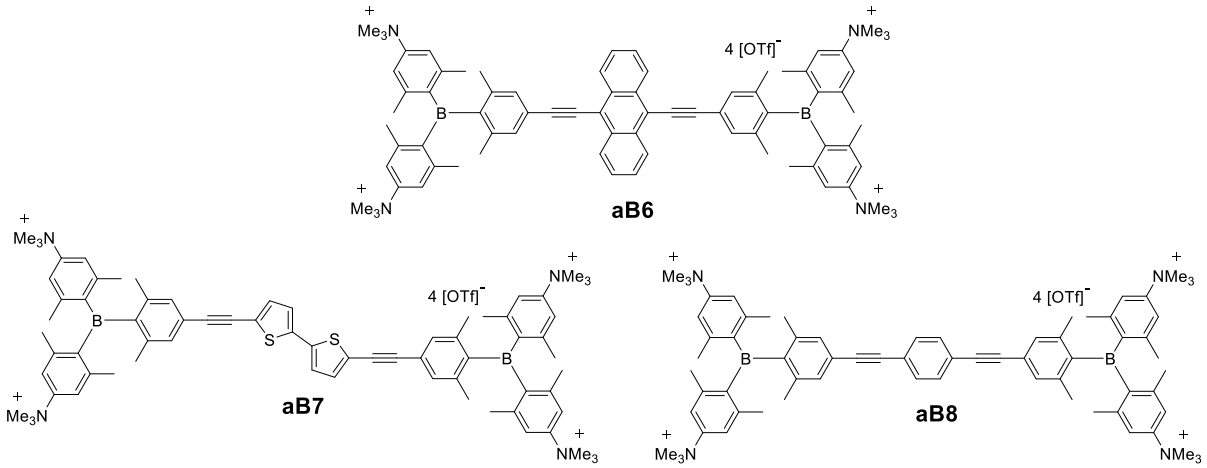

Figure 5-23: Chemical structures of the investigated quadrupolar bis-triarylborane chromophores **aB6** – **aB8** with different aromatic linkers.

The UV/Vis absorption and emission spectra of the three quadrupolar triarylborane chromophores were measured in acetonitrile and depicted in Figure 5-24. The **aB7** and **aB8** quadrupolar chromophores show related linear absorption spectra, which feature a main band at 24630 cm^{-1} and 26880 cm^{-1} respectively. This absorption band originates from the lowest exciton state S_1. The **aB6** anthracene compound provides additional peaks in the absorption spectrum. The low-energy absorption band at 20750 cm^{-1} is attributed to the $S_1 \leftarrow S_0$ transition accompanied by vibronic progression at *ca.* 21730 cm^{-1} and 28650 cm^{-1}. Furthermore, an additional less intense absorption band is observed at around 32480 cm^{-1} for all triarylborane chromophores and are assigned to an energetically higher-excited state. Simultaneously, the emission spectra are also broad, with maxima spread over a *ca.* 11000 cm^{-1} range for the three investigated compounds. By varying the bridging unit, a bathochromically shift of the linear absorption maxima, on going from **aB8** to **aB6** chromophore, are observed.

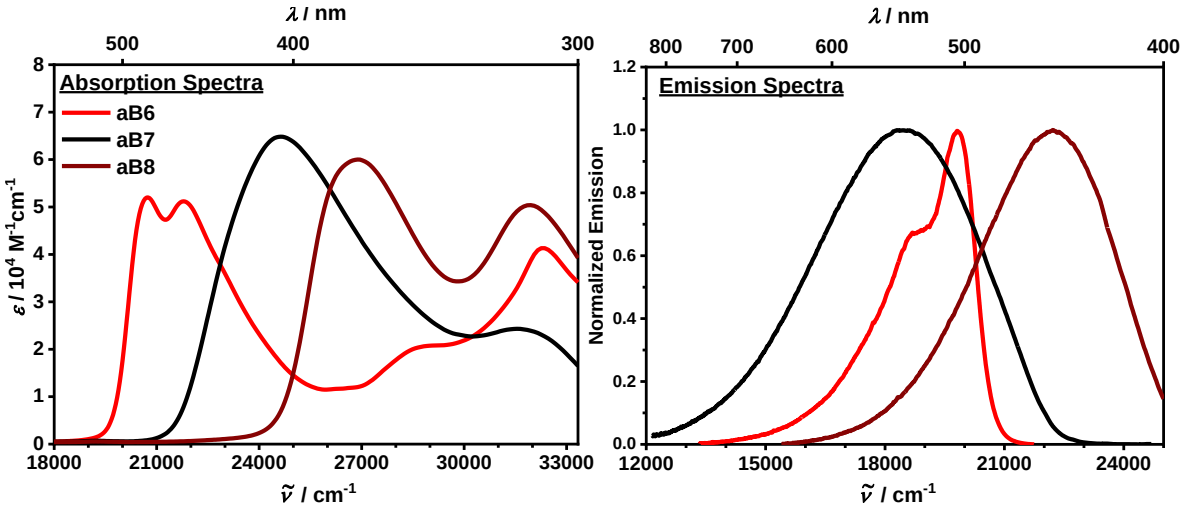

Figure 5-24: Linear absorption (left) and normalized fluorescence (right) spectra of triarylborane dimers **aB6**, **aB7** and **aB8** in acetonitrile.

The significant influence of the conjugation linker on the non-linear absorption properties of these quadrupolar triarylborane chromophores are indicated in Figure 5-25, in which their 2PA spectra in dry acetonitrile are depicted. In addition, the obtained optical data are summarized in Table 5-11.

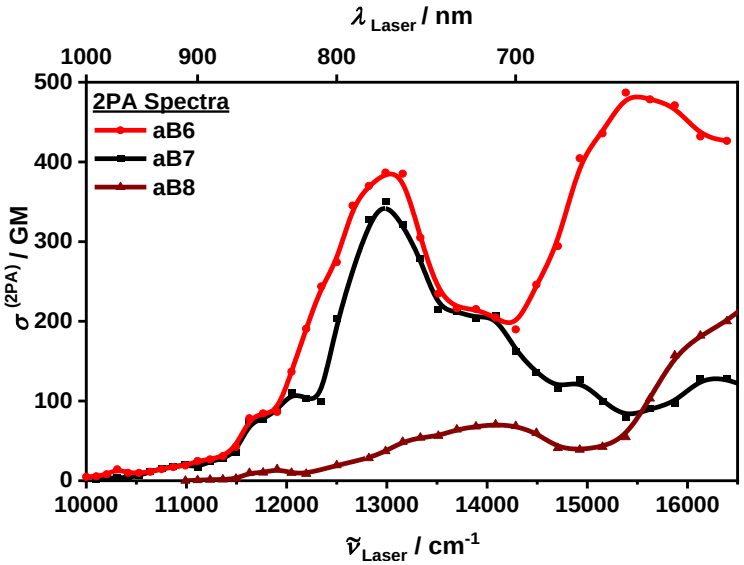

Figure 5-25: Plot of 2PA cross-section spectra versus the laser excitation energy of the investigated triarylborane homodimers **aB6** – **aB8** in acetonitrile.

The 2PA spectra of both **aB6** and **aB7** chromophores in acetonitrile display an enhanced broad band centered at 12990 cm^{-1} with similar 2PA cross section of 390 GM and 350 GM, respectively. In contrast, the spectra of **aB8** compound exhibits considerably lower 2PA cross section of 70 GM at 14080 cm^{-1}. In the higher-energies spectra region, several 2PA bands are visible for all the investigated compounds with the **aB6** compound achieving a 2PA cross section value of *ca.* 480 GM at 15520 cm^{-1}.

According to the TD-DFT calculation performed by the group of Prof. Marder, all the investigated compounds possess C_i symmetry, thus a center of inversion.[169] As a result, the 1PA and 2PA spectra are complementary to each other. For the sake of comparison, the linear and 2PA spectra are depicted together in Figure 5-26.

Table 5-11: The absorption maxima of S_1 state with the corresponding extinction coefficients, emission maxima, fluorescence quantum yields and the maximum 2PA cross-sections at the corresponding energies of the investigated triarylborane dimers in acetonitrile.

	$\tilde{\nu}_{S_1}$ / cm^{-1}	ε / M^{-1}cm^{-1}	$\tilde{\nu}_{em}$ / cm^{-1}	φ_{fl}	$\tilde{\nu}_{max}^{2PA}$ / cm^{-1}	σ_{max}^{2PA} / GM
aB6	20750	5.21 x 10^4	19800	0.72	12990	390
aB7	24630	6.48 x 10^4	18500	0.31	12990	350
aB8	26880	5.99 x 10^4	22300	0.58	14080	70

The nonlinear spectroscopic properties of the three chromophores are quite different from the linear one. The optimization of the intramolecular charge transfer by variation of the bridging unit causes enhanced 2PA cross section, without causing a red shift of the two-photon excitation wavelength.[170] Taking into account that all the three investigated compounds exhibit almost the same conjugation chain length[IX], this progressive red-shift of the lowest energy absorption band, which is observed in the linear absorption spectra, might be attributed to the higher electron density of the bridging units in **aB6** and **aB7**. This finding is further corroborated by the 2PA spectra characteristics, for which the chromophores **aB6** and **aB7** are similar, in contrast to the **aB8** compound, although all display the same spacer length. The **aB7** chromophore with thiophene linker moieties shows an almost 5 times higher 2PA cross section than the **aB8** chromophore owing comparable spacer length. Here, the thiophene rings play the role of electron relay in charge transfer process making the 2PA more effective. This strong electron-donating property of thiophene groups results in an increment of the permanent dipole moment difference $\Delta\mu_{gf}$ between the ground state and the first excited state (CT state) one half of the compounds. Since the $\Delta\mu_{gf}$ is equal to the transition dipole moment μ_{if} in quadrupolar compounds, the chromophores of the type A-π-D-π-A show exceptional larger 2PA cross section values than comparable A-π-A structures. [1,6,75,95]

On the other hand, the chromophore **aB6** possessing an anthracene moiety features similar 2PA cross sections to the **aB7** compound. By replacing the benzene core by anthracene, the size of the π-bridge is increased, which allows the electrons to be more delocalized around the linker, leading to enhanced

[IX] According to the X-ray diffraction analysis which were obtained Prof. Marder`s group, the distance between the two boron atoms for **aB6** is found to be *ca.* 22.5 Å and for **aB7** *ca.* 19.5 Å.

2PA cross sections and high fluorescence quantum yields.[171] Moreover, this is reflected by the significant red-shift of the lowest exciton state observed in **aB6** with respect to **aB8,** which results in a smaller detuning energy ($\tilde{\nu}_{1Ag} - \tilde{\nu}_{1Bu}/2$). Indeed, in the case of the **aB6** and **aB8** chromophore the estimated detuning energy is about 11600 cm^{-1} and 12600 cm^{-1}, respectively. As mentioned before, the small values of detuning energies can maximize the transition dipole moment between the one- and two-photon allowed states and consequently the 2PA cross sections of the centro-symmetric chromophores.[6,172] Several published studies indicate that anthracene-centered conjugated chromophores show a greatly enhanced 2PA effect, which are different from those of the benzene-centered analogues that show no enhancement.[172,173] Thus, anthracene might be a useful conjugation π-bridge center due to its excellent fluorescence properties and because its derivatives have been extensively used as fluorescence sensors.[174,175]

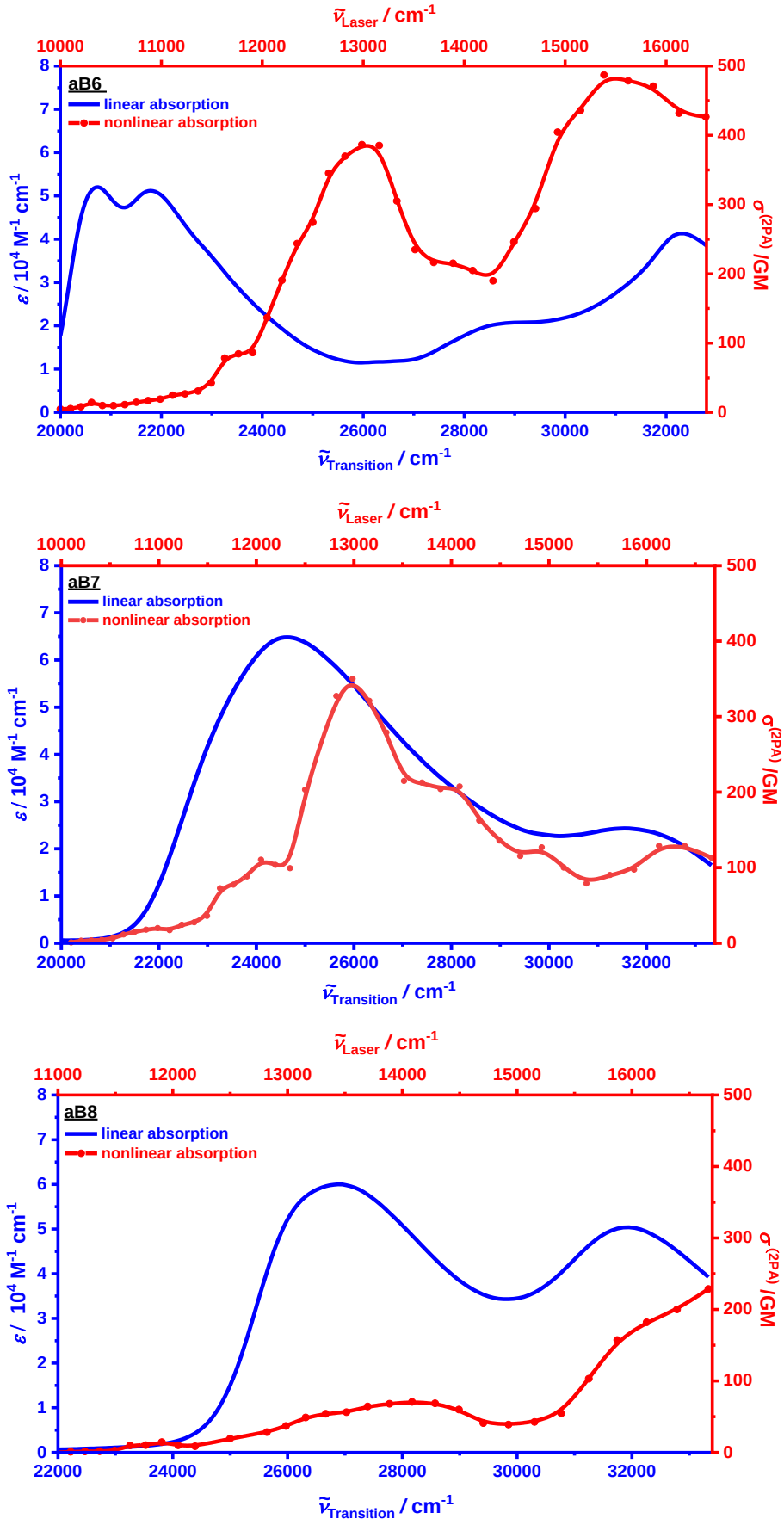

Figure 5-26: A comparison of the 1PA (blue line) and 2PA (red line) spectra of the investigated triarylborane compounds **aB6**, **aB7** and **aB8** in acetonitrile.

5.2.3 Conclusion

In this section, the nonlinear optical properties of a series of eight quadrupolar triarylborane chromophores with varying π-bridging centers were investigated. As expected, the choice of bridge which couples the two acceptor moieties leads to different 2PA properties. In the following, a spectroscopic comparison between the investigated chromophores **B1**-**B5** and **aB6**-**aB8** in acetonitrile are briefly summarized (Figure 5-27).

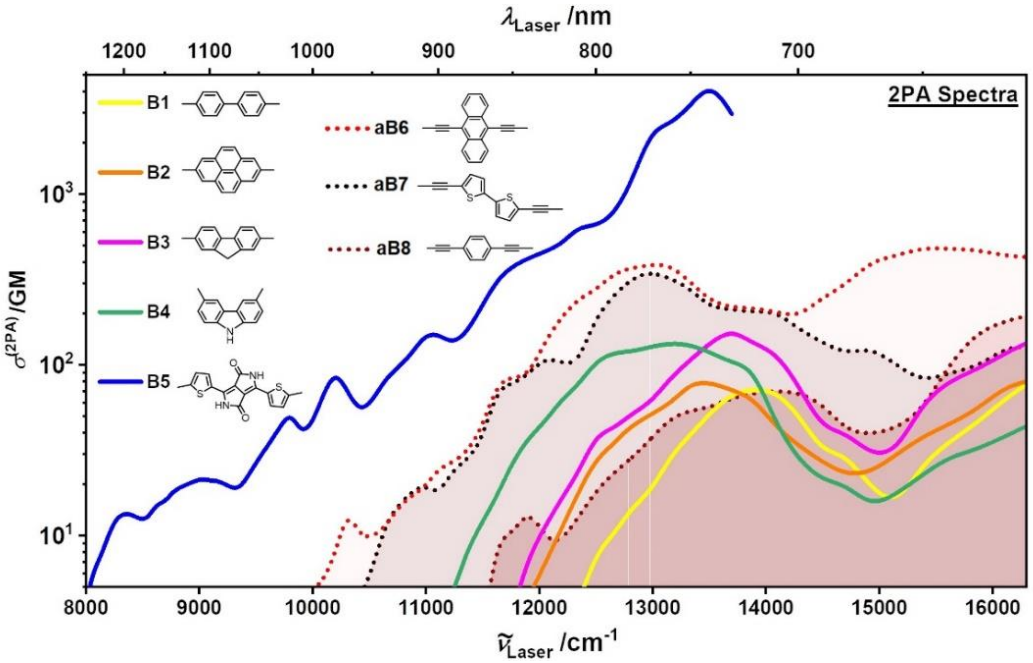

Figure 5-27: Logarithmic plot of 2PA spectra of all the investigated quadrupolar triarylborane compounds **B1** – **B5** and **aB6** – **aB8** in acetonitrile.

When comparing the 2PA spectra of the triarylborane chromophores **aB6** and **aB7** with long bis(phenylethynyl)arene linkers with those recorded from **B1** – **B4**, it can be concluded that the extension of the π-conjugated dimers and consequently somewhat the molecular size, leads to an increase of the 2PA cross section by enhancing 2PA bands in the red spectral region of the spectrum. In this context, H. Ågren *et al.* showed in several 2PA studies of conjugated oligomers that the maximum 2PA, which is often located in the UV side of the spectrum, is strongly correlated to the length of the oligomer and such length dependence does not hold for the dominating 2PA states in the visible side of the spectrum.[166,168,176] However, adding in that comparison the compounds **aB7**and **B5**, one sees that a most crucial role for sizable 2PA is played by the nature of the π-bridge. Based on the discussed findings, by increasing the size of the π-system, in combination with improving the molecular planarity, could be beneficial for enhancing the intramolecular charge transfer, leading to high 2PA. [175,177-179] Furthermore, in case of **B5** compound, there is a strong 2PA approaching twice the energy of the 1PA states because of double resonance conditions.[128,149,150] Additionally, the **aB7**

compound with the thiophene center consists of a symmetrical structure with a donor ability π-bridge unit, resulting in a substantial increase in the transition dipole moment between the first one-photon resonant and the final two photon resonant excited state, which is the major contributor to the 2PA cross section enhancement.[95,96,176]

In conclusion, the spectra features can be linked to the electronic characteristics of the bridges allowing for fine tuning. Thus, the engineering of the molecular architecture, using long, π-conjugated chains with enforced planarity leads to enhanced nonlinear response in these chromophores and allows targeting specific spectra features. Nevertheless, no quantifiable trends between the different bridges and spectroscopic properties were found. More systematic studies are still required in order to predict the specific dependence of the 2PA cross section on the length and bridging characteristics of a π-system.

5.3 Impact of Branching on the 2PA

A natural consequence of the bridging design led to the investigation of 2PA properties in molecules where two or more dipolar molecules are joined together with extended conjugation.[180] In light of this knowledge, molecular design strategies based on multidimensional branching were proposed to further enhance the 2PA cross section.[165] Critical issues in the case of branched systems concern excitation localization/delocalization and the role of coherent coupling between the chromophores.[181,182] The effect of branching on the 2PA properties strongly depends on the nature and the strength of the coupling between the branches. As soon as the coupling becomes stronger the excitation charge is more delocalized over all chromophore units leading to high 2PA cross section values.[183-185]

To this end, we investigated the effect of branching on the nonlinear optical properties of branched systems based on dipolar chromophores connected via a core moiety. In this regard, triphenylamine (TPA) derivatives have been applied successfully as an efficient core for cooperative 2PA enhancement. Due to their easy synthetic access and their strong donor character they show promising 2PA applications. The first branched chromophores used for studies of 2PA were reported by Prasad and *co*-workers in 1999.[180] Blanchard-Desce *et al.*[75] reported high 2PA response for triarylamine based branched chromophores. Goodson and *co*-workers[186] and Rebane *et al.*[187] observed a similar enhancement effect in dendrimer series based on substituted triarylamines. In our recent work by Ceymann *et al*.[128], we reported an enhancement of the 2PA cross section in a series of super-chromophores built up from squaraine dyes with a triarylamine core. Interestingly, the investigation of the (multi) branching effect on the 2PA cross section led to various trends, such as cooperative enhancement, additive behavior, or even reduction of 2PA. In this work we focused our attention on a study how the effect of branching affects the 2PA cross section quantitatively.

5.3.1 Triarylborane Chromophore Moieties[X]

As a continuation of the collaboration with the group of Prof. Marder in the framework of the investigations on nonlinear spectroscopic properties of triarylboron compounds, here we concentrate on the differences between dipolar and octupolar charge distribution. To this end, here we explored the dipolar system **TPA(BAr$_3$)** in which a triphenylamine donor and a triarylborane acceptor are connected and the octupolar analogue **TPA(BAr$_3$)$_3$** with a triphenylamine donor moiety connected to three triarylborane acceptors. As mentioned above, the triarylboranes are equipped with triarylamine

[X] Reprinted or adapted in part from: "*The Effect of Branching on the One- and Two-Photon Absorption, Cell Viability, and Localization of Cationic Triarylborane Chromophores with Dipolar versus Octupolar Charge Distributions for Cellular Imaging*.", S. Griesbeck, E. Michail, F. Rauch, H. Ogasawara, C. Wang, Y. Sato, R. M. Edkins, Z. Zhang, M. Taki, C. Lambert, S. Yamaguchi and T. B. Marder, Chem. Eur. J., 2019, 25, 13164-13175.

substituents in order to provide a good water solubility which is required for fluorescence microscopy of living cells and tissues (see subchapter 6.1). The chemical structures of the investigated compounds are shown in Figure 5-28 where the dipolar **TPA(BAr$_3$)** and octupolar **TPA(BAr$_3$)$_3$** has linear and star-shaped arrangement, respectively. Their syntheses were reported by Dr. S. Griesbeck.[160,188]

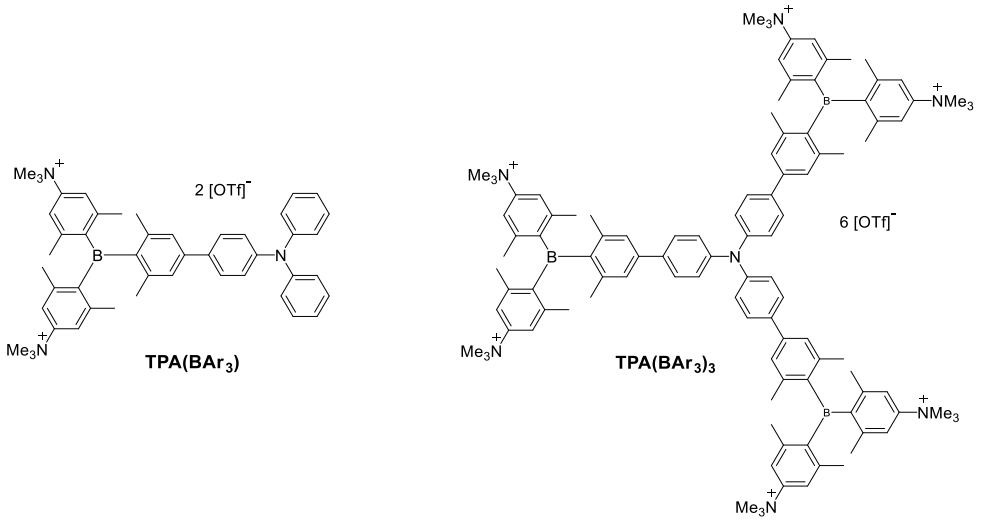

Figure 5-28: Chemical structure of dipolar **TPA(BAr$_3$)** and octupolar **TPA(BAr$_3$)$_3$** triarylborane compounds.

The steady-state linear and nonlinear absorption spectra were recorded in dry acetonitrile and are depicted together in Figure 5-29. Firstly, it is interesting to compare the changes in the linear UV/vis absorption spectra upon branching, in which the extinction coefficient is *ca.* 2.6-fold higher and a slight redshift (*ca.* 800 cm^{-1}) of the absorption maxima can be observed. According to the 2PA cross section, in the spectral region 20000 – 29000 cm^{-1} where the first 2PA structured band is located, the maximum 2PA cross section is 91 GM for the dipolar compound **TPA(BAr$_3$)** and increases *ca.* 3.7 times upon 3-fold branching to 335 GM for octupolar ones **TPA(BAr$_3$)$_3$**.

This factor is slightly larger (4.1) when estimating the experimental 2PA strength $<\delta^{(2PA)}>$ via equation (4–7) in that spectral region with integration limits 20000 – 29000 cm^{-1} and yields values of 4 x 10^4 a.u for the octupolar compound and 1 x 10^4 a.u for the dipolar one. This is probably due to integration area where includes enhanced vibronic progression.

However, this finding indicates that the octupolar system behaves approximately as a sum of the individual arms which can most likely attributed to no interaction (or little) between the branches.[184] Following this assumption, the interaction between the branches in the excited state is not dominant due to the weak coupling which leads to exciton localization on a dipolar chromophore branch prior to emission.[189,190] This is in agreement with the additive behavior of the respective linear absorption spectra and the experimental determined exciton coupling constant, which yields a small value (0.09 eV).[184]

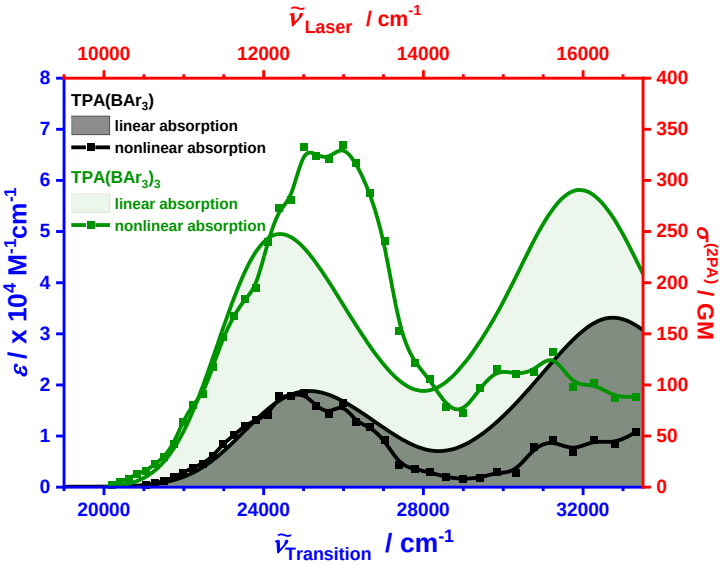

Figure 5-29: A comparison of the 1PA (shaded area) and 2PA (line with dots) spectra of dipolar **TPA(BAr$_3$)** (black colour) and octupolar **TPA(BAr$_3$)$_3$** (green colour) triarylborane compounds in acetonitrile.

5.3.2 Polychlorinated Triarylmethyl Radicals[XI]

In order to gain insight into the branching effect on the 2PA cross section, we investigated three radical compounds ranging from dipolar to octupolar branched structures. The compounds consist of three polychlorinated pyridyldiphenylmethyl radicals (PyBTM'') bridged by a triphenylamine carrying electron donating methoxy groups (TPA(OMe)). In this regard, the effect of branching on 2PA properties has roughly explored by growing the molecular complexity, from simple dipolar monoradical **TPA(OMe)$_2$(PyBTM'')**, to diradical **TPA(OMe)(PyBTM'')$_2$** and octupolar triradical **TPA(PyBTM'')$_3$** compounds. The chemical structures of the investigated compounds are shown in Figure 5-30 and a description of their synthesis is presented in the paper by Dr. Yohei Hattori.[191]

The linear and the nonlinear absorption spectra of the three investigated compounds are presented together in Figure 5-31. As expected, the molar extinction coefficient and 2PA cross section increase upon branching, however the observed behavior is not linear to the number of branches. Moreover, the lowest energy band is shifted towards higher energy for the branched systems showing a shift of *ca*. 800 – 1100 cm^{-1}, although it is difficult to give the energy of maximum absorption of this band because several electronic transitions are overlapping (one for monoradical, two for diradical and three for triradical compound). In the case of monoradical compound **TPA(OMe)$_2$(PyBTM'')** this shift is due to the strong triphenylamine donor which is consisted by two methoxy substituents.

[XI] Reprinted or adapted in part from: "*Luminescent Mono-, Di-, and Triradicals: Bridging Polychlorinated Triarylmethyl Radicals by Triarylamines and Triarylboranes.*" Y. Hattori, E. Michail, A. Schmiedel, M. Moos,M. Holzapfel, I. Krummenacher, H. Braunschweig, U. Meller, J. Pflaum, and C. Lambert, Chem. Eur. J., 2019, 25, 15463-15471.

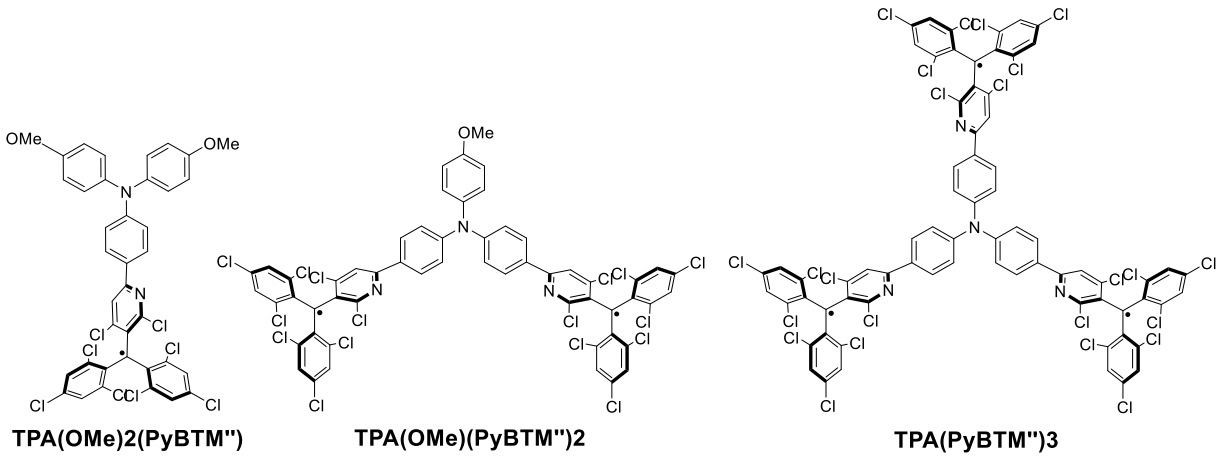

Figure 5-30: Chemical structures of monoradical **TPA(OMe)$_2$(PyBTM'')**, diradical **TPA(OMe)(PyBTM'')$_2$** and triradical **TPA(PyBTM'')$_3$** compounds.

According to the 2PA absorption spectra, for the first 2PA band at higher energies (12000 – 17000 cm^{-1}), we found 2PA cross sections which increase from *ca.* 90 GM for the monoradical **TPA(OMe)$_2$(PyBTM'')** to 840 GM for the diradical **TPA(OMe)(PyBTM'')$_2$** and 1200 GM for the triradical **TPA(PyBTM'')$_3$** compound. The same trend is also observed for the second 2PA band (17000 – 21000 cm^{-1}) where the 2PA cross section increases from 510 GM to 2980 GM on going from the dipolar to the octupolar compound. Thus, this increase cannot be explained by the simple additivity of individual chromophore moieties in the investigated compounds but must be caused by coherent interactions between the branches.[192]

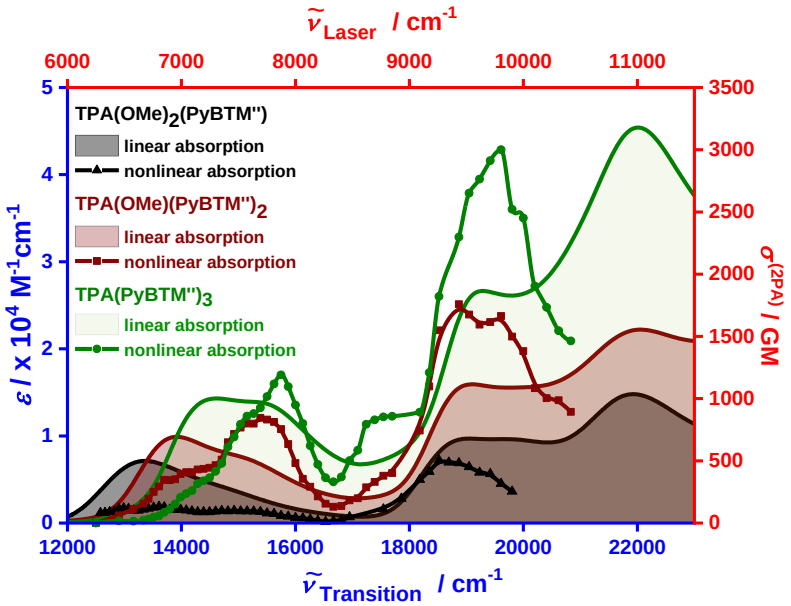

Figure 5-31: A comparison of the 1PA (shaded area) and 2PA (line with points) spectra of the dipolar **TPA(OMe)$_2$(PyBTM'')** (black colour), the quadrupolar **TPA(OMe)(PyBTM'')$_2$** (brown colour) and octupolar **TPA(PyBTM'')$_3$** (green colour) compounds in cyclohexane.

Again, the latter results are confirmed by estimation of the experimental 2PA strength $<\delta^{(2PA)}>$ via equation (4–7) for the two 2PA bands. For the first 2PA band, the 2PA strength $<\delta^{(2PA)}>$ in the spectral region with integration limits 14600 – 16700 cm^{-1} yields values of 0.5 x 10^4 a.u for the monoradical, 4.3 x 10^4 a.u for the diradical and 6 x 10^4 a.u for the triradical compound. In the second 2PA band the integrated 2PA strengths in the spectral region with integration limits 16700 – 21000 cm^{-1} increase from 0.2 x 10^5 a.u for the monoradical to 1 x 10^5 a.u for the diradical and to 1.6 x 10^5 a.u for the triradical compound.

5.3.3 Conclusion

In this chapter we explored how the coupling between the arms in branched systems affects the localization or delocalization of the ground or the excited state and therefore the 2PA cross section may be either enhanced or suppressed. Thus, we present the linear and the nonlinear spectroscopic properties of two characteristic examples of branching effect. In particular, we investigate an octupolar (three-branch) system based on triphenylamine donor core and triarylborane acceptor arms and its corresponding dipolar analogue. Herein, the 2PA response is nearly additive with respect to the number of branches. The latter indicates a breaking of the coherent coupling between the arms and the excitation localized on one of the branches prior to emission, leading to a dipolar emissive excited state. The experimental determined small exciton-coupling constant of 0.09 eV between the three branches allows us to confirm and explaine the observed additive trend in the 2PA spectra.

In contrast, for a series of polychlorinated pyridyldiphenylmethyl radical compounds bridged by a triphenylamine core, the 2PA cross sections show that the value for the octupolar branched radical is almost six times larger than that for the monomer. This large amplified 2PA response shown by branched chromophores is related to the interaction between the branched dipolar units.

A deeper understanding of the branching effect on nonlinear optical properties of multichromophoric structures demand further experimental and theoretical investigation. Notably, the study of localization phenomenon suggests also quantum-chemical excited-state calculations.[189]

6 Future Outlook

6.1 Proposes for 2PA Applications

Distinct spectroscopic and physical properties of the investigated compounds make them potentially applicable for diverse technological applications, such as nonlinear optical limiting and high-resolution biological imaging.

Nonlinear optical power limiting[XXVII]

Optical power limiting (OPL) application has attracted much interest for protection of human eyes or optical sensors from intense laser irradiation, optical pulse processing and laser mode locking.[193-198] It is a prerequisite for such applications that the materials possess a high transmission of low intensity near-IR light and a high extinction-coefficient at high intensities, greater than an optical limiting threshold. Thus, one of the requirements for optical limiting applications is a sizeable 2PA cross section at the wavelength of interest. In this regard, the benzodipyrrolenine-fused squaraine dimer **pySQB*trans*** (see subchapter 5.1.2) appears to be an ideal optical power limiter, as it shows extremely high 2PA cross section values in a broadband spectral range in the near-IR region. This energy region is important for optical communication and makes the **pySQB*trans*** chromophore interesting for protecting optical sensors. To this end, the OPL behavior of the **pySQB*trans*** was investigated at various incident energies by transmission measurements in the 2PIF apparatus.

The most straightforward way of treating this nonlinear absorption process is considering the transmitted intensity I through a two-photon absorbing sample with optical path length L as described by equation (6–1).[196,199]

$$I_{\mathrm{out}} = \frac{\alpha I_{\mathrm{in}}}{\alpha \exp(\alpha L) + [\exp(\alpha L) - 1]\beta I_{\mathrm{in}}} \qquad (6\text{–}1)$$

where I_{in} is the incident intensity, α [in cm^{-1}] is the attenuation coefficient due to linear absorption and β [in cm GW^{-1}] is the 2PA coefficient. This experiment, which consisted of measured transmitted pulse energy as a function of the incident laser energy, were performed using 150 fs pulses with 1 KHz repetition rate at the incident laser energies of 6700 cm^{-1}, 8000 cm^{-1} and 11000 cm^{-1} using a 10^{-3} M solution of **pySQB*trans*** in toluene in a 1 cm cuvette. Figure 6-1 shows the experimental results which consists of measured transmitted pulse energy I_{out} as a function of the incident laser energy I_{in}. [XXVIII]

[XXVII] Reprinted or adapted in part with permission from: "*Enhanced two–photon absorption and promising broad energy range optical power limiting properties of transoid and cisoid benzodipyrrolenine-fused squaraine dimers*", E. Michail, M. H. Schreck, L. Wittmann, M. Holzapfel and C. Lambert, Chem. Mater., **2021**, 33, 9, 3121-3131.

[XXVIII] In order to eliminate the effect of solvent in the experimental result, the energy detected after the cuvette filled with pure toluene is considered as the input energy.

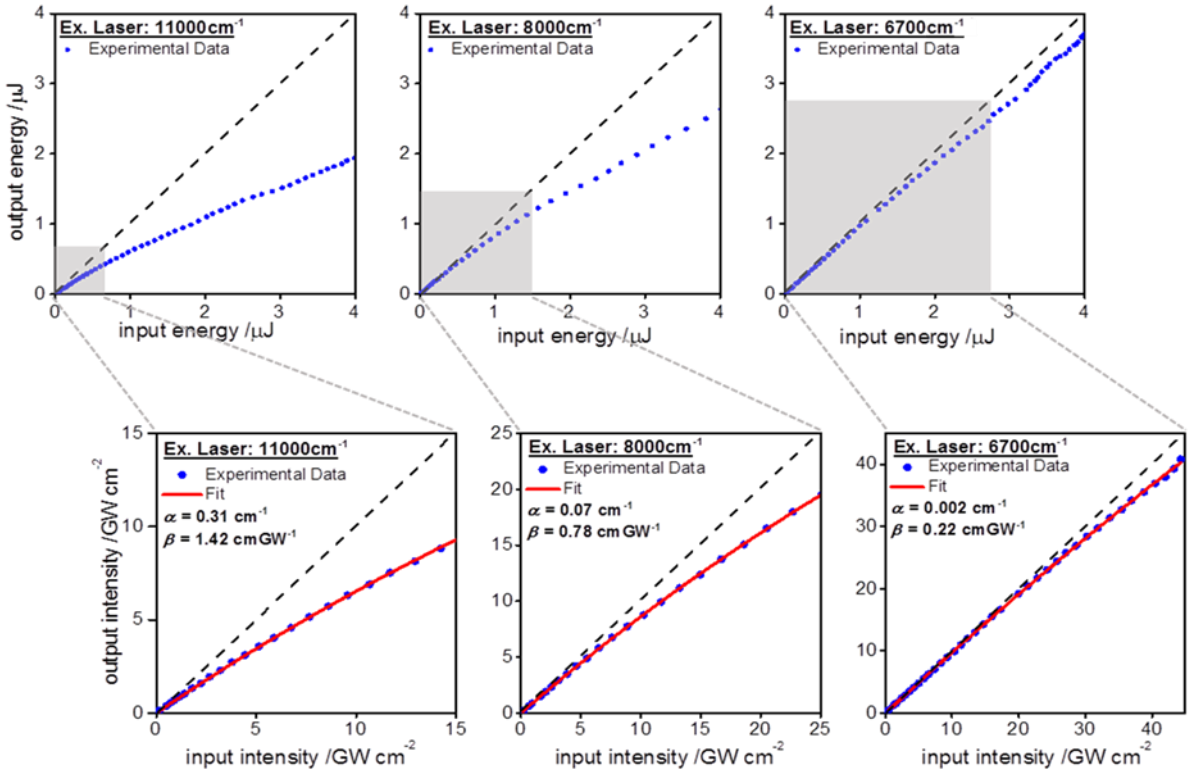

Figure 6-1: Measured output pulse energy (and intensity) as a function of the input pulse energy (and intensity) of **pySQB**$_{trans}$ in toluene solution using 150 fs pulses and 1 KHz repetition rate at 6700 cm^{-1}, 8000 cm^{-1} and 11000 cm^{-1}. The dotted lines show the behavior for a medium without non-linear absorption.

The **pySQB**$_{trans}$ in toluene solution exhibits strong OPL performance in the near-IR energy range 6700 – 11000 cm^{-1} even at rather low input intensities. When the input energy was increased to only 4 µJ the output energy dropped to less than half at 11000 cm^{-1}. The attenuation effect is smaller at smaller wavenumbers because it correlates with the 2PA cross section. The experimental data points at the three wavenumbers could be fitted by equation (6–1) at low incident intensities and the 2PA coefficient β could be extracted. When increasing the input intensity, other mechanisms such as 2PA saturation, excited state absorption, and three-photon absorption start to contribute to the nonlinear absorption process. The 2PA corresponding values of 2PA coefficient obtained from fittings and from the 2PIF spectroscopy through the 2PA cross section (see equation (1–2)) are presented in Table 6-1.

Table 6-1: The excitation laser energy, the 2PA cross-section and the corresponding 2PA coefficient values obtainted by 2PIF and nonlinear transmission measurments using 150 fs pulses of **pySQB**$_{trans}$ in toluene solution.

Laser Energy/cm^{-1}	$\sigma^{(2PA)}$/ GM	β/ cm GW^{-1} from $\sigma^{(2PA)}$	β/ cm GW^{-1} from non-linear transmission
11000	8.9 x 10^4	1.72	1.41
8000	1.4 x 10^4	0.37	0.73
6700	1.5 x 10^3	0.05	0.22

Therefore, the experimental data cannot be well fitted by a theoretical function that describes only a single mechanism.[200-202] Comparing our results with the few experimental studies that are available, where the OPL behaviours of organic compounds in the near-IR energy range of 6700 – 11000 cm^{-1} have been investigated,[203-207] shows that the **pySQB$_{trans}$** chromophore possesses an order of magnitude higher β values. Consequently, OPL measurements were also obtained for **pySQB$_{trans}$** as a film in polystyrene matrix[XXIX]. The optical limiting performance is presented in Figure 6-2 and displays a similar behavior as in toluene solution in Figure 6-2. Up to this intensity level the OPL behavior is mainly caused by 2PA processes both in solution and in film.

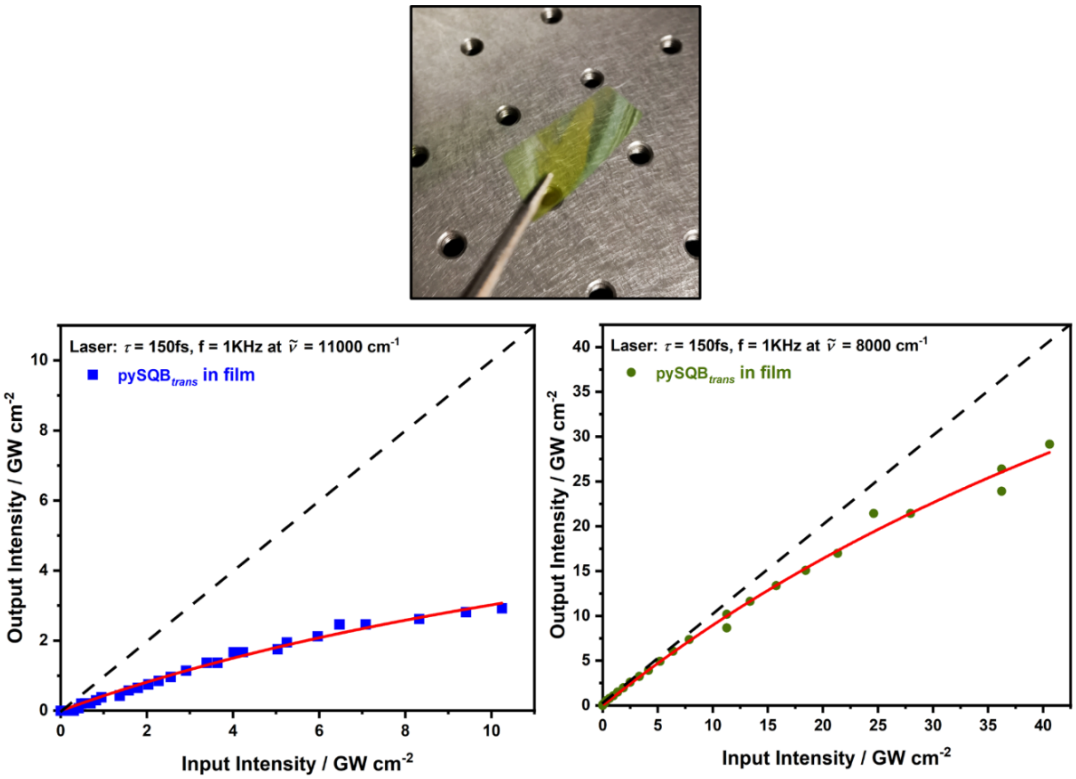

Figure 6-2: Top: **pySQB$_{trans}$** in polystyrene thin film. Bottom: measured output pulse intensity as a function of the input pulse intensity of **pySQB$_{trans}$** in a polystyrene film using 150 fs pulses with 1 kHz repetition rate at 8000 cm^{-1} and 11000 cm^{-1}. The dashed lines show the behavior for a medium without nonlinear absorption.

[XXIX] For film preparation, polystyrene (800 mg, Sigma-Aldrich) was dissolved in 3 mL toluene and mixed with 2 mL of a 1 x 10^{-3} M **pySQB$_{trans}$** solution in toluene. The resulting mixture was placed in an 8 cm diameter Petri dish and the solvent was slowly evaporated over 2 days. To slow down the evaporation, half of the dish was covered. A small piece of the film was cut out and placed in a sample holder for the measurements.

Two-Photon Biological Imaging

The low cytotoxicity and high photostability of the investigated triarylborane compounds (see subchapters 5.2.1 and 5.3.1), combined with high 2PA make them attractive materials for studying biological systems via two-photon imaging applications.[208,209] In addition, most of these compounds exhibit high fluorescence quantum yields φ_{fl}, which is a necessary parameter in order to achieve better signal-to-noise ratio in the imaging process. To this end, the quadrupolar compound **B5**, the dipolar one **TPA(BAr$_3$)** and its analogous octupolar compound **TPA(BAr$_3$)$_3$**, were applied in two-photon excited fluorescence live-cell imaging due to their high two-photon brightness $\sigma^{(2PA)}$ φ_{fl} [in GM] in acetonitrile (see Figure 6-3). The 2PA brightness (also so-called action 2PA cross section) is determined by the product of the 2PA cross section $\sigma^{(2PA)}$ with the fluorescence quantum yield φ_{fl}. It is well-know that a fluorophore should exhibit a 2PA brightness of at least 50 GM in order to observe bright two-photon microscope images. The two-photon imaging experiments were performed for monitoring and visualizing lysosomes[XXX] by the group of Prof. Dr. Shigehiro Yamaguchi at the Nagoya University in collaboration with the group of Prof. T.B. Marder. The compounds were taken up by the endocytosis pathway of the HeLa cells and localized at the lysosomes. As shown in Figure 6-4, the compounds stained the lysosomes in the cell being a very effective two-photon imaging agent.

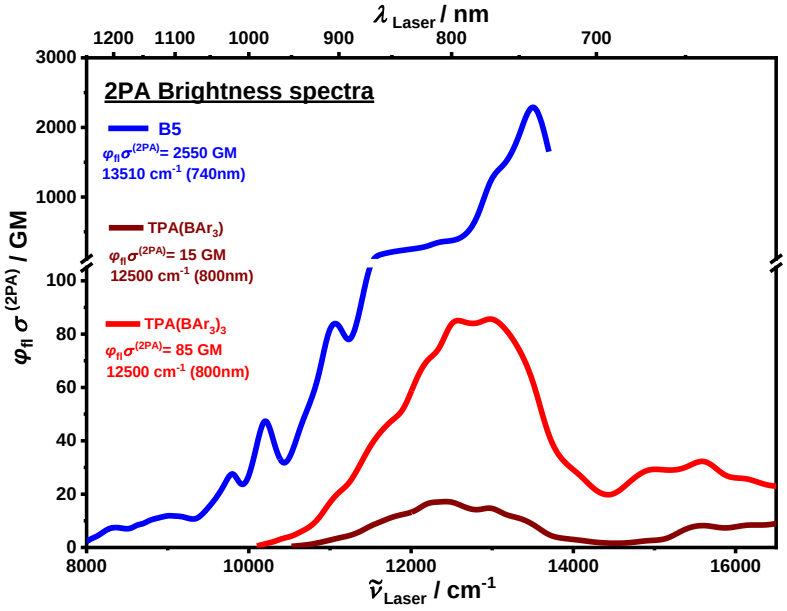

Figure 6-3: The two-photon brightness ($\sigma^{(2PA)}$ φ_{fl}) spectra in acetonitrile and the chemical structures of target molecules **B5, TPA(Bar$_3$)** and **TPA(Bar$_3$)$_3$** were used for live-cell imaging experiments.

[XXX] Lysosomes are membrane-bound organelles in eukaryotic cells which are responsible for many cell processes and the mutations of their genes lead to neurodegenerating disorders such as Parkinson's and Alzheimer's disease.

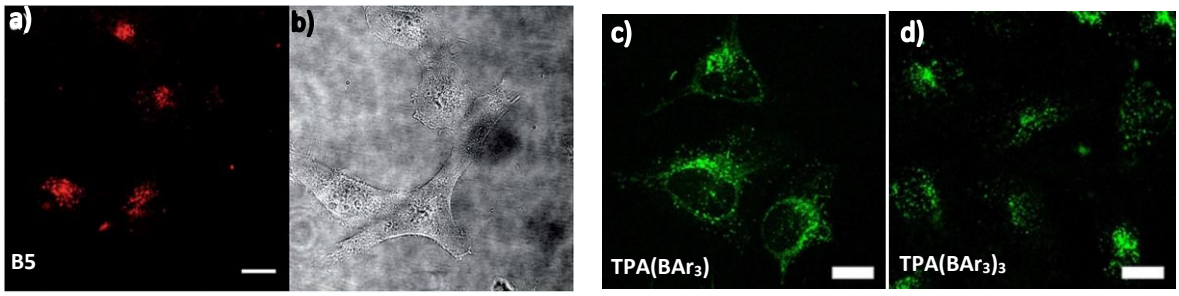

Figure 6-4: Left Panel: (a) Two-photon excited fluorescence and (b) bright field images of HeLa cells stained with **B5** (500nM). The TPEF image was recorded under excitation at 720nm (AOTF 38%) using an HyD detector with bandpass filter 650/50 and an HC Fluotar L 25x0.95 W VISIR objective. Scale bar: 20μm. Reproduced from ref. [161]

Right Panel: Two-photon excited fluorescence image of HeLa cells stained with 0.5μM **TPA(BAr$_3$)** (c) or **TPA(BAr$_3$)$_3$** (d). The TPEF images were recorded with excitation at 800 nm (AOTF 10%) using an HyD1 detector with bandpass filter 585/40 and an HCX APO L 40x0.80 W UVI objective. Scale bar: 20μm. Reproduced from ref. [188]

6.2 Preliminary Investigations

This thesis was motivated by the need to improve the understanding of the nonlinear properties and how the molecular structural parameters can affect these spectroscopic properties. Extensive investigation and significant progresses have been made on this research field in design and synthesis of chromophores with enhanced two-photon properties. However, the structure-property relations governing the 2PA has not been fully elucidated. Several studies in progress may support the knowledge for the development of materials with special nonlinear properties.

Conjugation effect[XXXI]

Future work concerns a deeper analysis of specific structural effects on the 2PA properties as mentioned in Chapter 5. Our goal in this preliminary work is to determine the influence of bridge conjugation on the 2PA cross section of a series of quadrupolar chromophores consisting of two methoxy substituted triphenylamine moieties that are connected to a benzene bridge via alkyne spacers at *para*- (***p*X**) and *meta*- (***m*X**) positions (see Figure 6-7), which were synthesized by Dr. Julian Schäfer.[210] As shown in Figure 6-7, the electron density at the benzene bridge varies by diverse substituents with different electron donating or accepting character, referred to as X. The electronic character of the substituents varies from strongly electron donating (X= OMe) to strongly electron accepting (X = NO_2).

[XXXI] This work has been investigated in a bachelor thesis under the supervision of E. Michail:
"*Linear and non-linear optical properties of triarylamine meta- and para- conjugated compounds with varying π - bridge electron densities*", C. Rimagmos, Bachelor Thesis, Julius-Maximilians-Universität, Würzburg, **2020**.

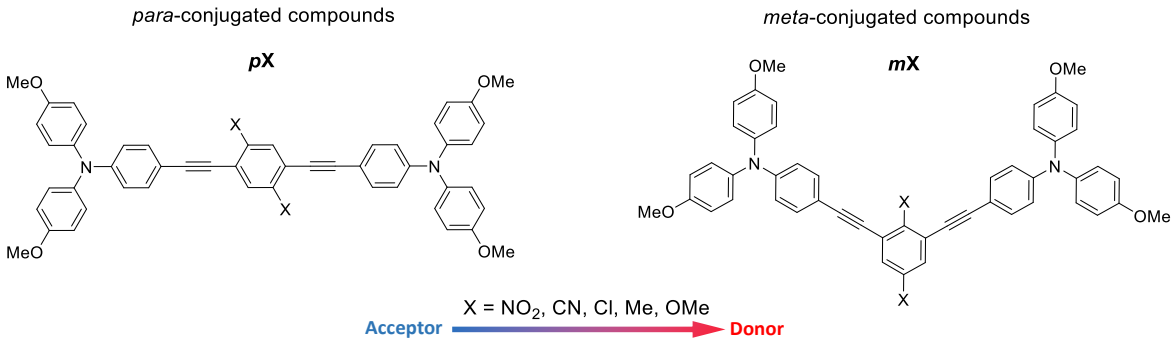

Figure 6-7: Chemical structure of the *para*- and *meta*- conjugated compounds ***p*X** and ***m*X**, with varying substituents at the benzene bridge.

The preliminary results of this study include the four quadrupolar *para*- and *meta*- conjugated chromophores with cyano (X = CN) and methyl (X = Me) substituents. The steady-state linear and nonlinear absorption spectra of ***p*Me**, ***p*CN**, ***m*Me** and ***m*CN** were recorded in toluene and are depicted together in Figure 6-8.

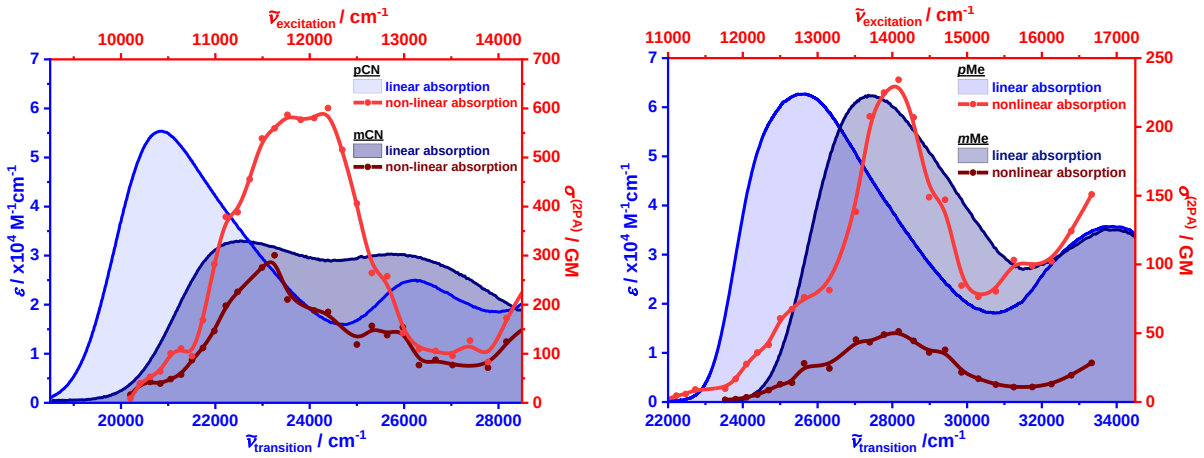

Figure 6-8: A comparison of the 1PA (shaded area) and 2PA (line with dots) spectra of pX (light colour) and mX (dark colour) conjugated compounds with substituents X=Me (left panel) and X=CN (right panel) in toluene.

The different conjugation pathway gives rise to different linear and 2PA spectra in toluene, as seen in Figure 6-8. The *para*-conjugated compounds ***p*Me** and ***p*CN** induce a shift of the main absorption band to the low energy region (*ca.* 1800 cm^{-1}) in respect to *meta*-conjugated compounds ***m*Me** and ***m*CN**. Simultaneously, at the higher energy side, a weak absorption band is observed which remains invariant in two isomers at *ca.* 33800 cm^{-1} for ***p*Me** and ***m*Me** and at *ca.* 26300 cm^{-1} for ***p*CN** and ***p*CN.** The 2PA cross section of *para*-conjugated compounds ***p*Me** and ***p*CN** reaches maximum values of 230 GM at 28200 cm^{-1} and 580 GM at 24400 cm^{-1} respectively, which are around five and two times higher than the corresponding *meta*-conjugated compounds ***m*Me** and ***m*CN** at the same energetic positions.

These spectral effects on 1PA and 2PA spectra were ascribed to an increased charge transfer ability with the direct conjugation pathway of *para*-compounds ***p*X** compared to the non-direct conjugation pathway of *meta*-compounds ***m*X** (see Figure 6.9). This assumption is supported by several previous works, which have investigated the influence of the different conjugative topologies on the ease of electron transfer.[211-215]

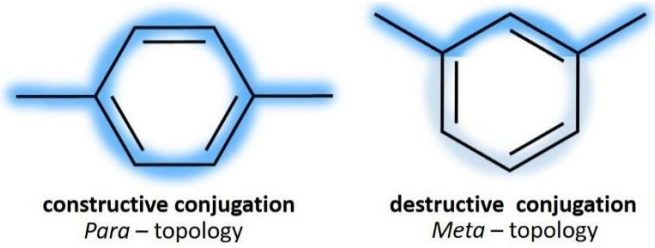

Figure 6-9: Illustration of constructive direct conjugation pathway of para-compounds and the destructive conjugation pathway of meta-compounds.

Moreover, these spectroscopic behavior of linear and nonlinear absorption spectra of the investigated compounds can be explained by a prevented electronic communication, where the *meta*-conjugation would effectively divide the molecule into two parts, each of which has its contribution to 2PA cross section.[216,217]

As mentioned before, by tuning the electron density at the bridge using substituents with different electron donating or accepting character, we can investigate how the nature of the π-bridge affects their nonlinear properties. Indeed, the 2PA cross section increases by changing the substituents from methyl (X = Me) to cyano (X = CN). Taking into consideration that the two methoxy substituted triphenylamine units serve as electron donor moieties, the 2PA cross section increases dramatically when cyano substituents, with more electron accepting character, are attached in the π-bridge (D-π-A-π-D). [167,218,219] Likewise in the case of the **aB7** quadrupolar triarylborane compound (see subchapter 5.2.2), a π-bridge exhibiting a strong electron donating character (A-π-D-π-A) results in an increased transition dipole moment between the first one-photon resonant and the final two photon resonant excited state and consequently in high 2PA cross section.

Albota *et al.*[95] reported first the concept of symmetric charge transfer from the ends of a conjugated system to the middle upon excitation which correlates to enhanced 2PA cross section values. Brédas *et al.*[96] showed that the 2PA cross section increases when electron acceptors are attached as a side group to the π-bridge, to form molecules of general structure D-π-A-π-D. These studies suggested that the symmetric charge transfer is effective in enhancing the two-photon absorptivity irrespective of the direction of the transfer (from the ends to the center or vice versa).

Solvent effect on 2PA cross section

This thesis` investigations have been focused on exciton coupling effects on 2PA as well as the correlation between the intramolecular charge transfer and the two-photon absorptivity, based on molecular structure characteristics. However, there are several other parameters which affect the two-photon absorptivity. An example is how the surrounding medium and specifically the role of solvent polarity can affect the 2PA process.[93,220-223]

Solvent effect studies on the 2PA of push-pull molecules show strong dependence of the molecular geometry in solution associated with the polarity of the solvent, thus leading to enhanced 2PA cross sections. [93,221,223,224] However, several theoretical and experimental studies have found that the 2PA cross section does not show a monotonic dependence on the polarity of the solvent.[72,220,225,226] Indeed, there is no general agreement due to a lack of systematic study in this direction. The theoretical and experimental efforts to address how the solvent affects the 2PA are limited, even though a significant number of works have been devoted to clarifying the solvent dependence of linear spectroscopy.

2PA circular and circular-linear dichroism

The polarization-depended 2PA spectroscopy principles can potentially be utilized as a grounding theory for nonlinear polarization-depended applications, which could be an interesting area of future research. A characteristic example is the 2PA circular dichroism (2PA-CD) spectroscopy.

The 2PA-CD spectroscopy was first proposed by Tinoco[227] and Power[228] in the 1970s and regained the attention of the research community during the last years. Important improvements were made in 2009 by Hernandez and *co*-workers[229,230] by introducing the double L-scan technique for the simultaneous measurements of polarization-depended nonlinear absorption. The 2PA-CD spectroscopy is a powerful tool for the investigation of optical effects beyond the electric dipole approximation of chiral systems.[231-234] The 2PA circular dichroism $\Delta\sigma^{(\text{2PA-CD})}$ is defined as the relative difference between the values of the 2PA cross-section for the left- and right-handed circular polarized light,[235-237]

$$\Delta\sigma^{(\text{2PA}-\text{CD})} = \sigma_{CL}^{(\text{2PA})} - \sigma_{CR}^{(\text{2PA})} \tag{6–3}$$

The estimation of this effect should be measurable using the 2PIF apparatus using the same procedure used to measure the 2PA polarization-dependent ratio $\Omega^{(\text{2PA})}$, as described in the experimental methods 8.2. Future studies of chiral fluorophores may combine the 2PA circular dichroism $\Delta\sigma^{(\text{2PA-CD})}$ spectroscopy, by using the 2PIF apparatus, with the linear circular dichroism spectroscopy, as well as with the 1PA and 2PA spectroscopy.

7 Summary and Conclusion

Main objectives of the present dissertation can be divided in two parts. The first part deals with setting up a spectroscopic technique for reliable and accurate measurements of the two-photon absorption (2PA) cross section spectra. In the second part, this firmly established experimental technique together with conventional spectroscopic characterization, quantum-chemical computations and theoretical modelling calculations was combined and therefore used as a tool to gain information for the so-called structure-property relationship through several molecular compounds.

The first part of the work initially introduces the main concept of the 2PA phenomenon and establishes the theoretical basis of the chosen experimental technique. Subsequently, the design and the development of a two-photon induced fluorescence (2PIF) spectroscopic apparatus for determination of the 2PA cross section are described, providing a complete experimental protocol. The 2PIF technique is based on the relative method, in which the intensity of the fluorescence emission induced by 2PA is measured. The 2PA cross section of a material is determined by comparing the material response to that of a reference substance of known 2PA cross section under identical experimental conditions. This technique was chosen for being sensitive to 2PA in a broad excitation energy range (550 – 1600 nm).

The setting up of this spectrometer is associated with two major challenges. Firstly, the excitation beam parameters and the fluorescence collection conditions must be the same for both the unknown sample and the reference standard. Secondly, the spectrometer with respect to the reference compound`s emission characteristics must be correctly calibrated. In order to overcome the first critical prerequisite, a set of irises and silver protected mirrors have to be aligned. This ensures that the excitation beam for the whole wavelength range achromatically passes through the reference and the sample compounds, placed in a precision rotation cuvette holder stage. Accordingly, the emission signal is collected at 90° using achromatic aspherical lenses, minimizing the colour and spherical aberration.

The second prerequisite demands the determination of the ratio between the fluorescence quantum yields of reference and sample as determined through the 2PIF spectrometer and obtained by the emission spectra for reference standards and samples in one-photon excitation. The latter helps avoiding errors due to the detection of the spectral response as the sample`s and reference`s emissions are not always spectrally overlapping. During the experimental procedure a critical parameter is the verification of the quadratic dependence between the excitation power and emitted fluorescence at every excitation wavelength, ensuring that only 2PA process takes place.

The second part deals with several new organic molecules, which were synthesized in the group of Prof. C. Lambert and Prof. T. B. Marder. The purpose was to investigate how structural parameters affect the 2PA cross section and lead to an alteration of their nonlinear optical properties. Particularly, this part focuses on electron delocalization and intra-molecular charge transfer phenomena since they are strongly correlated with the two-photon absorptivity. This investigation also includes theoretical approaches in order to interpret the experimental results and to estimate related quantities which therefore may be used as design criteria to achieve sizeable 2PA cross sections. Last but not least, polarization-depended nonlinear spectroscopic measurements turned out to be a powerful tool to substantiate the obtained results.

In order to gain insight into the strong correlation between the structural parameter effects and two-photon absorptivity, three separate parts were organized: i) the exciton coupling interaction between the chromophores, ii) the bridging unit characteristics and iii) the multi-branching concept. In this regard, a series of **SQA-based squaraine homodimers** was explored where the variation of the coupling unit between the two monomers leads to an alteration of their optical properties. Going a step further, two **SQB-based squaraine homodimers** forming two isomers were studied in which the molecular symmetry also has a great impact on their spectroscopic properties. Consequently, attention to the bridging effect on their nonlinear optical properties was drawn in a series of **π-bridged bis-triarylborane chromophores** with varying π-bridging units, where the 2PA spectra depend significantly on the characteristics and the nature of the bridge. To complete the picture of intramolecular charge transfer in the framework of 2PA, an exploration of the branched systems based on dipolar chromophores connected via a core moiety was taken place, which in this case consists of triphenylamine center. Thus, a series of **cationic triarylborane chromophores** was studied by concentrating on the differences between dipolar and octupolar charge distribution. Lastly, in this concept of multidimensional branching molecular design strategy, another series of **polychlorinated triarylmethyl radical compounds** was investigated on going from the simple dipolar to quadrupolar and octupolar compound.

Based on the discussed findings, some general conclusions can be drawn about the structure-property relationship on the 2PA properties. The major outcome is that the 2PA increment roughly follows the exciton coupling interaction between the conjugated chromophores, leading to the conclusion that the combination of a short and conjugated bridging unit between the two squaraine chromophores increases the exciton coupling strength and leads to an enhanced 2PA strength in such homodimers. The dominant factor that affects the two-photon absorptivity of these squaraine chromophores is demonstrated to be the exciton coupling interaction rather than the intramolecular charge transfer. Moreover, the 2PA spectra indicate that the symmetry has a huge impact on the two-photon

absorptivity, which emphasizes the effect of the *para*-conjugation *vs*. *meta*-conjugation. Indeed, the para-conjugation pathway increases the electronic coupling of the two chromophores when compared with the *meta*-conjugation pathway.

Moving forward to the π-conjugated triarylborane chromophores, co-planarity and the electron density of the conjugation have been identified, where in turn particularly important parameters define the intramolecular charge transfer ability. The extent of π-conjugation and consequently the molecular size has been found to increase the 2PA cross section as it is also a critical structure parameter. Finally, incorporating two or three chromophoric units in a single multichromophoric molecule has led to remarkable increase of the 2PA cross section through the synergetic co-operation of the chromophores.

Further studies have demonstrated that several of the investigated compounds with distinct spectroscopic and physical properties appear to be good candidates for specific applications such as high-resolution biological imaging and optical power limiting.

8 Appendix

8.1 Derivation of Expressions and Equations

Here we are going to derive expressions used in the previous chapters in order to provide a more comprehensive understanding of the physical quantities. The first subchapter 8.1.1 describes the excitation regimes in which the 2PIF measurements should be performed in order to achieve two-photon excitation conditions (see subchapter 3.3.1). Therefore, this chapter is a link between the key employed quantities (see Chapter 4, *i.e.* $P^{(2PA)}$, $<\delta^{(2PA)}>$, $r^{(2PA)}$, $\Omega^{(2PA)}$) and their origin. The mathematical framework is under the semi-classical theory of light-matter interaction, in which the matter is described by the quantum mechanical theory while the light is treated classically.

8.1.1 Two-Photon Excitation Fractional Equations

The Lambert-Beer law (see equations (1–1) and (1–2)) can be used to express the number of photons $p^{(2PA)}$ absorbed via 2PA process. Taking into account the propagation (*e.g. z*-axis) of the beam with photon flux F_L per unit area and time $p^{(2PA)}$ is given as:

$$p^{(2\mathrm{PA})} = \frac{dF_L}{dz} = -\sigma^{(2\mathrm{PA})} N {F_L}^2 \tag{8–1}$$

The number of molecules *N* per volume which are involved in the 2PA process refer to a quantity that depends on the photon flux (see Chapter 1.3.2). Furthermore, it can also be time dependent; *N* depends on the total number of photons absorbed since the beginning of the pulse, consider the fact that molecules which are promoted to an excited state via absorption cannot be excited further until they return to the ground state. Thus, by taking into consideration this condition, the number of molecules $N(\tau)$ is given by the equation,

$$N(\tau) = N_0 - \int_0^{\tau} \frac{p^{(2\mathrm{PA})}(t)}{2} dt = N_0 \mathrm{e}^{-\frac{1}{2}\sigma^{(2\mathrm{PA})}\tau {F_L}^2} \tag{8–2}$$

where N_0 represents the total number of molecules per unit volume in the material and the factor 1/2 accounts for the fact that two absorbed photons produce one excited molecule. Thus, the number of molecules $N^{(2PA)}(\tau)$ which are excited via 2PA during each pulse is:

$$N^{(2\mathrm{PA})}(\tau) = N_0 - N(\tau) \approx \frac{1}{2} N_0 \tau \sigma^{(2\mathrm{PA})} {F_L}^2 \tag{8–3}$$

Similarly, the number of photons $p^{(2PA)}$ absorbed by the materials during each pulse can be obtained from this equation and the excitation volume $V=\pi w_0^2 L$ as indicated in equation (8–4). As before the factor of 2 indicates the two photons absorbed per one molecule.

$$p^{(2PA)} = 2N^{(2PA)}V = N_0\tau\sigma^{(2PA)}{F_L}^2\,(\pi w_0^2 L) \tag{8–4}$$

Finally, in order to elaborate the experimental conditions in the 2PIF experiment the calculation of the fractional changes in molecular population and photon flux, by defining the quantities $\Delta N^{(2PA)}$ and $\Delta p^{(2PA)}$, is needed. Consequently, $\Delta N^{(2PA)}$ is the fraction of molecules excited per pulse via two-photon excitation and is defined as the ratio of the number of molecules of the sample which were excited via 2PA, $N^{(2PA)}$, divided by the total number of molecules in the illuminated sample volume N_0.

$$\Delta N^{(2PA)} = \frac{N^{(2PA)}}{N_0} \approx \frac{1}{2}\,\sigma^{(2PA)}\tau{F_L}^2 \tag{8–5}$$

Accordingly, $\Delta p^{(2PA)}$ is the fraction of photons absorbed per pulse via two-photon excitation and is defined as the ratio between the number of photons present in the excitation beam which were absorbed by the sample, $p^{(2PA)}$, divided by the total number of photons of the excitation beam p_0. The total number of photons of energy E can be expressed as $p_0 = E\lambda / hc$ and by substituting the photon flux $F_L = \lambda E / \tau hc(\pi w_0^2)$ in equation (8–4) we obtain:

$$\Delta p^{(2PA)} = \frac{p^{(2PA)}}{p_0} \approx\ \sigma^{(2PA)}N_0F_LL \tag{8–6}$$

The equations (8–5) and (8–6) are essential approximations for the selection of excitation regimes in which the 2PIF experiments are obtained (see subchapter 3.1.1).

Notably, the above approximations are applicable for the case where $f^{-1} >> \tau_{fl} >> \tau$; Since the excitation beam diameter remains almost constant over the cuvette length L, it has constant intensity over the beam cross section (πw_0^2). A train of laser pulses with pulse duration τ and repetition rate f excites the sample. Let us assume that the material is in the same condition every time and when a new pulse arrives the excitation is instantaneous on the timescale of the excited state lifetime τ_{fl}. Thus, after excitation by one pulse, the molecules relax completely before the arrival of the following pulse. In this situation, the number of photons being absorbed or emitted is additive in the number of pulses.

8.1.2 Two-Photon Absorption Probability

The quantum mechanical time-dependent perturbation theory sorts the interaction of light radiation and matter into a sequence of events (*i.g.* 1PA, 2PA) of decreasing probability. The key notion is the attempt to solve the Schrödinger equation deriving an analytical expression for two-photon transition probability $P^{(2PA)}$ by the second order time-depended perturbation theory. Within this frame, we start from the time-dependent Schrödinger equation:

$$i\hbar \frac{\partial \psi(\vec{r},t)}{\partial t} = \hat{H}\psi(\vec{r},t) \tag{8–7}$$

Where $\psi(\vec{r},t)$ is the atomic wave-function and $\hat{H}$ the Hamiltonian which can be represented as a sum, $\hat{H} = \hat{H}_0 + \lambda\hat{V}(t)$, of the unperturbed Hamiltonian $\hat{H}_0$ (Hamiltonian for a free atom) and the perturbation Hamiltonian $\hat{V}(t)$ (the time-dependent interaction potential) and λ is a small parameter. Using the perturbation theory, the above equation must be solved in two steps.

First, the eigenfunctions and the eigenvalues of the unperturbed Hamiltonian $\hat{H}_0$ which are later corrected and take into account the perturbation's influence are obtained. Choosing a basis for the space of degenerate levels, the wave-function $\psi(\vec{r},t)$ can be written as:

$$\psi(\vec{r},t) = \sum_{\mathrm{i}} \alpha_{\mathrm{i}}(t)\varphi_{\mathrm{i}}(\vec{r},t) \tag{8–8}$$

The wavefunction resulting from the solutions of Schrödinger`s equation for a free atom which interacts with an optical field $\vec{\mathrm{E}}(\mathrm{t}) = \mathrm{E}\mathrm{e}^{-i\omega \mathrm{t}}$ can be represented as:

$$\psi(\vec{r},t) = \sum_{n} \alpha_{\mathrm{i}}(t)\, u_{\mathrm{i}}(\vec{r})\mathrm{e}^{-i\omega_{\mathrm{i}}t} \tag{8–9}$$

in which $\alpha_i(t)$ is the probability amplitude that the system is at the i-th energy level at time t, where ω_i is the angular frequency of the transition from the ground state to the i-th excited state with energy E_i, since $\omega_i = E_i / \hbar$. The eigenvalue equation reads $\hat{H}_0\, u_i(\vec{r}) = E_i\, u_i(\vec{r})$ and expresses the energy eigenstates of unperturbed Hamiltonian from a complete set, as a linear combination of these eigenstates as is shown in equation (8–9). Therefore, substitution of equation (8–9) into (8–7),

$$\begin{aligned} i\hbar \sum_{\mathrm{i}} \frac{\partial[\alpha_{\mathrm{i}}(t)]}{\partial t} u_{\mathrm{i}}(\vec{r})e^{-i\omega_{\mathrm{i}}t} + i\hbar \sum_{\mathrm{i}} \alpha_n(t) \frac{\partial\left[u_{\mathrm{i}}(\vec{r})e^{-i\omega_{\mathrm{i}}t}\right]}{\partial t} \\ = \sum_{\mathrm{i}} \alpha_{\mathrm{i}}(t)\, E_{\mathrm{i}} u_{\mathrm{i}}(\vec{r})e^{-i\omega_{\mathrm{i}}t} + \sum_{\mathrm{i}} \alpha_{\mathrm{i}}(t)\left[\lambda\hat{V}\right]u_{\mathrm{i}}(\vec{r})e^{-i\omega_{\mathrm{i}}t} \end{aligned} \tag{8–10}$$

and by performing the time-derivatives can be obtained:

$$\begin{aligned} \hbar \sum_{\mathrm{i}} \frac{\partial[\alpha_{\mathrm{i}}(t)]}{\partial t} u_{\mathrm{i}}(\vec{r})e^{-i\omega_{\mathrm{i}}t} + i\hbar \sum_{\mathrm{i}} (-i\omega_{\mathrm{i}})\, a_{\mathrm{i}}(t)\, u_{\mathrm{i}}(\vec{r})e^{-i\omega_{\mathrm{i}}t} \\ = \sum_{\mathrm{i}} a_{\mathrm{i}}(t)\, (\hbar\omega_{\mathrm{i}}) u_{\mathrm{i}}(\vec{r})e^{-i\omega_{\mathrm{i}}t} + \sum_{\mathrm{i}} a_{\mathrm{i}}(t)\left[\lambda\hat{V}\right]u_{\mathrm{i}}(\vec{r})e^{-i\omega_{\mathrm{i}}t} \end{aligned} \tag{8–11}$$

The second and the third terms are equivalent and eliminated. Following the orthonormality condition, multiplication of both sides with the complex eigenfunction $\varphi_m^*(\vec{r},t) = u_m^*(\vec{r})e^{i\omega_m t}$ and by integrating over $\vec{r}$ ($d^3r = dx{\cdot}dy{\cdot}dz$) coordinates, the equation (8–11) can be rewritten as:

$$i\hbar \sum_{\mathrm{i}} \frac{\partial[a_{\mathrm{i}}(t)]}{\partial t}\left[e^{-i\omega_{\mathrm{i}}t}\right]\left[e^{i\omega_m t}\right] \int_V [u_{\mathrm{i}}(\vec{r})u_m^*(\vec{r})]\, d^3r = \sum_{\mathrm{i}} a_{\mathrm{i}}(t)\left[e^{-i\omega_{\mathrm{i}}t}\right]\left[e^{i\omega_m t}\right] \int_V \left[u_{\mathrm{i}}(\vec{r})\left[\lambda\hat{V}\right]u_m^*(\vec{r})\right] d^3r \tag{8–12}$$

As it is known, if each individual member of the set of wavefunctions is normalized, they constitute an orthonormal set, thus, using the orthonormality condition for eigenstates:

$$\int_V u_{\mathrm{i}}(\vec{r})\, u_m^*(\vec{r}) d^3r = \delta_{\mathrm{i}m} \quad \text{where} \quad \delta_{\mathrm{i}m} = \begin{bmatrix} 1 & \text{if } (\mathrm{i} = m) \\ 0 & \text{if } (\mathrm{i} \neq m) \end{bmatrix} \tag{8–13}$$

Therefore, when i = m the equation (8–11) can be expressed as,

$$i\hbar \frac{\partial[a_{\mathrm{i}}(t)]}{\partial t} = \sum_{\mathrm{i}} a_{\mathrm{i}}(t)\left[\lambda\hat{V}_{\mathrm{mi}}\right]e^{-i\omega_{\mathrm{mi}}t} \tag{8–14}$$

where $\omega_{\mathrm{mi}} = \omega_{\mathrm{i}} - \omega_{\mathrm{m}}$ and $\hat{V}_{\mathrm{im}} = \int \left[u_{\mathrm{i}}(\vec{r})\left[\lambda\hat{V}\right]u_m^*(\vec{r})\right] d^3r$, which represents the matrix element of the perturbation Hamiltonian $\hat{V}(t)$. The latter equation (8–14) cannot be solved exactly. For this reason the time-dependent perturbation theory technique is used, by expanding the parameter λ ($\lambda = \lambda_{(1)} + \lambda_{(2)} + \ldots$) and the coefficients α_{i} ($\alpha_{\mathrm{i}} = [\alpha_{\mathrm{i}}]_{(1)} + [\alpha_{\mathrm{i}}]_{(2)} + \ldots$) into a series

$$\left[\frac{\partial[a_n(t)]}{\partial t}\right]_{(N)} = (i\hbar)^{-1} \sum_{\mathrm{i}} [a_{\mathrm{i}}(t)]_{(N-1)} \hat{V}_{n\mathrm{i}} e^{-i\omega_{n\mathrm{i}}t} \qquad N = 1,2,3 \tag{8–15}$$

where *N* is an integer number. The case where *N* = 1 refers to a first-order interaction and describes the linear absorption process. The second-order interaction, *N* = 2 leads to the 2PA. The strategy is to solve the differential equation (8–15) for *N* = 1, and then substitute the latter into equation (8–15) for *N* = 2. The initial conditions can be expressed as:

(a) Before the excitation all the electrons are found in the ground state g *N*=0:

$$[a_{\mathrm{i}}(t)]_{(0)} = \begin{bmatrix} 1 & \text{if } (\mathrm{i} = \mathrm{g}) \\ 0 & \text{if } (\mathrm{i} \neq \mathrm{g}) \end{bmatrix} \tag{8–16}$$

(b) in the case of linear absorption, *N* = 1, the perturbation Hamiltonian $\hat{V}(t)$ may be represented as the interaction energy with the incident electromagnetic field $\vec{E}$,

$$\hat{V}(t) = \vec{\mu} \cdot \vec{E}(t) \;\rightarrow\; \hat{V}_{\mathrm{gi}} = -\left(\vec{\mu}_{\mathrm{gi}} \cdot \vec{e}\right)\left(\frac{E}{2}e^{-i\omega t} + \frac{E^*}{2}\, e^{i\omega t}\right) \tag{8–17}$$

where $\vec{\mu}_{\mathrm{gi}}$ is the transition moment between the ground state (g) and the i-th excited state. At the same time, $\vec{E}(t)$=$E\vec{e}$ is the incident electric field with amplitude *E* and polarization vector $\vec{e}$.

For $N = 1$ and taking into account the initial conditions (8–16) and (8–17), the differential equation (8–15) for $[\alpha_i(t)]_{(1)}$ can be integrated directly and we obtain:

$$[a_i(t)]_{(1)} = \frac{(\vec{\mu}_{gi} \cdot \vec{e})E}{2\hbar(\omega_{gi} - \omega)}\left(e^{i(\omega_{gi}-\omega)t} - 1\right) + \frac{(\vec{\mu}_{gi} \cdot \vec{e})E^*}{2\hbar(\omega_{gi} - \omega)}\left(e^{i(\omega_{gi}+\omega)t} - 1\right) \qquad (8–18)$$

Since the transition occurs from a lower energy state to a higher energy state *i.e.* $\omega_{gi} = \omega_i - \omega_g > 0$, the first term can be resonant and predominates when $\omega_{gi} \approx \omega$ and corresponds to the 1PA process. The second term can be predominant when $\omega_{gi} = \omega_i - \omega_g < 0$, which leads to a transition from a higher energy state to a lower energy state and corresponds to the stimulated emission process. Notably, the first term in the above equation gives the one-photon transition probability ($P^{(1PA)} = |[\alpha_i(t)]_{(1)}|^2$) of finding the system in the exciting state i at time $t > 0$ (see Chapter 4, equation (4–1)).

The second order probability amplitude, $[\alpha_i(t)]_{(2)}$ which eventually leads to the 2PA process, follows the initial conditions:

(a) The expression for the $N = 1$ is known (equation (8–18), and the second term neglected because it does not result in 2PA,

$$[a_i(t)]_{\{1\}} = \frac{(\vec{\mu}_{gi} \cdot \vec{e})E}{2\hbar(\omega_{gi} - \omega)}\left(e^{i(\omega_{gi}-\omega)t} - 1\right) \qquad (8–19)$$

(b) In the case of 2PA, the perturbation Hamiltonian $\hat{V}(t)$ may be represented as:

$$\hat{V}(t) = \vec{\mu} \cdot \vec{E}(t) \rightarrow \hat{V}_{if} = -(\vec{\mu}_{if} \cdot \vec{e})\left(\frac{E}{2}e^{-i\omega t} + \frac{E^*}{2}e^{i\omega t}\right) \qquad (8–20)$$

where $\vec{\mu}_{fi}$ is the transition moment between the intermediate one-photon resonant sate, i, and the final two-photon resonant excited state, f. By substituting equation (8–19) and (8–20) into equation (8–15) for $N = 2$ results in:

$$\left[\frac{\partial[a_f(t)]}{\partial t}\right]_{(2)} = (i\hbar)^{-1}\sum_i \frac{(\vec{\mu}_{gi} \cdot \vec{e})(\vec{\mu}_{if} \cdot \vec{e})E^2}{4\hbar(\omega_{gi} - \omega)}\left(e^{i(\omega_{gf}-2\omega)t}\right) \qquad (8–21)$$

In the time-dependent part of equation (6–9) we kept only the term which relates the instantaneous transition from a lower energy-state g to a higher energy-state f ($\omega_{gf} = \omega_f - \omega_g$) and thus the equation (8–21) corresponds to 2PA process.

The differential equation (8–21) can be integrated directly over time to obtain

$$[a_f(t)]_{(2)} = (i\hbar)^{-1}\sum_i \frac{(\vec{\mu}_{gi} \cdot \vec{e})(\vec{\mu}_{if} \cdot \vec{e})E^2}{4\hbar(\omega_{gi} - \omega)}\left(\frac{e^{i(\omega_{gf}-2\omega)t} - 1}{\omega_{gf} - 2\omega}\right) \qquad (8–22)$$

Thus, the time-dependent probability $P_{gf}^{(2PA)}$ of two-photon induced transition f ← g is:

$$P_{\mathrm{gf}}^{(2\mathrm{PA})} = \left|[a_{\mathrm{f}}(t)]_{\{2\}}\right|^2 = \frac{E^4}{16\hbar^4}\left|\sum_{\mathrm{i}} \frac{(\vec{\mu}_{\mathrm{gi}}\cdot\vec{e})(\vec{\mu}_{\mathrm{if}}\cdot\vec{e})}{(\omega_{\mathrm{gi}}-\omega)}\right|^2 \left(\frac{e^{i(\omega_{\mathrm{gf}}-2\omega)t}-1}{\omega_{\mathrm{gf}}-2\omega}\right)^2 \qquad (8\text{–}23)$$

At this point it is crucial to indicate the physical meaning of the subscripts g, i and f as indicated in Figure 8-1. Here, Dirac notation (bra/ket) represents the electronic states in a molecule, where $|\mathrm{g}\rangle$ indicates the ground state, $|\mathrm{i}\rangle$ assigns the intermediate one-photon resonant excited state and $|\mathrm{f}\rangle$ the final two-photon resonant excited state. The $\vec{\mu}_{\mathrm{gi}}$ and $\vec{\mu}_{\mathrm{if}}$ show the transition dipole moments between the corresponding states.

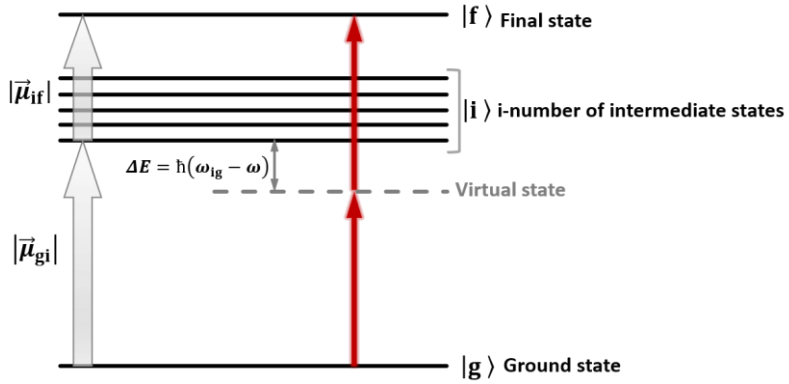

Figure 8-1: Schematic energy state diagram in a molecule. The red arrows indicate two-photon allowed transitions and the gray arrows the transition moments.

The sum in equation (8–23) contains all such potential intermediate one-photon resonant excited states and the contribution of each intermediate state is determined by the detuning energy $\Delta E = \hbar(\omega_{\mathrm{gi}} - \omega)$ between the energy of the intermediate one-photon allowed state $\hbar\omega_{\mathrm{gi}}$ and the excitation photon energy $\hbar\omega$.

In equation (8–23) the term enclosed in the second square bracket may describe the time dependence of the transition probability:[I]

$$\left(\frac{e^{i(\omega_{\mathrm{gf}}-2\omega)t}-1}{\omega_{\mathrm{gf}}-2\omega}\right)^2 = \frac{\sin^2\left[\frac{(\omega_{\mathrm{gf}}-2\omega)\mathrm{t}}{2}\right]}{\left[\frac{(\omega_{\mathrm{gf}}-2\omega)\mathrm{t}}{2}\right]^2} \qquad (8\text{–}24)$$

where in this approximation t^2 is the peak value ($2\omega \approx \omega_{\mathrm{gf}}$) and the width of the central peak is on the order of $2\pi t$. In the limit of large t, the limit of the time dependent function is proportional to t times a Dirac delta function $\delta(\omega)$ and the equation (8–24) can be written as:

[I] By using the trigonometric identity $\sin^2(x) = \frac{1-\cos(2x)}{2}$ and the Euler´s formula which express the cosine in terms of exponential functions $\cos(x) = \frac{e^{ix}+e^{-ix}}{2}$.

$$\lim_{t\to\infty}\left(\frac{e^{i(\omega_{gf}-2\omega)t}-1}{\omega_{gf}-2\omega}\right)^2 = 2\pi t\delta(\omega_{gf}-2\omega) \tag{8–25}$$

The Dirac delta function $\delta(\omega_{gf}-2\omega)$ confirms the condition that only if the transition energy is in resonance with the combined energy of the two incident photons the transition f ← g is possible. Organic chromophores usually exhibit spectra broadening of an excitation due to several reasons (*e.g.* vibrations, rotations, *etc.*). As a result, transitions occur between electronic states showing broad-band absorption spectra. By replacing the Dirac delta function with a line shape function $g(2\omega, \omega_{gf}, \Gamma)$ this line-broadening of the real electronic transition is taken into account. The line shape function is a normalized continuous distribution over all the frequency range

$$\int_0^\infty g(2\omega, \omega_{gf}, \Gamma)\, d(2\omega) = 1 \tag{8–26}$$

where ω is the incident photon energy, and Γ is the broadening factor which is an empirical damping parameter and describes the spectra broadening. Combing the equations (8–23) and (8–25) and according to the definition of photon flux F_L, which is related to the local intensity and the amplitude E of the electric field as follows:

$$F_L = \frac{I}{\hbar\omega} = \frac{nc\varepsilon_0}{2\hbar\omega}E^2 \tag{8–27}$$

The two-photon transition probability reads:

$$P_{gf}^{(2PA)} = \frac{1}{2}\frac{\pi\omega^2}{n^2c^2\varepsilon_0^2\hbar^2}tF_L^2\left|\sum_i \frac{(\vec{\mu}_{gi}\cdot\vec{e})(\vec{\mu}_{if}\cdot\vec{e})}{(\omega_{gi}-\omega)}\right|^2 g(2\omega, \omega_{gf}, \Gamma) \tag{8–28}$$

8.1.3 Rotationally averaged 2PA strength

According to the analytical expression of the two-photon transition probability, the sum in equation (8–28) defines the 2PA strength (see subchapter 4.2).

$$\delta^{(2PA)} = \left|\sum_i \frac{(\vec{\mu}_{gi}\cdot\vec{e})(\vec{\mu}_{if}\cdot\vec{e})}{(\omega_{gi}-\omega)}\right|^2 \tag{8–29}$$

where again, $\vec{\mu}_{gi}$ is the transition moment between the ground state and the intermediate one-photon allowed state and $\vec{\mu}_{if}$ the transition moment between the latter intermediate state and the final two-photon allowed state. At the same time $\omega_{gi} = \omega_i - \omega_g$ is the angular frequency of the transition to the intermediate state and ω is the frequency of the incident photon. The sum in the latter expression includes all the possible states counting also the initial and final states consisting of infinite number of

terms (so-called sum-over-state approximation, see Figure 4-1). However, the few-state model can be obtained by truncating the summation in equation (8–29) to include only a few excited states *i.e.* I = g, i and f. By this assumption, the sum may reduce to three terms,

$$\left|\sum_{\mathrm{i=g,i,f}} \frac{(\vec{\mu}_{\mathrm{gi}}\cdot\vec{e})(\vec{\mu}_{\mathrm{if}}\cdot\vec{e})}{(\omega_{\mathrm{gi}}-\omega)}\right|^2 = \left|\frac{(\vec{\mu}_{\mathrm{gg}}\cdot\vec{e})(\vec{\mu}_{\mathrm{gf}}\cdot\vec{e})}{-\omega}+\frac{(\vec{\mu}_{\mathrm{gf}}\cdot\vec{e})(\vec{\mu}_{\mathrm{ff}}\cdot\vec{e})}{(\omega_{\mathrm{gf}}-\omega)}+\frac{(\vec{\mu}_{\mathrm{gi}}\cdot\vec{e})(\vec{\mu}_{\mathrm{if}}\cdot\vec{e})}{(\omega_{\mathrm{gi}}-\omega)}\right|^2 \qquad (8\text{–}30)$$

The first two terms contain the permanent dipole moments $\vec{\mu}_{\mathrm{gg}}$, $\vec{\mu}_{\mathrm{ff}}$ of the ground and final states, respectively, as well as the transition moment $\vec{\mu}_{\mathrm{gf}}$ between the ground and the final excited state. Taking into account that the incident photon has half the transition frequency, $\omega \approx \omega_{\mathrm{gf}}/2$, we can combine them into one term. Thus, the 2PA strength under the few-state model approach yields the following expression

$$\delta^{(\mathrm{2PA})} = \left|\frac{(\vec{\mu}_{\mathrm{gf}}\cdot\vec{e})(\Delta\vec{\mu}_{\mathrm{gf}}\cdot\vec{e})}{\frac{\omega_{\mathrm{gf}}}{2}}+\frac{(\vec{\mu}_{\mathrm{gi}}\cdot\vec{e})(\vec{\mu}_{\mathrm{if}}\cdot\vec{e})}{\left(\omega_{\mathrm{gi}}-\frac{\omega_{\mathrm{gf}}}{2}\right)}\right|^2 \qquad (8\text{–}31)$$

which is composed by two terms. The first one is the "dipolar" term, denoted *D*, which contains the change of the permanent electric dipole moment upon transition $\Delta\vec{\mu}_{\mathrm{gf}} = \vec{\mu}_{\mathrm{ff}} - \vec{\mu}_{\mathrm{gg}}$ between the ground state and the final state. The second term is the "two-photon" term, denoted *T* which involves two excited states and is strongly dependent on their coupling.[6,93]

In order to take the random orientation into account we focus on the inner product of the vectors $(\vec{\mu}\cdot\vec{e})$ in the *D*- and *T*-term in equation (8–31), which must be averaged over all possible orientations of transition moment vector $(\vec{\mu})$ with respect to the excitation polarization $(\vec{e})$. Since each measurement yields an average response from many molecules in all possible orientations, the rotational-averaging methods[II] are used for the quantitative calculations. In these methods, when a molecule interacts with the incident light, the result depends upon the molecule`s orientation and is given by the function $f(\theta, \phi, \chi)$. The rotational-averaged value $\langle f \rangle$ integrates over all orientations and is given by:[238]

$$\langle f\rangle = \frac{1}{8\pi^2}\int_0^{\pi}\int_0^{2\pi}\int_0^{2\pi} f(\theta,\varphi,\chi)\sin(\theta)\,d\theta\,d\varphi d\chi \qquad (8\text{–}32)$$

where θ, ϕ and χ are the Euler angles that relate the coordinate systems as depicted in figure 4-2. A rotational average integrates over the full ranges of θ, ϕ and χ to account for the range of molecule

[II] Rotational-averaging methods are used routinely in spectroscopy *e.g.* absorption, emission, Raman, dichroism, pump-probe and several other spectroscopic methods. The goal is to calculate a statistical average over all orientation of a single molecule.

orientations in a sample. Thus, the numerator of the *D*-term on equation (8–31), for randomly orientated molecules under linearly polarized excitation light becomes[239]

$$\langle\left|\left(\vec{\mu}_{\mathrm{fg}}\cdot\vec{e}\right)\left(\Delta\vec{\mu}_{\mathrm{fg}}\cdot\vec{e}\right)\right|^2\rangle=\frac{1}{8\pi^2}\int_0^{\pi}\int_0^{2\pi}\int_0^{2\pi}\left|\vec{\mu}_{\mathrm{gf}}\cdot\vec{e}\right|^2\left|\Delta\vec{\mu}_{\mathrm{gf}}\cdot\vec{e}\right|^2\sin(\theta)\,d\theta\,d\varphi d\chi$$
$$=\frac{\left(2\cos^2\left(\theta_{\mathrm{gf}}\right)+1\right)}{15}\left(\mu_{\mathrm{gf}}^2\,\Delta\mu_{\mathrm{gf}}^2\right) \tag{8–33}$$

with θ_{fg} being the angle between the vectors $\vec{\mu}_{\mathrm{gf}}$ and $\Delta\vec{\mu}_{\mathrm{gf}}$. An averaging over space coordinates, such as in equation (8–33) can be performed yielding the following expression for the *T*-term of equation (8–31),

$$\langle\left|\left(\vec{\mu}_{\mathrm{gi}}\cdot\vec{e}\right)\left(\vec{\mu}_{\mathrm{if}}\cdot\vec{e}\right)\right|^2\rangle=\frac{1}{8\pi^2}\int_0^{\pi}\int_0^{2\pi}\int_0^{2\pi}\left|\vec{\mu}_{\mathrm{gi}}\cdot\vec{e}\right|^2\left|\vec{\mu}_{\mathrm{if}}\cdot\vec{e}\right|^2\sin(\theta)\,d\theta\,d\varphi d\chi$$
$$=\frac{\left(2\cos^2(\theta_{\mathrm{if}})+1\right)}{15}\left(\mu_{\mathrm{gi}}^2\,\mu_{\mathrm{if}}^2\right) \tag{8–34}$$

The Figure 8-2 illustrates all dipole moment vectors in the laboratory coordinate system (X, Y and Z) for the *D*- and *T*-term of the 2PA strength expression.

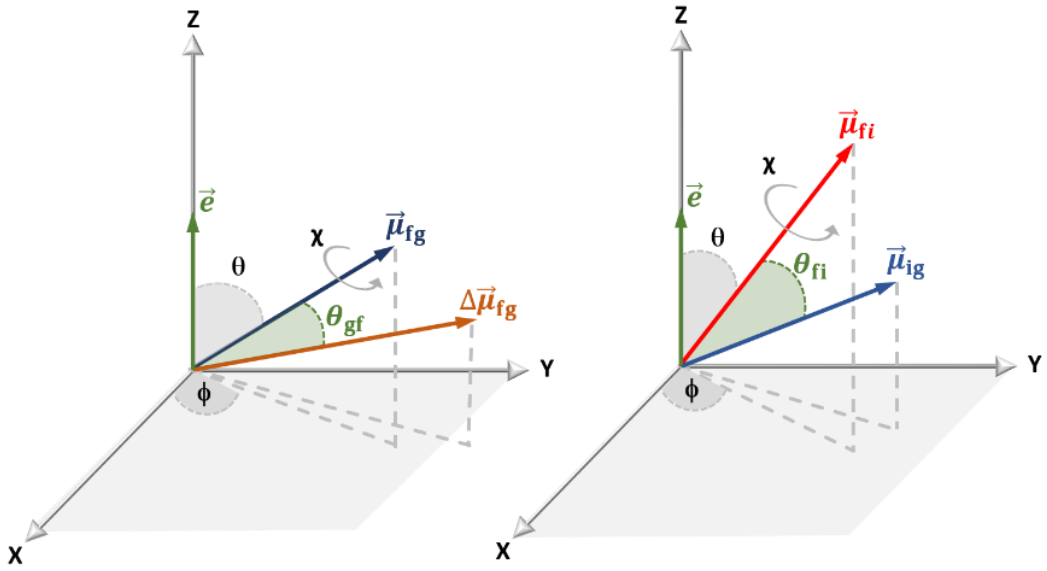

Figure 8-2: Schematic representation of the transition dipole moment vectors for the *D*-term (left) and *T*-term (right). X, Y and Z are the laboratory reference frame axes and θ, ϕ and χ are the Euler angles that relate to the coordinate system.

8.2 Experimental Methods

Steady-state UV/vis absorption spectroscopy

The linear optical absorption spectra were measured on a Jasco V670 UV/vis/NIR spectrometer (software SpectraManager v. 2.08.04) and Agilent Technologies Cary 5000 UV/vis/NIR spectrometer (software Agilent Cary WinUV Analysis and Bio v. 4.2) in 10 mm quartz cuvettes from Starna (Pfungstadt, Germany) at rt. Freshly prepared stock solutions were subsequently diluted (10^{-5}–10^{-6}M) aiming a concentration-independent behavior so that aggregation of the sample could be excluded.

Steady-state and time resolved fluorescence spectroscopy

The steady-state and time dependent fluorescence emission measurements were performed with an Edinburgh Instruments FLS980 spectrometer (software F980 version 1.2.2). The samples were strongly diluted (λ_{max} < 0.05 OD) in order to prevent self-absorption in 10 mm standard quartz cuvettes.

For the steady-state fluorescence measurements a 450 W Xenon lamp was used as excitation source and a R928P PMT detector (working range 11760-50000 cm^{-1}) as well as a R5509-42 PMT nitrogen-cooled detector (working range 7140-16660 cm^{-1}).

Fluorescence lifetime were determined by time-correlated single photon counting (TCSPC) by exciting the sample with pulsed laser diodes at 15240cm^{-1} and 12770 cm^{-1} under magic angle conditions. The fluorescence was detected with a H10720 high-speed PMT detector. The instrument response function was determined by using a scattering solution of colloidal silica in deionized water (LUDOX). Lifetimes were determined using the FAST software (version 3.4.2) by fitting with an (multi-) exponential decay function. The resulting expectation fluorescence lifetime value $\bar{\tau}_{fl}$ is:[240]

$$\bar{\tau}_{\mathrm{fl}} = \frac{a_1\tau_1 + a_2\tau_2}{a_1 + a_2} \tag{8–35}$$

where α_n are the amplitudes and the corresponding lifetimes τ_n. The radiative rate constant k_f was calculated using the fluorescence quantum yield (see below) by equation,

$$k_{\mathrm{fl}} = \frac{\varphi_{\mathrm{fl}}}{\bar{\tau}_{\mathrm{fl}}} \tag{8–36}$$

The squared fluorescence transition dipole moment μ_{fl} of the investigated compound was obtained by the Strickler–Berg equation

$$k_{\mathrm{fl}} = \frac{16 \times 10^6 \pi^3}{3h\varepsilon_0} \frac{n\,(n^2+2)^2}{9} \langle \tilde{\nu}_{\mathrm{fl}}{}^{-3} \rangle_{av}{}^{-1} \mu_{\mathrm{fl}}^2 \tag{8–37}$$

where $\langle \tilde{\nu}_{\mathrm{fl}}{}^{-3} \rangle_{\mathrm{av}}{}^{-1} = \int I_{\mathrm{fl}}\,\mathrm{d}\tilde{\nu} \;/\; \int \tilde{\nu}_{\mathrm{fl}}{}^{-3} I_{\mathrm{fl}}\,\mathrm{d}\tilde{\nu}$ is the average cubic fluorescence energy.

Fluorescence quantum yield

The fluorescence quantum yields were measured using an integration sphere combined with the FLS980 spectrometer applying the method of Bardeen *et. al.* and the observed photoluminescence quantum yield $\varphi_{\mathrm{fl,obs}}$, corrected for self-absorption by using the equation:[241]

$$\varphi_{\mathrm{fl}} = \frac{\varphi_{\mathrm{fl,obs}}}{1 - \alpha + (\alpha\, \varphi_{\mathrm{fl,obs}})} \tag{8–38}$$

where α is the probability of self-absorption of an emitted photon and is dependent on the overlap of the absorption and emission spectra.

One and two-photon fluorescence excitation anisotropy

The one-photon fluorescence excitation anisotropy (1P-FEA) measurements with the FLS980 spectrometer and the two-photon fluorescence excitation anisotropy (2P-FEA) with the 2PIF spectrometer were conducted using two thin broadband wavelength polarizers (ColorPol®IR 1300 BC5, CODIXX AG) for excitation and detection. The compounds in both type of anisotropy measurements were dissolved in highly viscous polyTHF ($M_n \approx 650$) in 10 mm standard quartz cuvettes. The anisotropy values $r^{(1PA)}$ and $r^{(2PA)}$ are defined by[242]

$$r = \frac{I_{\mathrm{VV}} - G I_{\mathrm{VH}}}{I_{\mathrm{VV}} + 2G I_{\mathrm{VH}}} \tag{8–39}$$

where, I_{VV} and I_{VH} are the detection fluorescence intensities with excitation polarizers aligned vertically and the detection polarizer vertically or horizontally, respectively. *G* is the grating factor which is the instrument sensitivity ratio of vertically and horizontally polarized light.

Representative example of the 2P-FEA measurements shown in Figure 8-3 which presented the 2P-FEA spectra together with the 2PA spectra for the **SQA**-based squaraine homodimers in subchapter 5.1.1 in toluene.

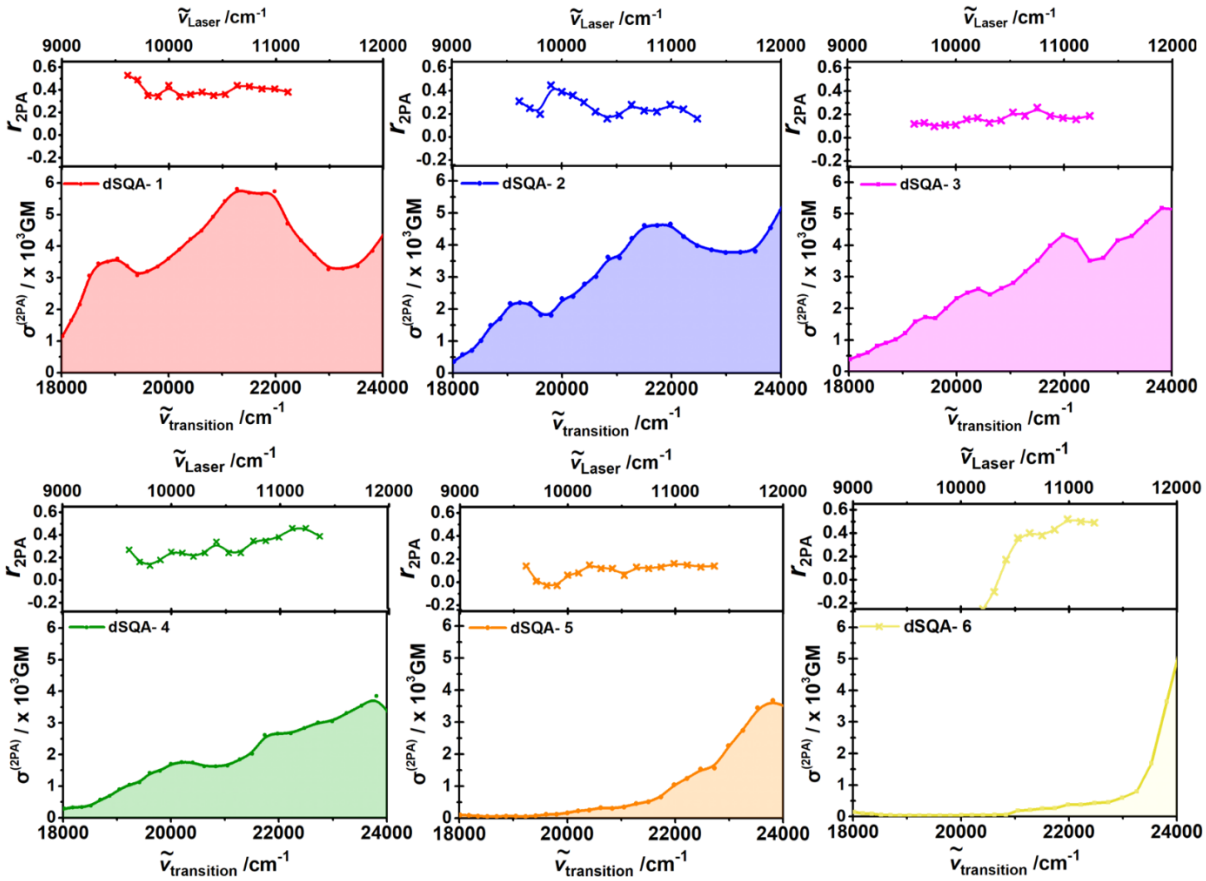

Figure 8-3: 2P-FEA spectra together with the 2PA spectra for all the **SQA**-based squaraine homodimers of subchapter 5.1.1.

Polarization-dependent 2PA ratio

Polarization-dependent 2PA measurements were performed in the 2PIF experimental apparatus by introducing an achromatic quarter-wave plate QP (SAQWP05M-1700, Thorlabs) into the excitation beam, after the focusing mirror. The polarization of the excitation beam was adjusted by the combination of the third polarizer P_3 and the waveplate. The polarization-dependent 2PA ratio $\Omega^{(2PA)}$ defined as:

$$\Omega^{(2\mathrm{PA})} = \frac{\left[I^{(2\mathrm{PA})}(\tilde{\nu}_{\mathrm{em.}})\right]_{(\mathrm{cir.})}}{\left[I^{(2\mathrm{PA})}(\tilde{\nu}_{\mathrm{em.}})\right]_{(\mathrm{lin.})}} \tag{8–40}$$

where $[I^{(2PA)}(\tilde{\nu}_{em.})]_{(cir.)}$ and $[I^{(2PA)}(\tilde{\nu}_{em.})]_{(lin.)}$ are the two-photon induced fluorescence signals recorded for circular and linear polarized excitation beam, respectively. One characteristic example of the determination of the polarization-dependent 2PA ratio is shown in Figure 8-4 where the quadratic power dependence of the 2PIF signal on the excitation power via circular and linear polarized light is depicted at selected excitation wavenumber for the **SQA**-based squaraine homodimers in fluid toluene.

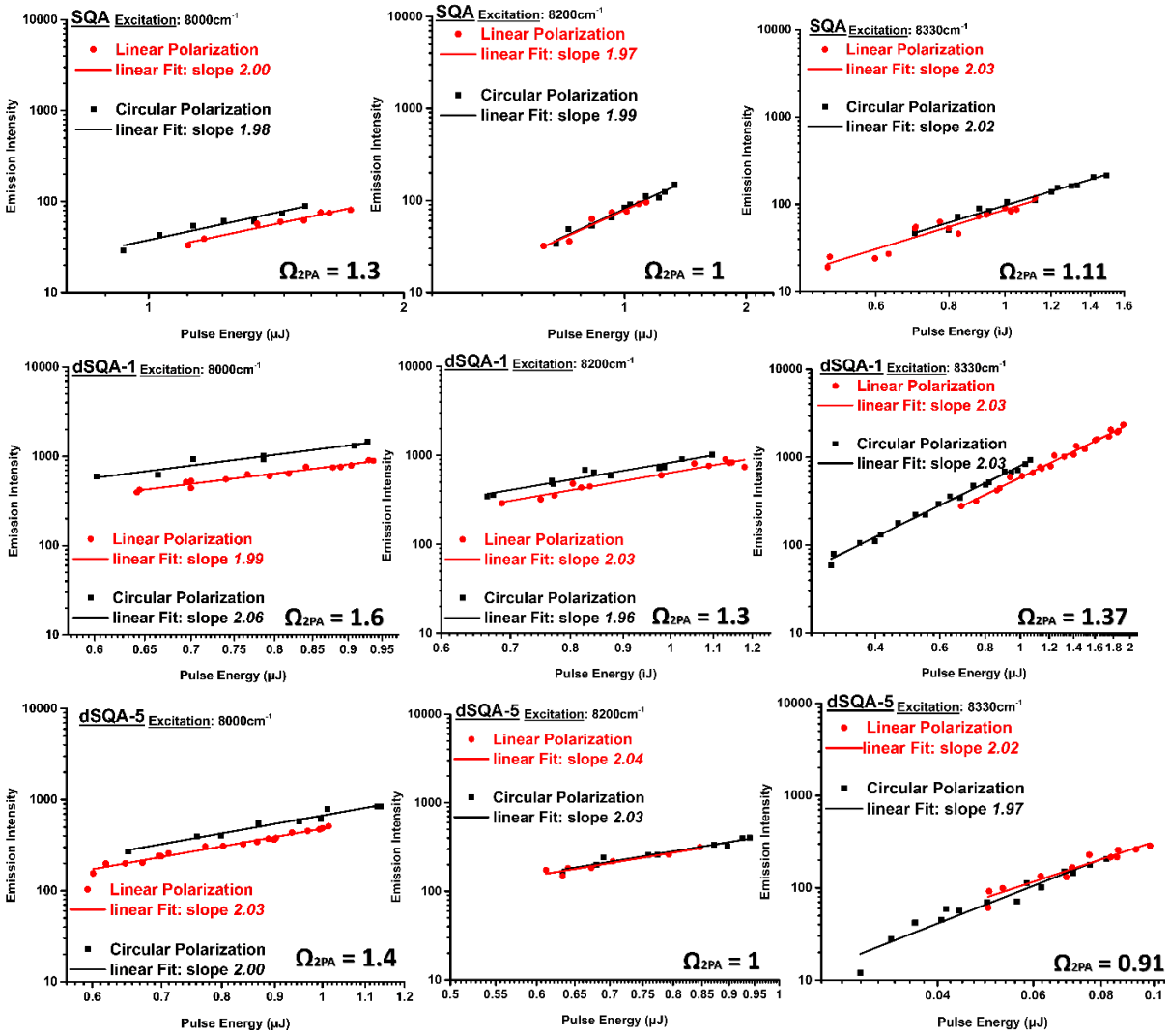

Figure 8-4: Energy-depended 2PA polarization measurements of **SQA**, **dSQA-1** and **dSQA-5** in toluene.

8.3 LabVIEW

In the context of building the 2PIF experimental apparatus, two LabVIEW programs, namely *2PIF Spectrometer* and *2PA Data Analysis*, have been developed to provide a complete control of the experimental procedure and for the subsequent data analysis, respectively. The *2PIF Spectrometer* program provides a user-friendly interface (see Figure 8-5) allowing the user to control the parameters of the measurement and to acquire the data. Moreover, through this interface a real-time display of the data was also provided allowing the user to evaluate the effectiveness of the experimental measurement and data processing selections. At the same time, this LabVIEW program consists of two more subroutines for the fluorescence quantum efficiency measurements and calibration of the detection. By using the second LabVIEW program, *2PA Data Analysis* (see Figure 8-6), we can perform the experimental data processing after the measurement. One can adjust the settings, such as the spectral integration range (λ_{min}, λ_{max}) and the sets of values ($I^{(2PA)}$, P_{ex}), which show slope of *ca.* 2 and thus indicate a 2PA process.

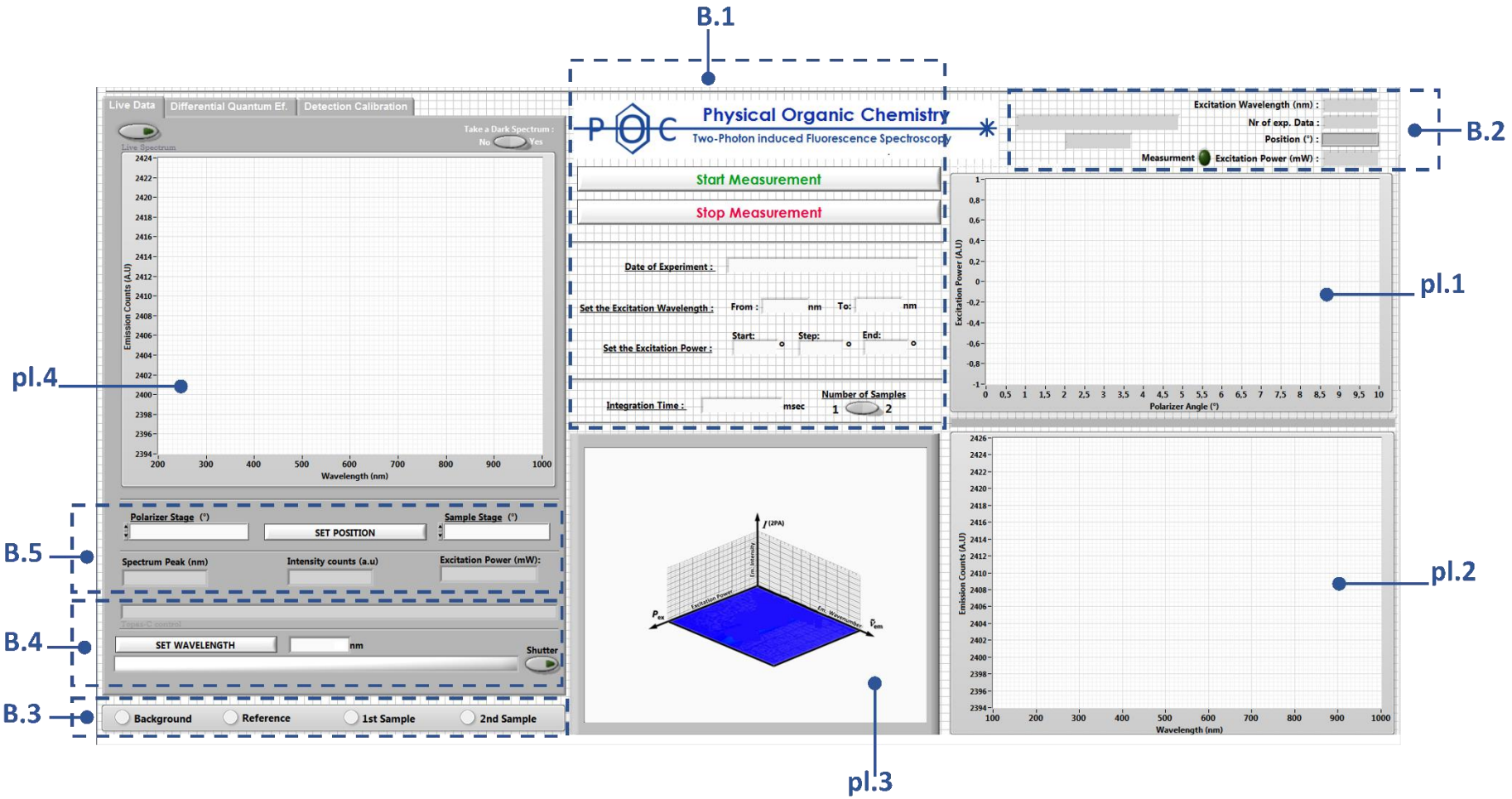

Figure 8-5: *2PIF spectrometer* LabVIEW interface program; **B.1** – Acquisition control parameters, which makes it possible to set the excitation wavelength and power range, as well as the acquisition`s integration time, the number of samples and the date of the experiment, which consists the file name of the auto-saved experimental data. **B.2** and **B.3**– real-time display of data upon measurement time. **pl.2** and **pl.3** – real-time display of plots upon measurement time: excitation power plotted against the polarizer`s RP_2 angle and emission spectrum recorded at the current excitation power, respectively. **pl.3** – (see Figure 3-5) **B.4** – Allows to control the TOPAS-C output. **B.5** and **pl.4** – designed for manual testing of the experimental parameters (e.g. excitation power) providing the live emission spectrum (**pl.4**) of the sample and the obtained counts in the corresponding excitation power.

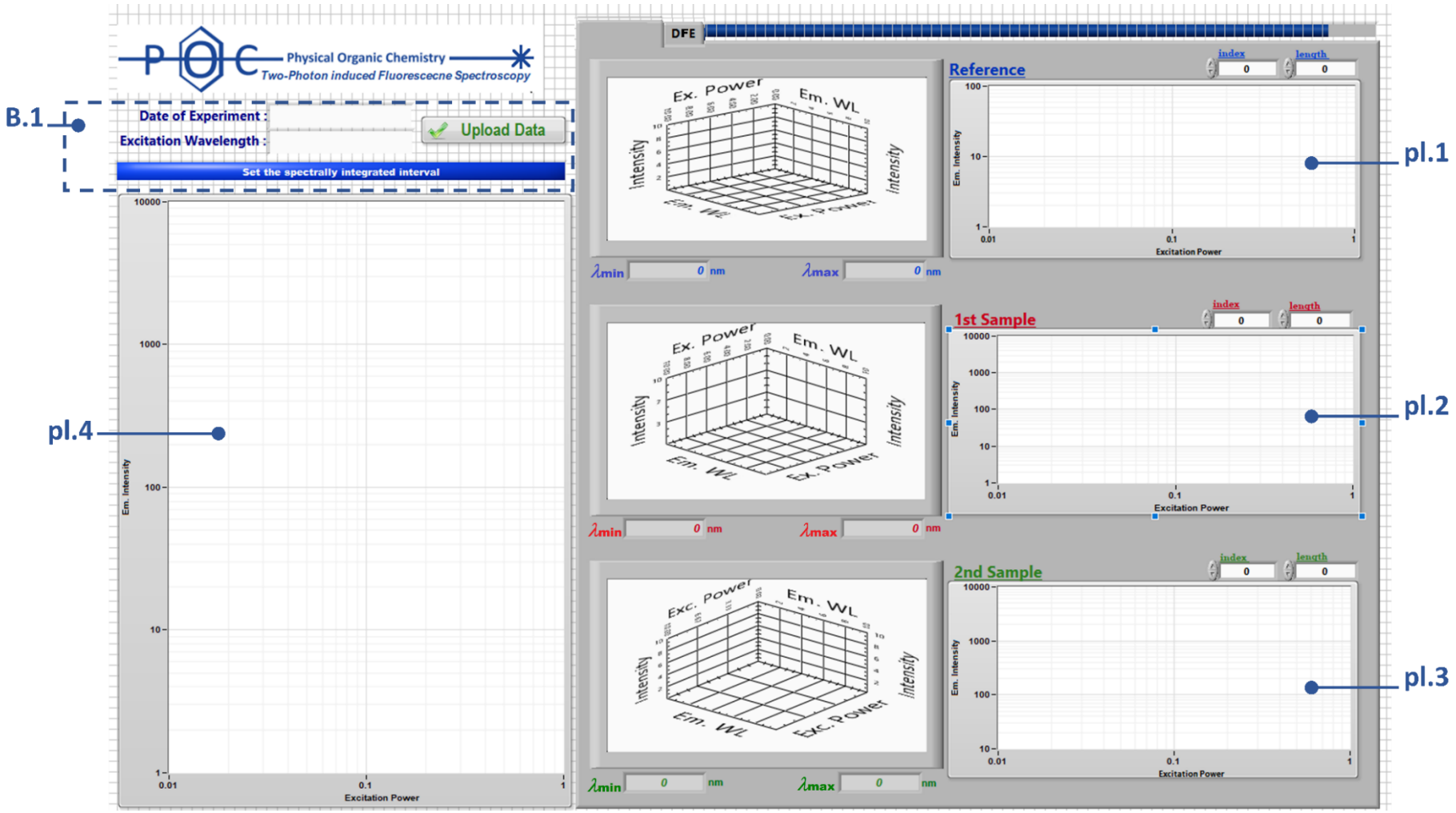

Figure 8-6: *2PIF experimental data processing LabVIEW interface program*; **B.1** – by filling the tabs the system uploads the corresponding experimental data. **pl.1**, **pl.2** and **pl.3** – the quadratic power dependence by log-log linear fit of fluorescence intensity $I^{(2PA)}$ versus the excitation power P_{ex}. The index and the length tabs allow users to set the spectral integration limit λ_{min} and λ_{max} for the reference and two investigated compounds. **pl.4** – indicate all the obtained experimental results together.

8.4 Theoretical Calculations

The theoretical calculations were done by time depended (TD-) and quadratic response (QR-) density functional theory (DFT) using the Gaussian09[105] and the DALTON[106,243] program packages. The BHandHLYP hybrid functional was used for optical properties and the B3LYP functional for optimization of the geometries. The 6-31G* basis set was used for all calculations. A combination of the experimental and theoretical results for the two benzodipyrrolenine-based squaraine dimers **pySQB*trans*** and **pySQB*cis*,** are presented in Figure 8-7 (see also Table 5-9).

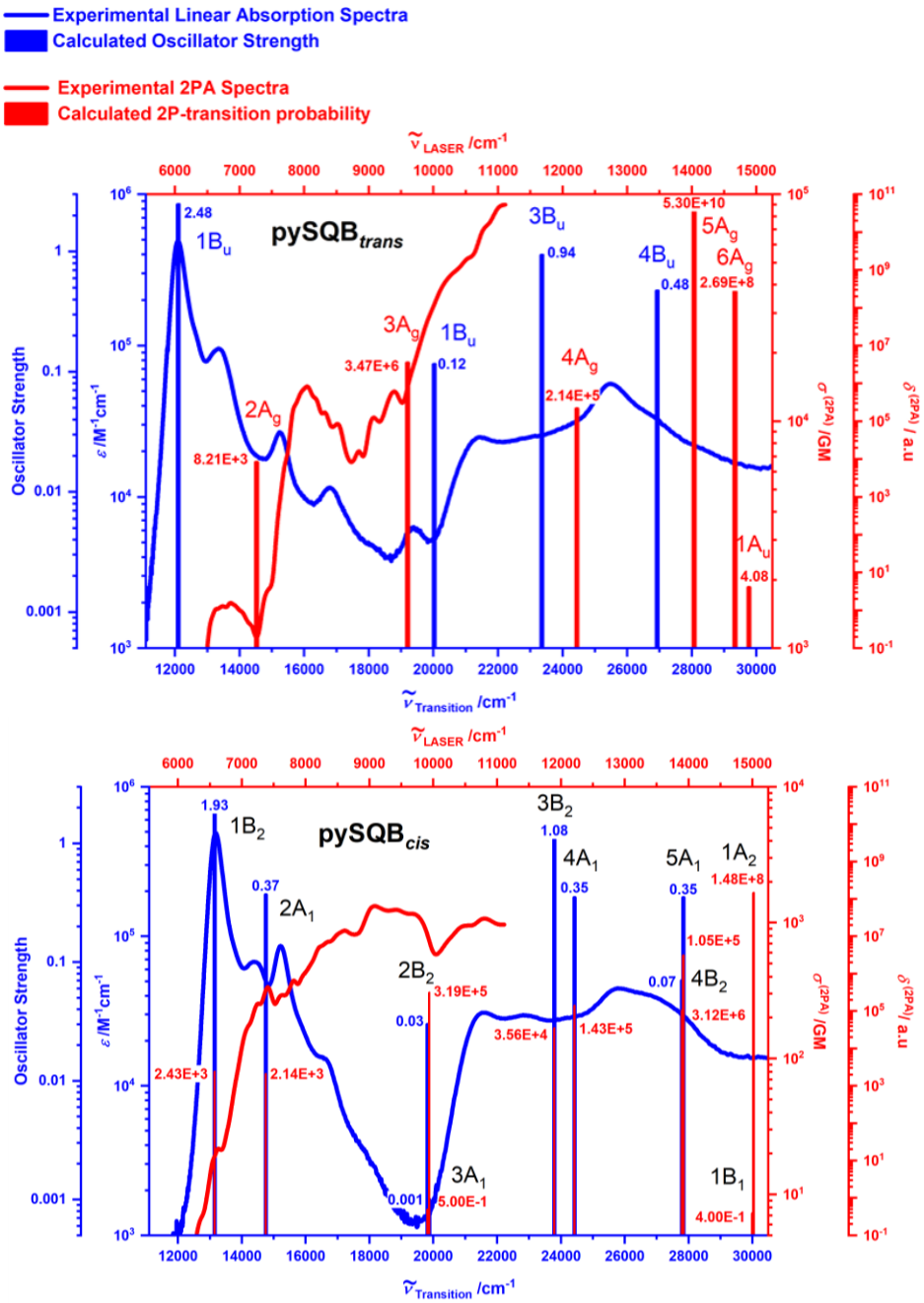

Figure 8-7: A comparison of the 1PA (blue line), 2PA spectra (red line) and the QR-DFT, TD-DFT (BHandHLYP/6-31G*) calculated transition energies (columns) with the values of oscillator strengths *f* (blue) and 2PA strengths $<\delta^{(2PA)}>$ (red) of the **pySQB*trans*** (shifted by 4000cm^{-1}) and **pySQB*cis*** (shifted by 3600cm^{-1}).

9 Literature

[1] G. S. He; L.-S. Tan; Q. Zheng; P. N. Prasad, "*Multiphoton Absorbing Materials: Molecular Designs, Characterizations, and Applications*." Chem. Rev. **2008**, 108 (4), 1245-1330.

[2] T. H. Maiman, "*Stimulated Optical Radiation in Ruby*." Nature **1960**, 187 (4736), 493-494.

[3] A. L. Aleksei Zheltikov, Ferenc Krausz, "*Handbook of Lasers and Optics*." Springer **2007**, Vol.: 4 "Nonlinear Optics", p.:157-248.

[4] M. Göppert-Mayer, "*Über Elementarakte mit zwei Quantensprüngen*." Annalen der Physik **1931**, 401 (3), 273-294.

[5] W. Kaiser; C. G. B. Garrett, "*Two-Photon Excitation in CaF2:Eu2+*." Phys. Rev. Lett. **1961**, 7 (6), 229-231.

[6] M. Pawlicki; H. A. Collins; R. G. Denning; H. L. Anderson, "*Two-Photon Absorption and the Design of Two-Photon Dyes*." Angew. Chem. Int. Ed. **2009**, 48 (18), 3244-3266.

[7] R. L. Sutherland, "*Handbook of Nonlinear Optics*." CRC Press **2003**, Chapter. 9 "*Nonlinear absorption*", p.: 579-584.

[8] A. F. J. Levi, "*"Essential Classical Mechanics for Device Physics"*." IOP Science **2016**, Chapter 5: "The Lorentz oscillator model", p.: 1-21.

[9] R. W. Boyd, "*"Nonlinear Optics"*." Elsevier **2008**, Chapter 1 "The Nonlinear Optical Susceptibility", p.: 1-67.

[10] J. Burris; T. J. McIlrath, "*Theoretical study relating the two-photon absorption cross section to the susceptibility controlling four-wave mixing*." J. Opt. Soc. Am. B **1985**, 2 (8), 1313-1317.

[11] S. Y. K. D. Belfield, M. V. Bondar, "*Advances in polymer science*." Springer **2008**, Chapter 2: "*Two-photon absorbing photonic materials: from fundamentals to applications*.", 97-156.

[12] D. M. Friedrich, "*Two-photon molecular spectroscopy*." J. Chem. Educ. **1982**, 59 (6), 472.

[13] R. M. Hochstrasser; H. N. Sung; J. E. Wessel, "*Two-photon excitation spectra. New and versatile spectroscopic tool*." J. Am. Chem. Soc. **1973**, 95 (24), 8179-8180.

[14] R. M. Hochstrasser; H. N. Sung; J. E. Wessel, "*High resolution two-photon excitation spectra*." J. Chem. Phys **1973**, 58 (10), 4694-4695.

[15] W. R. Zipfel; R. M. Williams; W. W. Webb, "*Nonlinear magic: multiphoton microscopy in the biosciences*." Nat. Biotechnol. **2003**, 21 (11), 1369-1377.

[16] L. I. Markova; E. A. Terpetschnig; L. D. Patsenker, "*Comparison of a series of hydrophilic squaraine and cyanine dyes for use as biological labels*." Dyes Pigm. **2013**, 99 (3), 561-570.

[17] L. Xu; J. Zhang; L. Yin; X. Long; W. Zhang; Q. Zhang, "*Recent progress in efficient organic two-photon dyes for fluorescence imaging and photodynamic therapy*." J. Mater. Chem. C **2020**, 8 (19), 6342-6349.

[18] A. Desponds; A. Banyasz; G. Montagnac; C. Andraud; P. Baldeck; S. Parola, "*Microfabrication by two-photon lithography, and characterization, of SiO2/TiO2 based hybrid and ceramic microstructures*." J. Sol-Gel Sci. Technol. **2020**, 95 (3), 733-745.

[19] V.P. Gupta, "*Molecular and Laser Spectroscopy, Advances and Applications.*" Elsevier, **2018**, Chapter 2, p.: 11-38.

[20] J. W. Lichtman; J.-A. Conchello, "*Fluorescence microscopy*." Nat. Methods **2005**, 2 (12), 910-919.

[21] A. S. Laura; P. Sebastião; P. Yang; S.-R. Kaliris; S. Lingyan; Z. Lin; B. Yury; R. R. Alfano In *Third therapeutic spectral window for deep tissue imaging*, Proc.SPIE, **2014**.

[22] A. S. Laura; P. Yang; P. Sebastião; B. Yury; R. A. Robert, "*Deep optical imaging of tissue using the second and third near-infrared spectral windows*." J. Biomed. Opt. **2014**, 19 (5), 1-6.

[23] Stanley Brown, "*Two photons are better than one*." Nat. Photonics **2008**, 2, 394-395.

[24] C. Xu; W. Zipfel; J. B. Shear; R. M. Williams; W. W. Webb, "*Multiphoton fluorescence excitation: new spectral windows for biological nonlinear microscopy*." Proc. Natl. Acad. Sci. U.S.A **1996**, 93 (20), 10763.

[25] J. D. Bhawalkar; N. D. Kumar; C. F. Zhao; P. N. Prasad, "*Two-Photon Photodynamic Therapy*." J. Clin. Laser Med. Surg. **1997**, 15 (5), 201-204.

[26] K. Ogawa; Y. Kobuke, "*Two-Photon Photodynamic Therapy by Water-Soluble Self-Assembled Conjugated Porphyrins*." Biochem. J. Int. **2013**, 2013, 125658.

[27] H. Abrahamse; Michael R. Hamblin, "*New photosensitizers for photodynamic therapy*." Biochem. J. **2016**, 473 (4), 347-364.

[28] K. Plaetzer; M. Berneburg; T. Kiesslich; T. Maisch, "*New Applications of Photodynamic Therapy in Biomedicine and Biotechnology*." Biochem. J. Int. **2013**, 2013, 161362.

[29] P. Agostinis; K. Berg; K. A. Cengel; T. H. Foster; A. W. Girotti; S. O. Gollnick; S. M. Hahn; M. R. Hamblin; A. Juzeniene; D. Kessel; M. Korbelik; J. Moan; P. Mroz; D. Nowis; J. Piette; B. C. Wilson; J. Golab, "*Photodynamic therapy of cancer: An update*." CA: Cancer J. Clin. **2011**, 61 (4), 250-281.

[30] C. N. LaFratta; J. T. Fourkas; T. Baldacchini; R. A. Farrer, "*Multiphoton Fabrication*." Angew. Chem. Int. Ed. **2007**, 46 (33), 6238-6258.

[31] K. J. Schafer; J. M. Hales; M. Balu; K. D. Belfield; E. W. Van Stryland; D. J. Hagan, "*Two-photon absorption cross-sections of common photoinitiators*." J. Photochem. Photobiol. A **2004**, 162 (2), 497-502.

[32] S. M. Kuebler; K. L. Braun; W. Zhou; J. K. Cammack; T. Yu; C. K. Ober; S. R. Marder; J. W. Perry, "*Design and application of high-sensitivity two-photon initiators for three-dimensional microfabrication*." J. Photochem. Photobiol. A **2003**, 158 (2), 163-170.

[33] X. Zhou; Y. Hou; J. Lin, "*A review on the processing accuracy of two-photon polymerization*." AIP Advances **2015**, 5 (3), 030701.

[34] J. Fischer; M. Wegener, "*Three-dimensional optical laser lithography beyond the diffraction limit*." Laser Photonics Rev. **2013**, 7 (1), 22-44.

[35] B. H. Cumpston; S. P. Ananthavel; S. Barlow; D. L. Dyer; J. E. Ehrlich; L. L. Erskine; A. A. Heikal; S. M. Kuebler; I. Y. S. Lee; D. McCord-Maughon; J. Qin; H. Röckel; M. Rumi; X.-L. Wu; S. R. Marder; J. W. Perry, "*Two-photon polymerization initiators for three-dimensional optical data storage and microfabrication*." Nature **1999**, 398 (6722), 51-54.

[36] E. P. Walker; Y. Zhang; A. Dvornik; P. Rentzepis; S. Esener, "*Two-photon volumetric optical disk storage systems experimental results and potentials*" Optics in Computing, Ed., Vol.90 of OSA: Trends in Optics and Photonics, **2003**, paper OFB2.

[37] J. M. M. R. C. Maurya, "*Molecular symmetry and group theory, approaches in Spectroscopy and chemical reactions*." De Gruyter **2019**, Chapter 2, 29-33.

[38] N. S. Makarov; M. Drobizhev; G. Wicks; E. A. Makarova; E. A. Lukyanets; A. Rebane, "*Alternative selection rules for one- and two-photon transitions in tribenzotetraazachlorin: quasi-centrosymmetrical π-conjugation pathway of formally non-centrosymmetrical molecule*." J. Chem. Phys **2013**, 138 (21), 214314-214314.

[39] O. Laporte; W. F. Meggers, "*Some Rules of Spectral Structure**." J. Opt. Soc. Am. **1925**, 11 (5), 459-463.

[40] P. Atkins and J. Paula, "*Physical Chemistry for the Life Sciences*." Oxford University Press **2006**, Chapter 13, p. 494.

[41] C. Brand; W. L. Meerts; M. Schmitt, "*How and Why Do Transition Dipole Moment Orientations Depend on Conformer Structure?*" J. Phys. Chem. A **2011**, 115 (34), 9612-9619.

[42] W. L. Peticolas, "*Multiphoton Spectroscopy*." Annu. Rev. Phys. Chem. **1967**, 18 (1), 233-260.

[43] M. Drobizhev; N. S. Makarov; S. E. Tillo; T. E. Hughes; A. Rebane, "*Two-photon absorption properties of fluorescent proteins*." Nat. Methods **2011**, 8 (5), 393-399.

[44] C. V. D. Mark G. Kuzyk, "*Characterization techniques and tabulations for organic nonlinear optical materials*." Springer, New York **2017**, Chapter 7-9, .

[45] P. Esherick; P. Zinsli; M. A. El-Sayed, "*The low energy two-photon spectrum of pyrazine using the phosphorescence photoexcitation method*." Chem. Phys. **1975**, 10 (2), 415-432.

[46] C. Xu; W. W. Webb, "*Measurement of two-photon excitation cross sections of molecular fluorophores with data from 690 to 1050 nm*." J. Opt. Soc. Am. B **1996**, 13 (3), 481-491.

[47] M. Hotzel; S. Urban; D. A. M. Egbe; T. Pautzsch; E. Klemm, "*Degenerate four-wave mixing measurements of the third-order nonlinearity of poly(aryleneethynylenes) and their model substances*." J. Opt. Soc. Am. B **2002**, 19 (11), 2645-2649.

[48] K. A. Drenser; R. J. Larsen; F. P. Strohkendl; L. R. Dalton, "*Femtosecond, Frequency-Agile, Phase-Sensitive-Detected, Multi-Wave-Mixing Nonlinear Optical Spectroscopy Applied to π-Electron Photonic Materials*." J. Phys. Chem. A **1999**, 103 (14), 2290-2301.

[49] S.-Y. Tseng; W. Cao; Y.-H. Peng; J. M. Hales; S.-H. Chi; J. W. Perry; S. R. Marder; C. H. Lee; W. N. Herman; J. Goldhar, "*Measurement of complex χ(3) using degenerate four-wave mixing with an imaged 2-D phase grating*." Opt. Express **2006**, 14 (19), 8737-8744.

[50] M. Rumi; J. W. Perry, "*Two-photon absorption: an overview of measurements and principles*." Adv. Opt. Photon. **2010**, 2 (4), 451-518.

[51] W. V. S. Eric; S.-B. Mansoor In *Z-scan technique for nonlinear materials characterization*, Proc.SPIE, 1997.

[52] M. A. Albota; C. Xu; W. W. Webb, "*Two-photon fluorescence excitation cross sections of biomolecular probes from 690 to 960 nm*." Appl. Opt. **1998**, 37 (31), 7352-7356.

[53] Enrique J. Galvez, "*Gaussian Beams*." Department of Physics and Astronomy, Colgate University **2014**, Chapter 1, Fundamental Gaussian Beams, p. 1-12.

[54] C. Xu; W. W. Webb, "*Measurement of two-photon excitation cross sections of molecular fluorophores with data from 690 to 1050 nm*." J. Opt. Soc. Am. B **1996**, 13 (3), 481-491.

[55] M. A. Albota; C. Xu; W. W. Webb, "*Two-photon fluorescence excitation cross sections of biomolecular probes from 690 to 960 nm*." Appl. Opt. **1998**, 37 (31), 7352-7356.

[56] N. S. Makarov; M. Drobizhev; A. Rebane, "*Two-photon absorption standards in the 550–1600 nm excitation wavelength range*." Opt. Express **2008**, 16 (6), 4029-4047.

[57] P. A. M. Dirac, Oxford University Press, 3rd Edition **1947**, Vol.: 1, "The principle of superposition", p.: 1-18.

[58] I. Damian, "*Malus' Law for a Real Polarizer*." arxiv.org **2006**, arXiv preprint physics/0604073.

[59] K. Shahrul; C. David; W. Bor; J. Rosly In *Student activity: verification on Malus's law of polarization at low cost*, Proc.SPIE, 2014.

[60] C. Elliott; V. Vijayakumar; W. Zink; R. Hansen, "*National Instruments LabVIEW: A Programming Environment for Laboratory Automation and Measurement*." JALA, **2007**, 12 (1), 17-24.

[61] P. S. S. Sumathi, "*LabVIEW based advanced instrumentation systems*." Springer **2007**.

[62] N. S. Makarov; M. Drobizhev; A. Rebane, "*Two-photon absorption standards in the 550–1600 nm excitation wavelength range*." Opt. Express **2008**, 16 (6), 4029-4047.

[63] N. S. Makarov; J. Campo; J. M. Hales; J. W. Perry, "*Rapid, broadband two-photon-excited fluorescence spectroscopy and its application to red-emitting secondary reference compounds*." Opt. Mater. Express **2011**, 1 (4), 551-563.

[64] S. de Reguardati; J. Pahapill; A. Mikhailov; Y. Stepanenko; A. Rebane, "*High-accuracy reference standards for two-photon absorption in the 680-1050 nm wavelength range*." Opt. Express **2016**, 24 (8), 9053-9066.

[65] S. d. Reguardati; J. Pahapill; M. Rammo; A. Rebane In *Improving the fidelity of two-photon absorption reference standards*, Proc.SPIE, **2017**.

[66] J. A. Gardecki; M. Maroncelli, "*Set of Secondary Emission Standards for Calibration of the Spectral Responsivity in Emission Spectroscopy*." Appl. Spectrosc. **1998**, 52 (9), 1179-1189.

[67] C. Würth; M. Grabolle; J. Pauli; M. Spieles; U. Resch-Genger, "*Relative and absolute determination of fluorescence quantum yields of transparent samples*." Nat. Protoc **2013**, 8 (8), 1535-1550.

[68] R. M. Williams; J. W. Verhoeven, "*On the applicability of the Kasha—Vavilov rule to C60*." Spectrochimica Acta Part A." Mol. Spectrosc **1994**, 50 (2), 251-254.

[69] D. H. McMahon; R. A. Soref; A. R. Franklin, "*Quantitative Measurements of Double-Photon Absorption in the Polycyclic Benzene Ring Compounds*." Phys. Rev. Lett. **1965**, 14 (26), 1060-1062.

[70] J. P. Hermann; J. Ducuing, "*Absolute Measurement of Two-Photon Cross Sections*." Phys. Rev. A **1972**, 5 (6), 2557-2568.

[71] A. Penzkofer; Y. Lu, "*Fluorescence quenching of rhodamine 6G in methanol at high concentration*." Chem. Phys **1986**, 103 (2), 399-405.

[72] A. Nag; D. Goswami, "*Solvent effect on two-photon absorption and fluorescence of rhodamine dyes*." J. Photochem. Photobiol. A **2009**, 206 (2), 188-197.

[73] N. S. Makarov, "*Ultrafast two-photon absorption in organic molecules: Quantitative spectroscopy and applications.*" Dissertation thesis, Montana State University, **2010**, Chapter: 4, p.: 26-31.

[74] S. d. Reguardati, "*High-accuracy reference standards for quantitative two-photon absorption spectroscopy*." Dissertation thesis, Tallinn University of technology **2017**, Chapter 4, p.: 56-80.

[75] F. Terenziani; C. Katan; E. Badaeva; S. Tretiak; M. Blanchard-Desce, "*Enhanced Two-Photon Absorption of Organic Chromophores: Theoretical and Experimental Assessments*." Adv. Mater. **2008**, 20 (24), 4641-4678.

[76] R. Aleksander; S. M. Nikolay; D. Mikhail In *Quantitative description of two-photon absorption with few essential states models*, Proc.SPIE, 2008.

[77] R. Aleksander; D. Mikhail; S. M. Nikolay; B. Erich; Z. Yujie; W. S. Charles In *Maximizing two-photon absorption cross section within few essential state model*, Proc.SPIE, 2010.

[78] M. M. Alam; M. T. P. Beerepoot; K. Ruud, "*Channel interference in multiphoton absorption*." J. Chem. Phys **2017**, 146 (24), 244116.

[79] P. R. Callis, "*Two-photon-induced fluorescence*." Annu. Rev. Phys. Chem. **1997**, 48 (1), 271-297.

[80] P. R. Callis, "*Topics in fluorescence spectroscopy*." edited by J. Lakowicz. Plenum Press, New York, **2002**, Volume 5: "*Nonlinear and two-photon-induced fluorescence*", Chapter 1, p.:1-39.

[81] M. J. Wirth; A. Koskelo; M. J. Sanders, "*Molecular Symmetry and Two-Photon Spectroscopy*." Appl. Spectrosc. **1981**, 35 (1), 14-21.

[82] R. Fortrie; H. Chermette, "*Two-photon absorption strength: A new tool for the quantification of two-photon absorption*." J. Chem. Phys **2006**, 124 (20), 204104.

[83] D. H. Friese; M. T. P. Beerepoot; K. Ruud, "*Rotational averaging of multiphoton absorption cross sections*." J. Chem. Phys **2014**, 141 (20), 204103.

[84] P. R. Monson; W. M. McClain, "*Polarization Dependence of the Two-Photon Absorption of Tumbling Molecules with Application to Liquid 1-Chloronaphthalene and Benzene*." J. Chem. Phys **1970**, 53 (1), 29-37.

[85] M. T. P. Beerepoot; D. H. Friese; N. H. List; J. Kongsted; K. Ruud, "*Benchmarking two-photon absorption cross sections: performance of CC2 and CAM-B3LYP*." Phys. Chem. Chem. Phys. **2015**, 17 (29), 19306-19314.

[86] W. M. McClain, "*Excited State Symmetry Assignment Through Polarized Two-Photon Absorption Studies of Fluids*." J. Chem. Phys **1971**, 55 (6), 2789-2796.

[87] L. W. T. Barros; T. A. S. Cardoso; A. Bihlmeier; D. Wagner; D. K. Kölmel; A. Hörner; S. Bräse; C. H. Brito Cruz; L. A. Padilha, "*Two-photon absorption in a series of 2,6-disubstituted BODIPY dyes*." Phys. Chem. Chem. Phys. **2017**, 19 (32), 21683-21690.

[88] A. H. Steindal; J. M. H. Olsen; K. Ruud; L. Frediani; J. Kongsted, "*A combined quantum mechanics/molecular mechanics study of the one- and two-photon absorption in the green fluorescent protein*." Phys. Chem. Chem. Phys. **2012**, 14 (16), 5440-5451.

[89] M. A. Salem; A. Brown, "*Two-Photon Absorption in Fluorescent Protein Chromophores: TDDFT and CC2 Results*." J. Chem. Theory Comput. **2014**, 10 (8), 3260-3269.

[90] P. Cronstrand; Y. Luo; H. Ågren, "*Generalized few-state models for two-photon absorption of conjugated molecules*." Chem. Phys. Lett. **2002**, 352 (3), 262-269.

[91] D. Beljonne; W. Wenseleers; E. Zojer; Z. Shuai; H. Vogel; S. J. K. Pond; J. W. Perry; S. R. Marder; J. L. Brédas, "*Role of Dimensionality on the Two-Photon Absorption Response of Conjugated Molecules: The Case of Octupolar Compounds*." Adv. Funct. Mater. **2002**, 12 (9), 631-641.

[92] P. Cronstrand; P. Norman; Y. Luo; H. Ågren, "*Few-states models for three-photon absorption*." J. Chem. Phys. **2004**, 121 (5), 2020-2029.

[93] T. Kogej; D. Beljonne; F. Meyers; J. W. Perry; S. R. Marder; J. L. Brédas, "*Mechanisms for enhancement of two-photon absorption in donor–acceptor conjugated chromophores*." Chem. Phys. Lett. **1998**, 298 (1), 1-6.

[94] M. M. Alam; R. Misra; K. Ruud, "*Interplay of twist angle and solvents with two-photon optical channel interference in aryl-substituted BODIPY dyes*." Phys. Chem. Chem. Phys. **2017**, 19 (43), 29461-29471.

[95] M. Albota; D. Beljonne; J.-L. Brédas; J. E. Ehrlich; J.-Y. Fu; A. A. Heikal; S. E. Hess; T. Kogej; M. D. Levin; S. R. Marder; D. McCord-Maughon; J. W. Perry; H. Röckel; M. Rumi; G. Subramaniam; W. W. Webb; X.-L. Wu; C. Xu, "*Design of Organic Molecules with Large Two-Photon Absorption Cross Sections*." Science **1998**, 281 (5383), 1653.

[96] M. Rumi; J. E. Ehrlich; A. A. Heikal; J. W. Perry; S. Barlow; Z. Hu; D. McCord-Maughon; T. C. Parker; H. Röckel; S. Thayumanavan; S. R. Marder; D. Beljonne; J.-L. Brédas, "*Structure–Property*

Relationships for Two-Photon Absorbing Chromophores: Bis-Donor Diphenylpolyene and Bis(styryl)benzene Derivatives." J. Am. Chem. Soc. **2000**, 122 (39), 9500-9510.

[97] J. E. Lewis; M. Maroncelli, "*On the (uninteresting) dependence of the absorption and emission transition moments of coumarin 153 on solvent*." Chem. Phys. Lett. **1998**, 282 (2), 197-203.

[98] J. R. Lakowicz, "*Molecular Fluorescence: Principles and Applications*." Wiley-VCH, New York, **2010**, 3rd Ed., Chapter: 10 "*Fluorescence anisotropy*", p.: 353-364.

[99] J. R. Lakowicz; I. Gryczynski; E. Danielsen; J. Frisoli, "*Anisotropy spectra of indole and N-acetyl-L-tryptophanamide observed for two-photon excitation of fluorescence*." Chem. Phys. Lett. **1992**, 194 (4), 282-287.

[100] I. Gryczynski; H. Malak; J. R. Lakowicz, "*Three-photon induced fluorescence of 2,5-diphenyloxazole with a femtosecond Ti:sapphire laser*." Chem. Phys. Lett. **1995**, 245 (1), 30-35.

[101] K. D. Belfield; M. V. Bondar; J. M. Hales; A. R. Morales; O. V. Przhonska; K. J. Schafer, "*One- and Two-Photon Fluorescence Anisotropy of Selected Fluorene Derivatives*." J. Fluoresc. **2005**, 15 (1), 3-11.

[102] J. Fu; O. V. Przhonska; L. A. Padilha; D. J. Hagan; E. W. Van Stryland; K. D. Belfield; M. V. Bondar; Y. L. Slominsky; A. D. Kachkovski, "*Two-photon anisotropy: Analytical description and molecular modeling for symmetrical and asymmetrical organic dyes*." Chem. Phys. **2006**, 321 (3), 257-268.

[103] M. G. Vivas; C. Diaz; L. Echevarria; C. R. Mendonca; F. E. Hernández; L. De Boni, "*Two-Photon Circular–Linear Dichroism of Perylene in Solution: A Theoretical–Experimental Study*." J. Phys. Chem. B **2013**, 117 (9), 2742-2747.

[104] R. P. Drucker; W. M. McClain, "*Polarized two-photon studies of biphenyl and several derivatives*." J. Chem. Phys. **1974**, 61 (7), 2609-2615.

[105] G. W. T. M. J. Frisch, H. B. Schlegel, G. E. Scuseria,; J. R. C. M. A. Robb, G. Scalmani, V. Barone,; G. A. P. B. Mennucci, H. Nakatsuji, M. Caricato,; H. P. H. X. Li, A. F. Izmaylov, J. Bloino, G. Zheng,; M. H. J. L. Sonnenberg, M. Ehara, K. Toyota, R. Fukuda,; M. I. J. Hasegawa, T. Nakajima, Y. Honda, O. Kitao,; T. V. H. Nakai, J. J. A. Montgomery, J. E. Peralta,; M. B. F. Ogliaro, J. J. Heyd, E. Brothers,; V. N. S. K. N. Kudin, R. Kobayashi, J. Normand,; A. R. K. Raghavachari, J. C. Burant, S. S. Iyengar,; M. C. J. Tomasi, N. Rega, J. M. Millam, M. Klene,; J. B. C. J. E. Knox, V. Bakken, C. Adamo, J. Jaramillo,; R. E. S. R. Gomperts, O. Yazyev, A. J. Austin,; C. P. R. Cammi, J. W. Ochterski, R. L. Martin,; V. G. Z. K. Morokuma, G. A. Voth, P. Salvador,; S. D. J. J. Dannenberg, A. D. Daniels, O¨. Farkas,; J. V. O. J. B. Foresman, J. Cioslowski and D. J. Fox,, Gaussian 09 R. D., Gaussian, Inc, Wallingford CT, **2009**.

[106] K. Aidas; C. Angeli; K. L. Bak; V. Bakken; R. Bast; L. Boman; O. Christiansen; R. Cimiraglia; S. Coriani; P. Dahle; E. K. Dalskov; U. Ekström; T. Enevoldsen; J. J. Eriksen; P. Ettenhuber; B. Fernández; L. Ferrighi; H. Fliegl; L. Frediani; K. Hald; A. Halkier; C. Hättig; H. Heiberg; T. Helgaker; A. C. Hennum; H. Hettema; E. Hjertenæs; S. Høst; I. M. Høyvik; M. F. Iozzi; B. Jansík; H. J. Jensen; D. Jonsson; P. Jørgensen; J. Kauczor; S. Kirpekar; T. Kjærgaard; W. Klopper; S. Knecht; R. Kobayashi; H. Koch; J. Kongsted; A. Krapp; K. Kristensen; A. Ligabue; O. B. Lutnæs; J. I. Melo; K. V. Mikkelsen; R. H. Myhre; C. Neiss; C. B. Nielsen; P. Norman; J. Olsen; J. M. Olsen; A. Osted; M. J. Packer; F. Pawlowski; T. B. Pedersen; P. F. Provasi; S. Reine; Z. Rinkevicius; T. A. Ruden; K. Ruud; V. V. Rybkin; P. Sałek; C. C. Samson; A. S. de Merás; T. Saue; S. P. Sauer; B. Schimmelpfennig; K. Sneskov; A. H. Steindal; K. O. Sylvester-Hvid; P. R. Taylor; A. M. Teale; E. I. Tellgren; D. P. Tew; A. J. Thorvaldsen; L. Thøgersen; O. Vahtras; M. A. Watson; D. J. Wilson; M. Ziolkowski; H. Agren, "*The Dalton quantum chemistry program system*." Wiley Interdiscip Rev Comput Mol Sci **2014**, 4 (3), 269-284.

[107] S. Sanyal; A. Painelli; S. K. Pati; F. Terenziani; C. Sissa, "*Aggregates of quadrupolar dyes for two-photon absorption: the role of intermolecular interactions*." Phys. Chem. Chem. Phys. **2016**, 18 (40), 28198-28208.

[108] S.-J. Chung; S. Zheng; T. Odani; L. Beverina; J. Fu; L. A. Padilha; A. Biesso; J. M. Hales; X. Zhan; K. Schmidt; A. Ye; E. Zojer; S. Barlow; D. J. Hagan; E. W. Van Stryland; Y. Yi; Z. Shuai; G. A. Pagani; J.-L. Brédas; J. W. Perry; S. R. Marder, "*Extended Squaraine Dyes with Large Two-Photon Absorption Cross-Sections*." J. Am. Chem. Soc. **2006**, 128 (45), 14444-14445.

[109] A. R. Ballestas-Barrientos; A. W. Woodward; W. V. Moreshead; M. V. Bondar; K. D. Belfield, "*Synthesis and Linear and Nonlinear Photophysical Characterization of Two Symmetrical Pyrene-Terminated Squaraine Derivatives*." J. Phys. Chem. C **2016**, 120 (14), 7829-7838.

[110] M. G. Kuzyk, "*Fundamental limits on two-photon absorption cross sections*." J. Chem. Phys **2003**, 119 (16), 8327-8334.

[111] J. Pérez Moreno; M. G. Kuzyk, "*Fundamental limits of the dispersion of the two-photon absorption cross section*." J. Chem. Phys **2005**, 123 (19), 194101.

[112] C.-L. Sun; S.-K. Lv; Y.-P. Liu; Q. Liao; H.-L. Zhang; H. Fu; J. Yao, "*Benzoindolic squaraine dyes with a large two-photon absorption cross-section*." J. Mater. Chem. C **2017**, 5 (5), 1224-1230.

[113] H.-J. Chang; M. V. Bondar; T. Liu; X. Liu; S. Singh; K. D. Belfield; A. Sheely; A. E. Masunov; D. J. Hagan; E. W. Van Stryland, "*Electronic Nature of Neutral and Charged Two-Photon Absorbing Squaraines for Fluorescence Bioimaging Application*." ACS Omega **2019**, 4 (12), 14669-14679.

[114] R. R. Avirah; D. T. Jayaram; N. Adarsh; D. Ramaiah, "*Squaraine dyes in PDT: from basic design to in vivo demonstration*." Org. Biomol. Chem. **2012**, 10 (5), 911-920.

[115] S. F. Völker; M. Renz; M. Kaupp; C. Lambert, "*Squaraine Dyes as Efficient Coupling Bridges between Triarylamine Redox Centres*." Chem. Eur. J. **2011**, 17 (50), 14147-14163.

[116] D. Scherer; R. Dörfler; A. Feldner; T. Vogtmann; M. Schwoerer; U. Lawrentz; W. Grahn; C. Lambert, "*Two-photon states in squaraine monomers and oligomers*." Chem. Phys **2002**, 279 (2), 179-207.

[117] C. Brüning; E. Welz; A. Heilos; V. Stehr; C. Walter; B. Engels; S. F. Völker; C. Lambert; V. Engel, "*Macrocyclic cis-Indolenine Squaraine Dyes as Efficient Near Infrared Emitters*." J. Phys. Chem. C **2015**, 119 (11), 6174-6180.

[118] C. Lambert; T. Scherpf; H. Ceymann; A. Schmiedel; M. Holzapfel, "*Coupled Oscillators for Tuning Fluorescence Properties of Squaraine Dyes*." J. Am. Chem. Soc. **2015**, 137 (10), 3547-3557.

[119] M. H. Schreck; M. I. S. Röhr; T. Clark; V. Stepanenko; F. Würthner; C. Lambert, "*A Self-Assembled Unit Comprising 12 Squaraine Dyes Built Up from Two Star-Shaped Hexasquarainyl-Benzene Molecules*." Chem. Eur. J. **2019**, 25 (11), 2831-2839.

[120] C. Lambert; F. Koch; S. F. Völker; A. Schmiedel; M. Holzapfel; A. Humeniuk; M. I. S. Röhr; R. Mitric; T. Brixner, "*Energy Transfer Between Squaraine Polymer Sections: From Helix to Zigzag and All the Way Back*." J. Am. Chem. Soc. **2015**, 137 (24), 7851-7861.

[121] S. F. Völker; A. Schmiedel; M. Holzapfel; K. Renziehausen; V. Engel; C. Lambert, "*Singlet–Singlet Exciton Annihilation in an Exciton-Coupled Squaraine-Squaraine Copolymer: A Model toward Hetero-J-Aggregates*." J. Phys. Chem. C **2014**, 118 (31), 17467-17482.

[122] S. F. Völker; A. Schmiedel; M. Holzapfel; C. Böhm; C. Lambert, "*Charge transfer dynamics in squaraine–naphthalene diimide copolymers*." Phys. Chem. Chem. Phys. **2013**, 15 (45), 19831-19844.

[123] S. F. Völker; C. Lambert, "*Exciton Coupling Effects in Polymeric cis-Indolenine Squaraine Dyes*." Chem. Mater. **2012**, 24 (13), 2541-2553.

[124] S. F. Völker; S. Uemura; M. Limpinsel; M. Mingebach; C. Deibel; V. Dyakonov; C. Lambert, "*Polymeric Squaraine Dyes as Electron Donors in Bulk Heterojunction Solar Cells*." Macromol. Chem. Phys. **2010**, 211 (10), 1098-1108.

[125] K. D. Belfield; K. J. Schafer; Y. Liu; J. Liu; X. Ren; E. W. V. Stryland, "*Multiphoton-absorbing organic materials for microfabrication, emerging optical applications and non-destructive three-dimensional imaging*." J. Phys. Org. Chem. **2000**, 13 (12), 837-849.

[126] Y. Zhang; B. Kim; S. Yao; M. V. Bondar; K. D. Belfield, "*Controlled Aggregation and Enhanced Two-Photon Absorption of a Water-Soluble Squaraine Dye with a Poly(acrylic acid) Template*." Langmuir **2013**, 29 (35), 11005-11012.

[127] C.-L. Sun; Q. Liao; T. Li; J. Li; J.-Q. Jiang; Z.-Z. Xu; X.-D. Wang; R. Shen; D.-C. Bai; Q. Wang; S.-X. Zhang; H.-B. Fu; H.-L. Zhang, "*Rational design of small indolic squaraine dyes with large two-photon absorption cross section*." Chem. Sci **2015**, 6 (1), 761-769.

[128] H. Ceymann; A. Rosspeintner; M. H. Schreck; C. Mützel; A. Stoy; E. Vauthey; C. Lambert, "*Cooperative enhancement versus additivity of two-photon-absorption cross sections in linear and branched squaraine superchromophores*." Phys. Chem. Chem. Phys. **2016**, 18 (24), 16404-16413.

[129] M. H. Schreck, "*Synthesis and Photophysics of Linear and Star-Shaped Oligomers of Squaraine Dyes*." Dissertation Thesis, Universität Würzburg **2018**, Chapter 3, p.: 102-106.

[130] E. Michail; M. H. Schreck; M. Holzapfel; C. Lambert, "*Exciton coupling effects on the two-photon absorption of squaraine homodimers with varying bridge units*." Phys. Chem. Chem. Phys. **2020**, 22 (33), 18340-18350.

[131] M. I. S. Röhr; H. Marciniak; J. Hoche; M. H. Schreck; H. Ceymann; R. Mitric; C. Lambert, "*Exciton Dynamics from Strong to Weak Coupling Limit Illustrated on a Series of Squaraine Dimers*." J. Phys. Chem. C **2018**, 122 (15), 8082-8093.

[132] M. Kasha; H. R. Rawls; M. Ashraf El-Bayoumi, "*The exciton model in molecular spectroscopy*." Pure Appl. Chem. **1965**, 11 (3-4), 371-392.

[133] P. Ottiger; H. Köppel; S. Leutwyler, "*Excitonic splittings in molecular dimers: why static ab initio calculations cannot match them*." Chem. Sci **2015**, 6 (11), 6059-6068.

[134] M. Schröter; S. D. Ivanov; J. Schulze; S. P. Polyutov; Y. Yan; T. Pullerits; O. Kühn, "*Exciton–vibrational coupling in the dynamics and spectroscopy of Frenkel excitons in molecular aggregates*." Phys. Rep. **2015**, 567, 1-78.

[135] W. W. Parson, "*Modern Optical Spectroscopy*." Springer **2009**, p.: 293.

[136] H. Marciniak; N. Auerhammer; S. Ricker; A. Schmiedel; M. Holzapfel; C. Lambert, "*Reduction of the Fluorescence Transition Dipole Moment by Excitation Localization in a Vibronically Coupled Squaraine Dimer*." J. Phys. Chem. C **2019**, 123 (6), 3426-3432.

[137] C. Zhong; D. Bialas; C. J. Collison; F. C. Spano, "*Davydov Splitting in Squaraine Dimers*." J. Phys. Chem. C **2019**, 123 (30), 18734-18745.

[138] F. C. Spano; S. Mukamel, "*Superradiance in molecular aggregates*." J. Chem. Phys **1989**, 91 (2), 683-700.

[139] A. S. Davydov, "*Theory of Molecular Excitons*." Plenum, New York **1971**.

[140] F. Meinardi; M. Cerminara; A. Sassella; R. Bonifacio; R. Tubino, "*Superradiance in molecular H aggregates*." Phys. Rev. Lett. **2003**, 91 (24), 247401.

[141] S. Ohira; I. Rudra; K. Schmidt; S. Barlow; S.-J. Chung; Q. Zhang; J. Matichak; S. R. Marder; J.-L. Brédas, "*Electronic and vibronic contributions to two-photon absorption in donor-acceptor-donor squaraine chromophores*." Chem. Eur. J. **2008**, 14 (35), 11082-11091.

[142] P. Macak; Y. Luo; H. Ågren, "*Simulations of vibronic profiles in two-photon absorption*." Chem. Phys. Lett **2000**, 330 (3), 447-456.

[143] M. R. Momeni; A. Brown, "*Why Do TD-DFT Excitation Energies of BODIPY/Aza-BODIPY Families Largely Deviate from Experiment? Answers from Electron Correlated and Multireference Methods*." J. Chem. Theory Comput. **2015**, 11 (6), 2619-2632.

[144] B. Le Guennic; D. Jacquemin, "*Taking Up the Cyanine Challenge with Quantum Tools*." Acc. Chem. Res **2015**, 48 (3), 530-537.

[145] F. Bassal; A. D. Laurent; B. Le Guennic; D. Jacquemin, "*Exploring the excited-states of squaraine dyes with TD-DFT, SOS-CIS(D) and ADC(2)*." Dyes Pigm. **2017**, 138, 169-175.

[146] K. Srinivas; C. Prabhakar; C. L. Devi; K. Yesudas; K. Bhanuprakash; V. J. Rao, "*Enhanced Diradical Nature in Oxyallyl Derivatives Leads to Near Infra Red Absorption: A Comparative Study of the Squaraine and Croconate Dyes Using Computational Techniques†*." J. Phys. Chem. A **2007**, 111 (17), 3378-3386.

[147] H. Feki; A. B. Ahmed; N. Fourati; Y. Abid; C. Minot, "*Theoretical studies of molecular structure and vibrational spectra of the asymmetric squaraine [(2-dimethylamino-4-anilino) squaraine]*." Comput. Theor. Chem. **2009**, 895 (1), 21-25.

[148] M. Drobizhev; N. S. Makarov; S. E. Tillo; T. E. Hughes; A. Rebane, "*Describing Two-Photon Absorptivity of Fluorescent Proteins with a New Vibronic Coupling Mechanism*." J. Phys. Chem. B **2012**, 116 (5), 1736-1744.

[149] K. Kamada; K. Ohta; Y. Iwase; K. Kondo, "*Two-photon absorption properties of symmetric substituted diacetylene: drastic enhancement of the cross section near the one-photon absorption peak*." Chem. Phys. Lett. **2003**, 372 (3), 386-393.

[150] M. Drobizhev; A. Karotki; M. Kruk; A. Rebane, "*Resonance enhancement of two-photon absorption in porphyrins*." Chem. Phys. Lett **2002**, 355 (1), 175-182.

[151] V. Barone, *"Computational strategies for spectroscopy from small molecules to Nano systems"*, John Wiley & Sons, **2012**,.

[152] S. Ohira; I. Rudra; K. Schmidt; S. Barlow; S.-J. Chung; Q. Zhang; J. Matichak; S. R. Marder; J.-L. Brédas, "*Electronic and Vibronic Contributions to Two-Photon Absorption in Donor–Acceptor–Donor Squaraine Chromophores*." Chem. Eur. J. **2008**, 14 (35), 11082-11091.

[153] S. J. Strickler; R. A. Berg, "*Relationship between Absorption Intensity and Fluorescence Lifetime of Molecules*." J. Chem. Phys **1962**, 37 (4), 814-822.

[154] E. G. Buchanan; P. S. Walsh; D. F. Plusquellic; T. S. Zwier, "*Excitonic splitting and vibronic coupling in 1,2-diphenoxyethane: Conformation-specific effects in the weak coupling limit*." J. Chem. Phys **2013**, 138 (20), 204313.

[155] W. Mary J; K. Aaron; S. Matthew J, "*Molecular Symmetry and Two-Photon Spectroscopy*." Appl. Spectrosc. **1981**, 35 (1), 14-21.

[156] J. E. Ehrlich; X. L. Wu; I. Y. S. Lee; Z. Y. Hu; H. Röckel; S. R. Marder; J. W. Perry, "*Two-photon absorption and broadband optical limiting with bis-donor stilbenes*." Opt. Lett. **1997**, 22 (24), 1843-1845.

[157] A. D. Slepkov; F. A. Hegmann; R. R. Tykwinski; K. Kamada; K. Ohta; J. A. Marsden; E. L. Spitler; J. J. Miller; M. M. Haley, "*Two-photon absorption in two-dimensional conjugated quadrupolar chromophores*." Opt. Lett. **2006**, 31 (22), 3315-3317.

[158] P. Norman; Y. Luo; H. Ågren, "*Large two-photon absorption cross sections in two-dimensional, charge-transfer, cumulene-containing aromatic molecules*." J. Chem. Phys **1999**, 111 (17), 7758-7765.

[159] M. Barzoukas; M. Blanchard-Desce, "*Molecular engineering of push–pull dipolar and quadrupolar molecules for two-photon absorption: A multivalence-bond states approach*." J. Chem. Phys **2000**, 113 (10), 3951-3959.

[160] S. I. Griesbeck, "*A very positive image of Boron: Triarylborane Chromophores for live cell imaging*." Dissertation Thesis, Universität Würzburg, **2019**, Chapter 3, p.: 55-56.

[161] S. Griesbeck; E. Michail; C. Wang; H. Ogasawara; S. Lorenzen; L. Gerstner; T. Zang; J. Nitsch; Y. Sato; R. Bertermann; M. Taki; C. Lambert; S. Yamaguchi; T. B. Marder, "*Tuning the π-bridge of quadrupolar triarylborane chromophores for one- and two-photon excited fluorescence imaging of lysosomes in live cells*." Chem. Sci **2019**, 10 (20), 5405-5422.

[162] N. Jiang; J. Fan; F. Xu; X. Peng; H. Mu; J. Wang; X. Xiong, "*Ratiometric Fluorescence Imaging of Cellular Polarity: Decrease in Mitochondrial Polarity in Cancer Cells*." Angew. Chem. Int. Ed. **2015**, 54 (8), 2510-2514.

[163] S. Griesbeck; Z. Zhang; M. Gutmann; T. Lühmann; R. M. Edkins; G. Clermont; A. N. Lazar; M. Haehnel; K. Edkins; A. Eichhorn; M. Blanchard-Desce; L. Meinel; T. B. Marder, "*Water-Soluble Triarylborane Chromophores for One- and Two-Photon Excited Fluorescence Imaging of Mitochondria in Cells*." Chem. Eur. J. **2016**, 22 (41), 14701-14706.

[164] Z. Liu; T. Chen; B. Liu; Z.-L. Huang; T. Huang; S. Li; Y. Xu; J. Qin, "*Two-photon absorption of a series of V-shape molecules: the influence of acceptor's strength on two-photon absorption in a noncentrosymmetric D–π–A–π–D system*." J. Mater. Chem. **2007**, 17 (44), 4685-4689.

[165] E. Collini, "*Cooperative effects to enhance two-photon absorption efficiency: intra- versus inter-molecular approach*." Phys. Chem. Chem. Phys. **2012**, 14 (11), 3725-3736.

[166] P. Norman; Y. Luo; H. Ågren, "*Structure-to-property relations for two-photon absorption of hydrocarbon oligomers*." Chem. Phys. Lett **1998**, 296 (1), 8-18.

[167] B. Strehmel; S. Amthor; J. Schelter; C. Lambert, "*Two-Photon Absorption of Bis[4-(N,N-diphenylamino)phenylethynyl]arenes*." ChemPhysChem **2005**, 6 (5), 893-896.

[168] P. Norman; Y. Luo; H. Ågren, "*Two-photon absorption in five-membered heteroaromatic oligomers*." Opt. Commun. **1999**, 168 (1), 297-303.

[169] M. Ferger; Ž. Ban; I. Krošl; S. Tomić; L. Dietrich; S. Lorenzen; F. Rauch; D. Sieh; A. Friedrich; S. Griesbeck; A. Kenđel; S. Miljanić; I. Piantanida; T. B. Marder, "*Bis(phenylethynyl)arene Linkers in Tetracationic Bis-triarylborane Chromophores Control Fluorimetric and Raman Sensing of Various DNAs and RNAs*." Chem. Eur. J. **2021**, n/a (n/a).

[170] P. L. Wu; P. F. Xia; Z. H. Li; X. J. Feng; H. L. Tam; K. F. Li; Y. Jiao; M. S. Wong; K. W. Cheah, "*Non-coplanar 9,9-diphenyl-substituted oligofluorenes with large two-photon absorption enhancement*." Chem. Comm. **2009**, (36), 5421-5423.

[171] Y. Wan; L. Yan; Z. Zhao; X. Ma; Q. Guo; M. Jia; P. Lu; G. Ramos-Ortiz; J. L. Maldonado; M. Rodríguez; A. Xia, "*Gigantic Two-Photon Absorption Cross Sections and Strong Two-Photon Excited Fluorescence in Pyrene Core Dendrimers with Fluorene/Carbazole as Dendrons and Acetylene as Linkages*." J. Phys. Chem. B **2010**, 114 (36), 11737-11745.

[172] X. Li; X. Zhang; W. Li; Y. Wang; T. Liu; B. Zhang; W. Yang, "*Synthesis and enhanced two-photon absorption properties of tetradonor-containing anthracene-centered 2-D cross-conjugated polymers*." J. Mater. Chem. **2011**, 21 (11), 3916-3924.

[173] H. C. Zhang; E. Q. Guo; Y. L. Zhang; P. H. Ren; W. J. Yang, "*Donor–Acceptor-Substituted Anthracene-Centered Cruciforms: Synthesis, Enhanced Two-Photon Absorptions, and Spatially Separated Frontier Molecular Orbitals*." Chem. Mater **2009**, 21 (21), 5125-5135.

[174] W. J. Yang; C. H. Kim; M.-Y. Jeong; S. K. Lee; M. J. Piao; S.-J. Jeon; B. R. Cho, "*Synthesis and Two-Photon Absorption Properties of 9,10-Bis(arylethynyl)anthracene Derivatives*." Chem. Mater **2004**, 16 (14), 2783-2789.

[175] W. Zhou; Y. Fang; X. Wu; Y. Han; J. Yang; L. Shen; Y. Song, "*Anthracene derivatives as broadband nonlinear optical materials: nonlinear absorption and excited-state dynamics analysis*." RSC Advances **2020**, 10 (34), 19974-19981.

[176] C.-K. Wang; P. Macak; Y. Luo; H. Ågren, "*Effects of π centers and symmetry on two-photon absorption cross sections of organic chromophores*." J. Chem. Phys **2001**, 114 (22), 9813-9820.

[177] M. Planells; M. Pizzotti; G. S. Nichol; F. Tessore; N. Robertson, "*Effect of torsional twist on 2nd order non-linear optical activity of anthracene and pyrene tricyanofuran derivatives*." Phys. Chem. Chem. Phys. **2014**, 16 (42), 23404-23411.

[178] Q. Xu; Z. Li; N. Liu; J. Jia; J. Yang; Y. Song, "*Third order nonlinear optical properties and transient dynamics of thiophene-contained pyrene derivatives: Effect of peripheral substituent group*." Opt. Laser Technol. **2019**, 109, 666-670.

[179] X. Wu; J. Xiao; R. Sun; T. Jin; J. Yang; G. Shi; Y. Wang; X. Zhang; Y. Song, "*Spindle-Type Conjugated Compounds Containing Twistacene Unit: Synthesis and Ultrafast Broadband Reverse Saturable Absorption*." Adv. Opt. Mater **2017**, 5 (2), 1600712.

[180] S.-J. Chung; K.-S. Kim; T.-C. Lin; G. S. He; J. Swiatkiewicz; P. N. Prasad, "*Cooperative Enhancement of Two-Photon Absorption in Multi-branched Structures*." J. Phys. Chem. B **1999**, 103 (49), 10741-10745.

[181] T. G. Goodson, "*Optical Excitations in Organic Dendrimers Investigated by Time-Resolved and Nonlinear Optical Spectroscopy*." Acc. Chem. Res **2005**, 38 (2), 99-107.

[182] F. Terenziani; C. Le Droumaguet; C. Katan; O. Mongin; M. Blanchard-Desce, "*Effect of Branching on Two-Photon Absorption in Triphenylbenzene Derivatives*." ChemPhysChem **2007**, 8 (5), 723-734.

[183] C. Sissa; V. Parthasarathy; D. Drouin-Kucma; M. H. V. Werts; M. Blanchard-Desce; F. Terenziani, "*The effectiveness of essential-state models in the description of optical properties of branched push–pull chromophores*." Phys. Chem. Chem. Phys. **2010**, 12 (37), 11715-11727.

[184] N. S. Makarov; S. Mukhopadhyay; K. Yesudas; J.-L. Brédas; J. W. Perry; A. Pron; M. Kivala; K. Müllen, "*Impact of Electronic Coupling, Symmetry, and Planarization on One- and Two-Photon Properties of Triarylamines with One, Two, or Three Diarylboryl Acceptors*." J. Phys. Chem. A **2012**, 116 (15), 3781-3793.

[185] C. Le Droumaguet; A. Sourdon; E. Genin; O. Mongin; M. Blanchard-Desce, "*Two-photon polarity probes built from octupolar fluorophores: synthesis, structure-properties relationships, and use in cellular imaging*." Chem. Asian J. **2013**, 8 (12), 2984-3001.

[186] O. Varnavski; X. Yan; O. Mongin; M. Blanchard-Desce; T. Goodson, "*Strongly Interacting Organic Conjugated Dendrimers with Enhanced Two-Photon Absorption*." J. Phys. Chem. C **2007**, 111 (1), 149-162.

[187] M. Drobizhev; A. Karotki; Y. Dzenis; A. Rebane; Z. Suo; C. W. Spangler, "*Strong Cooperative Enhancement of Two-Photon Absorption in Dendrimers*." J. Phys. Chem. B **2003**, 107 (31), 7540-7543.

[188] S. Griesbeck; E. Michail; F. Rauch; H. Ogasawara; C. Wang; Y. Sato; R. M. Edkins; Z. Zhang; M. Taki; C. Lambert; S. Yamaguchi; T. B. Marder, "*The Effect of Branching on the One- and Two-Photon Absorption, Cell Viability, and Localization of Cationic Triarylborane Chromophores with Dipolar versus Octupolar Charge Distributions for Cellular Imaging*." Chem. Eur. J. **2019**, 25 (57), 13164-13175.

[189] C. Katan; F. Terenziani; O. Mongin; M. H. V. Werts; L. Porrès; T. Pons; J. Mertz; S. Tretiak; M. Blanchard-Desce, "*Effects of (Multi)branching of Dipolar Chromophores on Photophysical Properties and Two-Photon Absorption*." J. Phys. Chem. A **2005**, 109 (13), 3024-3037.

[190] J. C. Collings; S.-Y. Poon; C. Le Droumaguet; M. Charlot; C. Katan; L.-O. Pålsson; A. Beeby; J. A. Mosely; H. M. Kaiser; D. Kaufmann; W.-Y. Wong; M. Blanchard-Desce; T. B. Marder, "*The Synthesis and One- and Two-Photon Optical Properties of Dipolar, Quadrupolar and Octupolar Donor–Acceptor Molecules Containing Dimesitylboryl Groups*." Chem. Eur. J. **2009**, 15 (1), 198-208.

[191] Y. Hattori; E. Michail; A. Schmiedel; M. Moos; M. Holzapfel; I. Krummenacher; H. Braunschweig; U. Müller; J. Pflaum; C. Lambert, "*Luminescent Mono-, Di-, and Triradicals: Bridging Polychlorinated Triarylmethyl Radicals by Triarylamines and Triarylboranes*." Chem. Eur. J. **2019**, 25 (68), 15463-15471.

[192] L. Xu; W. Lin; B. Huang; J. Zhang; X. Long; W. Zhang; Q. Zhang, "*The design strategies and applications for organic multi-branched two-photon absorption chromophores with novel cores and branches: a recent review*." J. Mater. Chem. C **2021**.

[193] S. David; D. Chateau; H.-J. Chang; L. H. Karlsson; M. V. Bondar; C. Lopes; B. Le Guennic; D. Jacquemin; G. Berginc; O. Maury; S. Parola; C. Andraud, "*High-Performance Optical Power Limiting Filters at Telecommunication Wavelengths: When Aza-BODIPY Dyes Bond to Sol–Gel Materials*." J. Phys. Chem. C **2020**, 124 (44), 24344-24350.

[194] J. M. Hales; M. Cozzuol; T. E. O. Screen; H. L. Anderson; J. W. Perry, "*Metalloporphyrin polymer with temporally agile, broadband nonlinear absorption for optical limiting in the near infrared*." Opt. Express **2009**, 17 (21), 18478-18488.

[195] S. Pascal; Q. Bellier; S. David; P.-A. Bouit; S.-H. Chi; N. S. Makarov; B. Le Guennic; S. Chibani; G. Berginc; P. Feneyrou; D. Jacquemin; J. W. Perry; O. Maury; C. Andraud, "*Unraveling the Two-Photon and Excited-State Absorptions of Aza-BODIPY Dyes for Optical Power Limiting in the SWIR Band*." J. Phys. Chem. C **2019**, 123 (38), 23661-23673.

[196] Q. Li; C. Liu; Z. Liu; Q. Gong, "*Broadband optical limiting and two-photon absorption properties of colloidal GaAs nanocrystals*." Opt. Express **2005**, 13 (6), 1833-1838.

[197] P. Feneyrou; O. Doclot; D. Block; P. L. Baldeck; J. Zyss, "*Two-photon absorption and optical-limiting properties in dimethylaminocyanobiphenyl crystal*." J. Nonlinear Opt. Phys. Mater **1996**, 05 (04), 767-774.

[198] D. Dini; M. J. F. Calvete; M. Hanack, "*Nonlinear Optical Materials for the Smart Filtering of Optical Radiation*." Chem. Rev **2016**, 116 (22), 13043-13233.

[199] L. W. Tutt; T. F. Boggess, "*A review of optical limiting mechanisms and devices using organics, fullerenes, semiconductors and other materials*." Prog. Quantum. Electron. **1993**, 17 (4), 299-338.

[200] Y. Lihua; Z. Junxiang; C. Yiping; L. Zhenhua; H. Anzhi, "*Two-photon absorption and optical-limiting properties of a novel organic compound*." Proc.SPIE **2002**, 4919.

[201] G. S. He; Q. Zheng; A. Baev; P. N. Prasad, "*Saturation of multiphoton absorption upon strong and ultrafast infrared laser excitation*." J. Appl. Phys. **2007**, 101 (8), 083108.

[202] S. M. Kirkpatrick; R. R. Naik; M. O. Stone, "*Nonlinear Saturation and Determination of the Two-Photon Absorption Cross Section of Green Fluorescent Protein*." J. Phys. Chem. B **2001**, 105 (14), 2867-2873.

[203] Q. Zheng; G. S. He; P. N. Prasad, "*A novel near IR two-photon absorbing chromophore: Optical limiting and stabilization performances at an optical communication wavelength*." Chem. Phys. Lett. **2009**, 475 (4), 250-255.

[204] G. S. He; Q. Zheng; K.-T. Yong; A. I. Ryasnyanskiy; P. N. Prasad; A. Urbas, "*Two-photon absorption based optical limiting and stabilization by using a CdTe quantum dot solution excited at optical communication wavelength of ~1300nm*." Appl. Phys. Lett. **2007**, 90 (18), 181108.

[205] M. C. J. M. Hales, T. E. O. Screen, H. L. Anderson, and J. W. Perry, "*Metalloporphyrin polymer with temporally agile, broadband nonlinear absorption for optical limiting in the near infrared*." Optics Express **2009**, 17 (21), 18478-18488.

[206] N. Schiccheri; M. Meneghetti, "*Excited State Two Photon Absorption of a Charge Transfer Radical Dimer in the Near Infrared*." J. Phys. Chem. A **2005**, 109 (21), 4643-4645.

[207] Purnima; D. Mohan; S. Rani, "*Optical nonlinear refractive and limiting behavior of nickel complex dye doped solid-state matrix for both visible and near infra-red nanosecond excitations*." Optik **2013**, 124 (14), 1741-1745.

[208] C. C. Jiménez; A. Enríquez-Cabrera; O. González-Antonio; J. Ordóñez-Hernández; P. G. Lacroix; P. Labra-Vázquez; N. Farfán; R. Santillan, "*State of the Art of Boron and Tin Complexes in Second- and Third-Order Nonlinear Optics §*." Inorganics **2018**, 6 (4).

[209] H. M. Kim; B. R. Cho, "*Small-Molecule Two-Photon Probes for Bioimaging Applications*." Chem. Rev **2015**, 115 (11), 5014-5055.

[210] J. Schäfer, "*Synthesis and Photophysical Investigation of Donor-Acceptor-Substituted meta- and para-Benzene Derivatives*." Dissertation Thesis, Universität Würzburg **2017**, Chapter 3, p.: 24-45.

[211] C. Rovira; D. Ruiz-Molina; O. Elsner; J. Vidal-Gancedo; J. Bonvoisin; J.-P. Launay; J. Veciana, "*Influence of Topology on the Long-Range Electron-Transfer Phenomenon*." Chem. Eur. J. **2001**, 7 (1), 240-250.

[212] A. Stockmann; J. Kurzawa; N. Fritz; N. Acar; S. Schneider; J. Daub; R. Engl; T. Clark, "*Conformational Control of Photoinduced Charge Separation within Phenothiazine−Pyrene Dyads*." J. Phys. Chem. A **2002**, 106 (34), 7958-7970.

[213] G. C. Solomon; D. Q. Andrews; T. Hansen; R. H. Goldsmith; M. R. Wasielewski; R. P. Van Duyne; M. A. Ratner, "*Understanding quantum interference in coherent molecular conduction*." J. Chem. Phys **2008**, 129 (5), 054701.

[214] R. H. Goldsmith; M. R. Wasielewski; M. A. Ratner, "*Electron Transfer in Multiply Bridged Donor−Acceptor Molecules: Dephasing and Quantum Coherence*." J. Phys. Chem. B **2006**, 110 (41), 20258-20262.

[215] Y. Tsuji; A. Staykov; K. Yoshizawa, "*Orbital Views of Molecular Conductance Perturbed by Anchor Units*." J. Am. Chem. Soc. **2011**, 133 (15), 5955-5965.

[216] S. Lee; K. R. J. Thomas; S. Thayumanavan; C. J. Bardeen, "*Dependence of the Two-Photon Absorption Cross Section on the Conjugation of the Phenylacetylene Linker in Dipolar Donor−Bridge−Acceptor Chromophores*." J. Phys. Chem. A **2005**, 109 (43), 9767-9774.

[217] K. M. Gaab; A. L. Thompson; J. Xu; T. J. Martínez; C. J. Bardeen, "*Meta-Conjugation and Excited-State Coupling in Phenylacetylene Dendrimers*." J. Am. Chem. Soc **2003**, 125 (31), 9288-9289.

[218] B. Strehmel; A. M. Sarker; H. Detert, "*The Influence of σ and π Acceptors on Two-Photon Absorption and Solvatochromism of Dipolar and Quadrupolar Unsaturated Organic Compounds*." ChemPhysChem **2003**, 4 (3), 249-259.

[219] J. Schäfer; M. Holzapfel; B. Mladenova; D. Kattnig; I. Krummenacher; H. Braunschweig; G. Grampp; C. Lambert, "*Hole Transfer Processes in meta- and para-Conjugated Mixed Valence Compounds: Unforeseen Effects of Bridge Substituents and Solvent Dynamics*." J. Am. Chem. Soc. **2017**, 139 (17), 6200-6209.

[220] H. Y. Woo; B. Liu; B. Kohler; D. Korystov; A. Mikhailovsky; G. C. Bazan, "*Solvent Effects on the Two-Photon Absorption of Distyrylbenzene Chromophores*." J. Am. Chem. Soc. **2005**, 127 (42), 14721-14729.

[221] Y. Luo; P. Norman; P. Macak; H. Ågren, "*Solvent-Induced Two-Photon Absorption of a Push−Pull Molecule*." The Journal of Physical Chemistry A **2000**, 104 (20), 4718-4722.

[222] R. Zaleśny; W. Bartkowiak; S. Styrcz; J. Leszczynski, "*Solvent Effects on Conformationally Induced Enhancement of the Two-Photon Absorption Cross Section of a Pyridinium-N-Phenolate Betaine Dye. A Quantum Chemical Study*." J. Phys. Chem. A **2002**, 106 (16), 4032-4037.

[223] C.-K. Wang; K. Zhao; Y. Su; Y. Ren; X. Zhao; Y. Luo, "*Solvent effects on the electronic structure of a newly synthesized two-photon polymerization initiator*." J. Chem. Phys **2003**, 119 (2), 1208-1213.

[224] E. Zojer; D. Beljonne; T. Kogej; H. Vogel; S. R. Marder; J. W. Perry; J. L. Brédas, "*Tuning the two-photon absorption response of quadrupolar organic molecules*." J. Chem. Phys **2002**, 116 (9), 3646-3658.

[225] I. Fitilis; M. Fakis; I. Polyzos; V. Giannetas; P. Persephonis; P. Vellis; J. Mikroyannidis, "*A two-photon absorption study of fluorene and carbazole derivatives. The role of the central core and the solvent polarity*." Chem. Phys. Lett **2007**, 447 (4), 300-304.

[226] Y. Yan; B. Li; K. Liu; Z. Dong; X. Wang; S. Qian, "*Enhanced Two-Photon Absorption and Ultrafast Dynamics of a New Multibranched Chromophore with a Dibenzothiophene Core*." J. Phys. Chem. A **2007**, 111 (20), 4188-4194.

[227] I. Tinoco, "*Two-photon circular dichroism*." J. Chem. Phys **1975**, 62 (3), 1006-1009.

[228] E. A. Power, "*Two-photon circular dichroism*." J. Chem. Phys **1975**, 63 (4), 1348-1350.

[229] L. De Boni; C. Toro; F. E. Hernández, "*Synchronized double L-scan technique for the simultaneous measurement of polarization-dependent two-photon absorption in chiral molecules*." Opt. Lett. **2008**, 33 (24), 2958-2960.

[230] C. Toro, "*Dissertation Thesis, "Polarization dependent 2PA properties of chiral molecules."*." University of Central Florida **2010**.

[231] H. Mojzisova; J. Olesiak; M. Zielinski; K. Matczyszyn; D. Chauvat; J. Zyss, "*Polarization-Sensitive Two-Photon Microscopy Study of the Organization of Liquid-Crystalline DNA*." Biophys. J. **2009**, 97 (8), 2348-2357.

[232] P. P. Markowicz; M. Samoc; J. Cerne; P. N. Prasad; A. Pucci; G. Ruggeri, "*Modified Z-scan techniques for investigations of nonlinear chiroptical effects*." Opt. Express **2004**, 12 (21), 5209-5214.

[233] C. Diaz; N. Lin; C. Toro; R. Passier; A. Rizzo; F. E. Hernández, "*The Effect of the π-Electron Delocalization Curvature on the Two-Photon Circular Dichroism of Molecules with Axial Chirality*." J. Phys. Chem. Lett **2012**, 3 (13), 1808-1813.

[234] A. Nag; D. Goswami, "*Polarization induced control of single and two-photon fluorescence*." J. Chem. Phys. **2010**, 132 (15), 154508.

[235] Y. Vesga; F. E. Hernandez, "*Study of the Effect of the Pulse Width of the Excitation Source on the Two-Photon Absorption and Two-Photon Circular Dichroism Spectra of Biaryl Derivatives*." J. Phys. Chem. A **2016**, 120 (34), 6774-6779.

[236] C. Díaz; Y. Vesga; L. Echevarria; I. G. Stará; I. Starỳ; E. Anger; C. Shen; M. El Sayed Moussa; N. Vanthuyne; J. Crassous; A. Rizzo; F. E. Hernández, "*Two-photon absorption and two-photon circular dichroism of hexahelicene derivatives: a study of the effect of the nature of intramolecular charge transfer*." RSC Advances **2015**, 5 (23), 17429-17437.

[237] C. Toro; L. De Boni; N. Lin; F. Santoro; A. Rizzo; F. E. Hernandez, "*Two-Photon Absorption Circular Dichroism: A New Twist in Nonlinear Spectroscopy*." Chem. Eur. J. **2010**, 16 (11), 3504-3509.

[238] S. S. Andrews, "*Using Rotational Averaging To Calculate the Bulk Response of Isotropic and Anisotropic Samples from Molecular Parameters*." J. Chem. Educ. **2004**, 81 (6), 877.

[239] W. J. Meath; E. A. Power, "*On the importance of permanent moments in multiphoton absorption using perturbation theory*." Journal of Physics B: Atomic and Molecular Physics **1984**, 17 (5), 763-781.

[240] A. Sillen; Y. Engelborghs, "*The Correct Use of "Average" Fluorescence Parameters*." Photochem. Photobiol. **1998**, 67 (5), 475-486.

[241] T.-S. Ahn; R. O. Al-Kaysi; A. M. Müller; K. M. Wentz; C. J. Bardeen, "*Self-absorption correction for solid-state photoluminescence quantum yields obtained from integrating sphere measurements*." Rev. Sci. Instrum **2007**, 78 (8), 086105.

[242] J. R. Lakowicz, "*Principles of Fluorescence Spectroscopy.*" **2010**, New York: 2010; Vol. 10.

[243] Dalton, a molecular electronic structure program, Release vDalton2020.alpha, http://daltonprogram.org. **2020**.

10 Zusammenfassung

Die Hauptziele der vorliegenden Dissertation lassen sich in zwei Teile gliedern. Der erste Teil befasst sich mit dem Aufbau einer spektroskopischen Technik zur zuverlässigen und genauen Messung der Zwei-Photonen-Absorptionsquerschnittsspektren (2PA). Im zweiten Teil wurde diese fest etablierte experimentelle Technik zusammen mit konventioneller spektroskopischer Charakterisierung, quantenchemischen Berechnungen und theoretischen Modellrechnungen kombiniert und damit als Werkzeug genutzt, um über mehrere molekulare Verbindungen Informationen für die sogenannte Struktur-Eigenschafts-Beziehung zu gewinnen.

Im ersten Teil der Arbeit wird zunächst das Hauptkonzept des 2PA-Phänomens vorgestellt und die theoretische Grundlage der gewählten experimentellen Technik geschaffen. Anschließend werden der Aufbau und die Entwicklung einer spektroskopischen Apparatur zur Bestimmung des 2PA-Querschnitts mittels Zwei-Photonen-induzierter Fluoreszenz (2PIF) beschrieben und ein vollständiges experimentelles Protokoll erstellt. Die 2PIF-Technik basiert auf der Relativmethode, bei der die Intensität der durch 2PA induzierten Fluoreszenzemission gemessen wird. Der 2PA-Querschnitt eines Materials wird durch den Vergleich der Materialantwort mit der einer Referenzsubstanz mit bekanntem 2PA-Querschnitt unter identischen Versuchsbedingungen bestimmt. Diese Technik wurde gewählt, weil sie für 2PA in einem breiten Anregungsenergiebereich (550 - 1600 nm) empfindlich ist.

Der Aufbau dieses Spektrometers ist mit zwei großen Herausforderungen verbunden. Erstens muss sichergestellt werden, dass die Parameter des Anregungsstrahls und die Bedingungen für die Fluoreszenzsammlung sowohl für die unbekannte Probe als auch für den Referenzstandard gleich sind. Zweitens muss das Spektrometer in Bezug auf die Emissionscharakteristik der Referenzsubstanz korrekt kalibriert werden. Um die erste kritische Bedingung zu erfüllen, muss ein Satz von Irisblenden und Silberschutzspiegeln so ausgerichtet werden, dass der Anregungsstrahl für den gesamten Wellenlängenbereich achromatisch durch die Referenz- und die Probenverbindung verläuft, die in einem Präzisionsrotations-Küvettenhaltertisch platziert sind. Dementsprechend wird das Emissionssignal unter Verwendung achromatischer asphärischer Linsen im 90°-Winkel gesammelt, wodurch die Farb- und sphärische Aberration minimiert wird.

Die zweite Voraussetzung erfordert die Bestimmung des Verhältnisses zwischen den Fluoreszenz-Quantenausbeuten von Referenz und Probe, wie sie durch das 2PIF-Spektrometer bestimmt und aus den Emissionsspektren für Referenzstandards und Proben bei Ein-Photonen-Anregung gewonnen werden. Letzteres hilft, Fehler aufgrund des Detektionsspektrums zu vermeiden, da sich die Emissionen von Probe und Referenz nicht immer spektral überlappen. Ein kritischer Parameter während des experimentellen Ablaufs ist die Überprüfung der quadratischen Abhängigkeit zwischen

Anregungsleistung und emittierter Fluoreszenz bei jeder Anregungswellenlänge, um sicherzustellen, dass nur ein 2PA-Prozess stattfindet.

Der zweite Teil beschäftigt sich mit mehreren neuen organischen Molekülen, die in der Gruppe von Prof. C. Lambert und Prof. T. B. Marder synthetisiert wurden. Ziel war es, zu untersuchen, wie strukturelle Parameter den 2PA-Querschnitt beeinflussen und zu einer Veränderung ihrer nichtlinearen optischen Eigenschaften führen. Insbesondere konzentriert sich dieser Teil auf die Phänomene der Elektronen-Delokalisation und des intramolekularen Ladungstransfers, da diese stark mit dem Zwei-Photonen-Absorptionsvermögen korreliert sind. Diese Untersuchung beinhaltet auch theoretische Ansätze, um die experimentellen Ergebnisse zu interpretieren und verwandte Größen abzuschätzen, die somit als Designkriterien verwendet werden können, um einen großen 2PA-Querschnitt zu erreichen. Nicht zuletzt erwiesen sich polarisationsabhängige nichtlineare spektroskopische Messungen als ein mächtiges Werkzeug, um die erhaltenen Ergebnisse zu untermauern.

Um einen Einblick in die starke Korrelation zwischen den strukturellen Parametereffekten und der Zwei-Photonen-Absorptionsfähigkeit zu erhalten, wurden drei separate Teile organisiert: i) die Exziton-Kopplungswechselwirkung zwischen den Chromophoren, ii) die Eigenschaften der Brückeneinheiten und iii) das Multi-Verzweigungskonzept. In diesem Zusammenhang wurde eine Serie von SQA-basierten Squarain-Homodimeren untersucht, bei denen die Variation der Kopplungseinheit zwischen den beiden Monomeren zu einer Veränderung der optischen Eigenschaften führt. Einen Schritt weitergehend wurden zwei SQB-basierte Squarain-Homodimere untersucht, die zwei Isomere bilden, bei denen die molekulare Symmetrie ebenfalls einen großen Einfluss auf ihre spektroskopischen Eigenschaften hat. Folglich wurde die Aufmerksamkeit auf den Verbrückungseffekt auf ihre nichtlinearen optischen Eigenschaften in einer Reihe von π-verbrückten Bis-Triarylboran-Chromophoren mit variierenden π-Verbrückungseinheiten gelenkt, wobei die 2PA-Spektren signifikant von den Eigenschaften und der Art der Brücke abhängen. Um das Bild des intramolekularen Ladungstransfers im Rahmen von 2PA zu vervollständigen, erfolgte eine Untersuchung der verzweigten Systeme auf der Basis von dipolaren Chromophoren, die über einen Kernteil verbunden sind, der in diesem Fall aus einem Triphenylamin-Zentrum besteht. So wurde eine Reihe von kationischen Triarylboran-Chromophoren untersucht, wobei man sich auf die Unterschiede zwischen dipolarer und oktupolarer Ladungsverteilung konzentrierte. Schließlich wurde im Rahmen dieses Konzepts der mehrdimensionalen Verzweigungsmoleküldesign-Strategie eine weitere Serie von polychlorierten Triarylmethyl-Radikalverbindungen untersucht, indem man von der einfachen dipolaren über die quadrupolare bis zur octupolaren Verbindung ging.

Basierend auf den diskutierten Ergebnissen können einige allgemeine Schlussfolgerungen über die Struktur-Eigenschafts-Beziehung auf die 2PA-Eigenschaften gezogen werden. Das wichtigste Ergebnis ist, dass der 2PA-Zuwachs grob der Exzitonenkopplungswechselwirkung zwischen den konjugierten Chromophoren folgt, was zu der Schlussfolgerung führt, dass die Kombination von kurzen und konjugierten Brückeneinheiten zwischen den beiden Squarain-Chromophoren die Exzitonenkopplungsstärke erhöht und zu einer erhöhten 2PA-Stärke in solchen Homodimeren führt. Der dominierende Faktor, der die Zwei-Photonen-Absorptionsfähigkeit dieser Squarain-Chromophore beeinflusst, ist nachweislich die Exzitonenkopplungs-Wechselwirkung und nicht der intramolekulare Ladungstransfer. Darüber hinaus zeigen die 2PA-Spektren, dass die Symmetrie einen großen Einfluss auf das Zwei-Photonen-Absorptionsvermögen hat, was den Effekt der para-Konjugation gegenüber der meta-Konjugation hervorhebt. Tatsächlich erhöht der para-Konjugationspfad die elektronische Kopplung der beiden Chromophore im Vergleich zum meta-Konjugationspfad.

Bei den π-konjugierten Triarylboran-Chromophoren wurden die Koplanarität und die Elektronendichte der Konjugation identifiziert, die wiederum besonders wichtige Parameter für die intramolekulare Ladungstransferfähigkeit sind. Es wurde festgestellt, dass das Ausmaß der π-Konjugation und damit die Molekülgröße den 2PA-Querschnitt erhöht, da sie ebenfalls ein kritischer Strukturparameter ist. Schließlich hat der Einbau von zwei oder drei chromophoren Einheiten in ein einzelnes multichromophores Molekül zu einer bemerkenswerten Erhöhung des 2PA-Querschnitts durch die synergetische Zusammenarbeit der Chromophore geführt.

Weitere Studien haben gezeigt, dass mehrere der untersuchten Verbindungen mit ausgeprägten spektroskopischen und physikalischen Eigenschaften, gute Kandidaten für spezifische Anwendungen wie hochauflösende biologische Bildgebung und optische Leistungsbegrenzung zu sein scheinen.

11 List of Publications

1. E. Michail, M. H. Schreck, L. Wittmann, M. Holzapfel, C. Lambert, "*Enhanced two–photon absorption and promising broad energy range optical power limiting properties of transoid and cisoid benzodipyrrolenine-fused squaraine dimers"*, Chem. Mater., **2020**, Chem. Mater., **2021**, 33, 9, 3121-3131.

2. Y. F. Saal, F. Zhang, M. Holzapfel, M. Stolte, E. Michail, M. Moos, A. Schmiedel, A.-M. Krause, C. Lambert, F. Würthner, P. Ravat, *"[n]Helicene diimides (n = 5, 6, and 7): Through-Bond versus Trough-Space Conjugation.*" J. Am. Chem. Soc., **2020**, 142, 21298-21303.

3. E. Michail, M. H. Schreck, M. Holzapfel, C. Lambert, "*Exciton coupling effects on the two-photon absorption of squaraine homodimers with varying bridge units."*, PhysChemChemPhys., **2020**, 22, 18340-18350.

4. S. Griesbeck, E. Michail, C. Wang, H. Ogasawara, S. Lorenzen, L. Gerstner, T. Zang, J. Nitsch, Y. Sato, R. Bertermann, M. Taki, C. Lambert, S. Yamaguchi, T. B. Marder, "*Tuning the pi-Bridge of Quadrupolar Triarylborane Chromophores for One- and Two-Photon Excited Fluorescence Imaging of Lysosomes in Live Cells."*, Chem. Sci., **2019**, 10, 5405-5422.

5. S. Griesbeck, E. Michail, F. Rauch, H. Ogasawara, C. Wan<g, Y. Sato, R. Edkins, Z. Zhang, M. Taki, C. Lambert, S. Yamaguchi, T. B. Marder, "*The effect of branching one- and two-photon absorption, cell viability and localization of cationic triarylborane chromophores with dipolar vs. octopular charge distributions for cellular imaging."*, Chem. Eur. J., **2019**, 25, 13164-13175.

6. Y. Hattori, E. Michail, A. Schmiedel, M. Holzapfel, I. Krummenacher, H. Braunschweig, U. Müller, J. Pflaum, C. Lambert, "*Luminescent mono-, di-, and tri-radicals: bridging polychlorinated triarylmethyl radicals by triarylamines and Triarylboranes.",* Chem. Eur. J., **2019**, 25, 15463-15471.

7. F. Zhang, E. Michail, F. Saal, A. Krause, P. Ravat, "*Stereospecific Synthesis and Photophysical Properties of Propeller-Shaped C90H48 PAH."* Chem. Eur. J., **2019**, 25, 16241-16245.

DOI: https://doi.org/10.1039/D0CP03410J

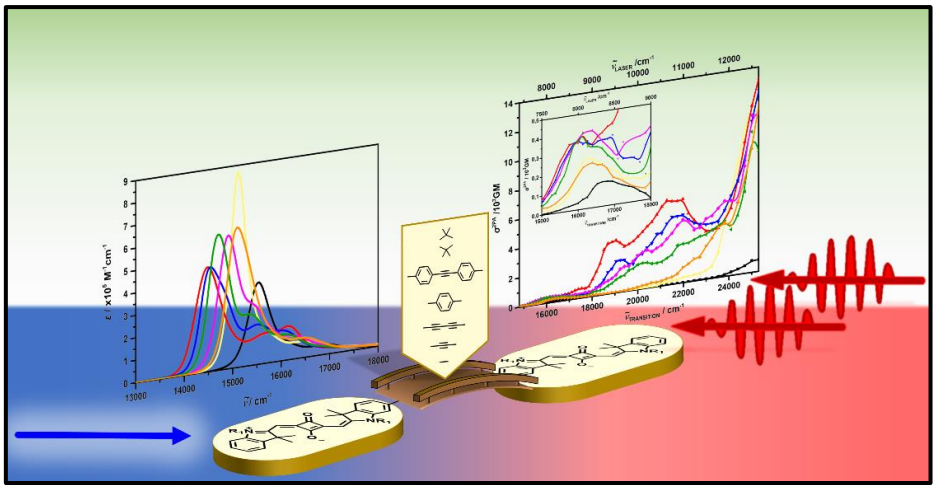

DOI: https://doi.org/10.1021/acs.chemmater.0c04780

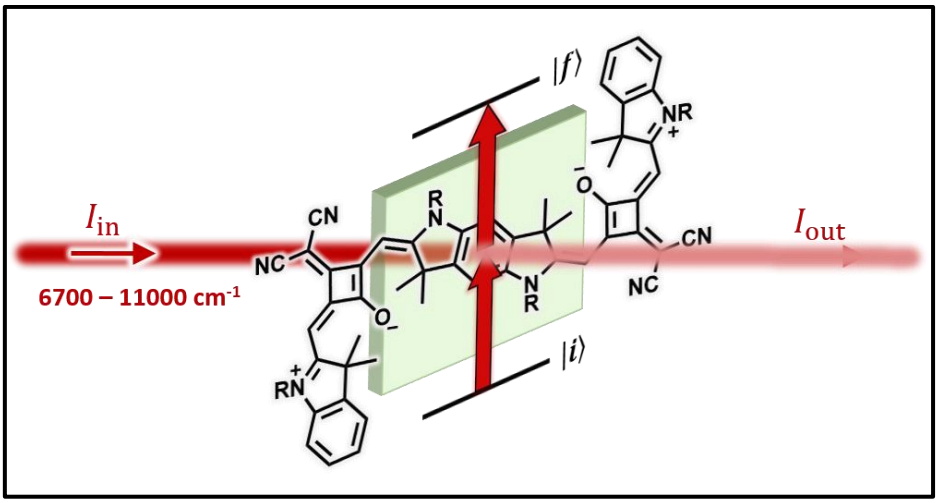

DOI: https://doi.org/10.1039/C9SC00793H